UBFC
UNIVERSITÉ
BOURGOGNE FRANCHE-COMTÉ

uB
UNIVERSITÉ DE BOURGOGNE

THÈSE DE DOCTORAT

DE L'ÉTABLISSEMENT UNIVERSITÉ BOURGOGNE FRANCHE-COMTÉ

PRÉPARÉE À L'UNIVERSITÉ DE BOURGOGNE

École doctorale n°37

Sciences Pour l'Ingénieur et Microtechniques

Doctorat d'Instrumentation et Informatique de l'image

par

ALIYU ISAH

Memristors in Nonlinear Network: Application to Information (Signal and Image) Processing

Thèse présentée et soutenue à Dijon, le 6 Juillet, 2021

Composition du Jury :

MICHEL AILLERIE	Professeur à l'Université de Lorraine & Centrale Supélec, Paris-Saclay	Rapporteur
SERGE DOS SANTOS	MCF HDR à l'INSA Centre Val de Loire	Rapporteur
SABIR JACQUIR	Professeur à l'Université Paris-Saclay	Examinateur
JEAN-MARIE BILBAULT	Professeur à l'Université de Bourgogne	Directeur de thèse
STÉPHANE BINCZAK	Professeur à l'Université de Bourgogne	Codirecteur de thèse
A.S NGUETCHO TCHAKOUTIO	Professeur à l'Université de Maroua, Cameroun	Codirecteur de thèse

N° | X | X | X |

ACKNOWLEDGMENT

I would like to thank and convey my warmest appreciation to my supervisor - Professor Jean-Marie BILBAULT for his remarkable support, guidance and attentiveness to ensure success in this work and above all - for opening my eyes as a researcher in the scientific community. His positive impact on me will continue to grow throughout my career. It is always my pleasure to work under his supervision. I would also like to thank my co-supervisors in persons of Professor Stéphane BINCZAK and Professor Aurélien Serge NGUETCHO TCHAKOUTIO for their outstanding contributions. In fact, we have a very nice and hardworking team. I would like to thank my rapporteurs Michel AILLERIE and Serge DOS SANTOS and the examiner Sabir JACQUIR for their suggestions, overview and insights of this study and future perspectives. I would like to thank my sponsor - The Kano State government of Nigeria in collaboration with Campus France, for giving me the opportunity to reach this milestone. I am always very grateful.

My appreciation goes to my parents Hama Isah and Isah Ibrahim for their encouragement, prayers and support, may Allah bless them in this life and hereafter. I would like to thank my wife Maimuna and my daughter Anisah for their patient during this period. I would also like to thank my brothers, sisters and friends for their well wishes and prayers.

Finally, I would like to thank the community of Université de Bourgogne (UB), Ècole Supérieure d'ingénieurs Numérique Et Matériaux (ESIREM), the doctoral school (Sciences Physiques pour L'Ingénieur et Microtechniques - *SPIM*) and the laboratory *Imagerie Vision Artificielle (ImViA)* for giving me the environment and equipment to carry out my research. I am very grateful to all the staff and my doctoral colleagues. It has been a very nice experience to meet you. Thank you all.

Contents

I Context and Issues 1

1 Introduction 3

1.1 Context . . . 3
1.2 Aims and Objectives of the thesis . . . 6
1.3 Organization . . . 7

2 Review on circuit elements and memristor interpretation 9

2.1 Resistor . . . 11
2.2 Capacitor . . . 16
2.3 Inductor . . . 20
2.4 Memristor . . . 24
2.4.1 Memristive device and system . . . 26
2.4.2 Verifying a memristor device . . . 27
2.4.3 Fingerprints of a memristor . . . 27
2.4.3.1 First fingerprint . . . 28
2.4.3.2 Second fingerprint . . . 31
2.4.3.3 Third fingerprint . . . 36
2.4.4 Not every nonlinear dynamical system is an ideal memristor . . . 36
2.4.5 Memristor by mode of excitation . . . 37
2.4.5.1 Charge−Controlled memristor (CCM) . . . 37
2.4.5.2 Flux−controlled memristor (FCM) . . . 40
2.4.6 *Why memristor*? . . . 42
2.4.7 Some potential applications of memristor . . . 42
2.4.8 Memory elements (Mem-elements) . . . 43
2.4.9 Remark on the four basic circuit elements . . . 44

3 Memristor technologies and models 47

3.1 HP (TiO_2) memristor: analysis and interpretation . . . 47

3.1.1 Model description . . . 48

3.1.2 Window function $g(x)$ . . . 51

3.2 Linear dopant drift model: Analysis . . . 56

3.2.1 CCM with linear dopant drift model . . . 56

3.2.2 FCM with linear dopant drift model . . . 58

3.3 Nonlinear dopant drift model: Analysis . . . 60

3.3.1 CCM with nonlinear dopant drift model . . . 61

3.3.2 FCM with nonlinear dopant drift model . . . 61

3.3.3 Effect of window function in memristor modeling: circuit point of view 63

3.4 SPICE and Analogue models of Memristor . . . 67

3.4.1 SPICE models of memristor . . . 68

3.4.2 Analogue models of Memristor . . . 70

3.4.2.1 Sine input . . . 71

3.4.2.2 Triangular input . . . 72

3.4.2.3 Rectangular or square wave input . . . 75

3.4.3 Passive models of the memristor emulator . . . 75

3.4.4 Proposition of Modification . . . 78

3.4.4.1 Current transformer . . . 78

3.4.4.2 Current mirror . . . 78

3.4.4.3 Hall effect sensor . . . 80

3.5 Conclusion . . . 80

II Main Contribution (1) 83

4 ϕ-q curve description and the New model 85

4.1 Introduction . . . 85

4.2 Memory effect . . . 85

4.3 ϕ-q curve . . . 87

4.4 The new memristor model . . . 92
4.5 Conclusion . . . 96

III Main Contribution (2) 97

5 CNN - Memristor dynamics in Nonlinear Network 99
5.1 Introduction . . . 99
5.2 Possibilities of the memristor-based 2D CNN . . . 101
5.3 RC cellular nonlinear network . . . 102
5.3.1 Voltage and current evolution: $V_m(t)$, $V_s(t)$ and $i(t)$ . . . 103
5.3.2 Charge $q(t)$ evolution . . . 106
5.3.3 Phase portraits: RC network . . . 107
5.3.4 Remarks on the RC network . . . 108
5.4 Memristor in the coupling mode . . . 110
5.5 Linear resistors R in the cell unit . . . 111
5.5.1 Analytical description of a specific case: System of two cells . . . 112
5.5.2 Expressions for the evolution of $V_m(t)$ and $V_s(t)$ . . . 113
5.5.3 Charge $q(t)$ evolution for memristor coupling mode: using the *$M(q)$ model (5.24)* . . . 115
5.5.3.1 Effect of initial charge q_0 on system dynamics . . . 122
5.5.3.2 Variation of $(V_{m_0} - V_{s_0})$ or specifically V_{m_0} . . . 123
5.6 Memristor dynamics involved in cells communication . . . 125
5.6.1 Evolution of $q(t)$ in phase portraits:– system solution using the new model . . . 125
5.6.2 Case A3 results comparison: Analytical, SPICE and Numerical . . . 147
5.6.3 System solution with HP model . . . 148
5.7 Memristor Asymmetry . . . 150
5.8 Memristor asymmetry from circuit point of view . . . 152
5.8.1 Memristor fuse . . . 155
5.9 Memristor fuse in the coupling mode . . . 167
5.9.1 Analytical interpretation of Memristor fuse in nonlinear network . . . 168

5.10 Conclusion . . . 171

6 Memristor coupled 2 cells with cubic resistance 173

6.1 Nonlinear resistor R_{NL} in the cell unit . . . 173

6.2 Analytical study . . . 175

6.3 Numerical solution – with MatLab . . . 180

6.3.1 Correlating V_m, V_s, V_a and V_b . . . 180

6.4 SPICE simulation . . . 185

6.4.1 R_{NL} circuit schematic description . . . 186

6.4.2 Verification of the R_{NL} SPICE component . . . 190

6.4.3 SPICE simulation of the 2-cells system – with Memristor and R_{NL} . . 192

6.4.3.1 SPICE - Correlating V_m, V_s, V_a and V_b . . . 192

6.4.3.2 Effect of R_2, R_3 and R_4 on the system stability decision . . . 194

6.5 Diffusion effects in a nonlinear electrical lattice using memristive coupling . 198

6.6 Description . . . 198

6.7 Conclusion . . . 201

IV General Conclusion 203

7 General conclusion and perspectives 205

7.1 General Conclusion . . . 205

7.2 Future Perspectives . . . 207

7.3 Publications . . . 207

V Appendices 235

A Memristor SPICE netlist file 237

B R_{NL} SPICE netlist file 239

Context and Issues

1

INTRODUCTION

1.1/ CONTEXT

Electronics engineering plays a crucial role in human civilization in both analogue and digital domains. This was made possible by the contribution of the circuit elements, generally called electronic components that are basically classified into two classes: (1.) Passive circuit elements: e.g resistor, capacitor, inductor, thermistor, transformer, light dependent resistor (LDR) etc. (2.) Active circuit elements: e.g transistor, diode, operational amplifiers, LED, integrated circuit, photodiode, voltage and current sources, etc,... The application of diode to either the passive or the active elements are not yet well defined. Some scientists consider the diode as a passive element as it cannot produce power to the remaining part of the circuit and as it constitutes 2-port device with $I = 0$ when $V = 0$. However, other ones claim that it is active as it allows to transform the signal power to a load. Our will is not to go into this debate, which is not of these thesis objectives, and we will only sort diodes in active class, because 2 diodes can give a transistor, which is clearly an active element.

One key component so far is the transistor owing to its reliable capabilities in switching, amplification and micro-scaleability. The performances of an electronic device are improved by incorporating smaller and faster circuit components. This approach serves many purposes, for example: reliability because fewer components are involved. However, transistor scaling is under challenging as it is presently few nano-meters in size, hence the need for an alternative to transistor for future electronic systems design. Scalability of electronic components becomes an important factor in order to meet the increasing demand of reliable digital electronic systems.

Nowadays, nano-scaleability is one of the main challenges in the electronics industries [1], especially due to the high demand of faster and more reliable systems (small, medium and large scales). For seven decades, transistor is the leading component contributing to the exponential advancement in electronic systems and designs [2]. However,

modern transistor suffers nano-scaleability owing to its infinitesimal dimension [3]. The performance of devices and systems improves with the reduction in the size of their constitutive circuitries [4] and often brings about the advantages such as reliability, lower power consumption, speed, cheapness, efficient handling etc, thanks to memristor nano-scaleability.

Memristor is a two-terminals nonlinear dynamic electronic device and is typically a passive nano-device whose conductivity is controlled by the time-integral of the applied voltage (also known as flux) across it or the time-integral of the current (also known as charge) flowing through it. This new component is proclaimed to be the fourth basic passive circuit element (along side resistor, capacitor and inductor) having interesting features that make it to be a proper replacement of transistor in various applications. For example: high density memory applications, bio-electronics or bio-inspired applications, storage and processing of big data, and image recognition and processing. It is impossible to completely discard transistor due to the emergence of memristor because it is an active device while memristor is a passive one. However, using both of them in a circuit will tremendously improve its performances, because one memristor can replace multiple transistors.

Memristive behaviour has been observed experimentally for two centuries but remained unidentified because no one had ever thought on the contingency of the fourth basic circuit element in electronics. The first man-made memristor dated in 1801 by English chemist Humphry Davy [5], in which the fingerprint of a memristor manifested experimentally with carbon arc discharge lamp (incandescent light) and was considered as the first artificial electric light source. Some devices and systems were shown to possess the now well known signature of a memristive device (pinched hysteresis loop) owing to their inholding inertia [6] which occurs from the movement of mobile ions or oxygen vacancies, the formation and splitting of conductive filaments and phase change transition of some materials for data storage, e.g sputtered $Ge_2Sb_2Te_5$ films [7, 8]. This inertia causes latency in the system mechanism, thereby making it to exhibit memory effect. Contemporarily, memory effect is also seen in nano devices [9] in which the dynamics of electrons and ions depends on the previous history of the device.

In 1971, a circuit theorist in person of Professor Leon Chua [10] observed from symmetrical argument of the circuit elements (shown in Fig. 2.2) that for the sake of completeness there should be a fourth passive circuit element in addition to the conventional resistor, capacitor and inductor. He theorized the existence of the memristor and its electromagnetic interpretation. However, memristor differs from the 3 other passive circuit elements in the sense that it is a nonlinear element and capable of storing information. As clearly presented in [10], some theories were established supporting the existence of the fourth basic circuit element, its electromagnetic interpretation and some promising applications.

Few years later, Chua and Kang [11] elaborated a broader class of nonlinear systems called the memristive systems, as discussed in section 2.4.1.

Although the principle theories of memristor exist [10], its realization remained a mystery for nearly four decades. Then in 2008 [12], a team of researchers from Hewlett Packard (HP) laboratory led by Stanley Williams published a paper in *Nature Journal* announcing their successful realization of a two-terminals solid state device bearing the characteristics of the memristor described by L. Chua in 1971 [10]. This discovery, that is described as accidental while working on nano crossbar grid [3], paved way for more awareness that kept attracting attention of many researchers, engineers and scientists in the world, therefore exploring more possible features of memristor in terms of applications and technologies. Some of the memristor technologies are Redox reaction, Ferro-electricity, Organic etc ..., and will be discussed in chapter 3.

The conventional resistance to the flow of charges through a conducting material or wire is often described analogously like flowing water through a pipe of uniform cross sectional area. The analogy of memristance with respect to the flowing charge is seen in a flowing water through a pipe having a variable diameter [13, 14]. The volume of water flowing through the pipe increases with increasing of the pipe's diameter, hence the water encounters a lower resistance path, while it decreases with decreasing of the pipe's diameter, hence encounters a higher resistance path. Considering a tap in between will enable water flowing in either direction, and allows to control the water flow. This analogy is demonstrated in Fig. 1.1. The *tap* is acting as the state variable of the system, thus maintaining the switching dynamics from high memristance state to the low memristance state and vice-versa. Notice that the most important aspect is the switching transition where the memristance is described relatively by the effect of R_{on} and R_{off}.

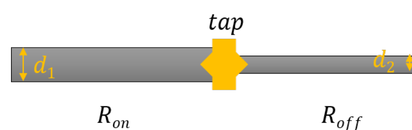

Figure 1.1: Memristance analogy to water flow through a pipe of varying diameter: where d is a diameter such that: $d_1 \gg d_2$.

Memristor is seen as the most promising element, not only capable to replace transistor for some applications, but also to revolutionize electronic industries virtually in every facets of electronic systems, design and applications [3]. Hence, memristor becomes a suitable component for nanotechnology. The most common properties that make memristor a good candidate for feature technologies are: Nano-scalability, Memory capabilities, Conductance modulation and Nonlinearities whose contemporary demand is at peak. For example, transistors suffer nano-scalability limitations due to their finite dimensions while it would be required that they can be of infinitesimal dimensions. Therefore they cannot effectively undergo any further reduction in size as it is presently a few nano-meter [15].

As it was stated by Gordon Moore, who is a co-founder of Intel cooperation, ”The number of transistors incorporated in a chip should approximately double every 18 months” and hence is called Moore’s Law. This law holds only if the sizes of chip’s associated circuitries keep reducing, otherwise the law will cease to be true. Transistors are tiny electrical switches, forming the fundamental unit that drives all the electronic gadgets. As the transistors get smaller, they also get faster and consume less electricity to operate. Obviously, there will be a limit when transistors can not undergo any further reduction in size, which seems to be different with memristor nano-scaleability.

However, the memristor discovery in [12] is still under criticism as some researchers do not believe in the found memristor [16, 17]. In [18], they showed that the real memristor stated in [10] is not found and even impossible. Intuitively, the three known passive circuit elements (R, L and C) are unquestionably independent of one another and they are in existence naturally, hence also refered to as the fundamental circuit elements. However, on the other hand, the claim for memristor as the fourth fundamental circuit element is challenging owing to its one-to-one resistor dependencies [19]. Namely, having exact same unit of measurement as ohm Ω and a deductive-like expression, as:

$$M = \frac{v}{i} = \frac{\frac{d\phi}{dt}}{\frac{dq}{dt}} = \frac{d\phi}{dq} = M(q) \; , \tag{1.1}$$

it resembles very much to resistor. Here $M(q)$ is the memristance and it is expressed in ohms like resistor. Notwithstanding, the fact that memristor cannot be realized by any simple combination of the three basic circuit elements (R, L and C) proves that memristor is actually a fundamental circuit element [3]. Although its position as the fourth passive circuit element is challenging [18, 19], memristor has massive technological impact and it appears to be a good candidate for numerous designs and applications. Moreover, since its inception in 2008, thousands of publications were published on memristor technologies and applications (too many to be all cited) and in doing so they affirmed memristor as the fourth basic circuit element. The number of memristor publications grows exponentially, hence outweighed the few criticisms.

1.2/ Aims and Objectives of the Thesis

The aim of this thesis is to develop a multipurpose Memristor based two-dimensional (2D) Cellular Nonlinear/Neural Networks (CNNs) for information processing. The process entails using memristor as synaptic link between neurons in electronic models, as for example in hybrid technologies with neuronal electronic prosthesis between real neurons. The network is initially composed of a linear capacitor and a nonlinear resistance in parallel for each cell and a linear resistor in series, see Fig. 1.2a. The equivalent memristor-based

network is shown in Fig. 1.2b where the series resistance is replaced by a memristor.

Figure 1.2 shows the conventional system composition and the equivalent Memristor-based network.

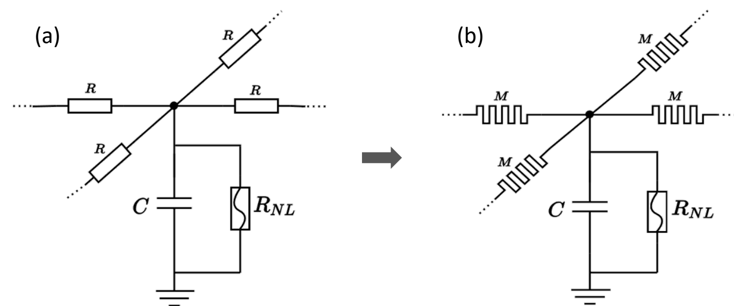

Figure 1.2: 2D cellular nonlinear networks (CNN). C is a linear capacitor and R_{NL} is a nonlinear resistance. (**a**) Coupling using linear resistance R and (**b**) coupling using memristor M.

1.3/ ORGANIZATION

This document is organized in three parts. The first part includes the first three chapters, containing the general introduction and the memristor insights. The second part contains the fourth and fifth chapters, presenting the contribution of this thesis on the memristor and its model. The third part includes the remaining chapters, presenting the applications of memristor in 2D CNN, 1D diffusive network and the general conclusion. The followings are the mentions of the chapters.

Chapter 1: Introduction: This chapter presents the general introduction and foresight for the need of memristor in nano-technology, motivation, the aims and objectives of this thesis.

Chapter 2: Review on the basic circuit elements and memristor interpretation: This chapter presents the general review on the four basic passive circuit elements, then a thorough interpretation of the memristor and some of its potential applications. The motivation is to explore more features of the memristor which could eventually guide researchers working in the field, from basic modeling up to practical implementation.

Chapter 3: Memristor technologies and models: This chapter presents the memristor technologies and insights into the HP TiO_2 memristor. It further explores some subtleties of the memristor.

Chapter 4: ϕ-q curve description of HP TiO_2 memristor and the new model: This chapter presents the graphical description of the ϕ-q curve, explaining the response of a memristor from its constitutive relationship. A new model is presented and it is used in the subsequent chapters to study the interaction of memristor within the cells.

Chapter 5: CNN - Memristor dynamics in Nonlinear Networks: This chapter intro-

duces the application of a memristor in cellular nonlinear network, then presents extensively, the dynamics of a charge-controlled memristor between two RC cells, the behavior of memristor in CNN neighborhood connections, memristor asymmetry and its effect in linking two RC cells bidirectionally. Furthermore, memristor fuse manifests symmetry features, hence it becomes part of the discussion.

Chapter 6: Memristor coupled 2 cells with cubic resistance: This chapter presents the interaction of memristor between two pixel cells, with the cells comparable to Fitzhugh-Nagumo cells. Then, the generalized memristor based 2D network is presented. The chapter is concluded by an introduction of one-dimensional (1D) diffusive network using memristive coupling.

Chapter 7: The general Conclusion and perspectives: Finally, the general conclusion and perspectives are presented, including the published contributions.

2

REVIEW ON CIRCUIT ELEMENTS AND MEMRISTOR INTERPRETATION

This chapter gives the review on the four basic passive circuit elements. Firstly, the three familiar passive circuit elements (R, L and C) are introduced briefly, focusing specifically on their geometrical features, while memristor is treated comprehensively. Electronic network comprises of causes and effects. The causes here refer to any various voltage or current sources and the effects are part of the network using or sinking the energy given by the sources. Active elements and passive elements are commonly used in place of causes and effects respectively. In general, active circuit elements are capable to generate electric power while passive circuit elements can only store, use or deny the generated power for example resistor, capacitor. Additionally, transistor is an active device owing to its ability to generate power gain. These circuit elements altogether form electronic devices (see Fig. 2.1) that have been one of the major bedrock for human civilization owing to their tremendous contribution in the advancement of electronic industries.

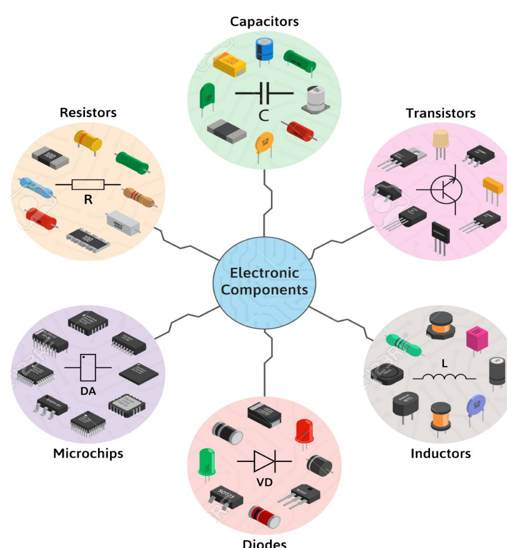

Figure 2.1: Display of some basic electronic components.

The basic active circuit elements are voltage and current sources in the form of dependent or independent sources. In addition, there are four fundamental circuit variables: electric current i, electric voltage v, electric charge q, and magnetic flux ϕ, where q and ϕ are defined as the time integrals of i and v respectively. These circuit variables are inter-related or linked accordingly to the basic passive circuit elements which include the three known conventional two-terminals basic passive circuit elements, namely: resistor R, capacitor C, and inductor L. These passive circuit elements are defined in terms of the constitutive relationships: $f(n, m) = 0$ between any pair of the four aforementioned circuit variables, where n and m could be any of i, v, q or ϕ variables. The three fundamental known passive circuit elements (R, L and C) in conjunction with the definitions of charge(q) and flux(ϕ) lead to five known possible relationships as shown in Fig. 2.2, and thus, in connection to other circuit elements have been the remarkable circuit components in the history of electronic system design.

In 1971, Leon Chua posited the missing basic circuit element [10] from symmetry argument, studying Fig. 2.2. He proposed that, for the sake of completeness, there should be a fourth fundamental passive circuit element defined by the mathematical relationship between electric charge q and magnetic flux ϕ, thus having a constitutive relation: $f(\phi, q) = 0$, see the red segment of Fig. 2.2. Leon Chua named the circuit element as *Memristor* M, a portmanteau of 'memory' and 'resistor'. The name (memory resistor) portrays that memristor is nothing else than a resistor with memory. This fact arises due to the peculiar nature of memristor to remember the history (memory effect) of its previous state (resistance), even after the power is disconnected and restarted from this previous state if the power is reconnected, irrespective of the duration upon which the power is ON or OFF (i.e it could be a day, a month or years) [3]. This special property suggests memristor to be a promising element in memory applications.

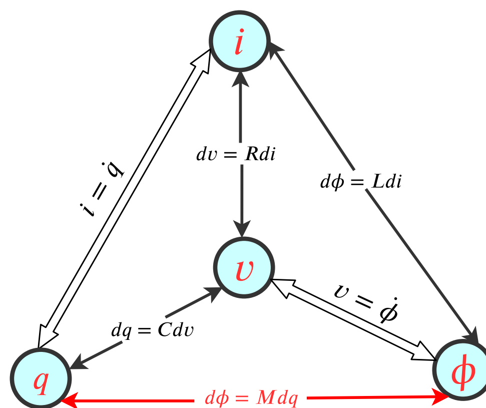

Figure 2.2: Symmetrical view of the four basic circuit elements and their correlations with the four circuit variables.

These four circuit variables in conjunction with the four passive circuit elements produced a set of six possible equations, one equation more than the previous five already known

equations, due to the presence of memristor. Hence, these relationships are summarized in Table 2.1. We first recognize the relationship between electric voltage v and magnetic flux ϕ, as typically known from Faraday's law, as:

$$v(t) = \frac{d\phi(t)}{dt} \text{ or equivalently : } \phi(t) = \int_{-\infty}^{t} v(\tau)d(\tau) \,, \tag{2.1}$$

that is,

$$\phi(t) = \int_{0}^{t} v(\tau)d(\tau) + \phi_0 \,,$$

where $\phi_0 = \int_{-\infty}^{0} v(\tau)d\tau$, is the initial flux at time $t = 0$ and may be zero or nonzero. Similarly, the relationship between electric current i and electric charge q is conventionally known as;

$$i(t) = \frac{dq(t)}{dt} \text{ or equivalently : } q(t) = \int_{-\infty}^{t} i(\tau)d(\tau) \tag{2.2}$$

$\Rightarrow$

$$q(t) = \int_{0}^{t} i(\tau)d(\tau) + q_0 \,,$$

where $q_0 = \int_{-\infty}^{0} i(\tau)d\tau$ is the initial charge at time $t = 0$ and may be zero or nonzero.

...	$i(t)$	$V(t)$	$q(t)$	$\phi(t)$
$i(t)$	...	$dV(t) = Rdi(t)$ Resistor	$i(t) = \frac{dq(t)}{dt}$ current & charge	$d\phi(t) = Ldi(t)$ Inductor
$V(t)$	$dV(t) = Rdi(t)$ Resistor	...	$dq(t) = CdV(t)$ Capacitor	$V(t) = \frac{d\phi(t)}{dt}$ voltage & flux
$q(t)$	$i(t) = \frac{dq(t)}{dt}$ current & charge	$dq(t) = CdV(t)$ Capacitor	...	$d\phi(t) = Mdq(t)$ Memristor
$\phi(t)$	$d\phi(t) = Ldi(t)$ Inductor	$V(t) = \frac{d\phi(t)}{dt}$ voltage & flux	$d\phi(t) = Mdq(t)$ Memristor	...

Table 2.1: Summary: Circuit elements visualization in tabular form.

2.1/ RESISTOR

Resistor is a passive two-terminals basic electronic component discovered by Georg Simon Ohm in 1827, in which, at a constant temperature, the current flowing through these terminals is directly proportional to the voltage drop across it.

Resistance is an inherent property of a material that resists to the flow of electric charge (or electric current) through it, dissipating power in the process as heat. Letter *R* is usually used to denote resistance and it has measurement unit as *Ohm* named after the inventor,

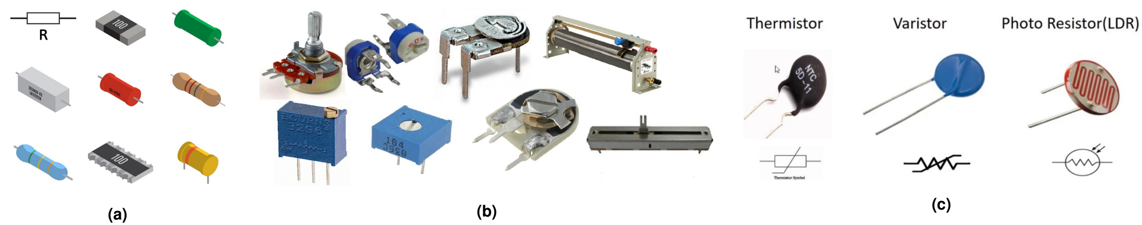

Figure 2.3: Different configurations of resistors. (a) Electronic symbol of resistor, surface mount resistor (or chip resistor) and other configurations depending upon applications. (b) Some examples of variable resistors. (c) Nonlinear resistors.

with symbol Ω. Resistors are components designed basically to offer resistance in the circuit, commonly used as a current limiting device. Virtually every electronic circuit is composed of at least one or more resistor, either a real component or by choosing the type of the material itself (resistivity). Nowadays, there are many types of resistors suitable for different applications, for example: *Fixed resistor, Rheostat or Variable resistor, Potentiometer (preset or post-set), Thermistor, Varistor, Thermocouple, Photo resistor or Light Dependent Resistor (LDR), Voltage Dependent Resistor (VDR), Barretter, Strain gauge, etc*. Some of them are nonlinear such as: Thermistor, Varistor, Photo resistor etc., as shown in Fig. 2.3.

The resistance of a material is expressed by the constitutive relationship between voltage v and current i such that $f(v, i) = 0$, or:

$$\mathrm{d}v = R\,\mathrm{d}i. \tag{2.3}$$

For nonlinear function, equation (2.3) can be expressed as $v = f_R(i)$. Hence, resistors are characterized by: the resistance, the tolerance, the maximum working voltage, the power rating, the temperature coefficient, the noise, and even an inductance effect [20]. We are not going into details by analyzing the effect of these factors on the resistance of a material. However, we highlight three important aspects as enumerated underneath. This is also applicable to capacitor and inductor. The expressions of resistance could be derived in the following point of view:

(i) Circuit viewpoint: A resistor of resistance R being connected across a voltage source V, then a current I will flow through the resistor according to:

$$V = IR\,, \tag{2.4}$$

this relationship is called Ohm's law and is considered as the circuit view point of a resistor.

(ii) Energy viewpoint: The energy in a resistor E_R is the heat dissipated as a result of the current flowing through it. This energy is also known as the Joule effect, it is caused by the inelastic collisions between electrons as they drift from one atom to

another, this phenomenon is given in eq. (2.10). Conventionally, the power in a circuit is given by:

$$P = V.I,$$

using (2.4), thus the power becomes:

$$P = I^2 R. \tag{2.5}$$

Recall that power P is given by:

$$P = \frac{d\mathscr{E}_R}{dt},$$

where $\mathscr{E}_R$ is the energy (heat dissipated) in a resistor and t is the time during which the current I flowed. It implies that:

$$\mathscr{E}_R = \int_0^t I^2 R \, dt \;\Rightarrow$$

$$\mathscr{E}_R = I^2 R \, t. \tag{2.6}$$

(iii) Geometry viewpoint: This refers to the physical resistor device given in Fig. 2.4. There are basically four factors affecting the resistance of a resistor and these factors are briefly discussed in the following.

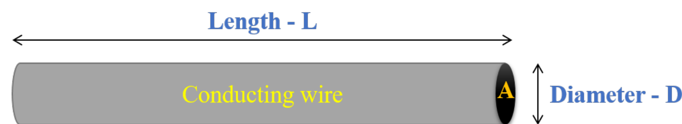

Figure 2.4: Geometry viewpoint of a resistor made up of uniformly conductive wire: A and L are the cross-sectional area and the length of the material respectively.

- ***Cross-sectional area of the conductor,*** A : We know that by definition, resistance is the opposition to the flow of electrons through a conductive material (Fig. 2.4) under the influence of potential difference. Obviously, for the same conductive material under the same applied voltage, a larger cross-sectional area A will allow the moving electrons to experience lower opposition or resistance and a lower area will make the moving electrons experience a higher opposition or resistance. We can easily observe this scenario in a non-uniform conductive wire whose resistance changes along its axial length due to the variation in width. It shows that: $R \propto \frac{1}{A}$.
- ***Length of the conductor,*** L : As the conductive wire becomes longer, electrons have to cover longer distance and would experience more collisions in the process which in essence will contribute to a higher opposition or resistance than usual. It follows that: $R \propto L$.

- ***Nature of the conducting material, Resistivity*** ρ : The nature of the material determines its opposition to the flow of electric current through it. It could be from the number of atoms, its organization and the number of free electrons. These are all put together and termed as *Resistivity* ρ (Ωm). The higher the resistivity of the material, the higher the opposition or resistance to the electrons flow and, the lower the resistivity, the lower resistance to the electrons flow. Note that the inverse of resistivity is called the conductivity σ. For example, silver metal has lower resistivity than copper metal: as a result, silver metal offers lower resistance to the current flow. Thus: $R \propto \rho$.
- ***Temperature,*** T : Change in temperature causes a change in the resistance of the material. As the temperature of the material increases, the kinetic energy of the electrons increases which will consequently increase the rate of collisions between atoms and electrons, hence an increasing resistance. Conversely, lower temperature signifies lower resistance.

Equation (2.4) can be rewritten as:

$$\mathbf{J} = \sigma \mathbf{E} = \frac{1}{\rho}\mathbf{E}, \tag{2.7}$$

where:

$\mathbf{J}$ is current density (in Ampere per meter-square) expressed as: $\mathbf{J} = \frac{I}{A}\vec{u}$, I is current (in Ampere), $\vec{u}$ is a unit vector of same direction than the current I and A is the enclosed area,

$\mathbf{E}$ is electric field (in V/m) expressed as: $\mathbf{E} = -\vec{\nabla}_l V$, i.e the gradient of V with respect to partial variable x, parallel to the length L,

L is the length of the conductive wire (in meter),

V is the potential difference, while σ and ρ are conductivity and resistivity respectively.

For uniform conductive wire (Fig. 2.4), the modulus of vectors $\vec{J}$ and $\vec{E}$ (or $\mathbf{J}$ and $\mathbf{E}$) can respectively be written as follows:

$$J = \frac{1}{\rho}E \ \text{ and } \ E = \frac{dV}{dL} = \frac{V}{L}.$$

Using the relation between $\mathbf{J}$ and $\mathbf{E}$ in (2.7), we get:

$$\frac{I}{A} = \frac{1}{\rho}\frac{V}{L} \quad \Rightarrow \quad V = \frac{\rho L}{A}I. \tag{2.8}$$

Finally, comparing (2.4) and (2.8), we get the resistance expression as:

$$R = \frac{\rho L}{A} \tag{2.9}$$

If the resistivity ρ of the material is known, then A and l are measured and its resistance R can be calculated using (2.9).

The resistivity ρ or conductivity σ can be obtained from the microscopic interpretation of Ohm's law, by simple derivation if the constituents of the material are known. We know that the electric conduction in a material is due to the electronic drifting from one side to another one under the influence of potential difference. If n is the density of charges contained in a given volume of material (e.g Fig. 2.4), $-e$ is the charge of the electrons and **v** is the drift velocity, while positive ions can be considered as static, then current density **J** can be written as follows:

$$\mathbf{J} = -ne\mathbf{v}.$$

If m is the electron's mass, excited by a force **F** such that $\mathbf{F} = -e\mathbf{E}$ and braked by a force proportional to its velocity, its acceleration **a** is given by:

$$m\mathbf{a} = -e\mathbf{E} - k\mathbf{v},$$

where k in $N.s.m^{-1}$ is a fixed parameter for braking. A maximum velocity $\mathbf{v}_{max}$ of the electron is attained as a limit according to this acceleration effect and the braking effect due to collisions with another electrons or fixed ions - before the electron collides with another electron or atom. If the average time to attain this maximum speed is $\langle t \rangle$, then; $\mathbf{v}_{max}$ becomes:

$$\mathbf{v}_{max} = -\frac{e\mathbf{E}}{k} = -\frac{e\mathbf{E}}{m}\langle t \rangle .$$

Moreover, the drift speed **v** is generally considered to be the average speed given by $\frac{\mathbf{v}_{max}}{2}$, such that:

$$\mathbf{v} = -\frac{e\mathbf{E}}{2m}\langle t \rangle .$$

The link between the velocity of the charges and the electric field being $\vec{v} = \mu\vec{E}$, we get the mobility $|\mu| = \frac{e}{2m}\langle t \rangle$. Substituting **v** into **J**'s expression, we also get:

$$\mathbf{J} = \frac{ne^2\mathbf{E}}{2m}\langle t \rangle \quad \Rightarrow$$

$$\rho = \frac{2m}{ne^2\langle t \rangle}. \tag{2.10}$$

2.2/ CAPACITOR

Capacitor is the first passive two-terminals basic electronic component invented by Ewald Georg von Kleist in 1745 [21]. It comprises of two conductive materials separated by a dielectric. The dielectric could be air or any appropriate insulation material. Condenser is almost synonymous to capacitor, condenser being for the circuit element, capacitance for the electric characteristic, then these terminologies are often used interchangeably.

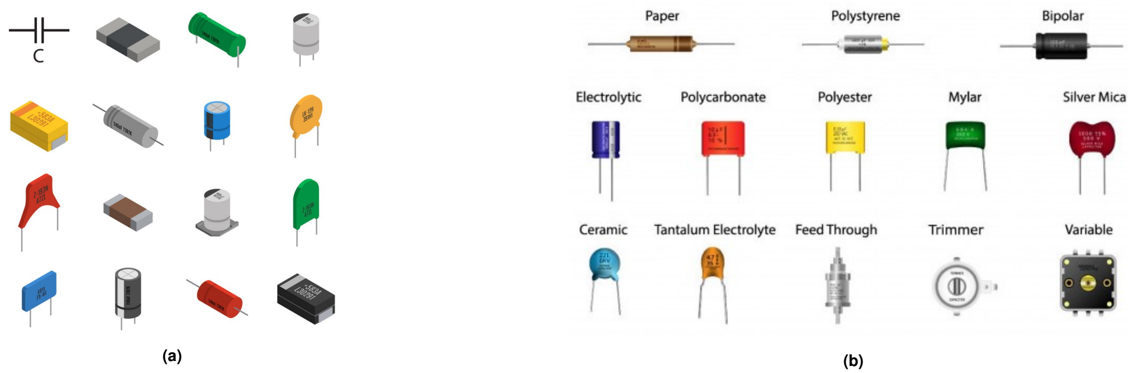

Figure 2.5: Different configurations of capacitors. (a) Electronic symbol of capacitor, surface mount capacitor (or chip capacitor) and other configurations. (b) Different types of capacitors.

Capacitance characterizes the amount of charge stored in the condensator between two parallel conducting materials subjected to potential difference. It is described by the constitutive relationship $f(v, q) = 0$, such that:

$$\mathrm{d}q = C\ \mathrm{d}v. \tag{2.11}$$

Therefore, $q = f_C(v)$. The function f_C may be nonlinear as for example in varicap diodes. Capacitance is measured in Farad F, often used with sub-multiple prefix such as micro (μ), nano (n), pico (p) etc, because Farad unit is very large. The size of 1 Farad capacitor will be extremely large and not met in real systems. Like resistor, there are many different types of capacitors used for different applications. For example: Ceramic capacitor, electrolytic, film, Tantalum, Silva Mica, variable, SMD capacitors etc. Some images of these capacitors are shown in Fig. 2.5.

Similarly, one can see the description of a capacitance in three different points of view as follows:

i) Circuit viewpoint: The current-voltage relationship in a capacitor is given by:

$$\begin{cases} i(t) = C\dfrac{dv(t)}{dt}, \text{ for a fixed capacitance.} \\ i(t) = C\dfrac{dv(t)}{dt} + v(t)\dfrac{dC}{dt}, \text{ for time-varying capacitances or nonlinear ones.} \end{cases} \tag{2.12}$$

Considering the first case of eq. (2.12), from eq. (2.11) giving also $i = C\frac{dv}{dt}$, the stored charge q is given by:

$$\begin{aligned} q &= \int_{-\infty}^{t} i \, d\tau, \\ &= C\int_{v_0}^{v(t)} dv = C(v - v_0), \quad \text{if for } t \to -\infty,\ v = v_0 \\ &= Cv, \qquad \text{if the initial condition } v_0 = 0. \end{aligned} \tag{2.13}$$

Equation (2.13) shows that the charge q accumulated in a capacitor is directly proportional to the applied voltage v across its terminals.

ii) Energy viewpoint: Capacitor stores energy in the form of electric field situated in between the plates due to the application of external electric potential difference v across its terminals. This energy is given by the electric potential energy U_E, such that (for the case where $v_0 = 0$):

$$\begin{aligned} U_E &= \int_0^q v dq, \\ &= \frac{1}{C}\int_0^q q dq, \\ &= \frac{q^2}{2C}. \end{aligned}$$

Therefore:

$$U_E = \mathscr{E}_c = \frac{1}{2}Cv^2 , \tag{2.14}$$

where $\mathscr{E}_c$ is the stored energy in a capacitor measured in Joule (J). Alternatively, one can derive equation (2.14) from the power expression:

$$d\mathscr{E}_c = Pdt = v.C\frac{dv}{dt}.dt = C\ vdv \ \Rightarrow$$

$$\mathscr{E}_c = U_E = C\int_0^v vdv = \frac{1}{2}Cv^2.$$

iii) Geometry viewpoint: Figure 2.6 shows the physical description of a basic capacitor: two parallel conductive plates placed apart by a distance d with a dielectric material sandwiched in between them. The two plates are identical, each having a cross-sectional area A. It follows that if a potential difference v is placed across the two external connection terminals, clouds of charges are established at both sides. However, the presence of dielectric material will prevent the charges from crossing, rather they pile up on the respective plate, and hence an electric field is created. The formed electric field has an energy expressed in (2.14) whose strength is influenced by the value of the capacitance C. As shown in Fig. 2.6, three factors affect

the capacitance of a capacitor as enumerated below.

- ***Surface area of the plates,*** A: By connecting the capacitor (shown in Fig. 2.6) to external voltage source, an electric field is generated and charges are accumulated on the respective plates. It implies that, the larger the plate's size, more charges can be stored and hence, the higher the capacitance, while a smaller plate's size yields lower capacitance. It shows that:

$$C \propto A.$$

- ***Distance between the plates,*** d: If V is the electric potential connected across the capacitor, then the electric field E is known to be:

$$E = \frac{V}{d} .$$

  Obviously, the shorter the distance between the plates, the higher electric field is generated and hence the higher capacitance. Conversely, the wider the distance between the plate, the lower electric field is generated, and hence the capacitance is lower. It follows that:

$$C \propto \frac{1}{l}.$$

- ***Dielectric or insulation***: In addition to the distance between the plates, the capacitance is affected by the nature or permittivity (ε) of the dielectric material (the section in magenta colour of Fig. 2.6) placed in between the plates. Recall that the field polarization $\vec{P}$ governs the electric dipole moment, given the dielectric material medium. The permittivity of the dielectric material determines the opposition to the electric charges: the higher the permittivity, the lower the opposition, and hence the higher the capacitance. Conversely, the smaller the permittivity, the higher the opposition, and hence the lower capacitance. For example: the permittivities of Air and Mica are approximately 1 and 8 respectively. Using Air in the medium as dielectric will give lower capacitance than with Mica having higher permittivity. Notice that ε is the absolute permittivity of the medium. The permittivity of vacuum is $\varepsilon_o = 8.85 \times 10^{-12}$ Farads/meter. The permittivity of vacuum is always considered as the reference, hence it becomes interesting to express the permittivity of any medium with respect to that of vacuum and that gives birth to what is called relative permittivity ε_r. Thus:

$$\varepsilon = \varepsilon_r.\varepsilon_o.$$

To derive the capacitance's expression of Fig. 2.6, we consider the surface area of the

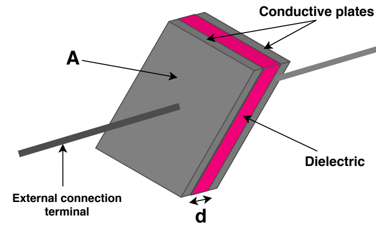

Figure 2.6: Geometrical viewpoint of a capacitor.

plates to be a Gaussian surface, such that from Gauss's law, we can write the following:

$$\oint \mathbf{E}.\, d\mathbf{A} = \frac{q}{\varepsilon},$$

that is in calculating the flux of $\vec{E}$ on the whole surface area surrounding the plates. Here:

E is the electric field vector (in volts per meter, V/m),

A is the normal surface area vector to the plates (in meter-square, m^2),

q is the total charge accumulated within the capacitor's plates (in Coulomb, C) and

ε is the permittivity of the dielectric material (in Farad per meter, F/m).

For a uniform electric field ⇒

$$E \oint dA = \frac{q}{\varepsilon}\,, \Rightarrow$$

$$EA = \frac{q}{\varepsilon} \quad \Rightarrow \quad E = \frac{q}{\varepsilon A}. \tag{2.15}$$

The relationship between electric field **E** and electric potential v is known to be:

$$\mathbf{E} = -\frac{dv}{d\mathbf{r}} \quad \Rightarrow \quad v = -\int \mathbf{E}.d\mathbf{r} \quad \Rightarrow \quad v = Ed. \tag{2.16}$$

Substituting (2.15) into (2.16), we get:

$$v = \frac{q}{\varepsilon A} d \tag{2.17}$$

Comparing equations (2.13) and (2.17), we get the capacitance expression as follows:

$$C = \varepsilon \frac{A}{d} = \varepsilon_r \varepsilon_o \frac{A}{d}\ . \tag{2.18}$$

Therefore, the capacitance is directly proportional to the area of the plates and inversely proportional to the distance d separating the plates. For a fixed distance between the plates d, fixed plates area A and dielectric material, the capacitance C is constant.

On the other hand, the second case of eq. (2.12) is important in the case of varicap capacitors, useful to produce solitonic effects, but it will not be considered here.

Capacitors have being used extensively in areas such as: power conditioning, signal processing, energy storage, coupling, filters, tuning radios and resonant, sensors, to regularize the output of power supply, ...

2.3/ INDUCTOR

Inductor is a passive two-terminals basic electronic component discovered by Michael Faraday in 1831. It is basically capable of storing energy in the form of magnetic field due to the passage of an electric current through it. Any current carrying conductor is associated with a magnetic field circulating around the conductor. The strength of the field or magnetic flux is directly proportional to the magnitude of the electric current flowing through it. A straight coil wire has one turn and as such it has less inductance. Moreover, the generated magnetic field becomes more significant if the wire is coiled to a certain number of turns, it could be air core or iron core format. However, the field is more concentrated if the coil is wound on a ferromagnetic material (or iron core format) and then has a higher inductance, see Fig. 2.7. Additionally, due to the variation of the formed magnetic flux, a voltage (self-induced voltage source according to Faraday's law) is induced in the coil and it acts in such a way to oppose itself to any change in the current that causes it (according to Lenz's law).

Figure 2.7: Air core inductor (left) has less inductance and iron core inductor (right) has more inductance

Figure 2.8: Different configurations of inductors. (a) Electronic symbol of inductor, SMD inductors (or inductor chips) and other configurations. (b) Different types of inductors.

Inductance is the property of a material to oppose to any change in the current flowing through it. Therefore, the ability of an inductor to oppose itself to any change in current flowing through it by generating self-induced voltage is called *self-inductance* or simply *inductance*, measured in *Henry, H*. The higher the opposition, the lower the change in the current will result. In other words, inductance is the property of a material associating its magnetic field and the rate of change of electric current flowing through it. It follows that:

$$v_L(t) = -L\frac{di(t)}{dt} ,$$

where L is the inductance and $v_L(t)$ is the self-induced voltage. The negative sign signifies that the induced voltage tends to oppose to any change in current flowing through the inductor at any given time, and can be dropped when considering the passive arrows rule. Nowadays, there are various types of inductors (just like resistor and capacitor) made of different sizes and shapes. Types of inductors are sorted by the kind of applications and the type of winding and core materials. Power inductors are more huge than general purpose inductors.

The constitutive relationship of an inductor is given by: $f(\phi, i) = 0$, such that:

$$\mathrm{d}\phi = L\,\mathrm{d}i\,. \tag{2.19}$$

Thus, for a nonlinear inductance, we have $\phi = f_L(i)$ with f_L a nonlinear inductance function. The expressions of the inductance can be seen in the following perspectives:

1. Circuit viewpoint: Consider an inductor of n-turns connected in a circuit. The magnetic field created by the current in each turn is proportional to the current, ϕ as for the magnetic flux in the area of the turn. In addition, the total flux Φ generated around the inductor, due to the current i flowing through it, is $n\phi$. We can then deduce that this total flux is directly proportional to the current flowing and the inductance L in henrys:

$$L \propto n^2$$

increases with the number square of turns. Therefore, equation (2.20) describes the circuit view point of an inductor and the inductance can be calculated for any known ϕ and i.

$$\Phi = Li. \tag{2.20}$$

2. Energy viewpoint: Inductor stores energy in the form of magnetic field. The power developed in the inductor due to the current flowing is:

$$P_L = v_L.i = L\frac{di}{dt}i.$$

If the rate of change of current $\frac{di}{dt}$ flowing through the inductor is positive, it implies that the power is positive and energy is being stored in the inductor. Conversely, if the rate of change of current is decreasing, then the power is negative and it implies that energy is giving out by the inductor.

The energy stored in an inductor $\mathscr{E}_L$ is thus obtained from: $\mathscr{E}_L = \int P_L.dt \quad \Rightarrow$

$$\begin{aligned} \mathscr{E}_L &= \int_0^i L\, idi, \\ &= \frac{1}{2} L i^2. \end{aligned} \tag{2.21}$$

3. Geometry viewpoint: The inductance L of the inductor is affected by the geometry of the material and coil formation. The factors affecting the inductance are shown in Fig. 2.9: a coil of wire wound around a soft iron core whose cross-sectional area determines the area occupied by the coil. These factors are briefly highlighted underneath.

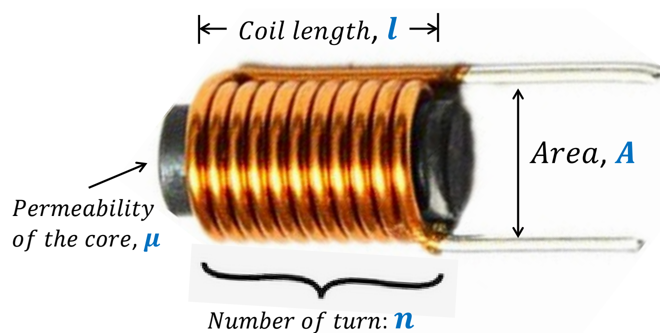

Figure 2.9: Geometry viewpoint of an inductor.

- ***Area of the coil,*** A : This refers to the area formed by the coil wound around the soft iron core. The higher the area of the coil, the lower rate of change of the current flowing through the inductor and vice-versa. It implies that the greater the coil area, the greater the inductance and conversely. Hence: $L \propto A$.
- ***Number of turns,*** n : This refers to the number of windings formed by the coil around the soft iron core. As seen above, the more the number of turns in the coil, the more the inductance and vice-versa, according to $L \propto n^2$.
- ***Length of the coil, l*** : This refers to the elongated length of the coil on the soft iron core. The longer the length of the coil, the less the inductance and the shorter the length of the coil, the greater the inductance. $\Rightarrow \; L \propto \frac{1}{l}$.
- ***Nature of the core material: Permeability*** μ : Using a core material with higher magnetic permeability yields a stronger magnetic field. Hence, the more

magnetic permeability of the core, the more the inductance and the less magnetic permeability of the core, the less the inductance. Soft iron core has a permeability 600 times more than air. It implies that using soft iron core will produce more inductance than with air core. Note that the permeability of free space or vacuum is designated as μ_o and it has a typical value of $4\pi\times 10^{-7} H/m$. It is more convenient to express the permeability of a material μ with respect to that of free space μ_o; and hence we have what is called relative permeability μ_r. It implies that:

$$\mu = \mu_r \mu_o \ .$$

We know that the magnetic induction field **B** is defined as the flux per unit area:

$$\mathbf{B} = \frac{\phi}{A} \ \Rightarrow \ \phi = \mathbf{B}A,$$

and the magnetic field **H** is expressed from Maxwell-Ampere's law, as:

$$H = \frac{n.i}{l} \ ,$$

meanwhile the relationship between flux density **B** and magnetic field **H** is:

$$\mathbf{B} = \mu\mathbf{H} = \mu\frac{n.i}{l} \ .$$

Therefore, the flux ϕ becomes for each turn:

$$\phi = \mathbf{B}A = \mu\frac{n.i.A}{l},$$

while the total flux is $\Phi = n\phi$, thus

$$\begin{aligned} L &= \frac{\Phi}{i}, \\ &= \mu\frac{n^2 A}{l}, \\ &= \mu_r\mu_o\frac{n^2 A}{l}. \end{aligned} \tag{2.22}$$

In addition to storage of energy, inductor is used extensively in numerous applications, such as: transformers, induction motors, relays, radio tuning, television, filters, transmission systems, sensors and many other applications in conjunction with capacitors and resistors.

2.4/ MEMRISTOR

Memristor, the fourth basic circuit element [10] (alongside resistor, capacitor and inductor), is a nonlinear passive two-terminals electronic component defined by the relationship between the magnetic flux linkage ϕ and the electric charge q. The name memristor is the contraction of memory resistor owing to its peculiar nature to resist the flow of electric current (as done by a resistor) and at the same time to remember the last amount of charge passed through it at the time when the power has been disconnected, hence to give the memory of the previous device resistance. Memristor keeps track of its dynamic resistance with respect to the current or electric charge flowing through it.

Memristor symbol

The unmarked side (the plus sign terminal) and the marked side (the minus sign terminal) indicate, respectively, the higher and lower potential terminal [22]. This is an important point which will be considered later: is the memristor a symmetrical or non symmetrical 2-ports element?

The definition of a *memristor* is given by its pioneer [23], as: "***any 2-terminals device, exhibiting a pinched hysteresis loop which always passes through the origin in the voltage-current plane when driven by any periodic input current source, or voltage source, with zero DC component. If the input is a current source, it is called a current-controlled memristor. If it is a voltage source, it is called a voltage-controlled memristor.***"

Recall that the magnetic flux ϕ represents the time-integral of voltage $v(t)$ and the electric charge q is the time-integral of electric current $i(t)$, hence these quantities are to be determined between two reference points. The fact that memristor is always defined by the integral of its input and output quantities ($v(t)$ and or $i(t)$), explains in essence why memristor remembers its previous resistance or has a memory effect. The constitutive relationship of a Memristor is given by $f(\phi, q) = 0$, such that:

$$\mathrm{d}\phi = M\ \mathrm{d}q, \tag{2.23}$$

where: M is the memristance that is a short form for memory resistance. Memristance is the property of a memristor to remember its previous resistance state and it is defined by the functional relationship between magnetic flux ϕ and electric charge q. The instantaneous memristance can be deduced from the dynamic slope of the ϕ-q locus given in the ϕ-q plane as shown in Fig. 2.11. Memristance is measured in Ohms (Ω), the same measurement unit as resistance. The relationship between the magnetic flux ϕ and the

electric charge q could be:

$$\phi = f_M(q),$$

for a charge-controlled memristor (i.e memristor device excited by a current source) or

$$q = f_G(\phi),$$

for a flux-controlled memristor (i.e memristor device excited by a voltage source), where f_M and f_G are nonlinear functions denoting memristance and memductance respectively.

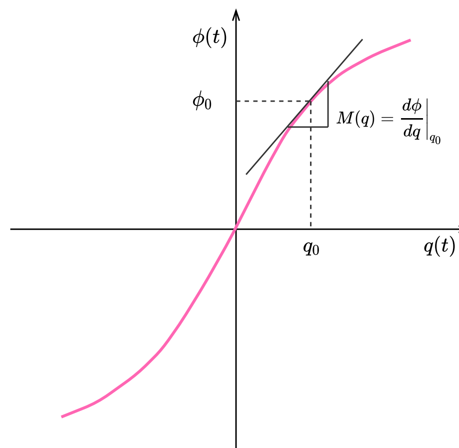

Figure 2.11: Memristance expression from a ϕ-q curve. Remark that, due to integration constants, this curve can be shifted horizontally and/or vertically.

In the introduction, we gave a memristor analogy to water flowing through a pipe whose diameter is changing with respect to water flowing characteristics, Fig. 1.1. The resistance of the memristor (or memristance) changes dynamically with the amount and direction of current flowing through it. People often confuse memristance with resistance. However, memristor differs from resistor in the sense that:

- It has entirely different constitutive relationship in comparison to resistor.
- Its resistance changes according to the quantity of charges having passed through it previously.
- Its resistance changes according to the direction of electric current flowing through it because it is not a bilateral device. Therefore, its connection mode matters.
- It preserves the previous history of electricity, according to the charge passed through it before, at any given time. In other words, it has memory of the previous electricity passed through it (memory effect).
- It is nonlinear in nature.
- It has pinched hysteresis loop in the voltage-current response in a circuit, depending

on its initial condition. Moreover, memristor has different circuit response according to its initial condition.

- It cannot be realized by any combination of the three known circuit elements (capacitor, resistor and inductor) and hence it can be considered as "fundamental".
- It has a uniqueness nature for the relationship between magnetic flux and electric charge (which is not directly available by measures).
- It behaves differently in DC and AC conditions.

Nevertheless, memristor and resistor have some similarities, for example:

- Both offer resistance to the flow of electric current.
- Their quantities (i.e memristance and resistance) have the same unit of measurement, i.e. Ohms, symbol: Ω.
- No phase shift in their voltage and current wave-forms, because $v(t) = M(q)i(t) \Rightarrow i(t) = 0$ if $v(t) = 0$ and vice-versa.
- They both dissipate energy as heat (Joule effect). They are not loss-less devices i.e. without preservation of energy. They are always associated to power (P) intake, i.e. $P \geq 0$.

2.4.1/ Memristive device and system

A broader class of nonlinear systems is reported [11], called memristive systems in which some nonlinear dynamic systems were found to exhibit memristive behaviour. Additionally, systems whose resistance depends on its internal state (e.g temperature) are believed to be memristive. Examples of these systems are: *Thermistor*, *Discharge tube*, *Hodgkin-Huxley (or Ionic) System* and *Tungsten filament lamps*. The memristive systems are generally described by one-port and state equations:

$$\begin{cases} y = f(x, u, t)u, \\ \dfrac{dx}{dt} = g(x, u, t), \end{cases} \tag{2.24}$$

where u is the input to the system, y is the output of the system, x is a vector denoting the set of internal state variables of the system, f is a nonlinear vector function and g is a nonlinear scalar function. Equation (2.24) affirms that memristive systems are nonlinear systems because the function f depends nonlinearly on the dynamic state variable x and both functions (f,g) depend on the input u to the system. Notice that (2.24) describes a

time-variant system, so all the variables are functions of time as well. For time-invariant memristive systems, eq. (2.24) is rewritten as follows:

$$\begin{cases} y = f(x,u)u, \\ \dfrac{dx}{dt} = g(x,u). \end{cases} \tag{2.25}$$

Moreover, an ideal memristor is considered as a special case of memristive system which can be expressed as:

$$\begin{cases} y = f(x)u, \\ \dfrac{dx}{dt} = g(u), \end{cases} \tag{2.26}$$

where the state variable x depends solely on the time-integral of the voltage applied across the device or the time-integral of the current flowing through it, for a flux-controlled and charge-controlled memristor respectively.

2.4.2/ VERIFYING A MEMRISTOR DEVICE

In Fig. 2.12, a two-terminals device under test $(D.U.T)$ is subjected to a periodic input source s(t): s(t) could be voltage or current source as highlighted in the aforementioned definition of memristor. If the current-voltage response of Fig. 2.12 on the left corresponds to that of Fig. 2.12 on the right, for any s(t) source respecting the definition in [23], then the black box is called a *memristor*. More details to check if a candidate system is indeed a memristive system is given in section 2.4.3.

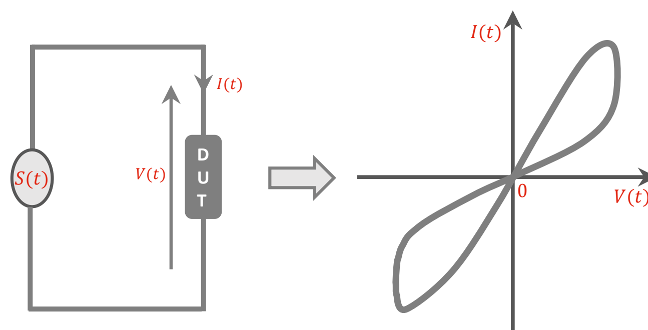

Figure 2.12: Testing memristor device as a black box (left) and current-voltage response of the black box (right).

2.4.3/ FINGERPRINTS OF A MEMRISTOR

Circuit elements such as resistor, capacitor, inductor etc..., are often characterized by their voltage-current response (V-I characteristics) in any given circuit. Memristor is not an exception, it has a peculiar voltage-current response which is a unique identifier that

distinguishes it from any other known circuit element. Hence, it is called fingerprint of a memristor and it is used to characterize a memristive system.

The most three known memristor fingerprints are enumerated in [24–26], as:

1. The V-I response of a memristor (with positive memristance) is always a pinched hysteresis loop (Lissajous figure) when subjected to a bipolar periodic input signal without offset.

2. The hysteresis lobe area decreases monotonically when the excitation frequency increases.

3. For a fixed input amplitude, the pinched hysteresis loop shrinks to a single-valued function as the frequency of the input supply tends to infinity.

More fingerprints of an ideal memristor are given in [25], including constitutive relationship (CR) between flux and charge and parameter versus state map (PSM) [27]. In fact, nine fingerprints of memristor are given in [25] including the three above mentioned and they give birth also to a valid test to assess a memristor device. However, we give here only the description of the three aforementioned signatures of a memristor.

2.4.3.1/ First fingerprint

The voltage-current response of a memristor in a circuit is always a pinched hysteresis loop [26,28]. As seen in Fig. 2.13a, the maxima and minima of the current $i(t)$ and voltage $v(t)$, through and across the memristor respectively, are not reached simultaneously and this is the cause of the formation of the hysteresis lobe area. The term "pinched hysteresis loop (or PHL)" [27] *refers to a double-valued Lissajous figure in the V-I plane that is always pinched at the origin for any given time, for any input amplitude (voltage or current), for any initial condition and for any input frequency*.

The term *pinched* also signifies that $v(t) = 0$ whenever $i(t) = 0$ and vice-versa. In other words, for any given value of current $i(t)$, there will be two corresponding values of voltage $v(t)$ except at $i(t) = 0$. The converse is also true, for any given value of voltage $v(t)$, there will be two corresponding values of current $i(t)$ except at $v(t) = 0$. This can be observed from Fig. 2.13a: it shows that current ($i(t)$ in gold) is zero whenever the voltage ($v(t)$ in black) is zero and as a result the hysteresis loop always passes through the origin, see Fig. 2.13b.

It turned out that memristive systems exhibit two different kinds of *PHL* [24,25] depending upon the system's constituents (i.e f and g as defined in eq. (2.24)) and the type of excitation (odd-type or even-type) [25]. The two types of PHL are: Self-crossing PHL

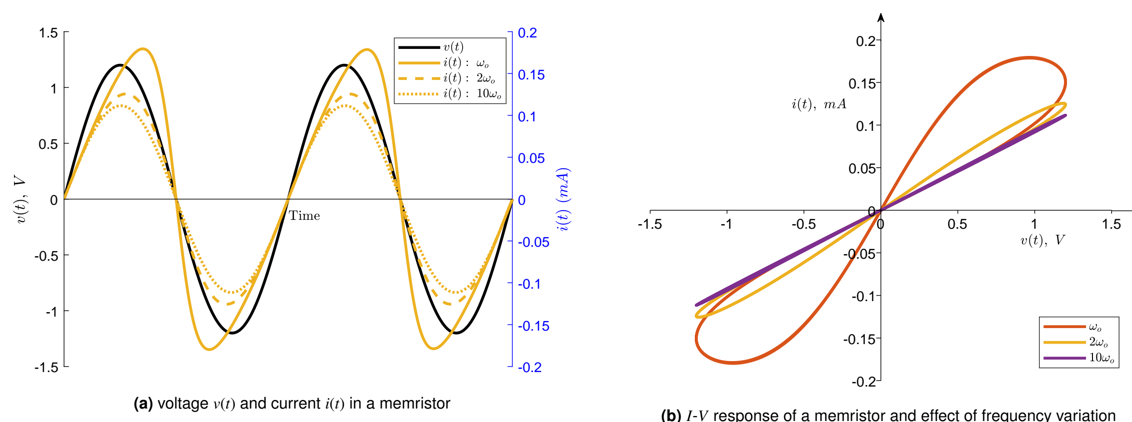

(a) voltage $v(t)$ and current $i(t)$ in a memristor

(b) I-V response of a memristor and effect of frequency variation

Figure 2.13: Demonstration of a memristor fingerprint for $R_{on} = 100\Omega$, $R_{off} = 16K\Omega$, $f_o = 1Hz$, $\omega_o = 2\pi f_o$ and $v(t) = 1.2sin(\omega t)$: $\omega = \omega_o$, $\omega = 2\omega_o$ and $\omega = 10\omega_o$.

(also known as Transversal or crossing PHL) and Tangential PHL (also known as non-tranversal or non-crossing PHL).

i. **Self-crossing or transversal pinched hysteresis loop (SPHL):** In this type of PHL, the locus cuts across at the origin (or pinched point). Additionally, one can see that the slope of the locus moving toward the origin is different from that of the locus leaving the origin. Figure 2.14a shows a typical transversal PHL.
An example of memristive system with transversal pinched hysteresis loop is the mathematical model of HP memristor (presented in section 3.1):

$$\begin{cases} v(t) = M(x)\, i(t), \\ M(x) = R_{off}(1-x) + R_{on}x \ , \\ \dfrac{dx}{dt} = k\ i(t)\ . \end{cases} \tag{2.27}$$

ii. **Tangential or non-transversal pinched hysteresis loop (TPHL):** As the name implies, the locus doesn't cut across, rather it passes tangentially as confirmed by the arrow directions, see Fig. 2.14b. Notice that it is still pinched at the origin i.e $v(t) = 0$ whenever $i(t) = 0$ and vice versa, however, there is always a fixed slope (for both the two slopes, i.e R_{off} and R_{on}) when the locus moves toward the origin and immediately after leaving the origin. This observation is obvious because the separate line slopes coincide together before reaching the origin and remain together even after leaving the origin until a certain amount of voltage or current is reached, then the loci separate and hence the hysteresis lobe area becomes visible, see Fig. 2.14b.

There are many memristive systems whose current-voltage response is a tangential PHL, some of these systems being mentioned in [11,24,29] and we highlight some

of them briefly in the following. Moreover, tangential PHL is met in the memristive behaviour of plants (Aloe vera and Mimosa pudica) [30].

(a) Thermistor: The current-voltage response of a voltage-controlled thermistor, whose mathematical model is given in (2.28), is also an example of a memristor with a tangential pinched hysteresis loop.

$$\begin{cases} i = G(T)v, \\ G(T) = \left(R_0 e^{\beta\left(\frac{1}{T}-\frac{1}{T_0}\right)}\right)^{-1}, \\ \frac{dT}{dt} = \frac{\delta}{C}(T_0 - T) + \frac{G_0}{C}v^2, \end{cases} \tag{2.28}$$

where i is the output current, v is the input voltage, G is the memductance, T is the absolute temperature, β is the material specific constant, C is the heat capacity, δ is the dissipation constant, R_0 is the base resistance of thermistor and T_0 is its base temperature.

(b) Tungsten filament lamp: It was shown experimentally [29] that the current-voltage response of a tungsten filament lamp exhibits a tangential pinched hysteresis loop. Its mathematical model is given in (2.29).

$$\begin{cases} i(t) = G(T)\ v(t), \\ G(T) = \frac{A}{\rho(T)L}, \\ \frac{dT}{dt} = \frac{1}{c(T)L^2}\left(\frac{v^2(t)}{\rho(T)} - e\sigma\left(4\pi\frac{R_0}{\rho_0}\right)^{\frac{1}{2}} L^{\frac{3}{2}}T^4\right), \end{cases} \tag{2.29}$$

where $i(t)$ is the output current, $v(t)$ is the input voltage, G is the memductance, T is the absolute temperature, A is the cross-sectional area of the filament, $\rho(T)$ is the resistivity of tungsten, L is the length of the filament, $c(T)$ is the volumetric specific heat capacity, e is emissivity and σ is Boltzmann constant, while R_0 and ρ_0 are the values of the resistance and the resistivity at room temperature T_0.

(c) Discharge tube: A charge-controlled discharge tube is an example of memristor with a tangential or non-crossing pinched hysteresis loop. It is described by the mathematical model, as:

$$\begin{cases} v = M(x)i, \\ M(x) = \frac{F}{x}, \\ \frac{dx}{dt} = -\beta x + \alpha M i^2, \end{cases} \tag{2.30}$$

where M is the memristance, x refers to the internal state vector, i is the harmonic input current, v is the harmonic output current while α, β and F are constants fixed by the size of the tube and its inner gas.

(d) Compact fluorescent lamp:

$$\begin{cases} v = M(T)i, \\ M(T) = a_5 T^{-\frac{3}{4}} \, e^{\left(\frac{ea_6}{2kT}\right)}, \\ \frac{dT}{dt} = a_1 \left[M(T)i^2 - a_4(T - T_0) - a_2 \, e^{\left(-\frac{ea_3}{kT}\right)} \right], \end{cases} \quad (2.31)$$

where e is the magnitude of the electron charge, k is the Boltzmann's constant, T is the temperature, a_1-a_6 are the lamp dependent coefficients.

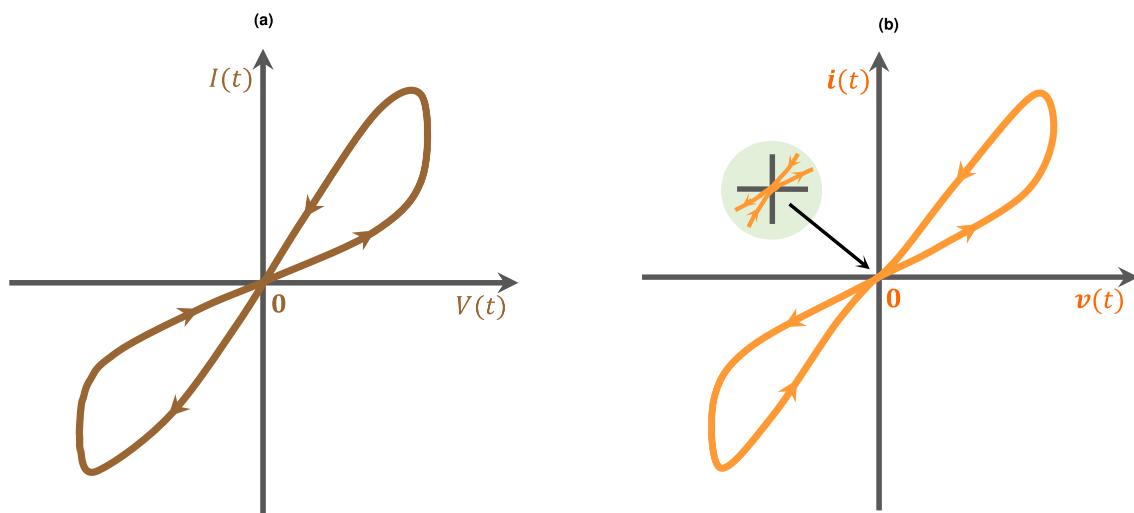

Figure 2.14: (a) Self-crossing or transversal pinched hysteresis loop (PHL) and (b) Tangential or non-transversal pinched hysteresis loop (PHL).

However, it is reported that the pinched hysteresis loop of ideal memristors, memcapacitors and meminductors is always self-crossing PHL [31]. It is even emphasized that self-crossing PHL is another signature or fingerprint of an ideal memristor. Moreover, TiO_2 memristor (from HP lab [12]) and SDC memristor (from KNOWM [32]) are examples memristors with self-crossing PHL. We can then focuse from now on specifically on this type of hysteresis loop. Note that memcapacitor and meminductor will be briefly discussed in section 2.4.8.

2.4.3.2/ Second fingerprint

The hysteresis lobe area decreases when the input frequency increases. Recall that the memristor is a nano device, therefore small input signal is enough to generate a big

electric field to trigger the device according to:

$$E = -\frac{dV}{dx},$$

when x, the internal state corresponds to the displacement of charge carriers. Therefore, any small increment in the potential difference V will lead to a large magnitude of electric field **E** to be generated. However, the resistance of the memristor depends on its internal state, hence any change in the input signal results in a behavioural change of its internal state as well. Therefore, for example considering an input current $i(t)$ such that:

$$i(t) = I_0 sin(\omega t), \tag{2.32}$$

the flowing charge will be:

$$\begin{aligned} q(t) &= \int_{-\infty}^{t} I_0 sin(\omega\tau)d\tau, \\ &= Q\,[1 - cos(\omega t)] + q_0 \,, \end{aligned} \tag{2.33}$$

where $q_0 = \int_{-\infty}^{0} I_0 sin(\omega\tau)d\tau$ is the initial charge just before the current starts to flow and $Q = \frac{I_0}{\omega}$ is the charge delivered by the current source during the first quarter of the period $T = \frac{2\pi}{\omega}$. Let us use a shifted charge $q' = q - q_0$, then:

$$q' = Q\,[1 - cos(\omega t)]\,. \tag{2.34}$$

Therefore, the magnitude peak to peak of the flowed charge is given by:

$$\frac{2I_0}{\omega} = 2Q. \tag{2.35}$$

For ideal charged-controlled memristor, its state variable is rather the charge flowing through the device. It is obvious from (2.35) that increasing the frequency ω for a fixed amplitude I_0, leads $q(t)$ peak to peak amplitude to decrease significantly and hence causes the shrinkage of the pinched hysteresis loop towards a linear graph.

Figure 2.15a shows the effect of increasing input frequency on the PHL lobe area of the memristor. The input frequency ω is considered in three steps ω_1, ω_2 and ω_3 with the corresponding lobe areas A_1, A_2 and A_3 respectively, such that:

$$\omega_1 < \omega_2 < \omega_3$$

and

$$A_1(\omega_1) > A_2(\omega_2) > A_3(\omega_3)$$

It follows that: as $\omega \to \infty$, $A \to 0$, this behaviour is shown in Fig. 2.15b.

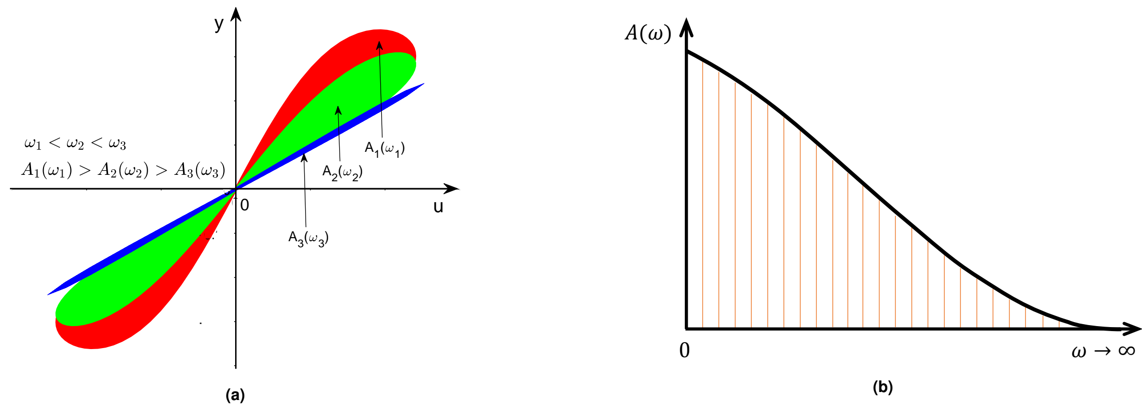

Figure 2.15: Effect of increasing frequency on the PHL lobe area. (a) Hysteresis lobe area shrinkage due to the increase in the input frequency and (b) PHL lobe area versus frequency.

CALCULATING THE LOBE AREA OF A PHL:

Let us consider a memristor excited by a current source given by (2.32) with $\omega = \frac{2\pi}{T}$, T being the period. By considering a half cycle (i.e $\frac{T}{2}$) of the input $i(t)$, we get the hysteresis loop given in Fig. 2.16, having enclosed area A and surface boundary S, altogether enclosed in a triangle OCD [33–35].

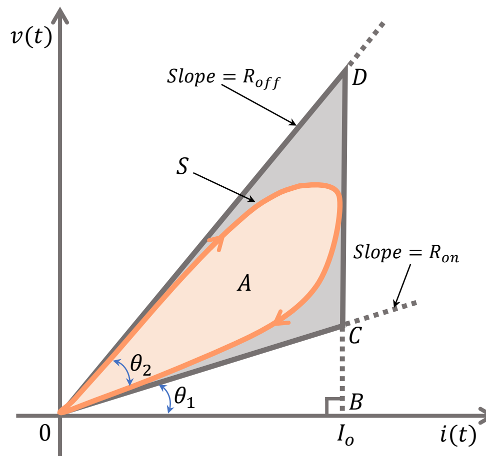

Figure 2.16: Calculating the area of PHL.

The area A is obtained from the surface integral of the voltage with respect to the current, as:

$$A = \oint_S v\,di. \tag{2.36}$$

Figure 2.17 shows the operating point of a memristor in the plane (q,ϕ) starting with an initial charge q_0, corresponding to an initial flux ϕ_0, with the so-called shifted flux $\phi' = \phi - \phi_0$. From (2.34) and (2.35), the operating point is within the interval $[q_0, q_0+2Q]$, hence the normalized form of the constitutive relationship becomes:

$$\hat{f}(\phi', q') = 0. \tag{2.37}$$

The corresponding normalized expression of the memristance-versus-state map, becomes:

$$M'(q') = M(q' + q_0) = \frac{d\phi'(q')}{dq'}.$$

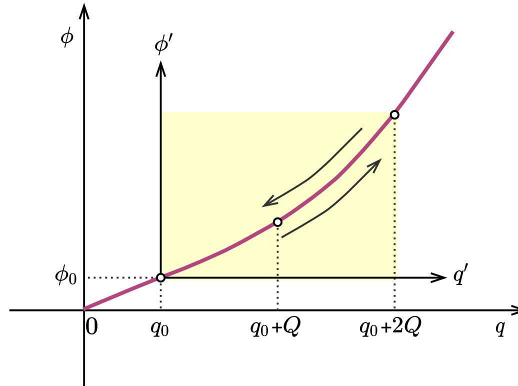

Figure 2.17: Memristor operating point from the constitutive relationship.

From equations (2.32)-(2.33), we get an algebraic relation between the charge q' and the current source $i(t)$:

$$i^2 = \omega^2(2Q - q')q'. \tag{2.38}$$

From (2.36), with $v(t) = M'(q'(t))i(t)$, the area during the first half cycle can be expressed as:

$$A = \frac{1}{2}\int_0^{\frac{T}{2}} M'(q'(t))\frac{d(i^2)}{dt}dt.$$

The integration by parts gives:

$$A = \frac{1}{2}\left[M'(q'(t))i^2(t)\right]_0^{\frac{T}{2}} - \frac{1}{2}\int_0^{\frac{T}{2}} \dot{M}'(q'(t))i^2(t)\, dt, \tag{2.39}$$

where the dot in M' represents the derivative with respect to time. In [33], the authors consider that the memristance function $M'(q')$ can exhibit step discontinuity points q'_j in the charge interval $[0, 2Q]$, with $j = 1, 2, ..., n$, hence, they considered some step changes of the memristance at point q'_j. However, we will exclude in the following the case of any discontinuities for $M'(q')$. In this simplified case, the first term of equation (2.39) is zero. Noting that $\frac{dM'}{dt} = \frac{dM'}{dq'}.\frac{dq'}{dt} = \frac{dM'}{dq'}.i(t)$, equation (2.39) gives then:

$$A = -\frac{1}{2}\left(\int_0^{\frac{T}{2}} \left.\frac{dM'}{dq'}\right|_{q'\neq q'_j} i^3 dt\right). \tag{2.40}$$

For example, the pinched hysteresis lobe area of the memristance expression given by

(2.27) is described in the following. The given memristance function is rewritten as:

$$M'(q') = R_i - \delta R \frac{q'}{q_d}, \tag{2.41}$$

where $\delta R = R_{off} - R_{on}$, $R_i = R_{off} - \delta R \frac{q_0}{q_d}$ is the initial memristance at time $t = 0$ and q_d is the charge necessary for the modification of the memristance by the value δR [33]. Since R_i is constant, then $\frac{dM'}{dq'} = -\frac{\delta R}{q_d}$. Using the current source (2.32), we get:

$$A = \frac{1}{2} \frac{\delta R}{q_d} I_0^3 \int_0^{\frac{T}{2}} sin^3(\omega t) dt.$$

Using the identity: $sin^3(\alpha) = \frac{3}{4} sin(\alpha) - \frac{1}{4} sin(3\alpha)$, then $\int_0^{\frac{T}{2}} sin^3(\omega t) dt = \frac{4}{3\omega}$ and the area is finally expressed as:

$$A = \frac{2}{3} \frac{\delta R}{\omega} \frac{I_o^3}{q_d}. \tag{2.42}$$

The area is independent of the initial memristance, however, it is directly proportional to the cubic power of the exciting current and inversely proportional to the input frequency.

Note that eq. (2.42) is determined according to the mathematical model of HP memristor, thus q_d is the charge required to move the tunneling dopant barrier between doped and undoped region from $x \to 0$ toward $x \to 1$ (see section 3.1 for more details).

Moreover, a generalized formulation for computating the hysteresis lobe area of *mem-elements* is reported in [34], taking into account whether the input is a voltage or current. Thus, for a mem-element having input $u(t)$, output $y(t)$, state variable $x(t)$ and a differentiable function $h(x)$, this mem-element can be characterized by:

$$\begin{cases} y(t) = h(x)u(t), \\ \frac{dx(t)}{dt} = u(t), \end{cases} \tag{2.43}$$

where:

$$u(t) = U_{max} sin(\omega t).$$

Thus, the loop area during the first half cycle is given by:

$$A = -\frac{1}{2} \int_0^{\frac{T}{2}} \frac{dh(x)}{dx} u^3 dt. \tag{2.44}$$

2.4.3.3/ THIRD FINGERPRINT

For a fixed input amplitude, the pinched hysteresis loop (PHL) shrinks to a single-valued function as the frequency of the input supply tends to infinity. In this case, the PHL is called the *Degenerating PHL*, i.e when the locus of both slope lines (R_{on} and R_{off}) merge to a single-valued function or in other words, the PHL has disappeared, thus resembling an ordinary resistor. From Fig. 2.16, the angle θ_2 formed by the lines $\overline{OC}$ and $\overline{OD}$ at the origin O, is a function of the input frequency. θ_2 diminishes to 0 as the input frequency increases toward infinity, thereby consequently causes the lines $\overline{OC}$ and $\overline{OD}$ to become the same. See also (2.42), with $\omega \to \infty$, the area $A \to 0$. This explains also easily this third fingerprint. Thus, at high input frequency memristor behaves like a normal resistor and as such it has nothing special.

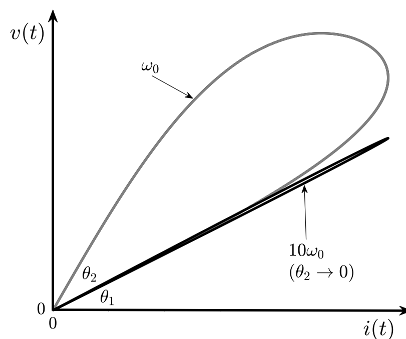

Figure 2.18: Third fingerprint illustration for tenfold increase in frequency: $\omega = 10\omega_o$, $\theta_2 \approx 0$.

2.4.4/ NOT EVERY NONLINEAR DYNAMICAL SYSTEM IS AN IDEAL MEMRISTOR

Memristive systems are a class of nonlinear dynamical systems whose current voltage response resembles the fingerprint of an ideal memristor. However, it is known that not every nonlinear dynamical system is ideally a memristor, even though it exhibits a pinched hysteresis loop in its current-voltage characteristic. Hence, the above outlined criteria of memristor identification are not enough to distinguish a memristor device from some nonlinear dynamical systems which are not memristors. As we have shown earlier, the pinched hysteresis loop is the major criterion used to authenticate a given system as memristor or not [24]. In fact, it states that some memory elements may not exhibit pinched hysterisis loop, and an example of memcapacitor is even given [36]. There are concerns in the scientific community of what a memristor is and what is not [16–19, 28, 37–41].

Leon Chua generalized the concept of memristor to include all resistance switching memories [27], however it is shown experimentally that resistance switching memories are not memristors [37]. Blaise Mouttet reported that L. Chua contradicted himself in [27], against

his axiomatic definition of a memristor in 1971 [10]. He further concluded that the HP's memristor lacks a scientific merit [17].

It is further clarified that the pinched hysteresis loop as the fingerprint of a memristor, or a memristive device, must hold for all amplitudes, for all frequencies, and for all initial conditions, of any periodic testing waveform, such as sinusoidal or triangular signals, which assumes both positive and negative values over each period of the waveform [28]. However, still some dynamical systems fulfilling these conditions are yet not memristor [38, 39]. Notwithstanding, a simple testing technique to identify an ideal memristor is reported in [41], which could, together with the concept of pinched hysteresis loop, help to identify a memristor from a non-memristor. However, there is no memristor reported in the literature, adhering to the axiomatic definition that relates charge and flux. Therefore we may conclude that all the reported memristors are resistive switching devices and they are special class of memristive systems, hence not an ideal memristor. The fact that an ideal memristor is not yet found and or simply does not exist, does not discredit the hitherto findings about memristors, as they are still valuable in ReRAM and many other applications, and justify all efforts to better understand this new element.

An ideal memristor is described axiomatically by the constitutive relationship between the charge and the flux, but there is not a memristor discovery based on this principle. Contemporarily, all the memristor technologies are based on bipolar resistance switching mechanisms. This is the main reason used by some scientists to critic memristor discovery. In fact, whenever someone thinks about the existence of an ideal memristor, the possible conclusion is that such a device is likely to be impossible [42]. Optimistically, we do think that one-day such a device will be found. But for the moment, all the memristors are resistance switching devices with potential applications. And because they possess signatures of an ideal memristor, they can be categorised as a special class of memristor.

2.4.5/ Memristor by mode of excitation

Depending on the type of excitation, memristor can be characterized as charge-controlled memristor (CCM) or flux-controlled memristor (FCM), see Fig. 2.19.

2.4.5.1/ Charge–Controlled memristor (CCM)

For charge-controlled memristor, the input applied to the memristor is a current source. The set-up is given in Fig. 2.19a, whereby a current source $i(t)$ is connected to a memristor M. Thus, the current flowing through the memristor will cause a voltage drop $v_m(t)$ across it. From (2.24), the three variables u, x and y become i, q and v respectively, q being the time domain integral of the input current i and v the output voltage of the

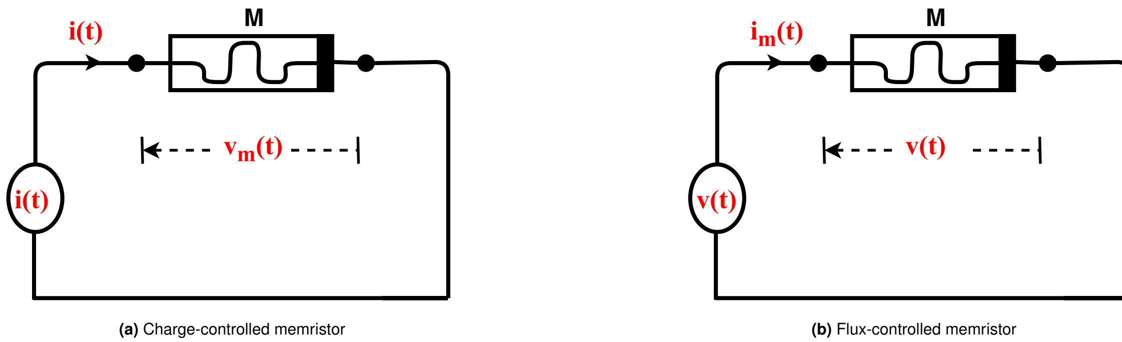

(a) Charge-controlled memristor

(b) Flux-controlled memristor

Figure 2.19: Memristor subjected to current and voltage excitation respectively

memristor. Hence, the constitutive relation of charge-controlled memristor should always represent the flux (ϕ) dependence on the charge (q), as:

$$\phi = \hat{\phi}(q). \tag{2.45}$$

Substituting the variables i, q and v into eq. (2.26), we get:

$$\begin{cases} v = M(q)i, \\ \dfrac{dq}{dt} = i. \end{cases} \tag{2.46}$$

N.B: The notation $\hat{\phi}$ in eq. (2.45) stands for a function definition: it could be any letter, for example f, such that: $\phi = f(q)$, so the ($\hat{}$) will often be removed in the following. Also notice that equations (2.45) and (2.46) are identical, with $M(q)$ a charge-controlled memristance whose expression can be obtained by differentiating both sides of equation (2.45) with respect to t. Thus:

$$\frac{d\phi}{dt} = \frac{d}{dt}\left(\hat{\phi}(q)\right).$$

As the right hand side is a composite function, then by applying chain rule, we get:

$$\frac{d\phi}{dt} = \frac{d\phi(q)}{dq} \times \frac{dq}{dt} \Rightarrow \frac{d\phi}{dt} = M(q)\,\frac{dq}{dt} = M(q)i. \tag{2.47}$$

Therefore, $M(q) = \dfrac{d\phi(q)}{dq} = \dfrac{d\phi}{dq}$. This equation can be rewritten conveniently as:

$$\mathrm{d}\phi = M(q)\,\mathrm{d}q. \tag{2.48}$$

Moreover, (2.47) also gives the voltage drop $v_m(t)$ (see Fig. 2.19a) across the charge-controlled memristor $M(q)$:

$\frac{\mathrm{d}\phi}{\mathrm{d}t} = M(q)\,\frac{\mathrm{d}q}{\mathrm{d}t}$, such that:

$$v_m(t) = M(q)\ i(t), \tag{2.49}$$

Example 1: Suppose a charge-controlled memristor characterized by the cubic function as follows:

$$\phi(t) = \beta q(t) + \frac{\alpha}{3}\ q(t)^3 \tag{2.50}$$

where α and β are in $Wb.C^{-3}$ and $Wb.C^{-1}$ respectively, (Wb and C mean Weber and Coulomb respectively). Equation (2.50) is a modified version of the one used by Chua [27], by adding parametric coefficients α and β in order for the equation to be homogeneous. It implies that:

$$M(q) = \frac{d\phi}{dq} = \beta + \alpha\ q(t)^2 \tag{2.51}$$

Let the input current $i(t)$ be:

$$i(t) = I_o sin(\omega t),$$

then the charge is computed as follows:

$$\begin{aligned} q(t) &= \int_{-\infty}^{t} i(\tau)d\tau \\ &= q_0 + \int_{0}^{t} i(\tau)d\tau \\ &= q_0 + \frac{I_o}{\omega}\left(1 - cos(\omega t)\right). \end{aligned} \tag{2.52}$$

Knowing q_0 and $q(t)$, then $M(q)$ and $v_m(t)$ can be calculated from equations (2.51) and (2.49) respectively. Hence, q_0 is the memristor initial charge that determines its previous state. Figure 2.20 shows some examples for $I_o = 1A$, $f = 4Hz$, $\alpha = 1Wb.C^{-3}$, $\beta = 1mWb.C^{-1}$ and two different values of q_0 as $0C$ and $0.05C$, respectively shown by Figs. 2.20a and b.

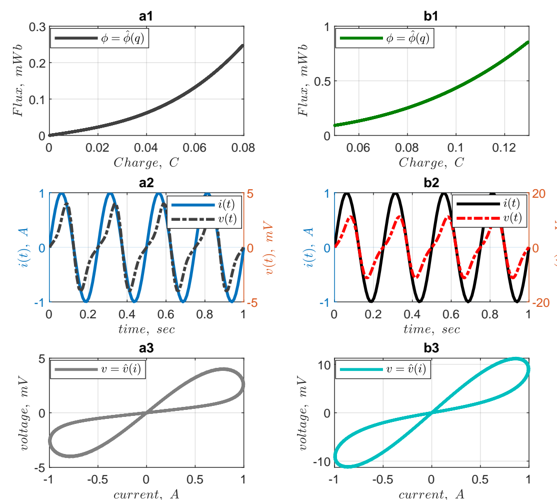

Figure 2.20: Results of Example 1: $I_o = 1A$, $f = 4Hz$, $\alpha = 1Wb.C^{-3}$, $\beta = 1mWb.C^{-1}$, (**a**)$q_0 = 0C$ and (**b**) $q_0 = 0.05C$.

It is expected that taking different values for q_0, the operating point in Fig. 2.20a1 will be changed, so will be the hysteresis curve of Fig. 2.20a3, compare Figs. 2.20**a** and **b**.

2.4.5.2/ FLUX–CONTROLLED MEMRISTOR (FCM)

Memristor is flux-controlled if the input applied to the memristor is a voltage source (see Fig. (2.19b). The applied voltage $v(t)$ causes current $i_m(t)$ to flow through the memristor M. One can see that the triad variables u, x and y in (2.26) become v, ϕ and i respectively. Hence the output of a flux-controlled memristor is current and its constitutive relationship represents the charge dependence on flux. The constitutive relationship of the memristor of this type is given in (2.53).
The state variable is controlled by the flux as the result of time-domain integral of the applied input voltage.

$$q = \hat{q}(\phi). \tag{2.53}$$

Similarly, substituting the variables v, ϕ and i into (2.24), we get:

$$\begin{cases} i = Y(\phi)\, v, \\ \dfrac{d\phi}{dt} = v, \end{cases} \tag{2.54}$$

where $Y(\phi)$ is the flux-controlled memductance, measured in Siemens S, the same S.I unit as conductance. Note that $Y(\phi)$ is the inverse of $M(q)$. Thus, ϕ is the time domain integral of v:

$$\begin{aligned} \phi &= \int_{-\infty}^{t} v(\tau)\, d\tau, \\ &= \phi_0 + \int_{0}^{t} v(\tau)\, d\tau. \end{aligned}$$

Similarly, we can deduce an expression of $Y(\phi)$ by differentiating both sides of eq. (2.53) with respect to time.

$\therefore \dfrac{dq}{dt} = \dfrac{d}{dt}(q(\phi))$ and by applying chain rule differentiation method:

$$\frac{dq}{dt} = \frac{dq(\phi)}{d\phi} \times \frac{d\phi}{dt} \quad \Rightarrow \quad \frac{dq}{dt} = Y(\phi)\,\frac{d\phi}{dt}. \tag{2.55}$$

With $Y(\phi) = \dfrac{dq(\phi)}{d\phi} = \dfrac{dq}{d\phi} \quad \Rightarrow$

$$dq = Y(\phi)\, d\phi. \tag{2.56}$$

The current through the memristor $i_m(t)$ can be expressed from eq. (2.55), and is finally given by:

$$i_m(t) = Y(\phi)\ v(t). \tag{2.57}$$

EXAMPLE 2:

Suppose a flux-controlled memristor described by:

$$q = \frac{\psi_1}{3}\phi^3 + \psi_2\phi, \tag{2.58}$$

ψ_1 and ψ_2 are appropriate constants in $C.Wb^{-3}$ and $C.Wb^{-1}$ respectively. Given a source voltage:

$$v(t) = V_0 sin(\omega t),$$

the equivalent expression of the flux is obtained to be:

$$\phi = \frac{V_0}{\omega}(1 - cos(\omega t)) + \phi_0.$$

Using (2.56), then:

$$Y(\phi) = \psi_1\phi^2 + \psi_2. \tag{2.59}$$

Hence, knowing $Y(\phi)$, then $i(t)$ is calculated and some examples are given in Fig. 2.21**a** and **b** respectively for $\phi_0 = 0Wb$ and $\phi_0 = 0.08Wb$. Similar to Fig. 2.20, here also the initial conditions affect the ϕ-q operating point and hence the I-V curve.

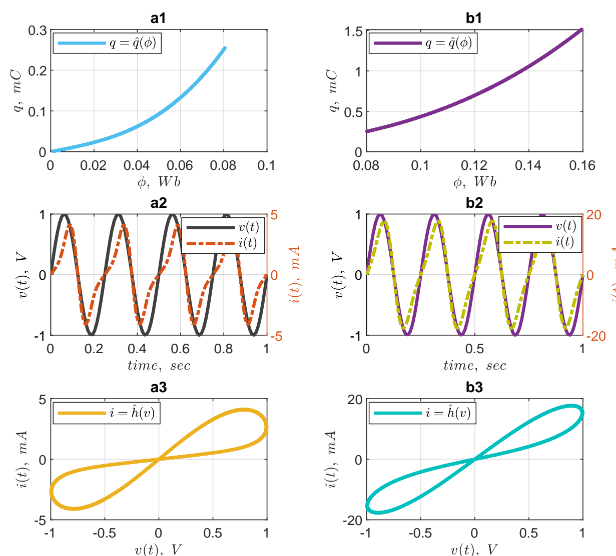

Figure 2.21: Result obtained for example 2: $V_0 = 1V, f = 4Hz$, $\psi_1 = 1\ C.Wb^{-3}$, $\psi_2 = 1m\ C.Wb^{-1}$, (**a**) $\phi_0 = 0Wb$ and (**b**) $\phi_0 = 0.08Wb$.

2.4.6/ *Why memristor?*

During my presentation in the event ***Doctoral day 2019*** *on March 2019 at Le Creusot, France*, organized by ***ImViA*** laboratory, someone asked me a question "*why is the need for the memristor?*" He seemed comfortable about electronics, but not knowing about memristor. As shown earlier, memristor is the fourth fundamental passive circuit element having interesting features in electrical and electronics systems design. The following are some features associated to a memristor:

- It stores information, hence reliable for memory applications.
- It undergoes nano-scalability, hence suitable for the modern-day nano-technology.
- Conductance modulation resembling chemical synapse.
- It has connection flexibility, that is, series-parallel connections, and it can form stack of memory cells for high density storage applications.
- It is a nonlinear circuit element, by its nature.
- It has low power consumption. As nano device, it requires little power to operate.
- One memristor can replace multiple transistors in a circuit, thus it will ensure better performances and most reliable systems.
- These features, among many others, suggest memristor to be the promising element for designing very effective neuromorphic systems and memory applications [43–47].

2.4.7/ SOME POTENTIAL APPLICATIONS OF MEMRISTOR

The aforementioned features suggest memristor to be a proper candidate in the modern-day electronics industries. Since the discovery of HP memristor, the number of published memristive based applications increase exponentially. Hence, utilizing memristive device in existing applications gives numerous advantages, for example: non-volatility, scalability, no leakage current, compatibility with CMOS technology in terms of both electrical connections and manufacturing processes.

Many memristor based applications are reported [48–50], including implementation of chaotic circuits and field programmable gate array [51, 52], high density memory applications [53] such as non-volatile random access memory (NVRAM) due to its long retention and fast switching times [54], storage and processing of big data, image recognition and processing [48,55,56], cellular nonlinear or neural networks CNNs [57–59], neuromorphic

system and bio-electronics (or bio-inspired systems) due to its dynamics conductance resembling the chemical synapse [60–64], programmable analogue logic circuits [65–67], edge detection [68] and amplitude and frequency modulation [69].

Memristor is reported to be a promising element as synapse owing to its flexibility in conductance modulation and very effective high density connectivity [59, 60, 70]. There are many implemented electronic memristor-based synapses for various neuromorphic computing architectures [71–77]. In fact, there is a great progress in the phase of using memristor in neural network and artificial intelligence [78–87].

A new function of a memristor as transducer - called the memosducer - is demonstrated experimentally, and it is particularly interesting in the optimization of ultrasonic excitation for Time Reversal - Nonlinear Elastic Wave Spectroscopy (TR-NEWS) dedicated to nonlinear acoustic imaging [88, 89]. It was shown that the features of memristor such as hysteretic properties, nonlinearity and memory effect etc... are promising in TR-NEWS based ultrasonic imaging.

The main application of this work is to use memristor as synaptic link between neurons in electronic models, as for example in hybrid technologies with neuronal electronic prosthesis between real neurons. Using memristor for image processing technique was also reported by [48], where a memristive grid is employed to performed edge detection.

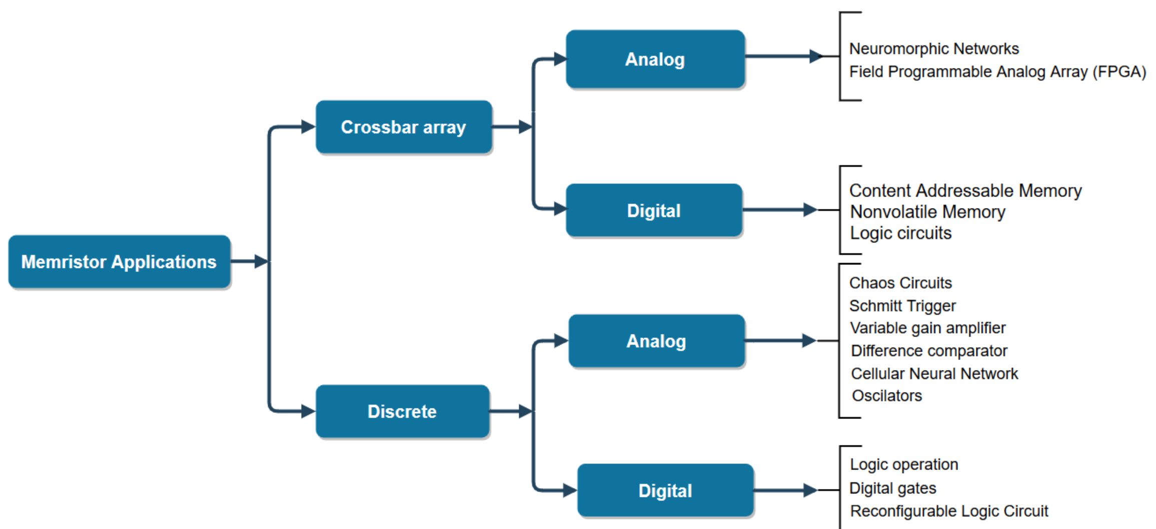

Figure 2.22: Some memristor applications in analog and digital circuit [49].

2.4.8/ Memory elements (Mem-elements)

The emergence of memristor led to the discovery of two other memory elements, namely: *Memcapacitor* and *Meminductor* [9, 90–92]. The Memristor M_R is not a loss-less device while memcapacitor M_C and meminductor M_L are loss-less devices. Their names are derived accordingly from the conventional three circuit elements (resistor, capacitor and

inductor respectively) due to some common features, for example, each having the same unit of measurement as Ohm, Farad and Henry respectively.

Then is posed a question of whether memristor is indeed the fourth circuit element due to its resistance dependency and appearance of memcapacitor and meminductor. Instead of four circuit elements, why not six altogether? However, memristor, memcapacitor and meminductor are classified as memory circuit elements or simply mem-elements owing to the ability to remember their previous history, which is a manifestation of their memory effects [9, 90, 93–97].

We also think that due to relation $i = C\frac{dv}{dt}$ for capacitor and $v = L\frac{di}{dt}$ for inductance, the memory for these elements is already present by the occurrence of the time derivative (of voltage v for capacitor and of current i for inductance). This is not the case for $v = Ri$ through a resistance, and this is the heart of all interests for the new element: the memristor.

Notwithstanding, circuit elements can be classified into linear and nonlinear elements. Hence, resistor R, capacitor C and inductor L are rather linear elements, whereas memristor M_R, memcapacitor M_C and meminductor M_L are nonlinear elements. Note that M, R_M and M_R are the notations used for the memristance in this text.

2.4.9/ Remark on the four basic circuit elements

Undoubtedly, the four basic circuit elements *R*, *L*, *C* and *M* together with memcapacitor M_C and meminductor M_L, will have a massive technological impact in the twenty first century and beyond. We presented briefly the three conventional circuit elements and the general description of the fourth circuit element. The responses of the four basic passive circuit elements from their circuit point of view, are given in Figs. 2.23 and 2.24 obtained by simulation and experiments respectively. Hence in terms of Current-Voltage response, these elements are distinguishable from one another.

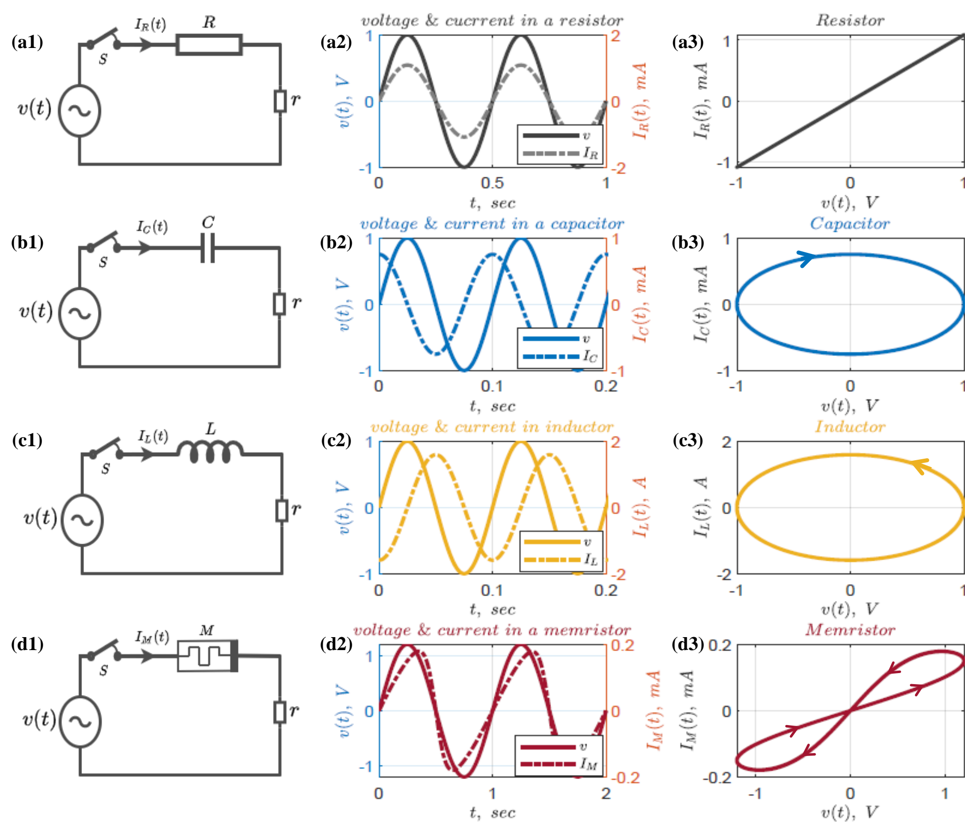

Figure 2.23: Simulation results comparison for the four basic passive circuit elements when $v(t) = V_0 sin(\omega t)$. r is a small resistor (say 100Ω) to allow easy measurements of the currents I_R, I_C, I_L and I_M. (**a1-a3**) Resistor $R = 920\Omega$: there is no phase difference in the $V(t)$ and I_R waveform and the I-V characteristic is a linear graph. (**b1-b3**) Capacitor $C = 12\mu F$: there is phase difference of $\frac{\pi}{2}$ in the V and I_C waveform, i.e I_C is leading the V by $\frac{\pi}{2}$ and the I-V characteristics is a clockwise circle. (**c1-c3**) Inductor $L = 10mH$: there is phase difference of $\frac{\pi}{2}$ in the I_L and V waveform, i.e V is leading I_L by $\frac{\pi}{2}$ and the I-V characteristic is a counter clockwise circle. (**d1-d3**) Memristor M: $R_{on} = 100\Omega$, $R_{off} = 16K\Omega$, there is no phase difference in the I_m and V waveform and the I-V characteristic is a pinched hysteresis loop.

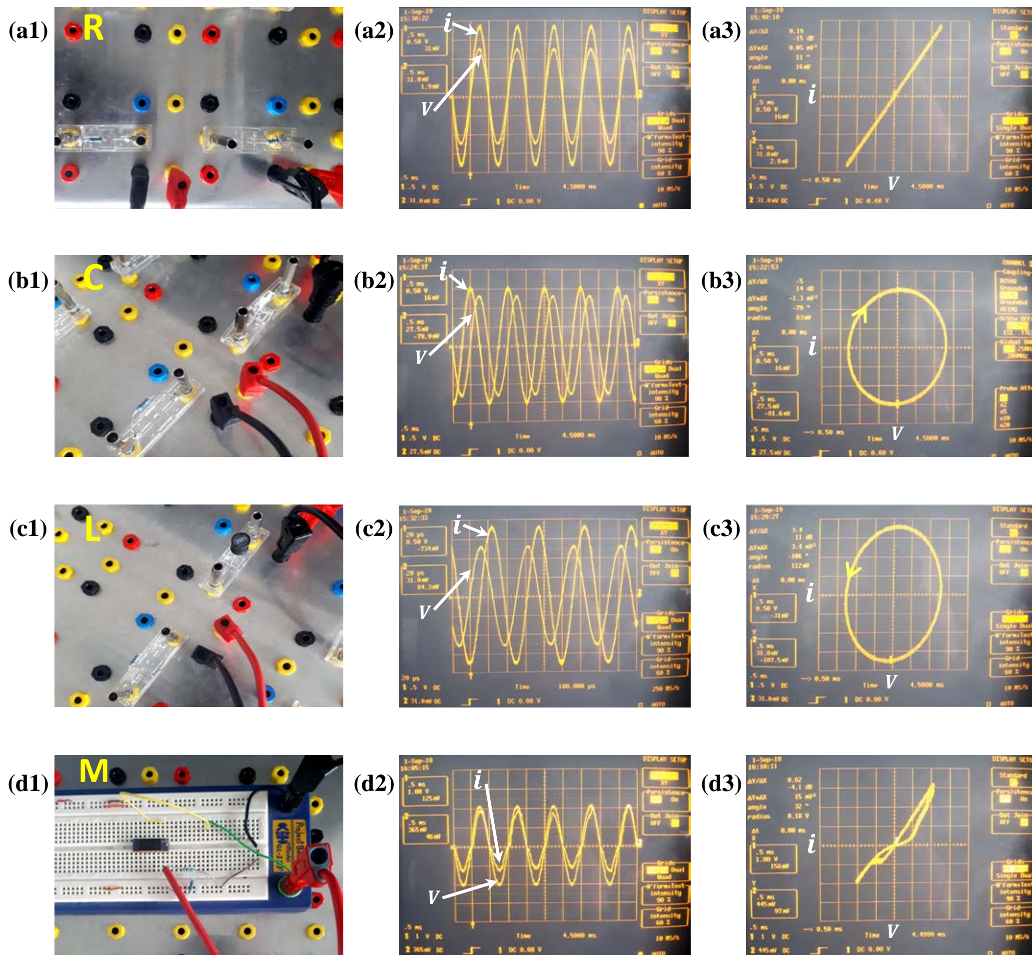

Figure 2.24: Experimental results of the four fundamental passive circuit elements. (**a1-a3**) $R = 1K\Omega$, (**b1-b3**) $C = 10nF$, (**c1-c3**) $L = 10mH$ and (**d1-d3**) KNOWM memristor chip. The current through each component is measured and the corresponding I-V characteristics are given. There is no phase difference in $V(t)$ and $I(t)$ waveforms for R and M, while there is a phase difference of $\frac{\pi}{2}$ for C and L. In the capacitor C, $I(t)$ is leading the $V(t)$ by $\frac{\pi}{2}$ and in an inductor L, $V(t)$ is leading $I(t)$ by $\frac{\pi}{2}$. The I-V characteristic of R is a linear graph, for C and L it is a circle (respectively with clockwise and anticlockwise) and for M it is a pinched hysteresis loop.
Scales: R: time t $[0.50ms/$div], current I $[0.31mA/$div] and voltage V $[0.50V/$div], C: time t $[0.50ms/$div], current I $[0.28mA/$div] and voltage V $[0.50V/$div],
L: time t $[20\mu s/$div], current I $[0.31mA/$div] and voltage V $[0.50V/$div] and M: time t $[0.50ms/$div], current I $[4.45\mu A/$div] and voltage V $[1.0V/$div].

3

MEMRISTOR TECHNOLOGIES AND MODELS

All memristor technologies follow similar principle of operation – called ***bipolar resistance switching***, which means resistance switching between two limits, namely: R_{on} and R_{off} accomplished by the evolution of the applied signal. R_{on} is the lower resistance limit (higher conducting state) while R_{off} is the higher resistance limit (lower conducting state). Although the principle of operation is the same, each technology differs from one another in terms of resistance switching mechanism (see Fig. 3.1).

The HP memristor is based on the principle of MIM (Metal-Insulator-Metal) device, where a titanium oxide TiO_2 bilayer is placed between two metal electrodes (specifically platinum), see Fig. 3.2b. One of the layer is doped with oxygen vacancies allowing for conduction while the other layer is a pure TiO_2, thus, the setup exhibits two resistance states due to the expansion and the contraction of the doped layer. Since the discovery in [12], many other memristor technologies are reported, such as self-directed channel devices using electropositive metal (Silver, Ag) for conduction and resistance changing due to the formation and dissolution of a conducting channel filament [13, 32]. Other memristor technologies are ferroelectric memristor [98, 99], polymeric (or organic) [100], spintronic memristor [101, 102], amorphous silicon memristor technology [60] and amorphous oxide semiconductor zinc-tin-oxide (ZTO) memristor [103].

Memristor technologies are based on ionic or magnetic effect. The texonomy of memristor technologies is presented in Fig. 3.1.

3.1/ HP (TiO_2) MEMRISTOR: ANALYSIS AND INTERPRETATION

The **TiO_2 memristor** is the first real two-terminals solid state memristor device announced by Hewlett Packard (HP) lab in 2008 [12], while working on nanoscale crossbar arrays of wires in which each junction formed a memristor [3, 104]. In this configuration,

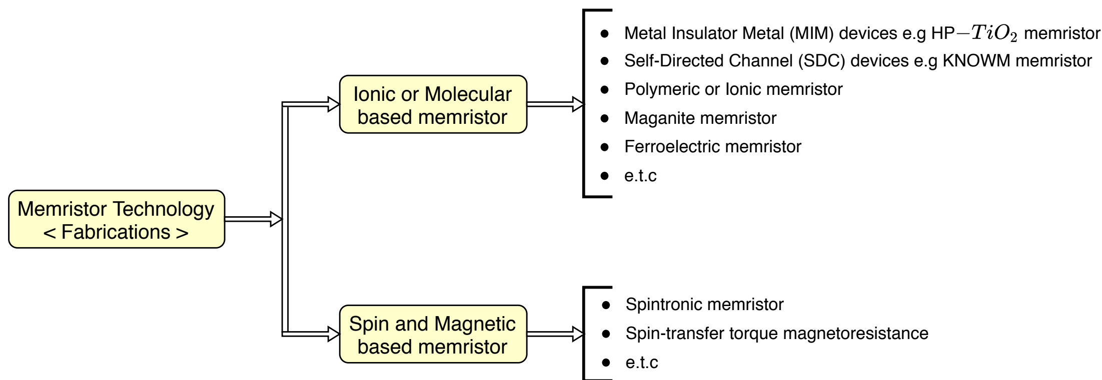

Figure 3.1: Some memristor fabrications technologies.

the memristor is acting as a storage element to give binary output for color images or as a switch to give different grayscale levels, thus allowing to process images [105]. Recall that the memristive systems are described by port and state equations given in equation (2.24). If the memristance is only a function of the state variable x, then we can transform (2.24), as:

$$V = R(x)\, i : \quad \text{port equation,} \tag{3.1a}$$

$$\frac{dx}{dt} = f(x, i) : \quad \text{state equation.} \tag{3.1b}$$

Equation (3.1a) is the state dependent Ohm's law relationship. Memristor is able to conserve the information of the total amount of charge passed through it and its resistance $R(x)$ is continuously changing within certain boundaries according to the passing current $i(t)$. $R(x)$ is the memristance function whose value depends upon the state variable of the device $x(t)$. The state equation (3.1b) of the memristor defines the dynamics relationship between the passing current $i(t)$ and the state variable $x(t)$. Furthermore, equation (3.1b) can be represented in a generic form as:

$$\frac{dx}{dt} = f(x, s),$$

where s could be a current i or a voltage v for a charge-controlled memristor and a flux-controlled memristor respectively. However, if s is a voltage source, then the port equation is rather rewritten as: $i = G(x)v$, where G is the memductance.

3.1.1/ Model description

The structural view of HP memristor is given in Fig. 3.2b. The device is made up of a thin film bilayer of Titanium-Oxide TiO_2 of thickness D sandwiched between two platinum (Pt) contacts which serve as electrodes. One portion of TiO_2 is initially doped with oxy-

gen vacancies, hence becomes $TiO_{2\text{-}e}$ and the other portion remains pure TiO_2. These oxygen vacancies let the layer become N-type semiconductor with electrons as charge carriers and thus adopt conductivity, the other undoped side has resistive property, such that the entire arrangement behaves as a semiconductor material. Notice that in reality the dopants are scattered along the device width, however, its concentration in one edge is negligible compared to that of the other edge, creating two different resistive regions. The structural arrangement constitutes two resistances R'_{on} and R'_{off} connected in series. R'_{on} resistance corresponds to the doped region ($TiO_{2\text{-}e}$ i.e higher conducting region) of width (w) while R'_{off} resistance corresponds to the undoped region (TiO_2, i.e lower conducting region) whose width is $(D - w)$. Note that when $w \to D$, $R'_{on} \to R_{on}$ and if $w \to 0$, $R'_{off} \to R_{off}$.

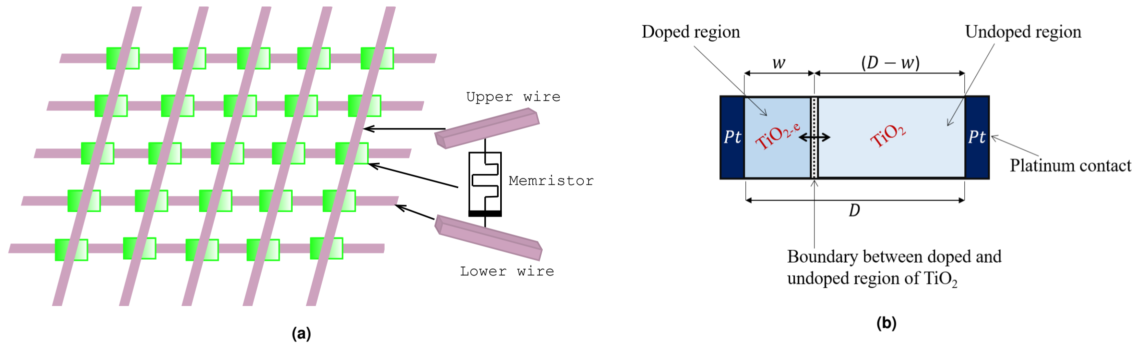

Figure 3.2: Geometry of HP (TiO_2) memristor. (a) Crossbar arrays of wires with memristor in each junction [3, 105]. (b) Structural view of the TiO_2 memristor, i.e enlargement of the memristor in the junction.

The boundary between doped and undoped regions (shown with two headed arrows) moves back and forth depending upon the direction of the flowing current or the polarity of the applied voltage. If the boundary moves leftward, w decreases and the opposite width $(D - w)$ increases, leading hence to higher resistance (becoming less conductive). Conversely, if the boundary moves rightward, w increases while $(D-w)$ decreases, leading hence to lower resistance (becoming more conductive). This further confirms bipolar resistance switching characteristic. HP memristor [12] is based on this principle and the modeling equations are direct replicate of (3.1a) and (3.1b). The boundary stops instantly (motionless) if the current stops to flow and continues from this position once the current flows again, irrespective of the duration, i.e even months or years [3]. Therefore, w acts as the state variable of the device characterizing the instantaneous memristance.

The mathematical description of the titanium-oxide memristor when a positive voltage $V(t)$ is applied to the 2-ports device is shown in Fig. 3.3, corresponding to a current $i(t)$ flowing into the memristor, while the voltage is shared in 2 parts: a voltage $V_1 = \dfrac{V(t)\, R_{on} w}{R_{on} w + R_{off}(D - w)}$ across the doped region (the left part of Fig. 3.3a), and the complementary part $V_2 = \dfrac{V(t)\, R_{off}(D - w)}{R_{on} w + R_{off}(D - w)}$ present across the undoped region (the right part of Fig. 3.3a). Let us consider the oxygen vacancies in the doped region. The charge

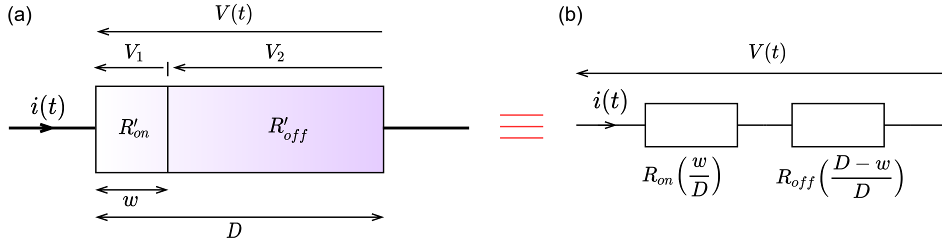

Figure 3.3: Memristor internal behavioural response. $R'_{on} = R_{on}\frac{w(t)}{D}$, $R'_{off} = R_{off}\left(1 - \frac{w(t)}{D}\right)$, $V_1 = R'_{on}i(t)$ and $V_2 = R'_{off}i(t)$.

carriers (electrons with mass m_e and charge $q = -e$) are accelerated by the electric field $E = \dfrac{V(t)\,R_{on}}{R_{on}w + R_{off}(D-w)}$ and braked as they collide together. Their velocity is then limited by the speed $u_l = \dfrac{q.E}{m_e}\langle t\rangle$, where $\langle t\rangle$ is the mean time between two consecutive collisions, leading to their averaged velocity $< u > = \mu_v\vec{E}$, where μ_v is the mobility of the charge carriers. Note that the electric field in the conductive region can be expressed as $E = \dfrac{V_1}{w} = \dfrac{R_{on}}{D}i(t)$. The charge carriers expand then the doped region towards the right ($w \uparrow$), whose boundary increases with a positive current $i(t)$ such that:

$$\frac{dw}{dt} = \mu_v E = \mu_v \frac{R_{on}}{D} i(t), \tag{3.2a}$$

$$V(t) = M(w)\, i(t), \tag{3.2b}$$

$$M(w) = R_{on}\frac{w(t)}{D} + R_{off}\left(1 - \frac{w(t)}{D}\right). \tag{3.2c}$$

Note that $\vec{u} = \mu_v\vec{E} \Rightarrow \dfrac{u}{\mu_v} = \dfrac{1}{\mu_v}\dfrac{dw}{dt}$ and $u = \dfrac{dw}{dt}$ is the drift speed of the boundary. The dopant mobility (μ_v) determines how quickly the boundary between doped and undoped regions (or the dopants) can move back and forth across the device for any applied signal. The tunneling of the barrier width w is determined by the magnitude and polarity of the applied voltage or current. It can be seen from equation (3.2a) that at any given time t, the width $w(t)$ of the doped region depends on the quantity of electric charge having passed through the device. Hence the conductivity of TiO_2 memristor and its switching dynamics between R_{on} (ON state) and R_{off} (OFF state) are determined by w [106].

Finally, with the normalized form $x(t) = \dfrac{w(t)}{D}$, the behaviour of the memristor is given by:

$$\frac{dx}{dt} = \mu_v \frac{R_{on}}{D^2}\, i(t), \tag{3.3a}$$

$$V(t) = M(x)\, i(t), \tag{3.3b}$$

$$M(x) = R_{off} - \delta R\, x, \tag{3.3c}$$

where: $V(t)$ is the voltage across the 2 ports-device, $i(t)$ is the current flowing through it, $M(x)$ is the memristance and $\delta R = R_{off} - R_{on}$. $M(x) = R_{off}$ if $x(t) = 0$ and R_{on} if $x(t) = 1$. Equation (3.3c) shows that HP memristor remembers the coordinate of the state variable x, not the charge. However, the coordinate of x is related to the amount of charge having flowed through the device and they are each of them directly proportional to one another. When a signal is applied to the device, the boundary between the doped and undoped regions moves, the direction of this movement depending on the polarity of the applied signal. It is always expected that:

$$0 \leq \frac{w(t)}{D} \leq 1 \;\Rightarrow\; x \in [0,1] \text{ or } 0 \leq x \leq 1.$$

When integrating (3.3a) for x from 0 to 1:

$$\begin{aligned} \int_0^1 dx = 1 &= \mu_v \frac{R_{on}}{D^2} \int_{w=0}^{w=D} i(t)dt, \\ &= \mu_v \frac{R_{on}}{D^2} q_d, \end{aligned} \tag{3.4}$$

where $q_d = \int_{w=0}^{w=D} i(t)dt = \frac{D^2}{\mu_v R_{on}}$ is the charge required to move completely the doped/undoped boundary from $w = 0$ to $w = D$. Then (3.3a) can be rewritten as:

$$\frac{dx}{dt} = \frac{1}{q_d} i(t). \tag{3.5}$$

3.1.2/ Window function $g(x)$

A window function $g(x)$ is often introduced as a factor in the right hand side of (3.5) for nonlinear dopant drift modeling, i.e. to avoid x from taking values outside of the interval $[0,1]$ [107], to give

$$\frac{dx}{dt} = \frac{1}{q_d} g(x)i(t). \tag{3.6}$$

The model of TiO_2 memristor is usually characterized by two models, namely: linear and nonlinear drift models, with the state equation given by (3.5) and (3.6), respectively.

Why is the need of a window function in memristor modeling?

There exist enriched intrinsic nonlinearity within the memristor device which also manifests in its hysteretic behaviour [12], however, when the dopants move toward either of the boundaries, that is, $w = 0$ (or $x = 0$) or $w = D$ (or $x = 1$), their speed decreases to zero which significantly affects the device dynamics and hence the performance. Due to the nano-nature of memristor device, small voltage can result in huge electric field to

be developed across the device, which in turn yields significant nonlinearities in the ionic transport [12]. These nonlinearities become more apparent in the boundaries where the drift speed of the dopant obviously reduces to zero. Hence, this phenomenon is called nonlinear dopant drift. However, the nonlinearity can be more pronounced at the boundary by inclusion of the window function $g(w)$ or $g(x)$ in the case of normalised quantities.

Since the state variable w is bounded between 0 and D, for an applied voltage bias, w is proportional to the quantity of charge q already passed through the device, until it approaches 0 or D, where it requires higher voltage to switch from OFF resistance state to ON resistance state under positive bias and from ON resistance state to OFF resistance state under negative bias. Hence, the switching transition at these extreme boundaries is described as *Hard Switching* because the transition, from OFF state to ON state and vice-versa, delays until certain amount of voltage threshold is reached. Thus, hard switching can be specified by considering different boundary conditions, hence the need of a window function. The window function $g(x)$ is basically a dimensionless function multiplied to the right hand side of eq. (3.5) for modeling the nonlinear dopant drift when x approaches 0 or 1 and for avoiding x from taking values outside of the limits $[0, 1]$. For example, the SPICE circuit simulation of the linear model often reports computation errors attributed to the values of x. On the other hand, there is no such error even for a hard switching case if a window function (i.e. nonlinear model) is used.

Some authors have tried to define the function $g(x)$ with a more physical description of the device, in modeling the non-linearity of the charge carriers along the device geometry. Due to the direct dependency of x on q, eq. (3.6) suggests that higher quantity of charge is needed for w to be closer to 0 or D [12].
Five sufficient and necessary conditions for any efficient window function are outlined by Prodromakis et al. [108]. Quoting them, $g(x)$ must:

- ***(1)*** *take into account the boundary conditions at the left and right electrodes of the device;*
- ***(2)*** *be capable of imposing nonlinear drift over the entire active core of the device;*
- ***(3)*** *provide linkage between the linear and nonlinear dopant drift models;*
- ***(4)*** *be scalable, meaning a range of $g_{max}(x)$ can be obtained such that $0 \leq g_{max}(x) \leq 1$;*
- ***(5)*** *utilize a built-in control parameter for adjusting the model.*

The proper choice of the window function is of significant importance for predictive modeling of memristors because the system may respond differently with respect to the window function used [109]. There are many suggested window functions essentially to resolve the boundary issues and to impose nonlinearities [12,107,108,110–120]. However, each

of them has their own advantages as well as own disadvantages. Some of the commonly used window functions are described briefly in the following.

- Strukov et al. [12, 110] proposed a window function, given by:

  $$g(w) = \frac{w(D-w)}{D^2},$$

  and is normalized as:

  $$g(x) = x(1-x). \tag{3.7}$$

  In the boundary limits, x will remain at 0 or 1 until the device has changed its resistance state.

- Joglekar et al. [107] proposed $g(x)$ to be:

  $$g(x) = 1 - (2x-1)^{2p}, \tag{3.8}$$

  where $p \in \mathbb{Z}^+$ is a positive integer serving as a control parameter. For large p, this window function gives a better nonlinear ionic drift than Strukov et al. However, the model reduces to linear dopant drift if $p \to \infty$. Notice that for $p = 1$, $g(x)$ in eq. (3.8) becomes: $g(x) = 4x(1-x)$, that is, 4 times Strukov's function. Hence, the control parameter p gives Joglekar's function more flexibility than Strukov's function.

- Prodromakis et al. [108] proposed $g(x)$ to be:

  $$g(x) = 1 - [(x-0.5)^2 + 0.75]^p, \tag{3.9}$$

  where $p \in \mathbb{R}^+$ is a positive real number. This function has hence more versatility than Joglekar's function, where p takes only positive integer values. Moreover, here p allows upward scaling of $g(x)$ such that its maximum value, i.e g_{max}, remains in the interval: $0 \leq g_{max} \leq 1$. One can also see that for $p = 1$, $g(x)$ in eq. (3.9) becomes:

  $$g(x) = x\,(1-x),$$

  the same as Strukov's function. Similarly, for $p \to \infty$, the model resembles linear drift model. Moreover, Prodromakis et al. take into account the unusual situation whereby the dopant's drift is such that $g_{max} \gtreqless 1$, by introducing a new scalar j serving as a second control parameter in expression (3.9), thus becoming:

  $$g(x) = j\left(1 - [(x-0.5)^2 + 0.75]^p\right). \tag{3.10}$$

  For a fixed value of parameter p with j varying suitably, $g(x)$ can be scaled up and

down in conformity with:

$$g_{max} \gtreqless 1.$$

- Biolek et al. [111] proposed $g(x)$ to be:

$$g(x) = 1 - (x - stp(-i))^{2p}, \tag{3.11}$$

where $p \in \mathbb{Z}^+$ and i is the current flowing through the memristor, such that:

$$stp(i) = \begin{cases} 1 & for\ i \geq 0, \\ 0 & for\ i < 0. \end{cases} \tag{3.12}$$

The flowing current i is considered as positive when the device is in the saturation mode, i.e $x \to 1$ corresponding to the expansion of the doped layer, and negative if the device is in depletion mode, i.e $x \to 0$ which corresponds to the contraction of the doped layer. Notice that there is a discontinuity in the boundaries due to the step function definition of the current i. We will return in chapter 5 to the fact that there is no symmetry in memristor behaviour when $i > 0$ or $i < 0$.

- Proposed window function:
  In accordance with the role of window function, we can also ourselves propose $g(x)$ as derived from Hann window apodisation function as follows:

$$g(x) = \frac{1}{2}\left[1 + cos\ 2\pi(\alpha(x))\right].$$

It is well known that:

$$for\ \ \alpha(x) = 0 \text{ or } 1: \quad 1 + cos\ 2\pi(\alpha(x)) = 2,$$

$$for\ \ \alpha(x) = \pm 0.5: \quad 1 + cos\ 2\pi(\alpha(x)) = 0.$$

Therefore, to fulfill the continuity constraints for $x = 0$ and $x = 1$, a sufficient condition stands:

$$\alpha(0) = -\tfrac{1}{2},$$

$$\alpha(\pm 0.5) = 0,$$

$$\alpha(1) = \tfrac{1}{2}.$$

Thus, $\alpha(x)$ becomes:

$$\alpha(x) = x - \frac{1}{2},$$

that is:

$$g(x) = \frac{1}{2}\left[1 + cos\,\pi(2x - 1)\right]. \tag{3.13}$$

Following the idea of [108], we can introduce a scalar control parameter j for up and down scaling of $g_{max}(x)$. Thus:

$$g(x) = \frac{j}{2}\left[1 + cos\,\pi(2x - 1)\right]. \tag{3.14}$$

Figure 3.4a shows the comparison of the aforementioned functions. The window functions by Strukov's team and Biolek's team lacking flexibility, a comparison is drawn between the models by Joglekar et al. on one hand, and Prodromakis et al. on the other one, that is, equations (3.8) and (3.9) respectively. The control parameter p is arbitrarily chosen in ascending order in order to observe the corresponding responses of $g(x)$: $p = 1,\ 2,\ 10,$ and 20, and the results are given in Fig. 3.4b. One can see that for all p, Joglekar model has $g(0.5) = 1$, unlike Prodromakis model where $g(0.5)$ is scaleable from 0 to 1 with increase in p, with $g(0.5) \equiv g_{max}(x)$. In addition, for $p \rightarrow \infty$, both models resembles linear drift model.

Finally, another known window function is the ThrEshold Adaptive Memristor (TEAM) model [112].

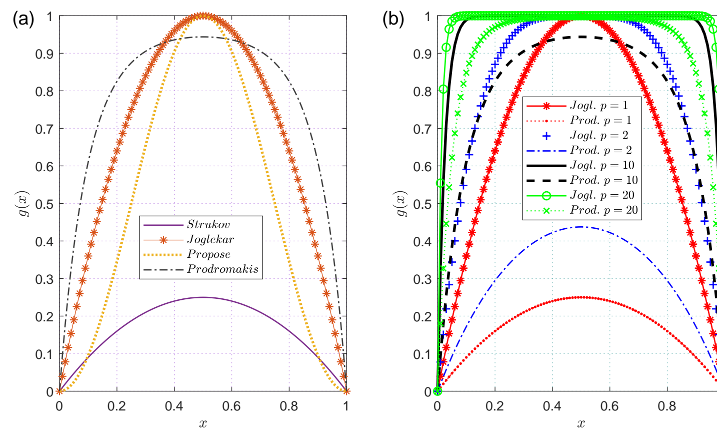

Figure 3.4: Window functions comparison. (a) Proposed window function and its comparison with the discussed functions. Joglekar ($p = 1$) and Prodromakis ($p = 10$), (b) Comparison of Joglekar and Prodromakis window functions, showing the effect of varying p.

The analytical solution of the memristor model is given in the subsequent section by observing the effect of window function $g(x)$ in the two possible scenarios: ***without any window function eq. (3.5)*** and ***with a window function according to eq. (3.6)***.

3.2/ LINEAR DOPANT DRIFT MODEL: ANALYSIS

This is the simplest model in which the dopant tunneling barrier width drifts at a speed $u = \frac{dw}{dt}$ under uniform electric field $\mathbf{E} = \frac{R_{on}\, i}{D}$ corresponding to the time-dependence description of the state variable given by equation (3.5). Notice that this is based on the assumption that the device can reach saturation (i.e virtually doped $w \to D$).

***Why Linear model*?** This term describes the displacement nature of the tunneling barrier width w with respect to the applied input signal, hence not the memristor itself. Equation (3.5) implies a linear relationship between the normalized tunneling barrier width $x(t)$ and the charge $q(t)$, i.e $x(t) \propto q(t)$. Hence, it is called linear dopant drift model. Moreover, it does not take into account the consequence when x reached 0 or 1.

Recall that the memristance notation is R or M, therefore, $R(x) = M(x)$ and $R(q) = M(q)$. These terms are used interchangeably throughout the text. The state equation (3.5) is considered solely, and the state variable x is calculated from this equation to be used in the memristance equation, and subsequently to determine the voltage drop across the memristor and the current flowing through it. Firstly, the case of a current excitation (charge controlled memristor: CCM) is considered and then followed by the case of a voltage excitation (flux controlled memristor: FCM). The analytical expressions are derived for each case and the results are given accordingly.

3.2.1/ CCM WITH LINEAR DOPANT DRIFT MODEL

In this case, the memristance is driven by a current source. Therefore, for a memristor with memristance $M(q)$ subjected to a time-varying current source $i(t)$, the voltage drop across the memristor will be:

$$v(t) = M(q)\, i(t).$$

The state variable $x(t)$ can be expressed from equation(3.5) by integration:

$$\int_{x_0}^{x(t)} dx' = \frac{1}{q_d} \int_0^t i(t')\, dt' \; ,$$

where $\int_0^t i(t')\, d(t') = q(t) - q_0$, then:

$$x(t) - x_0 = \frac{1}{q_d}(q(t) - q_0), \tag{3.15}$$

where $x_0 = \frac{w(0)}{D}$ is the state variable at $t = 0$, giving the previous history of the device with a charge q_0 having already flowed through the memristor. Actually, for a formed (used) memristor device, x_0 is likely to be non-zero because the dopants are dis-localized, hence

the device has some previous information preserved.
It is easy to predict x_0 if the initial memristance of $M(x)$ (i.e M_0) is known. From eq. (3.3c), we get:

$$M_0 = R_{off} - \delta R\ x_0, \tag{3.16}$$

and

$$x_0 = \frac{R_{off} - M_0}{\delta R}.$$

Note that: the subscript '$_0$' in x_0 does not necessarily imply $x(t) = 0$, but rather the value of $x(t)|_{t=0}$ and it could be any value in the interval $[0,\ 1]$. x_0 is simply a notation to represent the previous state of the device.
Therefore, having $q(t)$ known and $x(t)$ expressed in terms of $q(t)$, from (3.3c) and (3.15), $M(x)$ becomes $M(q)$, thus:

$$\begin{aligned} M(q) &= R_{off} - \delta R\left[x_0 + \frac{1}{q_d}(q(t) - q_0)\right], \\ &= R_{off} - \delta R\ x_0 - \delta R\ \frac{1}{q_d}(q(t) - q_0). \end{aligned}$$

Substituting for M_0 from (3.16) [i.e $M_0 = R_{off} - \delta R\ x_0$] $\Rightarrow$

$$\begin{aligned} M(q) &= M_0 - \delta R\frac{1}{q_d}(q(t) - q_0), \\ &= R_{off} - \delta R\frac{q(t)}{q_d}. \end{aligned} \tag{3.17}$$

Note that when $q(t) \geq q_d$, the expression of $M(q)$ must be replaced by: $M(q) = R_{on}$ as $x \to 1$, while: $M(q) = R_{off}$ as $x \to 0$ and the boundary cannot move any further. As suggested in [12], $\frac{R_{off}}{R_{on}} = 10^2 \sim 10^3$, this implies $R_{off} \gg R_{on}$ so that: $\delta R \simeq R_{off}$. In addition, we assume that $x_0 \ll 1$; so that, $M_0 \simeq R_{off}$. Then, we get the approximate memristance expression as:

$$M(q) = R_{off}\left(1 - \frac{q(t)}{q_d}\right) \tag{3.18}$$

Hence, the charge having flowed is simply:

$$q(t) - q_0 = \int_{x_0}^{x(t)} q_d\ \mathrm{d}x. \tag{3.19}$$

Now that from the expression of $M(q)$, $V(t)$ is known for any $i(t)$ and the result is given by Fig. 3.5. The memristance $M(q)$ in (3.18) depicts an ideal charge-controlled memristance having charge $q(t)$ as the only state variable.

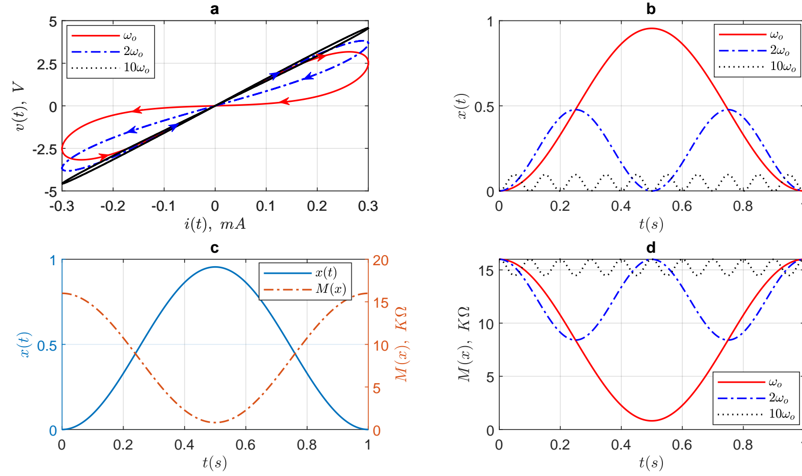

Figure 3.5: Analytical results of CCM with Linear model, $R_{on} = 100\Omega$, $R_{off} = 16K\Omega$, $q_d = 100\mu C$ and three different input frequencies. (a) I-V characteristics, (b) state variable, (c) state variable and memristance for $f = 1Hz$, (d) memristance.

3.2.2/ FCM WITH LINEAR DOPANT DRIFT MODEL

Here, the memristor is driven by a voltage source $v(t)$ connected across its two terminals, and the current flowing through the memristor $i(t)$ is given by:

$$i(t) = Y(\phi)\ v(t),$$

where $Y(\phi)$ is the memductance. From the definition of memristor:

$$M(q) = \frac{d\phi(q)}{dq},\ \text{or}\ d\phi = M(q)\ dq.$$

Let us substitute an expression of $M(q)$ from (3.17) in order to obtain the relationship between charge $q(t)$ and the flux $\phi(t)$, thus:

$$d\phi = \left[R_{off} - \delta R\ \frac{q(t)}{q_d}\right]\ dq.$$

Integrating both sides gives:

$$\int_{\phi_0}^{\phi(t)} d\phi^* = \int_{q_0}^{q(t)} \left(R_{off} - \frac{\delta R}{q_d}\ q^*\right)\ dq^*,$$

thus:

$$\phi(t) - \phi_0 = R_{off}\ (q(t) - q_0) - \frac{\delta R}{2q_d}\ (q(t)^2 - q_0^2). \tag{3.20}$$

Equation (3.20) is a quadratic equation in $q(t)$ and consequently will generate two possible solutions of $q(t)$. For simplicity let us take ϕ and q in place of $\phi(t)$ and $q(t)$ respectively.

Considering $q' = q - q_0$, such that $q^2 - q_0^2 = q\prime^2 + 2q_0 q'$, then equation (3.20) becomes:

$$q' = \left(\frac{R_{off}}{\delta R} q_d - q_0\right) \pm \sqrt{\left(\frac{R_{off}}{\delta R} q_d - q_0\right)^2 - \frac{2q_d(\phi - \phi_0)}{\delta R}} \Rightarrow$$

$$q = \frac{R_{off}}{\delta R} q_d \pm \sqrt{\left(\frac{R_{off}}{\delta R} q_d - q_0\right)^2 - \frac{2q_d(\phi - \phi_0)}{\delta R}}\ . \tag{3.21}$$

To vividly visualize (3.21), we have to apply the normal approximation: similar to what we did in obtaining equation (3.18). Thus, equation (3.21) becomes:

$$q = q_d \pm \sqrt{(q_d - q_0)^2 - \frac{2q_d(\phi - \phi_0)}{R_{off}}}.$$

Physically, the feasible value of $q(t)$ compatible with the boundary condition is given with only the minus sign of the quadratic equation solution. This ensures that the state variable is within the recommended range. Therefore, the charge $q(t)$ as a function of flux $\phi(t)$ is given by:

$$q = q_d - \sqrt{(q_d - q_0)^2 - \frac{2q_d(\phi - \phi_0)}{R_{off}}} \Rightarrow$$

$$q = q_d\left(1 - \sqrt{\left(1 - \frac{q_0}{q_d}\right)^2 - \frac{2(\phi - \phi_0)}{q_d R_{off}}}\right). \tag{3.22}$$

From (3.15), the expression of $x(t)$ is updated by substituting (3.22) into (3.15):

$$x(t) = x_0 + 1 - \sqrt{\left(1 - \frac{q_0}{q_d}\right)^2 - \frac{2(\phi - \phi_0)}{q_d R_{off}}} - \frac{q_0}{q_d}. \tag{3.23}$$

Suppose $x_0 = 0$, $q_0 = 0$ and $\phi_0 = 0$, then substituting (3.23) into (3.17), we have: $M(\phi) = R_{off} - \delta R\left(1 - \sqrt{1 - \frac{2\phi(t)}{q_d R_{off}}}\right)$, and after the simplification:

$$M(\phi) = R_{off}\ \sqrt{1 - \frac{2\phi(t)}{q_d R_{off}}}\ . \tag{3.24}$$

$M(\phi)$ is the flux-controlled memristance and the memductance $Y(\phi)$ is expressed as:

$$Y(\phi) = \frac{1}{M(\phi)}.$$

For any input voltage $V(t)$ connected across the memristor, the current $i(t)$ is given by:

$$i(t) = Y(\phi)\ v(t).$$

Figure 3.6 shows the current–voltage response and the corresponding state variables. All other important parameters could be visualized in the same way.

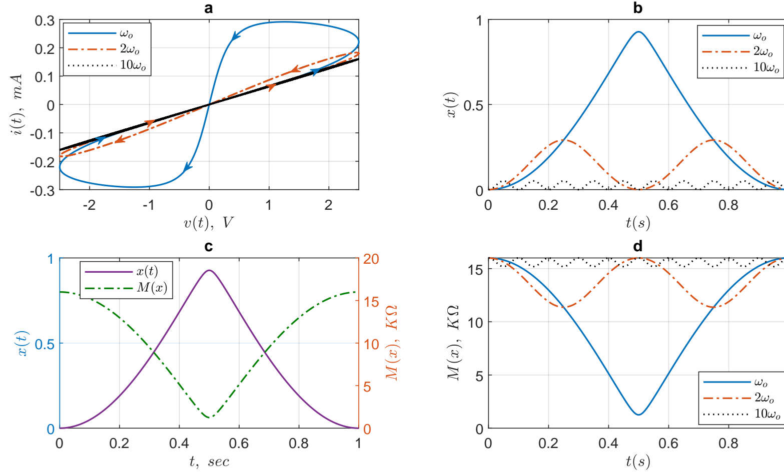

Figure 3.6: Analytical results of FCM with linear dopant drift model: $R_{on} = 100\Omega$, $R_{off} = 16K\Omega$, $q_d = 100\mu C$ and different input frequencies. (a) I-V characteristics, (b) state variable, (c) state variable and memristance for $f = 1Hz$, (d) memristance.

3.3/ Nonlinear dopant drift model: Analysis

The drawbacks of linear model can be overcome by adding an appropriate window function to the existing linear model which imposes nonlinear drift in the entire width of the device, see eq. (3.6). Moreover, the nonlinearity of the device improves and becomes even more significant at the boundaries under certain voltage threshold [12], hence it is called the nonlinear dopant drift model. In addition to enhancing nonlinearity, the window function is important in maintaining safe dynamic operating range of the memristor device model by disallowing w to take values outside of interval $[0, D]$, which would consequently cause memristance to take values outside its limits or even negative if $\delta R\ x > R_{off}$. Thus, $g(x)$ resolves the boundary issues by ensuring zero drift at the boundaries, i.e $x = 0$ and $x = 1$, such that:

$$g(0) = g(1) = 0.$$

Let us consider $g(x)$ by Joglekar and Wolf [107], for $p = 1$: $g(x) = 4x\ (1 - x)$ corresponding to the $g(x)$ in [12] multiplied by 4. The voltage across and current through the memristor can be calculated. That corresponds then rather to Strukov's window function that we will consider now, as:

$$g(x) = x(1 - x).$$

3.3.1/ CCM WITH NONLINEAR DOPANT DRIFT MODEL

Equation (3.6) is rewritten as follows:

$$\frac{dx}{dt} = \frac{1}{q_d}\, x\,(1-x)\, i(t).$$

Let us consider an input current: $i(t) = I_0\, sin(\omega t)$. Then, at $t = 0$, $i(t) = 0$, $q(t=0) = q_0$ and $x(t=0) = x_0$. Therefore, integration by variable separable method gives:

$$\int_{x_0}^{x} \frac{dx^*}{x^*\,(1-x^*)} = \frac{1}{q_d}\int_0^t i(t^*)\, dt^* = \frac{q-q_0}{q_d}.$$

$$\therefore\ \ln x\Big|_{x_0}^{x} - \ln(1-x)\Big|_{x_0}^{x} = \frac{q-q_0}{q_d},$$

$$\ln\left(\frac{x}{x_0}\right) - \ln\left(\frac{1-x}{1-x_0}\right) = \frac{q-q_0}{q_d},$$

$$\frac{x - x\,x_0}{x_0 - x\,x_0} = e^{\frac{q-q_0}{q_d}} \quad \Rightarrow$$

$$x(t) = \frac{x_0\, e^{\frac{q-q_0}{q_d}}}{1 - x_0 + x_0\, e^{\frac{q-q_0}{q_d}}}. \tag{3.25}$$

Therefore, the charge-controlled memristance $M(q)$ becomes:

$$M(q) = R_{off} - \delta R\, \frac{x_0\, e^{\frac{q-q_0}{q_d}}}{1 - x_0 + x_0\, e^{\frac{q-q_0}{q_d}}}. \tag{3.26}$$

At $t = 0$, x_0 is confirmed, while $x(t)$ always lies between 0 and 1, hence $x(t) \to 1$ when $t \to \infty$. From (3.26) we get the voltage drop across the memristor:

$$V(t) = M(q)\, i(t),$$

while the results are shown in Fig. 3.7.

3.3.2/ FCM WITH NONLINEAR DOPANT DRIFT MODEL

Recall that for any input voltage $v(t) = V_0 sin(\omega t)$ applied to the memristor:

$$\phi(t) = \int_0^t V(\tau)\, d\tau + \phi_0 \ \Rightarrow\ \phi(t) = \frac{V_0}{\omega}[1 - cos(\omega t)] + \phi_0$$

and the dynamic state of the memristor $x(t)$ is driven by flux $\phi(t)$. Therefore, once again by definition:

$$V(t) = M(q)\frac{dq(t)}{dt}\ .$$

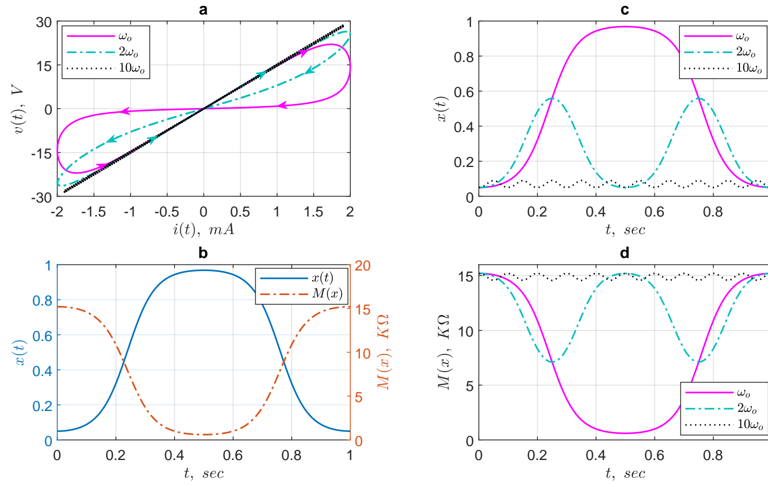

Figure 3.7: Analytical results of the CCM with nonlinear dopant drift model at different input frequencies. $I_0 = 2mA$, $x_0 = 0.05$, $q_d = 100\mu C$, $R_{off} = 16K\Omega$, $R_{on} = 100\Omega$ and $\delta R = 15.9K\Omega$. (a) I-V characteristics, (b) state variable and memristance for $f = 1Hz$, (c) state variable, (d) memristance.

From (3.26), it follows that:

$$V(t) = \left(R_{off} - \delta R \, \frac{x_0 \, e^{\frac{q-q_0}{q_d}}}{1 - x_0 + x_0 \, e^{\frac{q-q_0}{q_d}}} \right) \frac{dq(t)}{dt},$$

$$\int_0^t V(t^*) \, dt^* = \int_{q_0}^{q(t)} \left(R_{off} - \delta R \, \frac{x_0 \, e^{\frac{q^*-q_0}{q_d}}}{1 - x_0 + x_0 \, e^{\frac{q^*-q_0}{q_d}}} \right) dq^* \quad \Rightarrow$$

$$\phi(t) - \phi_0 = R_{off}(q(t) - q_0) - \delta R \int_{q_0}^{q(t)} \frac{x_0 \, e^{\frac{q^*-q_0}{q_d}}}{1 - x_0 + x_0 \, e^{\frac{q^*-q_0}{q_d}}} dq^*.$$

Let $y = 1 - x_0 + x_0 \, e^{\frac{q^*-q_0}{q_d}}$, then $\frac{dy}{dq^*} = \frac{x_0}{q_d} e^{\frac{q^*-q_0}{q_d}} \Rightarrow q_d \frac{dy}{x_0 \, e^{\frac{q^*-q_0}{q_d}}} = dq^*$. Moreover, at $t = 0,\ q^* = q_0 \Rightarrow y(0) = 1$ while at time t, $q^* = q(t)$, $y = 1 - x_0 + x_0 \, e^{\frac{q-q_0}{q_d}}$. Substituting these generated variables, the equation becomes:

$$\phi(t) - \phi_0 = R_{off}(q(t) - q_0) - \delta R \int_{y(0)}^{y(t)} \frac{x_0 \, e^{\frac{q^*-q_0}{q_d}}}{y} . q_d \frac{dy}{x_0 \, e^{\frac{q^*-q_0}{q_d}}},$$

$$\phi(t) - \phi_0 = R_{off}(q(t) - q_0) - q_d \delta R \, \ln\left(\frac{y(t)}{y(0)} \right) \quad \Rightarrow$$

$$\phi(t) = \phi_0 + R_{off}(q(t) - q_0) - q_d \delta R \, \ln\left(1 - x_0 + x_0 \, e^{\frac{q(t)-q_0}{q_d}} \right). \tag{3.27}$$

From equation (3.27), $q(t)$ can be expressed in terms of $\phi(t)$ as follows:

$$\ln\left(1 - x_0 + x_0 \, e^{\frac{q(t)-q_0}{q_d}} \right) - \frac{R_{off}}{q_d \delta R}(q(t) - q_0) = -\frac{1}{q_d \delta R}(\phi(t) - \phi_0),$$

Taking exponential of both sides and then simplifying:

$\left(1 - x_0 + x_0\ e^{\frac{q(t)-q_0}{q_d}}\right) \times e^{-\frac{R_{off}}{\delta R}\frac{q(t)-q_0}{q_d}} = e^{-\frac{1}{q_d \delta R}(\phi(t)-\phi_0)}$. Using $\delta R \approx R_{off}$, then:

$(1 - x_0)\ e^{-\frac{q(t)-q_0}{q_d}} = e^{-\frac{1}{q_d \delta R}(\phi(t)-\phi_0)} - x_0 \quad \Rightarrow$

$$q(t) = q_0 - q_d\ \ln\left(\frac{e^{-\frac{V_0[1-cos(\omega t)]}{q_d \delta R\ \omega}} - x_0}{1 - x_0}\right). \tag{3.28}$$

Similarly, $x(t)$ is obtained by substituting (3.28) into (3.25) and then $M(\phi)$ from (3.17). Thus: $G(\phi) = \dfrac{1}{M(\phi)}$, $i(t) = G(\phi)\ V(t)$ and the results are shown in Fig. 3.8.

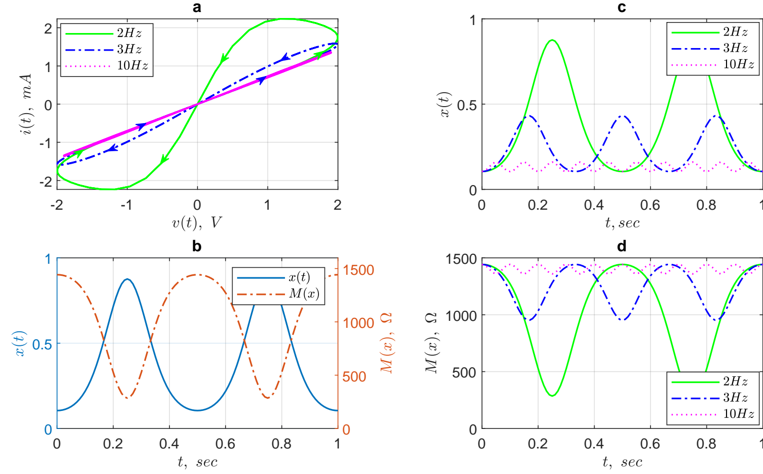

Figure 3.8: Analytical results of FCM with nonlinear dopant drift modal at different input frequencies. $v(t) = V_0 sin(\omega t)$, $V_0 = 2V$, $x_0 = 0.1$, $q_d = 100\mu C$, $R_{off} = 16K\Omega$, $R_{on} = 100\Omega$ and $\delta R = 15.9K\Omega$. (a) I-V characteristics, (b) state variable and memristance for $f = 2Hz$, (c) state variable (d) memristance.

3.3.3/ Effect of window function in memristor modeling: circuit point of view

Figure 3.9 shows the comparison of linear and nonlinear models on the memristance transition with respect to the flowing charge. For the linear dopant drift model, the memristance transits linearly from one state to the other, whereas in the nonlinear drift model, it transits nonlinearly and in a cubic fashion. For unity control parameter, that is $p = 1$, the nonlinearity is more pronounced, however, with the increase in p, the nonlinear model approaches the linear model [70, 107], see Fig. 3.9.

For the same initial conditions, Fig. 3.10 shows the nonlinear models comparison of the memristance transition from its highest resistance state ($R_{off} = 16K\Omega$) to the lowest state ($R_{on} = 100\Omega$) and vice-versa. It shows that the amount of charge q_R required for each

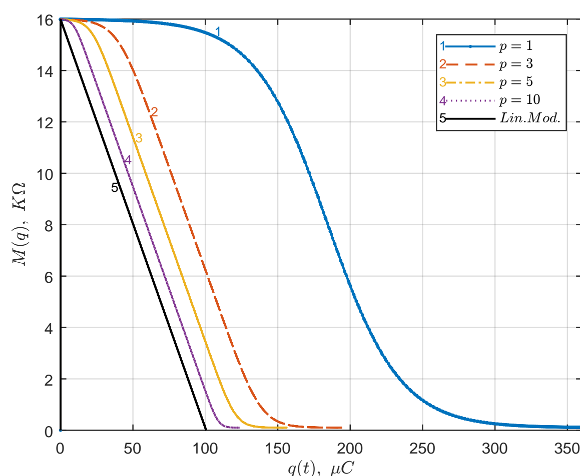

Figure 3.9: Memristance versus charge for linear and nonlinear drift models (Joglekar). It shows that as p increases, the nonlinear drift model tends to the linear model. Window function gives nonlinear model. Window function, in addition to nonlinearity, also increases the dynamics of the charge (or mobile carrier thereby affected by the value of q_d, because $q_d \propto \frac{1}{\mu_v} = \hat{h}(\mu_v)$). Therefore, for a fixed device dimension (i.e D) and doping, only μ_v is affected by the window function, hence q_d. This is due to the fact that window function ensures zero drift of the mobile carrier at the boundaries, thus significantly reduces their mobility and increases q_d.

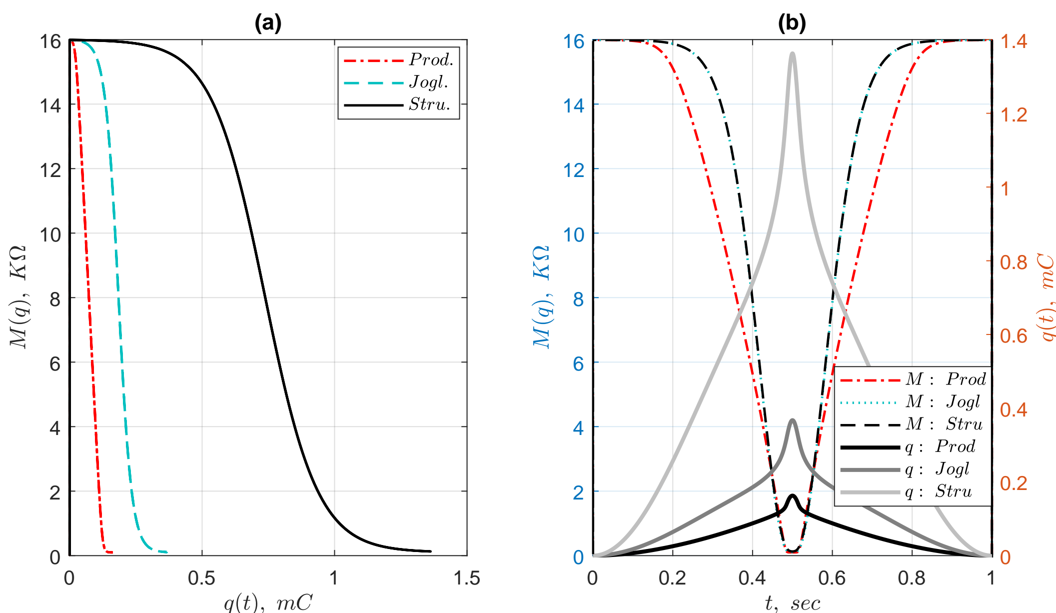

Figure 3.10: Nonlinear models comparison of the full memristance transition between $R_{off} = 16K\Omega$ and $R_{on} = 100\Omega$ with respect to the quantity of charge $q(t)$. The results are obtained under the same initial conditions. This is to show the amount of charge q_R needed for each model to fully transit until R_{off} and then R_{on}. Note that $p = 1$ and $p = 20$ for Joglekar and Prodromakis respectively, and $g_{max}(x) = 1$ for both models allowing for accurate comparison. (**a**) $M(q)$ versus $q(t)$ for Strukov (Stru.), Joglekar (Jogl.) and Prodromakis (Prod.). (**b**) $M(q)$ and $q(t)$ transients.

model to fully transit from R_{off} to R_{on} and vice versa, differs from one model to another. Hence, this is very important in deciding which model to use for any application. Figure 3.11 shows the expanded form of Fig. 3.10. For Joglekar function and for $p = 1$, $q_R = 0.365mC$. For Prodromakis function, $q_R = 0.145mC$, but here $p = 20$ so that $g_{max}(x)$ can scale up to 1 in order to accurately compare the result with the one obtained using Joglekar (i.e $g_{max}(x)$ can scale up to 1 for both models). For Strukov function, $q_R = 1.350mC$

and the detailed comparison of these models is illustrated in Table 3.1. It is to be noted that the amount of charge q_R required to fully drive memristor from R_{off} to R_{on} and vice-versa, depends strongly on the initial memristance and the value of p (i.e the p in the case of Joglekar and Prodromakis).

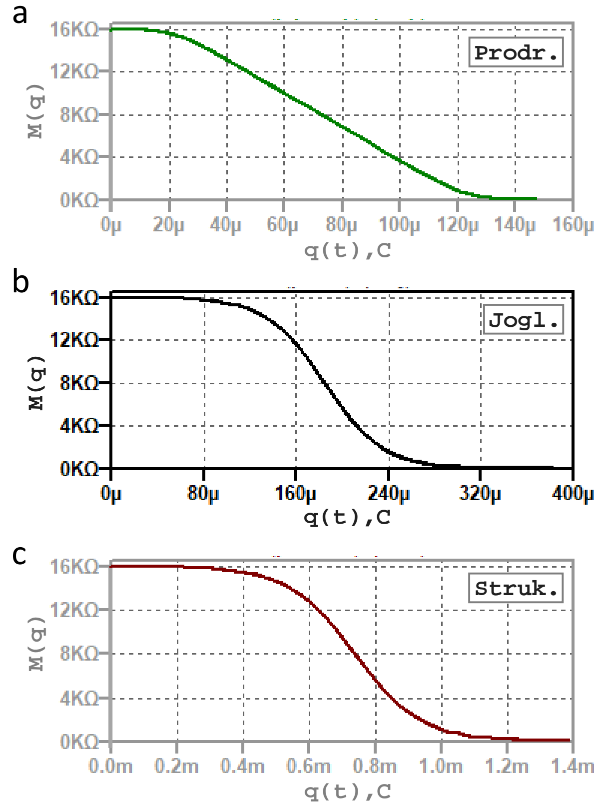

Figure 3.11: Nonlinear models comparison of the full memristance transition between $R_{off} = 16K\Omega$ and $R_{on} = 100\Omega$ with respect to the quantity of the flowing charge $q(t)$. It shows the amount of charge q_R needed for each model to fully transit from R_{off} to R_{on}. Note that $p = 1$ and $p = 20$ for Joglekar and Prodromakis respectively, allowing to have $g_{max}(x) = 1$ for both models. (**a**) Prodromakis (Prodr.) $q_R = 0.145mC$ with $p = 20$, (**b**) Joglekar (Jogl.) $q_R = 0.365mC$ with $p = 1$ and (**c**) Strukov (Struk.) $q_R = 1.350mC$.

To explore the effect of window function in memristor according to the circuit point of view, firstly, Fig. 3.12 compares the results of linear and nonlinear models using Joglekar's window function and for the same circuit parameters. The comparison aims to observe the dynamics of state variable x, the corresponding memristance and the current-voltage graph, by using a periodic input voltage source for three different values of the input amplitudes $0.7V$, $1V$ and $1.2V$, shown respectively, by Figs. 3.12**a1-a3**, **b1-b3** and **c1-c3**.

It is observed that for a small input voltage, for example $0.7V$ given by Fig. 3.12**a1-a3**, the behaviours of the linear and nonlinear models are virtually the same, as can be seen from the corresponding I-V characteristics (Fig. 3.12**a2**). This is due to the fact that the boundary between doped and undoped regions operates not close to the layer limit 0 or D, which means that a small voltage causes a small displacement of the state variable x and hence a small transition of the memristance. Both models respond in the same way when the input voltage is small.

Figures 3.12**b1-b3** show the case where the input voltage is increased to $1V$, hence the state variable displaces farther and the difference between linear and nonlinear models begins to be noticeable. Figures 3.12**c1-c3** show the case when the input voltage is increased to $1.2V$, in fact, the difference between the linear and nonlinear models becomes apparent. Figure 3.12**c1** shows a shift difference in the current transients for linear (i_l) and nonlinear (i_{nl}) models when the voltage is high and it becomes apparent in the corresponding Fig. 3.12**c2**. Figure 3.12**c3** shows that the displacement of the state variable and the memristance transition (x_l and M_{nl} resp.) in the case of the linear model are higher than the ones for nonlinear model (x_{nl} and M_{nl} resp.) when the input voltage is high.

Furthermore, it can be seen in Fig. 3.12**c3** that $x_l \approx 1$. Therefore, increasing the input voltage above $1.2V$, we observe that $x_l \geq 1$, i.e the state variable of the linear drift model is already greater than or equal to one, thus, leads to difficulties because it forces M(x) to take values outside its limiting values $[R_{on}, R_{off}]$. However, this problem is absent when it comes to nonlinear drift model, see Fig. 3.13, where even higher input voltage is used. Both curves of linear and nonlinear models coincide when the voltage is small. Therefore, the difference between linear and nonlinear dopant drift models is only noticeable when the input voltage is substantially high, and that is the point where $x \to 0$ or $x \to 1$.

Furthermore, the proposed window function is compared from the circuit point of view, with the ones proposed by Strukov et al., Joglekar et al., and Prodromakis et al.. The results of this comparison are shown in Fig. 3.13, where the abbreviation P, J, S and N are respectively, Prodromakis, Joglekar, Strukov and our new proposed function. The control parameter $p = 1$ for Joglekar's function, while $p = 20$ is used for Prodromakis window function so that $g(x)|_{x=0.5} = 1$ is the same for both functions except the one by Strukov. Thus, it allows easy comparison.

The setup responds differently with respect to each window function as shown in Figs. 3.13**a1-a4**, **b1-b4** and **c1-c4** for $1V$, $1.2V$ and $1.5V$ respectively. The dynamics of the memristance and the state variable increase with the voltage amplitude. Figures 3.13**c1-c4** show the hard switching case, that is, when the memristor is subjected to a substantial amount of input voltage. It is clear that the choice of a window function for a memristor modeling is very important because each function responds with different dynamics.

Physically, the presence of the window function seems to be artificial and without any physical argument. We will then present in chapter 4, precisely, another point of view to take into account the fact that x must remain in $[0, 1]$ while q can vary in a greater interval.

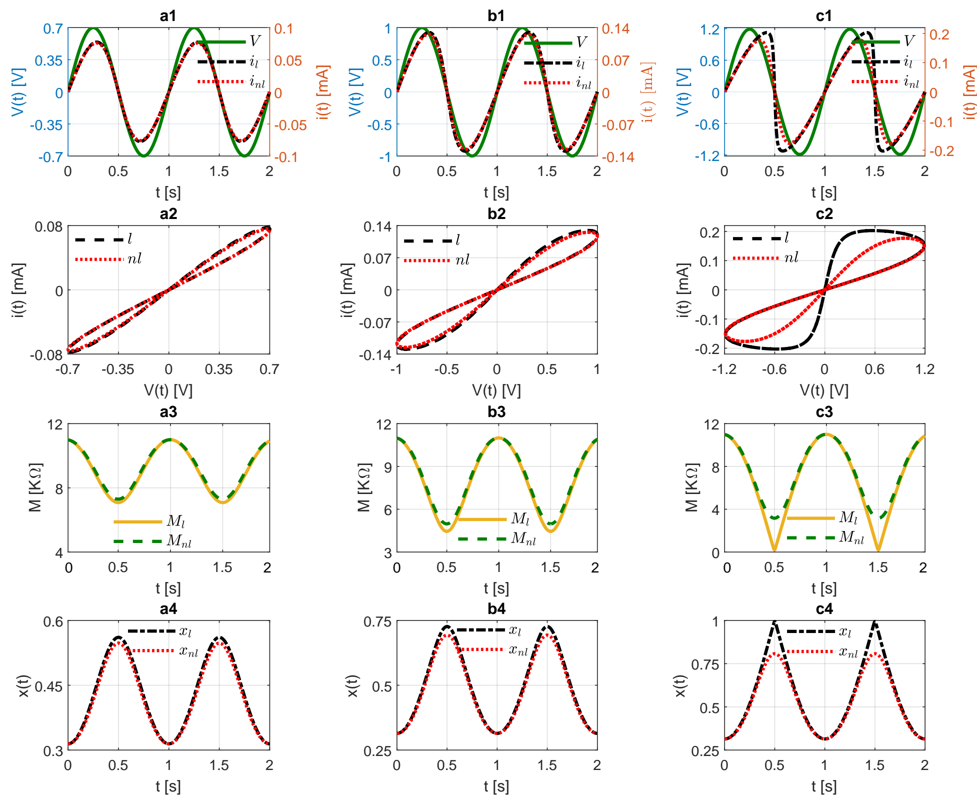

Figure 3.12: Comparison of the linear and nonlinear dopant drift models showing for each case, the nature of the flowing currents, the I-V characteristics, the memristance and the corresponding state variable transition respectively, for (**a1-a3**) $0.7V$, (**b1-b3**) $1V$ and (**c1-c3**) $1.2V$. Where: l and nl are linear and nonlinear models abbreviations, V(t) is the input voltage, i_l and i_{nl} are the flowing currents for linear and nonlinear drift model respectively, similarly, x_l, M_l, x_{nl} and M_{nl} are the state variables and memristances for the linear and nonlinear models.

Table 3.1: Comparison of the three nonlinear dopant drift models

Window function $g(x)$	Proposed	Strukov	Joglekar	Prodromakis
Resolve boundary issues	✓	✓	✓	✓
Impose nonlinear drift	✓	✓	✓	✓
Linkage with linear drift	✗	✗	✓	✓
Control parameter	✗	✗	✓	✓
g_{max} scalability	✗	✗	✗	✓
q_R value	$20mC$	$1.3mC$	$350\mu C$	$150\mu C$

3.4/ SPICE and Analogue models of Memristor

The **SPICE** (**S**imulation **P**rogram with **I**ntegrated **C**ircuit **E**mphasis) software is an electronic circuit simulator allowing to realize the circuit functionality before its fabrication. It is basically a software used for simulating and testing design. Nowadays, there are many developed SPICE softwares, for example PSPICE, LTSPICE, HSPICE, NGSPICE, MULTISIM, TINA and so on. SPICE allows to perform numerous circuit analysis such as transient, AC and DC analysis, parameter sweep, distortion analysis, temperature, noise etc,... under different scalings such as logarithmic, linear, octave etc. Furthermore, SPICE allows to create a schematic component from its equivalent analog circuit

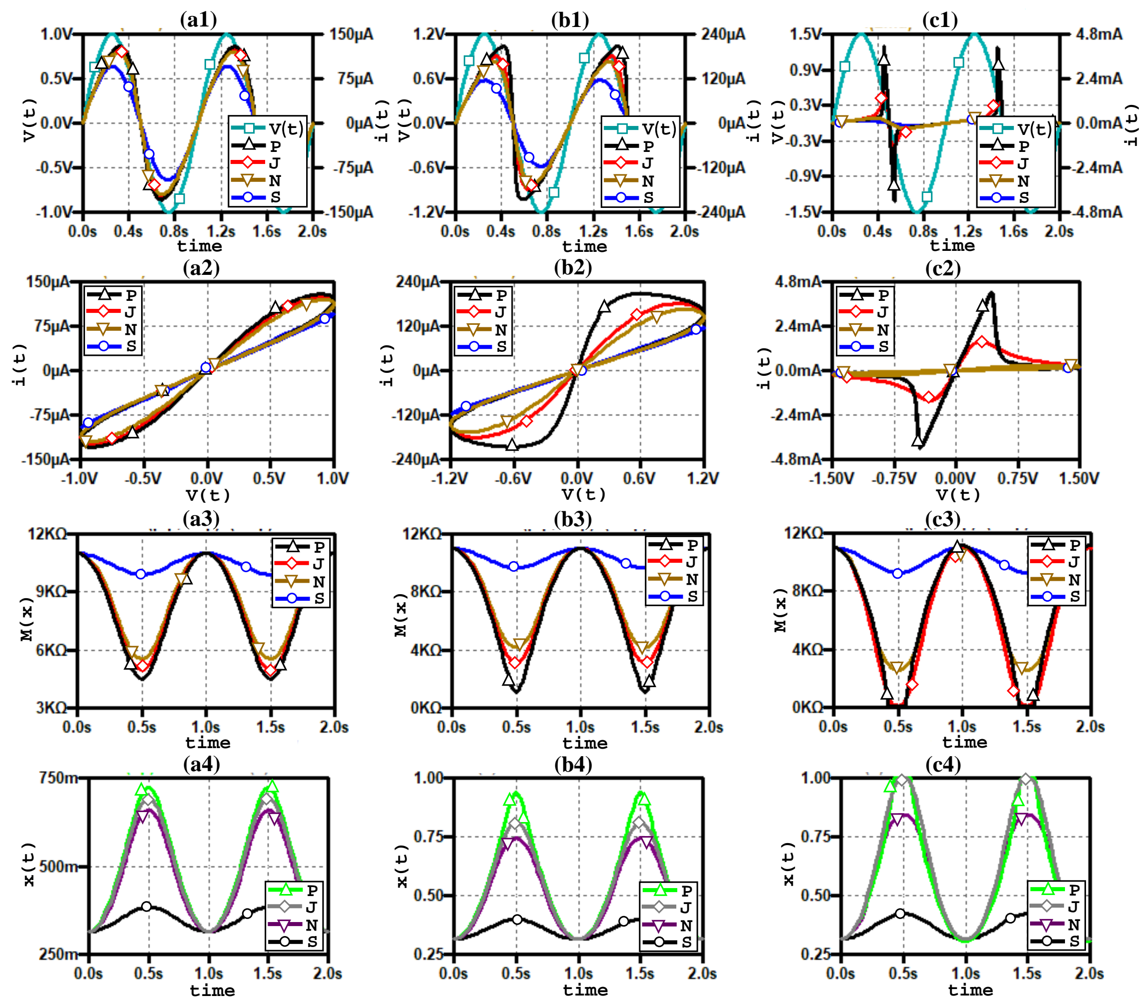

Figure 3.13: Comparing the effect of a window function from the circuit point of view. Our proposed new(N) function is compared with the ones by Strukov(S), Jolekar(J) and Prodromakis(P), for **(a1-a4)** $1V$, **(b1-b4)** $1.2V$ and **(c1-c4)** $1.5V$. V(t) is the input voltage, i(t) is the current, x and M(x) are state variable and memristance. See the ordinate and abscissa of each figure.

description.

One key important aspect is the SPICE and Analog model of a memristor for designing and testing memristor-based applications. Before the realization of physical memristor device by HP lab in 2008, with the exception of L. Chua proposal [10], there was no available memristor model. However, with the discovery of TiO_2 memristor, researchers started to develop different methods mimicking its behaviour.

3.4.1/ SPICE MODELS OF MEMRISTOR

The mathematical description of a given phenomenon can be modeled in SPICE with the aid of its built-in control sources (for example, voltage control voltage source, voltage control current source, behavioral sources, etc) and other components such as resistors, capacitors, OpAmps ... The mathematical description of HP TiO_2 memristor is used to

emulate memristor characteristics, as such many models are reported and some are based on particular applications [107, 110–112, 114, 116, 121–126]. The most commonly used SPICE model is the one developed by Biolek et al. [111], whose setup is shown in Fig. 3.14. Figure 3.14a shows the block diagram representation of the port and state equations of the memristor:

$$V(t) = (R_{off} - \delta R x) I(t) \text{ and } \frac{dx}{dt} = kI(t)f(x). \tag{3.29}$$

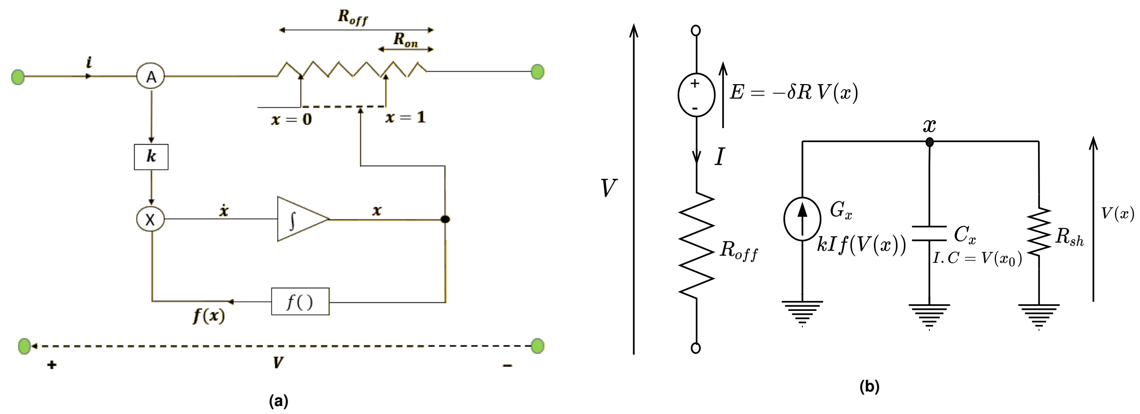

Figure 3.14: SPICE implementation of TiO_2 memristor model for simulation purpose. (a) Block diagram representation of the memristance function: $V = R(x)i$ and $\frac{dx}{dt} = kf(x)i$, (b) Equivalent SPICE model: E is an E-type voltage source (i.e voltage controlled voltage source), G is a G-type current source (voltage dependent current source) and R_{sh} is the shunt resistance of the integrator.

The ammeter (A) senses the current flowing through the memristor, meanwhile the memory effect is modelled by means of a feedback controlled integrator. The feedback of the nonlinear window function $f(x)$ models the nonlinear dopant drift and the influence of the boundary conditions. The memristance value between R_{off} and R_{on} is determined by the coordinate of $x \in (0, 1)$.

Figure 3.14b shows the equivalent SPICE schematic of equation (3.29). The capacitor C_x whose initial voltage models the initial state of the normalized width x_0, is used as the integrator of the differential state equation. The port equation is modelled with the aid of E-type voltage source (voltage dependent voltage source) whose source is the voltage of capacitor and then multiplied by the gain $-\delta R$, and it is connected in series with a resistor R_{off}. $V(x)$ is the voltage of the capacitor C_x and it models the normalized width x of the memristor, while R_{sh} is the shunt resistor grounding the integrator unit. The integrand, that is, the quantity on the right hand side of the state equation is modeled with the aid of a G-type current source (voltage dependent current source) that multiplies the memristor current I by the gain $kf(V(x))$. The SPICE netlist file of Fig. 3.14b is given in Table A.1 (Appendix A), and it is used to create memristor SPICE component for simulation purpose. The integral of the current (or charge) and voltage (or flux) respectively, flowing through and across the memristor can be modelled using the E-type voltage source,

hence allowing to visualize the monotonically increasing function of q versus ϕ in the ϕ-q plane.

The initial state of the memristor is given by the initial voltage $V(x_0)$ across the capacitor. The initial memristance R_i is determined as: $R_i = R_{off} - \delta R x_0$. Figure 3.15 shows the results of the memristor netlist file in Table A.1 (Appendix A). The result is obtained using a sine voltage source connected across the port terminals *pl* and *mn* of the memristor.

Figure 3.15a shows the transient results of voltage and current for an input voltage amplitude of $1.2V$ and the corresponding I-V characteristic is given in Fig. 3.15b. Furthermore, Fig. 3.15c shows the corresponding monotonically increasing ϕ-q function, thus matching the characteristics of the memristor from its constitutive relationship. Meanwhile, Fig. 3.15d shows the memristance with respect to the transition of the device state variable.

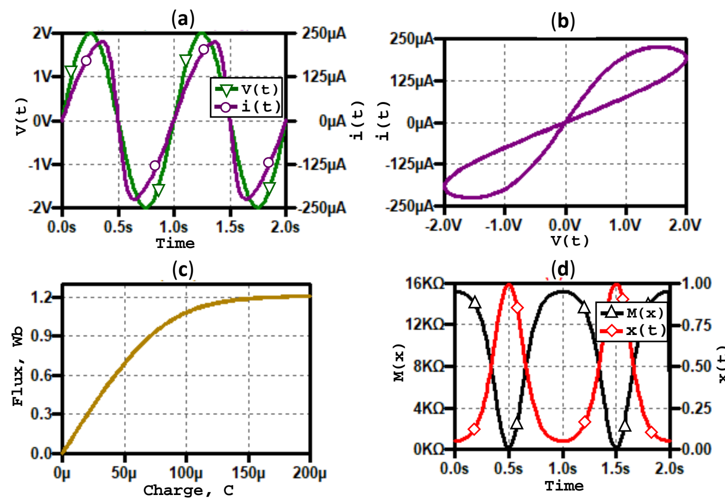

Figure 3.15: Simulation results of the memristor netlist file given in Table A.1. $V = V_0 sin(\omega t)$, $V_0 = 1V$, $f = 1Hz$, $R_{on} = 100\Omega$, $R_{off} = 16K\Omega$, $\mu_v = 10fm^2/(V.s)$ and $D = 10nm$, which gives $q_d = 100\mu C$. (**a**) V and i transients, (**b**) I-V characteristic, (**c**) ϕ-q curve and (**d**) memristance and state variable transitions.

3.4.2/ Analogue models of Memristor

Analogue memristor models are developed using analog and active components such as operational amplifiers, hence modeling the behaviour of memristor for simulation [51, 127–131]. Analog models can be easily implemented in the laboratory for practical and research purposes. For example, Fig. 3.16 shows an analog model of a flux-controlled memristor [127]. The model is analysed by considering different input signals, for example sinusoidal, triangular input voltage sources etc..., and it shows a pinched hysteresis loop which is the primary signature of a memristor.

Figure 3.14b is similar to Fig. 3.16 with difference in the integration unit, that is RC and operational amplifier respectively. Comparing the two figures, one can see that $R_{sh} = R$

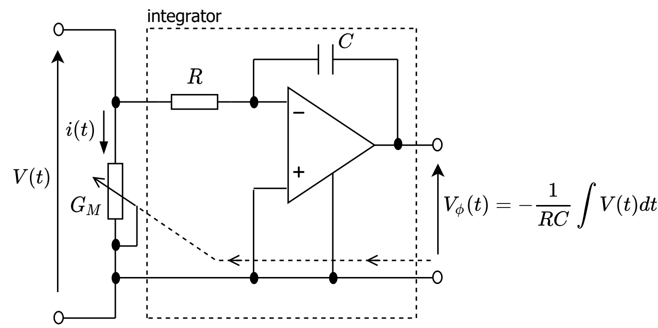

Figure 3.16: Analogue model of memristor [127].

and $C_x = C$. As shown in the introduction that for flux-controlled memristors, the state variable is a function of flux, in other words, the memristor dynamics depends upon the flux whose magnitude is proportional to the voltage across the memristor. In Fig. 3.16, the operational amplifier block is used as an integrator to generate its output voltage proportional to the flux. The output flux is expressed as

$$V_\phi(t) = \frac{1}{\tau}\int V(t)dt, \tag{3.30}$$

where $\tau = RC$ is a time constant. The memductance $G_M(t)$ depends linearly on $V_\phi(t)$, with:

$$G_M(t) = G_0 + K_G V_\phi(t), \tag{3.31}$$

where G_0 and K_G are constants. Finally, the current $i(t)$ is given by:

$$i(t) = G_M(t).V(t). \tag{3.32}$$

Equations (3.30)-(3.32) are analyzed using three different types of input voltage, namely: sine, triangular and square wave, respectively.

3.4.2.1/ Sine input

Let consider the applied input signal to be a sine voltage $V(t)$ as:

$$V(t) = V_0 sin(\omega t), \tag{3.33}$$

whose flux $\phi(t)$ is represented by the voltage $V_\phi(t)$ obtained by integrating (3.33):

$$V_\phi(t) = \frac{1}{\tau}\left[\int_0^t V_0 sin(\omega t')dt' + \phi_0\right],$$

$$V_\phi(t) = \frac{V_0}{\tau\omega}(1 - cos(\omega t)) + \frac{\phi_0}{\tau}, \tag{3.34}$$

where ϕ_0 is the initial flux. Knowing the flux $V_\phi(t)$, the memductance $G_m(t)$ and the current $i(t)$ are to be calculated using equations (3.31) and (3.32) respectively. Figure 3.17 shows the results of sinusoidal input voltage, observed for different frequencies and Fig. 3.17 shows the results obtained for sine input voltage with values parameters: $R = 1K\Omega$, $C = 1\mu F$, $G_0 = 0.5S$ and $K_G = 10S\,V^{-1}$. The results are significantly modified with the changes of G_0, K_G and frequency. Nevertheless, the model is working at low frequencies.

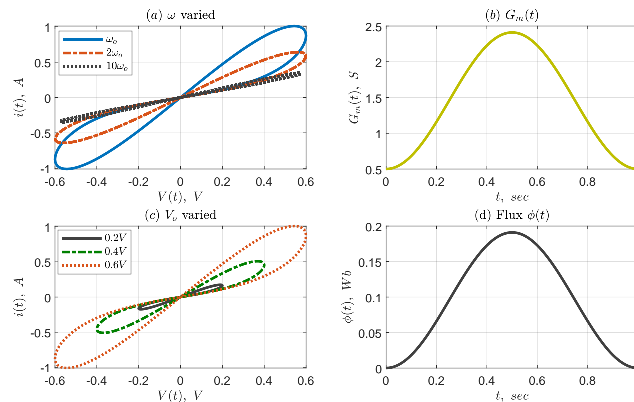

Figure 3.17: Results of the sinusoidal input voltage. Parameters set: $R = 1k\Omega$, $C = 1\mu F$, $G_0 = 0.5S$ and $K_G = 10S\,V^{-1}$ (a) $V_o = 0.6V$ and variation of input frequency, $\omega_o = 2\pi f_o$ with $f_o = 1Hz$. (b) memductance for ω_o and $V_o = 0.6V$, (c) at ω_o frequency and variation of voltage amplitude V_o, (d) the flux $\phi(t)$ for ω_o and $V_o = 0.6V$.

3.4.2.2/ Triangular input

Here, the periodic input voltage is a triangular one as shown in Fig. 3.18. The same approach is used as in the case of sine input but with new input voltage expression. The triangular waveform of Fig. 3.18 is symmetrical, hence:

$$t_2 = 2t_1, \quad t_3 = 3t_1 \text{ and } t_4 = 4t_1 \text{ with } t_1 = \frac{T}{4},$$

where T is the period in seconds. The voltage expressions of the various slopes are obtained to be:

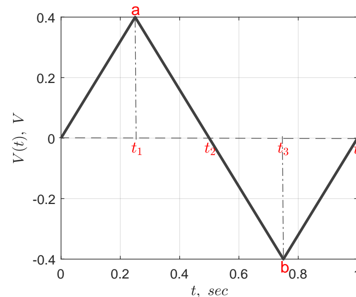

Figure 3.18: Triangular input voltage.

First rising slope for the time interval 0 to t_1 (i.e, 0 to point a):

$$V_{t_1} = \frac{V_p}{t_1}t.$$

Falling slope for the time interval t_1 to t_3 (i.e point a to b):

$$V_{t_3} = -\frac{V_p}{t_1}(t - 2t_1).$$

Second rising slope for the time interval t_3 to t_4:

$$V_{t_4} = -\frac{V_p}{t_1}(4t_1 - t).$$

Where V_{t_1}, V_{t_3} and V_{t_4} are the instantaneous voltages of $V(t)$ within the time t_1, t_3 and t_4 respectively. V_p is the peak value of $V(t)$. It implies that:

$$\begin{cases} V(t) = \frac{V_p}{t_1}t, & \text{if } t \in [0,\ t_1], \quad (3.35) \\ V(t) = -\frac{V_p}{t_1}(t - 2t_1), & \text{if } t \in [t_1,\ t_3], \quad (3.36) \\ V(t) = -\frac{V_p}{t_1}(4t_1 - t), & \text{if } t \in [t_3,\ t_4], \quad (3.37) \end{cases}$$

The corresponding flux expression ($V_\phi(t)$) is obtained by integrating (3.35), (3.36) and (3.37) accordingly, with a special care to ensure the voltage continuity:

$$\begin{cases} V_\phi(t) = \frac{1}{\tau}\int_0^{t_1} V_{t_1} dt, & \text{if } t \in [0,\ t_1], \quad (3.38) \\ V_\phi(t) = \frac{1}{\tau}\int_{t_1}^{t} V_{t_3} dt + k_1, & \text{if } t \in [t_1,\ t_3], \quad (3.39) \\ V_\phi(t) = \frac{1}{\tau}\int_{t_3}^{t} V_{t_4} dt + k_2, & \text{if } t \in [t_3,\ t_4], \quad (3.40) \end{cases}$$

$V_\phi(t)$ is proportional to the instantaneous flux of $V(t)$. k_1 and k_2 are constants to be calculated in order to eliminate the jump discontinuities. $V_\phi(t)$ must be continuous at $t = t_1$ and $t = t_3$, otherwise there will be discontinuities at points a and b (Fig. 3.18). The constants k_1 and k_2 are obtained respectively, by equating equations (3.38) and (3.39) for $t = t_1$, and then (3.39) and (3.40) for $t = t_3$.

From equations (3.38) and (3.39):

$$\frac{1}{\tau}\int_0^{t_1} V_{t_1} dt = \frac{1}{\tau}\int_{t_1}^{t_1} V_{t_3} dt + k_1.$$

$$\therefore \left.\left\{\frac{1}{\tau}\int \frac{V_p}{t_1} t\ dt = \frac{1}{\tau}\int -\frac{V_p}{t_1}(t-2t_1)\ dt + k_1\right\}\right|_{t=t_1} \Rightarrow$$

$$k_1 = -\frac{V_p\ t_1}{\tau} = -\frac{V_p\ T}{4\tau}. \tag{3.41}$$

Similarly at point 'b', i.e from equations (3.39) and (3.40):

$$\frac{1}{\tau}\int V_{t_3} dt + k_1 = \frac{1}{\tau}\int V_{t_4} dt + k_2.$$

$$\therefore \left.\left\{\frac{1}{\tau}\int \left(-\frac{V_p}{t_1}(t-2t_1)\right) dt + k_1 = \frac{1}{\tau}\int \left(-\frac{V_p}{t_1}(4t_1-t)\right) dt + k_2\right\}\right|_{t=t_3} \Rightarrow$$

$$k_2 = \frac{8V_p\ t_1}{\tau} = \frac{4V_p\ T}{\tau}. \tag{3.42}$$

The constants k_1 and k_2 are obtained from (3.41) and (3.42) respectively, and they are used in equations (3.38)-(3.40) to determine the flux $V_\phi(t)$. Hence knowing these parameters, the conductance $G_m(t)$ is obtained using (3.31), allowing to determine the current $i(t)$ given by (3.32). Figure 3.19 shows results for the voltage, the current, the flux, the conductance and the corresponding pinched hysteresis loop. Values of parameters: obtained for $V_p = 0.4V$, $G_0 = 10S$ and $K_G = 0.2S\,V^{-1}$.

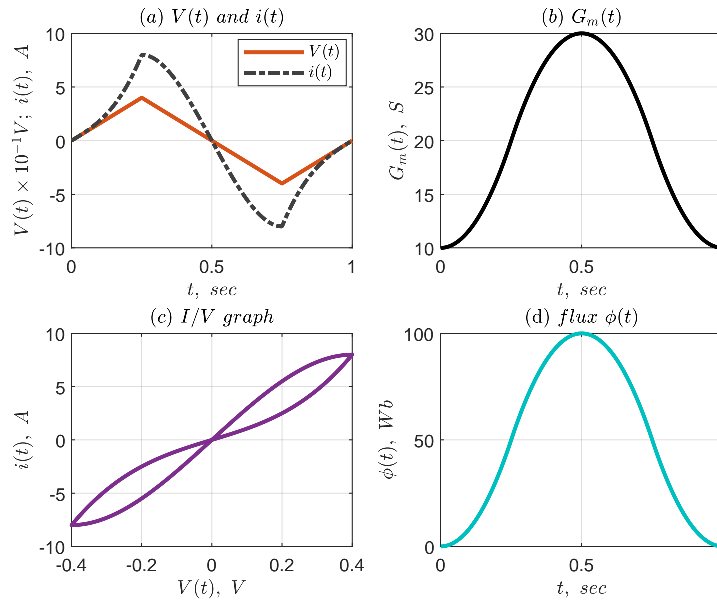

Figure 3.19: Results of triangular input voltage. $V_p = 0.4V$, $f = 1Hz$, $R = 1K\Omega$, $C = 1\mu F$, $G_0 = 10S$ and $KG = 0.2S\,V^{-1}$.

3.4.2.3/ RECTANGULAR OR SQUARE WAVE INPUT

The periodic input applied to the memristor is a square wave input voltage with amplitude $\pm V$. This type of input can be expressed as:

$$V(t) = \begin{cases} V_+, & \text{if } 0 \leq t < t_1 \\ V_-, & \text{if } t_1 \leq t < t_2 \\ V_+, & \text{if } t_2 \leq t < t_3 \\ V_-, & \text{if } t_3 \leq t < t_4 \\ \vdots, & \vdots \end{cases} \tag{3.43}$$

and the corresponding flux is obtained by integrating (3.43) as follows:

$$V_\phi(t) = \begin{cases} V_+t, & \text{if } 0 \leq t < t_1 \\ V_-t + Vi_1, & \text{if } t_1 \leq t < t_2 \\ V_+t + Vi_2, & \text{if } t_2 \leq t < t_3 \\ V_-t + Vi_3, & \text{if } t_3 \leq t < t_4 \\ \vdots, & \vdots \end{cases} \tag{3.44}$$

where Vi_1, Vi_2 and Vi_3 are constants for the continuity at time t_1, t_2 and t_3 respectively.

Let consider the time interval as 0.25s, then $t_1 = 0.25$, $t_2 = 0.5$, $t_3 = 0.75$ and $t_4 = 1$. The constants are obtained to be: $Vi_1 = 0.25V_+ - 0.25V_-$, $Vi_2 = -0.25V_+ + 0.25V_-$ and $Vi_3 = 0.5V_+ - 0.5V_-$. Similarly, the memductance $G_m(t)$ and the current $i(t)$ are calculated using equations (3.31) and (3.32) respectively. Figure 3.20 shows the result of the square wave input voltage for $V = \pm 1V$, $R = 1K\Omega$, $C = 1\mu F$, $G_0 = 1S$ and $KG = 5S\,V^{-1}$.

3.4.3/ PASSIVE MODELS OF THE MEMRISTOR EMULATOR

Figure 3.21 shows the schematic of a passive memristor emulator [130]. The model is similar to the one in Fig. 3.16 with the exception that junction field effect (JFET) transistor is used instead of the operational amplifier, but without any need of internal power to operate. The voltage across the gate (G) terminal with respect to the source (S) terminal corresponds to the voltage V_C across the capacitor C provided that the gate resistance (R_G) is infinite, that is no current flows through R_G. The role of the gate resistance R_G is to avoid leakage current through the gate, therefore, it separates the gate from the output of the RC cell which acts as a passive lossy integrator having the cutoff frequency (f_c), as:

$$f_c = \frac{1}{2\pi RC}.$$

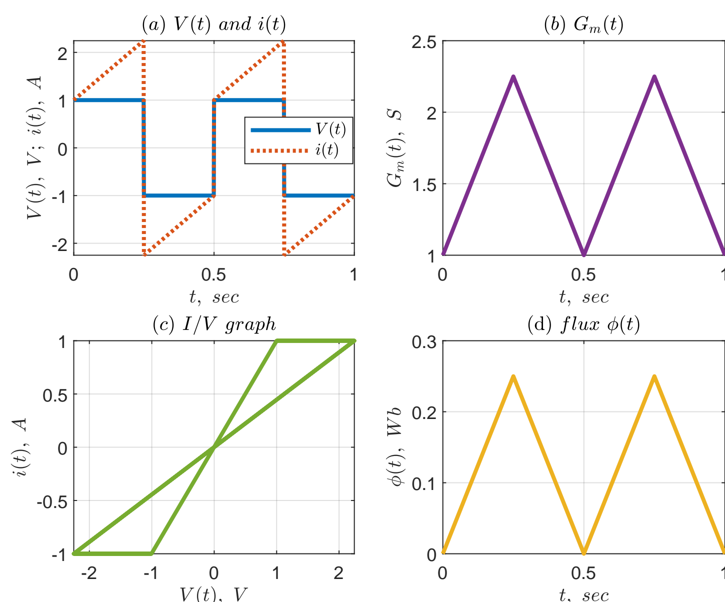

Figure 3.20: Results of square wave input voltage. $V = \pm 1V$, $f = 2Hz$, $R = 1K\Omega$, $C = 1\mu F$, $G_0 = 1S$ and $KG = 5S\,V^{-1}$.

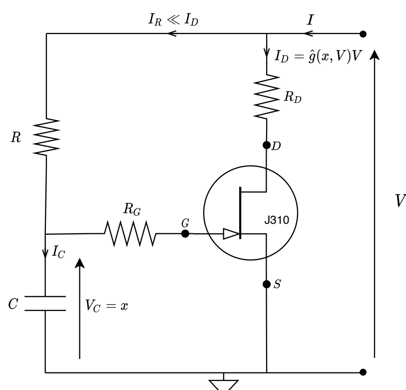

Figure 3.21: Schematic of a passive memristor emulator [130].

R_D is a small resistance (optional) connected to the drain terminal in order to measure the current flowing through drain and then the source terminal. Since no current goes into the gate terminal of the JFET, the current through the resistor R is the same than the one through the capacitor, that is: $I_R = I_C$. Therefore, $V_C = V_{GS}$, controls the current through the D-S junction. For frequencies above f_c, the characteristics of Fig. 3.21 corresponds to the characteristics of ideal integrator. Taking into account the differential equation of the RC cell and its high impedance level (i.e $I_R \ll I_D$), the mathematical relationship of Fig. 3.21 can be expressed from Kirchhoff's laws:

$$C\frac{dV_C}{dt} + \frac{V_C - V}{R} = 0 \quad \Rightarrow$$

$$\frac{dV_C}{dt} = \frac{1}{RC}(V - V_C). \tag{3.45}$$

The transconductance of the device is controlled by the voltage V_C across the capacitor

and hence it is equivalent to the state variable x of the system: $V_C = x$. Furthermore, the state variable V_C (or x) corresponds to the integral of the port voltage V and $V_{DS} = V$ because R_D is negligible. Therefore, the characteristics of JFET transistor as given in [127], is:

$$I_D = \hat{g}(V_{GS}, V_{DS})V_{DS} = \hat{g}(x, V)V. \tag{3.46}$$

From equations (3.45) and (3.46) we obtained the following state dependent Ohm's law relationship:

$$\frac{dx}{dt} = \frac{1}{RC}(V - x), \tag{3.47}$$

$$I = \hat{g}(x, V)V. \tag{3.48}$$

Recall that flux-controlled memristor and an ideal flux-controlled memristor are expressed respectively, by: $\left\{I = \hat{g}(x, V)V,\ \frac{dx}{dt} = \hat{f}(x, V)\right\}$ and $\left\{I = \hat{g}(x)V,\ \frac{dx}{dt} = \hat{f}(V)\right\}$, where $\hat{g}$ (a memductance) and $\hat{f}$ are nonlinear functions of the state variable and the voltage.

For appropriate choice of parameters and under specific conditions, equations (3.47) and (3.48) show that Fig. 3.21 models a flux-controlled memristive system. Furthermore, it could even model an ideal flux-controlled memristor provided that it meets two conditions as outlined in [130], thus: (1) *The memductance is independent of the voltage V (thus a small voltage swing) and* (2) *The state variable must be negligible compared to the voltage V (this will be fulfilled for relatively high signal frequencies when the passive integrating RC cell will show adequate attenuation)*.

Figure 3.22 shows that the pinched hysteresis loop can be observed by plotting I_D versus V (or V_{DS}) for different values of the input frequency, R and C.

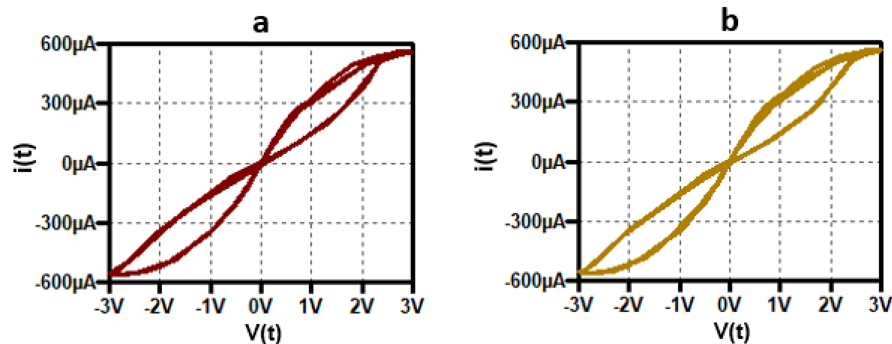

Figure 3.22: Response of the emulator in Fig. 3.21 (a) $R = 1.5M\Omega$, $R_G = 100M\Omega$, $C = 100pF$, $R_D = 1$, $V = 3V$ at $1KHz$. (b) $R = 1M\Omega$, $R_G = 100M\Omega$, $C = 100pF$, $R_D = 1$, $V = 3V$ at $1592KHz$ (i.e cutoff frequency). The response is affected by the value of of the input frequency, and the values of R and C which make the integrator causing different phase shifts.

3.4.4/ Proposition of Modification

The analogue model in Fig. 3.21 can be modified in certain ways to observe the pinched hysteresis curve. We propose that the condition $I_R \ll I_D$ and the condition $f \geq f_c$ can be avoided by using:

- Current Transformer.
- Current mirror.
- Hall effect sensor (H.E.S).

3.4.4.1/ Current transformer

Figure 3.23 shows the schematic model using current transformer (CT) in which the flowing current I_R through the RC branch is determined by the influence of the CT. The input current I is the same as the flowing current through the drain-source path of the JFET.

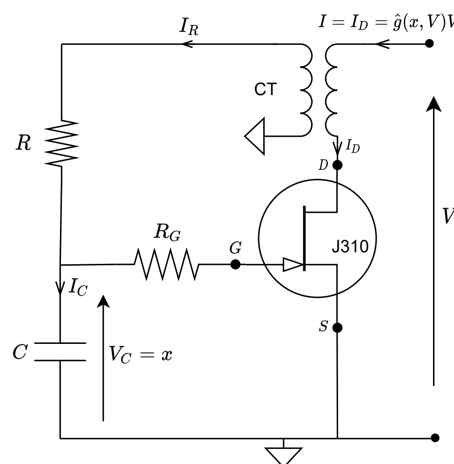

Figure 3.23: Analogue model using current transformer (CT), $I_D = I$, while $I_R = \alpha I$, α being the CT coefficient.

3.4.4.2/ Current mirror

A current mirror is a circuit designed to copy a current through one active device by controlling the current in another active device of a circuit, keeping the output current constant regardless of loading. It consist of two transistors with identical V_{GS}. One transistor is connected as diode and is driven by incoming or reference current I_{in}, and the other one provides desired outgoing current I_{out} according to the following relationships. Figure 3.24 shows three different formations of current mirror using MOSFET transistors. The current mirror will copy the current I_D to the RC branch, hence the condition $I_R \ll I_D$ can be avoided.

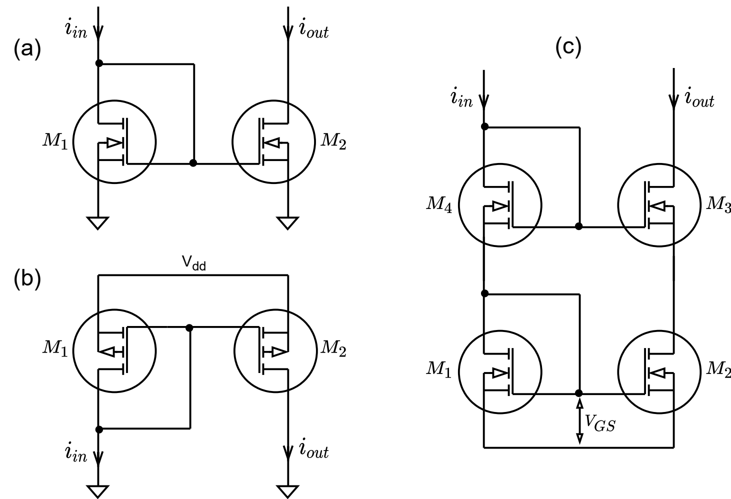

Figure 3.24: Some examples of current mirror formations. (a) N-type MOSFET, (b) P-type MOSFET and (c) Cascode current mirror [Perfect current mirror ($V_{DS_{M1}} = V_{DS_{M2}}$)].

For a MOSFET transistor with width W and length L, the current flowing through the device is described as:

$$I_D = \frac{\mu_n C_{ox}}{2}\frac{W}{L}(V_{GS} - V_{TH})^2(1 + \lambda V_{DS}), \tag{3.49}$$

where I_D is the drain current, V_{DS} is the drain-source voltage, V_{GS} is the gate-source voltage, V_{TH} is the threshold voltage, L is the length of the transistor, W is the width of the transistor, C_{ox} is the specific capacitance of the gate in F/m^2 and μ_n is the mobility. By ignoring the channel length modulation effect $(1 + \lambda V_{DS})$, the relationship reduces to:

$$I_D = \frac{\mu_n C_{ox}}{2}\frac{W}{L}(V_{GS} - V_{TH})^2. \tag{3.50}$$

The input and output currents of the current mirror are expressed respectively as:

$$I_{D_{in}} = \frac{\mu_n C_{ox}}{2}\left(\frac{W}{L}\right)_{in}(V_{GS} - V_{TH})^2,$$

$$I_{D_{out}} = \frac{\mu_n C_{ox}}{2}\left(\frac{W}{L}\right)_{out}(V_{GS} - V_{TH})^2.$$

By taking the ratio of output to input currents we have:

$$I_{D_{out}} = \left(\frac{\left(\frac{W}{L}\right)_{out}}{\left(\frac{W}{L}\right)_{in}}\right) I_{D_{in}} \tag{3.51}$$

If the two transistors have the same technological parameters and identical dimensions, then:

$$I_{D_{out}} = I_{D_{in}}$$

Choosing appropriate width sizes, desired output current can be obtained without affect-

ing the input current.

3.4.4.3/ Hall effect sensor

Figure 3.25 shows the model schematic using hall effect sensor (H.E.S). The H.E.S senses the current I_D and its output having to be passed through the digital to analog converter DAC, hence generating the current I_C from the effect of I_D. Therefore, V_C controls V_{GS} and hence the conductance of the memristor. Arduino board can be used for programming the sensor as well as its source, i.e $5V$. H.E.S has 3 pins: input, ground and output. The output pin is connected to the common node of the capacitor and gate of the JFET. The variation of the sensor ouput will be proportional to the voltage V_C across the capacitor C, which in turn is proportional to the system state x which determines the conductance of the memristor.

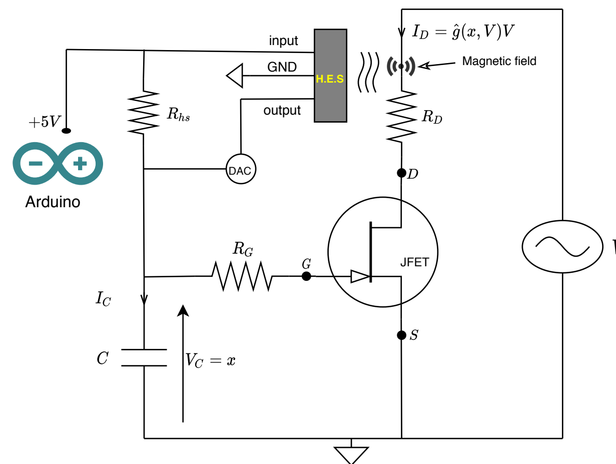

Figure 3.25: Modified passive memristor emulator with hall effect sensor.

3.5/ Conclusion

Memristor technologies are introduced, then followed by the details modeling analysis of TiO_2 memristor. According to the mode of excitation, the analytical solutions and results of linear and nonlinear dopant drift models are obtained. The difference between linear and nonlinear models is highly observable as the state variable of the system approaches 0 or 1. It shows that for a small input voltage applied to the memristor, the linear and nonlinear models respond fairly the same because the state variable operates within the bulk of the device, not toward the edge. The effect of increasing input frequency is shown for each model and the shrinkage of the pinched hysteresis loop is due to the inverse relationship between the flowing charge $q(t)$ and the input frequency ω [i.e $q(t) = \frac{I_o}{\omega}(1 - cos(\omega t))$]. Furthermore, a new window function is presented, which is derived from the Hann window

function. Its response is compared with the ones obtained from the three other functions by Strukov, Joglekar and Prodromakis. From the circuit point of view, it was shown that the choice of window function is very important for memristor modeling, because each model responds differently due to different level of imposed nonlinearities.

The model of TiO_2 memristor is used to create memristor component in SPICE for circuit simulation purposes. This approach is extended whereby analog components, such as operational amplifier, are used to mimic the behaviour of memristor in SPICE for simulation of memristor based applications. The passive model of the memristor is working under some restricted values of parameters. We proposed that these drawbacks can be avoided by using some devices, including current transformer, current mirror or Hall effect sensor. However, this part of the thesis is not yet achieved.

Main Contribution (1)

4

ϕ-q CURVE DESCRIPTION AND THE NEW MODEL

4.1/ INTRODUCTION

In this chapter, we give a detailed ϕ-q curve description of the TiO_2 memristor. Firstly, giving the role of the parameter q_0 for characterizing the memory effect of the device, then following the thorough description of the ϕ-q curve which also forms the foundation of our new memristor model. Then, the circuit response of the new model is obtained by SPICE simulation.

4.2/ MEMORY EFFECT

Memristor being a memory resistor, the memory effect of this device becomes a point of interest, especially in the context of applications. Having in mind that $M = \dfrac{d\phi}{dq}$ with $\phi = \int_{-\infty}^{t} V(\tau)d\tau$ and $q = \int_{-\infty}^{t} i(\tau)d\tau$, the fact that the memristance is expressed between two reference points – the previous and the present state – makes the memristor to exhibit memory effect, manifested in its hysteretic behaviour. The initial memristance is given by the relation $\hat{f}(\phi_0, q_0)$ defined by the initial conditions of the memristor at time $t = 0$.

The memristor is initially at M_0 from the last moment it was used. When the memristor is subjected to power supply once again and depending on the polarity of the voltage or current source, the memristance, expressed in ohms, transits towards R_{on} or R_{off} emanating from M_0 along the transition curve, see Fig. 4.1.

The forth or back movement of the boundary between doped and undoped regions is proportional to the quantity of charge flowing through the memristor. We have shown in

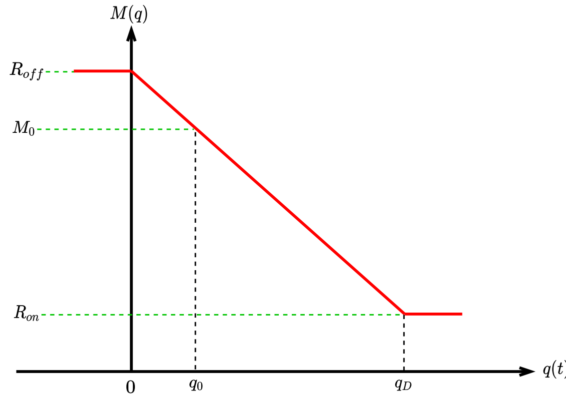

Figure 4.1: Memristance transition with respect to the flowing charges.

equation (3.4) that $q_d = \dfrac{D^2}{\mu_v R_{on}}$ is the amount of charge required to move the boundary between doped and undoped TiO_2 from $w \to 0$ to $w \to D$, or equivalently from $x \to 0$ to $x \to 1$. Moreover, the charge q_d can be viewed as the threshold charge serving as a charge scaling factor whose value is determined by the technology parameters. Typically [12], for $R_{off} = 16K\Omega$, $R_{on} = 100\Omega$, $D = 10^{-8}m$ and $\mu_v = 10^{-14}m^2/V.s$, then: $q_d = 100\mu C$. From equation (3.3), the equivalent memristance expression, in simplest case of linear dopant drift model, writes:

$$\begin{aligned} M(x) &= R_{off} - \delta R\, x, \\ \frac{dx}{dt} &= \frac{i(t)}{q_d}. \end{aligned} \tag{4.1}$$

To vividly explore the memory effect of the memristor device, here it is rather considered at time $t = 0$, $q(t) = \displaystyle\int_{-\infty}^{0} i(\tau)d\tau = q_0$ representing the previous amount of charge passed through the device, while $x(t) = x_0$ is the initial position of the boundary between the doped and the undoped regions, characterizing the initial memristance of the memristor. Then, at time $t \in [0 \cdots + \infty[$ and due to the flowing current $i(t)$, it becomes $q(t) = q_0 + q'(t)$ with $q'(t) = \displaystyle\int_{0}^{t} i(\tau)d\tau$. From equation set (4.1), $x(t)$ is processed with respect to the initial charge q_0 and the charge scaling factor q_d as:

$$\begin{aligned} x(t) &= \frac{q(t)}{q_d}, \\ &= \frac{1}{q_d}\left[q_0 + q'(t)\right], \end{aligned} \tag{4.2}$$

and the equivalent memristance becomes:

$$M(q) = R_{off} - \delta R \frac{(q' + q_0)}{q_d} = R_i - \delta R \frac{q'}{q_d}, \tag{4.3}$$

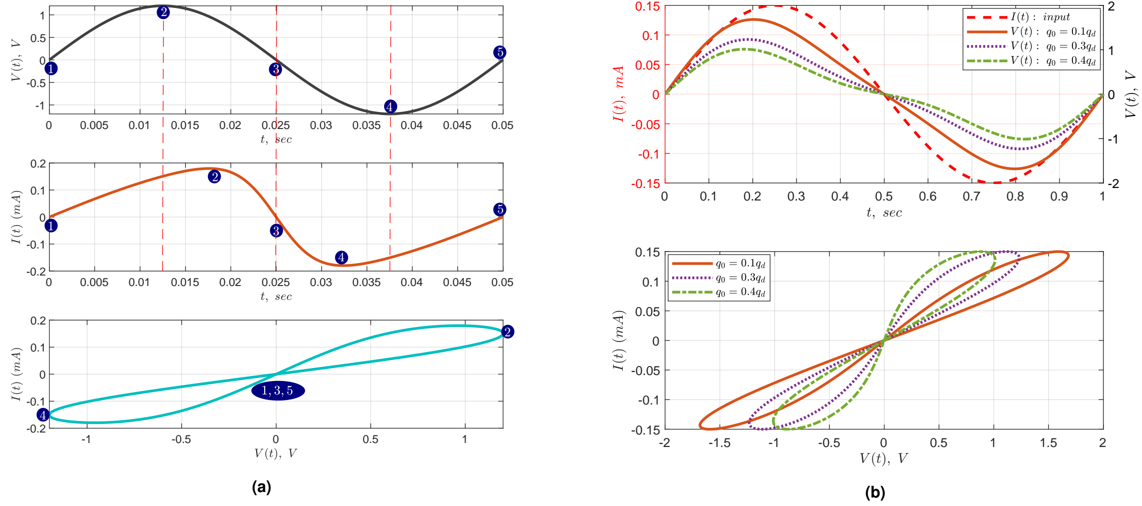

Figure 4.2: (a) The voltage and current waveforms in a memristor are always in phase. However, one can see that the current is not maximum even so the causative voltage is maximum (point 2), emphasizing the nonlinear nature of the device. Points 1, 3 and 5 are the evidence of pinched hysteresis loop at (0,0) i.e $I(t) = 0$ whenever $V(t) = 0$ and vice versa. (b) Effect of initial charge q_0 on the memristor I-V characteristic, thus reflecting the memory effect of the device. $R_{off} = 16K\Omega$, $R_{on} = 100\Omega$, $I_0 = 0.15mA$, $f = 1Hz$, $\mu_v = 10f\ m^2/V.s$, $D = 10nm$, then $q_d = 100\mu C$ and $q_0 = 0.1q_d,\ 0.3q_d$ and $0.4q_d$.

where $R_i = R_{off} - \delta R\ \dfrac{q_0}{q_d}$ is the initial memristance defining the memory effect of the memristor. Then, the Ohm's law $V(t) = M(q)I(t)$ depends not only on the current $I(t) = \dfrac{dq}{dt}$, but also on the initial charge q_0 having already flowed through the memristor before the initial conditions. Therefore, q_0 defines the initial memristance $M(q_0)$ of the device.

Figure 4.2b shows that for fixed input amplitude and frequency, the value of initial charge affects the I-V characteristic of the device. The result is obtained for three different initial conditions, as: $q_0 = 0.1q_d$, $q_0 = 0.3q_d$ and $q_0 = 0.4q_d$ respectively.

4.3/ ϕ-q CURVE

The pinched hysteresis loop is one of the known fingerprints of memristor [26] that basically characterize memristive systems by observing the device's voltage and current responses in the current versus voltage plane (i.e the I-V curve), but it can not define memristor model in any way [27], as it depends on initial condition, for example $q(t = 0) = q_0$. Therefore, to effectively model memristor behaviour, the flux−charge relationship also called the ϕ-q curve is to be studied. Considering an ideal charge-controlled memristor [23, 25, 27, 41] given by: $\phi = \hat{\phi}(q)$ and defining more generally the state variable $x(t)$ as the instantaneous charge $q(t)$ flowing through the device with respect to q_d, the memristance $M(x)$ becomes $M(q)$ whose dynamics depends solely on the charge $q(t)$, such

that:

$$V(t) = M(q)\ i(t), \qquad \frac{dq}{dt} = i(t), \tag{4.4}$$

representing the port and state equations of the device, respectively. Here $M(q) = \frac{d\phi}{dq}$ is the charge-controlled memristance defined by the slope at the operating point $(q(t), \phi(t))$ on the ϕ-q curve at any given time. In Fig. 4.3, the memristance $M(q)$ undergoes transition between two resistance states: R_{on} and R_{off}. As the charge having crossed through the memristor can be less than 0 or greater than q_d, we can use as state variable $x(t) = \frac{q(t)}{q_d}$ given by eq. (4.2), but it is emphasized that this variable is not limited in $[0, 1]$ as should be $x(t)$ defined previously. Let us recall that: $M(q) = R_{off}$ for $x \leq 0$ and $M(q) = R_{on}$ for $x \geq 1$. Depending upon memristor technology, the limiting values R_{on} and R_{off} are set by means of two possibilities: (i) by the manufacturer according to the technology parameters during the fabrication process (e.g Metal-Insulator-Metal such as HP technology) or (ii) by the user and depending upon the application (e.g Self Directed Channel (SDC) devices such as KNOWM memristor) [32, 132]. The equations linking the voltage $V(t)$ across the memristor and the current $i(t)$ flowing through it, are rewritten as:

$$V(t) = \left[R_{off} - \delta R\ x\right]\ i(t), \qquad \frac{dx}{dt} = \frac{i(t)}{q_d}. \tag{4.5}$$

Equation (4.5) characterizes a charge-controlled memristor whose dynamics is determined by the charge flowing through the device. However, a more realistic description of the memristance $M(q)$ with respect to q_d must avoid $M(q)$ to be out of $[R_{on}, R_{off}]$, if q is outside $[0, q_d]$. Using equation (4.2), we have then to modify (4.5) in:

$$M(q) = \begin{cases} R_{off}, & \text{if } q(t) \leq 0 \\ R_{off} - \delta R\ \frac{q(t)}{q_d}, & \text{if } 0 \leq q(t) \leq q_d \\ R_{on}, & \text{if } q(t) \geq q_d \end{cases} \tag{4.6}$$

Recall that the constitution relation of the memristor is given by $d\phi = M(q)dq$, then from equation (4.6) we obtained a quadratic expression of the ϕ-q loci by considering $q(t)$ in $[0, q_d]$:

$$\phi(q) = R_{off}\ q - \frac{\delta R}{2\ q_d} q^2. \tag{4.7}$$

In this q interval, as the flux $\phi(t)$ changes with respect to $q(t)$, one can see in Fig. 4.3 that

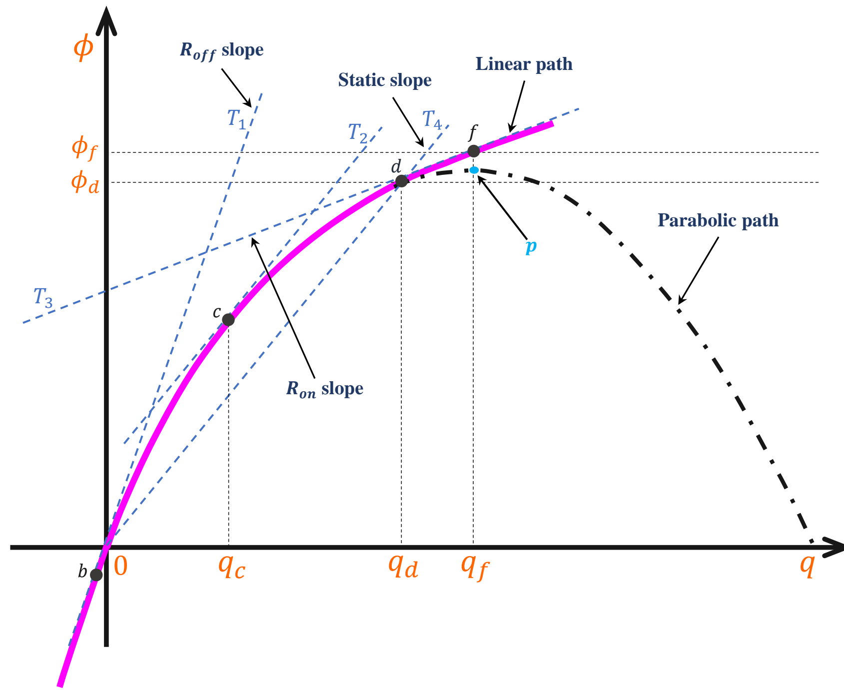

Figure 4.3: Memristance ϕ-q curve description of eq. (4.11). The flux ϕ is a continuous function of charge q and varies according to the operating point along the ϕ-q curve. Points b, c and d define some instances of memristance given by the lines T_1, T_2 and T_3 respectively. Point b is when $q(t) < 0$ and the memristance is R_{off} given by the slope of line T_1. However, points c and d describe the memristance transition as $q(t)$ increases until $q(t) = q_d$ where the ϕ-q loci leaves the parabolic path and becomes a straight line T_3 whose slope is R_{on}. For $q(t) > q_d$, the ϕ-q loci is no longer parabolic. Note that q_f is not far from q_d, see eq. (4.12). This curve is for $\phi_0 = 0$ and $q_0 = 0$.

$\phi(t)$ increases toward the summit of the imaginary dotted parabola (labeled as 'p') where the slope of the tangent is horizontal. Additionally, the area covered by the parabolic curve in eq. (4.7) depends upon the limiting values of R_{on} and R_{off}. The description of this model must be completed with a continuous variation of ϕ versus q. Furthermore, the complete mathematical description of the ϕ-q curve in Fig. 4.3, is as follows:

If $q \leq 0$:

$$V(t) = i(t)\, R_{off} \quad \Rightarrow \quad \phi(q) = R_{off}\, q. \tag{4.8}$$

If $0 \leq q \leq q_d$:

$$V(t) = \left(R_{off} - \delta R \frac{q}{q_d}\right)\, i(t) \quad \Rightarrow \quad \phi(q) = R_{off}\, q - \delta R \frac{q^2}{2\, q_d} + \phi_1. \tag{4.9}$$

If $q \geq q_d$:

$$V(t) = i(t)\, R_{on} \quad \Rightarrow \quad \phi(q) = R_{on}\, q + \phi_2. \tag{4.10}$$

ϕ_1 and ϕ_2 are constants describing the continuity of the ϕ-q curve at $q = 0$ and $q = q_d$

respectively. Thus, equations (4.8)-(4.10) give:

$$\text{at } q=0\text{: } \left\{R_{off}\, q = R_{off}\, q - \delta R \frac{q^2}{2\, q_d} + \phi_1\right\} \;\; \Rightarrow \;\; \phi_1 = 0,$$

$$\text{at } q=q_d\text{: } \left\{R_{off}\, q - \delta R \frac{q^2}{2\, q_d} = R_{on}\, q + \phi_2\right\} \;\; \Rightarrow \phi_2 = \delta R\, \frac{q_d}{2}.$$

The complete description of this model and its corresponding circuit response are given in equation (4.11), Fig. 4.3 and Fig. 4.4 respectively, and it adheres to the signatures of a charge-controlled memristor.

$$\begin{cases} \left.\begin{aligned} \phi(t) &= R_{off}\, q(t) \\ V(t) &= R_{off}\, i(t) \end{aligned}\right\} & \text{if } q(t) \leq 0 \\ \\ \left.\begin{aligned} \phi(t) &= R_{off}\, q(t) - \delta R\, \frac{q(t)^2}{2q_d} \\ V(t) &= \left(R_{off} - \delta R\, \frac{q(t)}{q_d}\right) i(t) \end{aligned}\right\} & \text{if } 0 \leq q(t) \leq q_d \\ \\ \left.\begin{aligned} \phi(t) &= R_{on}\, q(t) + \delta R\, \frac{q_d}{2} \\ V(t) &= R_{on}\, i(t) \end{aligned}\right\} & \text{if } q(t) \geq q_d \end{cases} \tag{4.11}$$

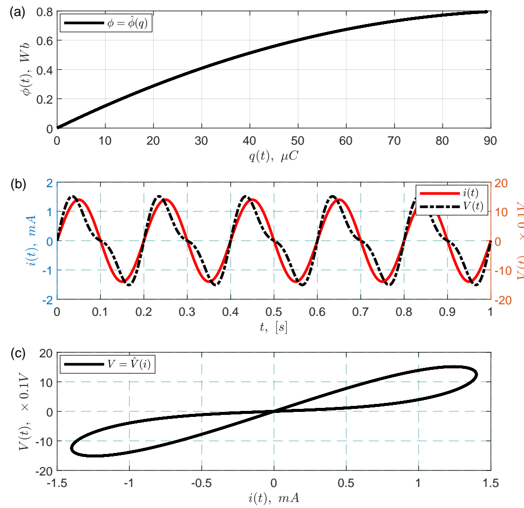

Figure 4.4: Characteristics of the memristor model given in eq. (4.11) by using a sine current input $i(t) = I_0\ sin(\omega t)$. The result is obtained for $R_{off} = 16K\Omega$, $R_{on} = 100\Omega$, $I_0 = 1.4mA$, $\mu_v = 10^{-14}m^2/V.s$, $D = 10^{-8}m$ which gives $q_d = 100\mu C$. (a) ϕ-q curve, (b) current and voltage transients and (c) I-V characteristics.

If the charge already flowed through the device is negative, the slope of the ϕ-q curve is R_{off}. On the other hand, if the total charge crossed through the memristor reaches $q(t) = q_d$, the slope becomes R_{on}. In Fig. 4.3, when the charge flowing through the device

increases, the conductivity increases simultaneously and the memristance moves toward R_{on} via the parabolic path describing the flux versus the charge by the black dotted curve. If $q(t) > q_d$, the ϕ-q loci is no longer on the dotted parabolic path, instead traverses a path whose slope is R_{on}.

Notice that the instantaneous memristance at some chosen points is represented by the slope of the lines, for example T_1, T_2 and T_3 (in blue dotted lines) to the ϕ-q curve at points b, c and d respectively. Following Fig. 4.3, these points are treated one after the other in the following.

Point b: as the initial charge q_0 is negative, the boundary between doped and undoped regions lets $M(q)$ be R_{off}. Then the memristor is not activated, however its effect is preserved and manifests itself in $\phi(t)$ resulting in straight line segment having exact slope R_{off} as the tangent T_1 at point b. Hence, as $q(t)$ increases, the locus follows along the parabolic path according to equation (4.7). Line T_1 is an example of line whose slope at point b is equal to R_{off} and this is met if $q(t) \leq 0$:

$$\left.\frac{d\phi}{dq}\right|_{q\leq 0} = R_{off}.$$

Point c: for any q_c, such that $0 < q_c < q_d$, the point $(q(t), \phi(t))$ belongs to the pink parabolic curve, with a tangent T_2 of slope:

$$\left.\frac{d\phi}{dq}\right|_{q=q_c} = M(q_c) = R_{off} - \delta R\frac{q_c}{q_d},$$

with $R_{on} < M(q_c) < R_{off}$.

Point d: as $q(t)$ increases, $\phi(t)$ increases correspondingly toward the summit of the dotted parabolic path (point p). However, the ϕ-q loci reaches the point d (when $q(t) = q_d$) before reaching the summit p, beyond which $\frac{d\phi}{dq} = R_{on}$. Note that the line T_4 sprouted from the origin through point d, corresponds to the static slope of the ϕ-q loci at $q(t) = q_d$, that is

$$\frac{\phi_d}{q_d} = \frac{R_{off} + R_{on}}{2},$$

while the dynamic slope of the ϕ-q loci at point d, whose tangent is the straight T_3 is obtained by differentiating (4.7) and substituting $q(t)$ by q_d, that is:

$$\left.\frac{d\phi}{dq}\right|_{q=q_d} = R_{off} - \delta R\ \frac{q_d}{q_d} = R_{on}.$$

Thus, line T_3 is tangent to the parabolic path at point d whose dynamic slope is exactly R_{on}.

Point f: obviously, one can see that point d is the point whereby the ϕ-q loci is just about to leave the parabolic path and to join a linear path. Moreover, this linear path depicts the R_{on} slope. Thus, $q(t)$ increasing and going beyond q_d, the ϕ-q loci is no longer on the dotted parabolic path, instead becomes a straight with R_{on} slope, see point f in Fig. 4.3. Note that at the summit of the parabola,

$$q_f = \frac{R_{off}}{\delta R} q_d \;\Rightarrow\; q_f > q_d, \tag{4.12}$$

the dynamic slope would be 0, which is not realistic. Additionally, Fig. 4.3 shows the ϕ-q curve for zero initial conditions, that is, $\phi_0 = 0$ and $q_0 = 0$, hence it goes through the origin ($\phi(t = 0) = 0$ if $q(t = 0) = 0$). Depending on the values of ϕ_0 and q_0, the curve can be shifted horizontally or vertically without changing the dynamical slopes.

4.4/ The new memristor model

The memristance function $M(q)$ of a charge−controlled memristor is studied with respect to the flowing charge through it. Fig. 4.5a shows the response of $M(q)$ versus the charge flowing through the memristor. In black trace is the result of equation (4.11) in which the memristance does not change at $q < 0$ and $q > q_d$ and for a real memristor device this phenomenon is modeled using window function by imposing zero drift at the two extreme boundaries (i.e $q = 0$ and $q = q_d$). In addition, it further affirms the passivity nature of memristance whereby:

$$P_M \geq 0 \;\Rightarrow\; M > 0,$$

where P_M is the power dumped in the memristor whose memristance is M. However, the model of HP TiO_2 memristor (shown in Fig. 4.5a) has not a continuous derivative at $q = 0$ and $q = q_d$, which causes angulation at these q values.

Furthermore, the study of memristance dynamics in the CNN neighborhood connection between pixels (as will be seen in section 5.6) requires $\frac{dM(q)}{dq}$ to be continuous at $q = 0$ or q_d in order to solve the system analytically. Hence, the main idea of this section is to modify the conventional TiO_2 memristor model given in eq. (4.11). The memristance function in red curve, shows a rather better result because it solves the problem of derivative discontinuity at $q(t) = 0$ or q_d.

The new model of $M(q)$ is developed in the following, as derived from a cubic polynomial function which is determined to be continuous and with a continuous first derivative with respect to q, at these extreme points. To begin with, consider the memristance represented by a third order polynomial with constants coefficients a, b, c and d, as:

$$M(q) = a + b\,q + c\,q^2 + d\,q^3 \quad for\; q \in [0,\;\; q_d]. \tag{4.13}$$

The derivative of $M(q)$ with respect to q is:

$$\frac{dM(q)}{dq} = b + 2c\, q + 3d\, q^2. \tag{4.14}$$

Following equation (4.13) and (4.14), the constants $a,\ b,\ c,$ and d are determined as follows:

$$for\ \ q < 0 : \quad M(q) = a = R_{off},$$

$$for\ \ q = 0 : \quad \left.\frac{dM(q)}{dq}\right|_{q=0} = 0 \ \Rightarrow\ b = 0,$$

$$for\ \ q = q_d : \quad \left.\frac{dM(q)}{dq}\right|_{q=q_d} = 0 \text{ and } \left.M(q)\right|_{q=q_d} = R_{on} \ \Rightarrow$$

$$\begin{aligned} b + 2c\, q_d + 3d\, q_d^2 &= 0, \\ q_d\, (2c + 3d\, q_d) &= 0 \ \Rightarrow \end{aligned}$$

$$q_d \neq 0 \ \Rightarrow\ 2c + 3d\, q_d = 0.$$

$$\therefore \quad c = -\frac{3}{2} d\, q_d. \tag{4.15}$$

Moreover, $\left.M(q)\right|_{q=q_d} = R_{on} = R_{off} + c\, q_d^2 + d\, q_d^3 \ \Rightarrow$

$$c\, q_d^2 + d\, q_d^3 = -\delta R, \tag{4.16}$$

where $\delta R = R_{off} - R_{on}$. Substituting c from (4.15) into (4.16), thus:

$$-\frac{3}{2} q_d^3 + d\, q_d^3 = -\delta R \ \Rightarrow$$

$$d = \frac{2\, \delta R}{q_d^3}, \tag{4.17}$$

and equation (4.15) becomes:

$$c = -\frac{3\, \delta R}{q_d^2}. \tag{4.18}$$

Substituting the expressions of the constants $a,\ b,\ c,$ and d into (4.13), yields:

$$M(q) = R_{off} - 3\, \delta R \left(\frac{q}{q_d}\right)^2 + 2\, \delta R \left(\frac{q}{q_d}\right)^3, \tag{4.19}$$

which implies that:

$$M(q) = \begin{cases} R_{off}, & \text{if } q(t) \leq 0 \\ R_{off} - \dfrac{3\,\delta R}{q_d^2}\,q^2 + \dfrac{2\,\delta R}{q_d^3}\,q^3, & \text{if } 0 \leq q(t) \leq q_d \\ R_{on}, & \text{if } q(t) \geq q_d \end{cases} \tag{4.20}$$

with its charge derivative given by:

$$\frac{dM(q)}{dq} = \begin{cases} -\dfrac{6\,\delta R}{q_d^2} q + \dfrac{6\,\delta R}{q_d^3}\,q^2, & \text{if } 0 \leq q(t) \leq q_d \\ 0, & \text{if } q \leq 0 \ \text{ or } \ q \geq q_d \end{cases} \tag{4.21}$$

Furthermore, with $d\phi = M(q)\,dq$, the corresponding flux expression of (4.20) is given by:

$$\phi = \begin{cases} R_{off}\,q, & \text{if } q(t) \leq 0 \\ R_{off}\,q - \dfrac{\delta R}{q_d^2}\,q^3 + \dfrac{\delta R}{2q_d^3}\,q^4, & \text{if } 0 \leq q(t) \leq q_d \\ R_{on}\,q + \dfrac{\delta R}{2}\,q_d, & \text{if } q(t) \geq q_d. \end{cases} \tag{4.22}$$

Note that here again, $\phi = \phi(q)$ can be shifted vertically or horizontally, according to the choice of initial conditions. The new model is shown by the red curve in Fig. 4.5a as comparison to the expression of $M(q)$ in (4.6). Additionally, the ϕ-q curves for both models are given in Fig. 4.5b. The response of the new model is shown in Fig. 4.6.

POINT OF INFLEXION:

To determine the point of inflexion, the first and second derivatives of $M(q)$ with respect to q are obtained from (4.20), leading to:

$$\frac{dM(q)}{dq} = 6\frac{\delta R}{q_d}\left(\frac{q^2}{q_d^2} - \frac{q}{q_d}\right), \tag{4.23}$$

Differentiating (4.23) once again, gives:

$$\frac{d^2M(q)}{dq^2} = 6\frac{\delta R}{q_d}\left(\frac{2q}{q_d^2} - \frac{1}{q_d}\right). \tag{4.24}$$

Therefore, $\frac{d^2M(q)}{dq^2} = 0 \;\; if \; 2q = \frac{q_d^2}{q_d} = q_d \;\Rightarrow\; q = \frac{q_d}{2}$. Substituting $q = \frac{q_d}{2}$ into (4.23), gives:

$$\begin{aligned}\frac{dM(q)}{dq} &= 6\frac{\delta R}{q_d}\left(\frac{1}{4} - \frac{1}{2}\right),\\ &= -\frac{3}{2}\frac{\delta R}{q_d}.\end{aligned}$$

The memristance $M(q)$ at $q = \frac{q_d}{2}$ is obtained by substituting the value of q into (4.20):

$$M(q)\Big|_{q=\frac{q_d}{2}} = R_{off} - 3\,\delta R\frac{1}{4} + 2\,\delta R\frac{1}{8} \Rightarrow$$

$$M(q)\Big|_{q=\frac{q_d}{2}} = \frac{1}{2}(R_{off} + R_{on}). \tag{4.25}$$

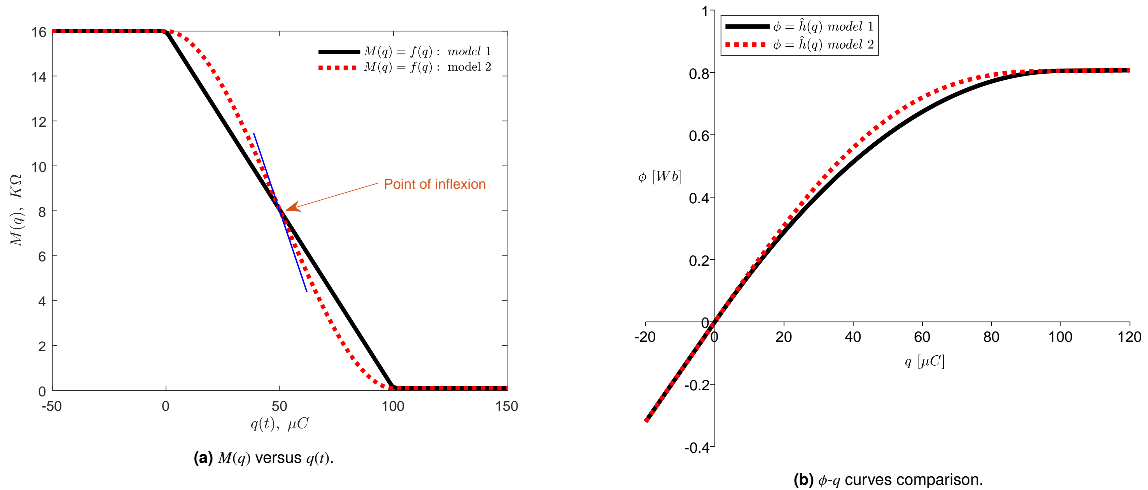

(a) $M(q)$ versus $q(t)$.

(b) ϕ-q curves comparison.

Figure 4.5: Results comparison of memristance as a function of charge for the HP model and our developed cubic model. Models 1 and 2 refer to the memristance expressions in (4.6) and (4.20) respectively. The charge $q(t)$ is taken in a larger interval, for example $q(t) = [-0.2,\; 1.2] \times 10^{-4}C$. Using the parameters value in [12]: $\mu_v = 10^{-14}m^2/V.s$, $D = 10nm$, $R_{off} = 16K\Omega$, $R_{on} = 100\Omega$, gives $q_d = 100\mu C$. Thus, $\frac{dM(q)}{dq}$ in eq. (4.6) has discontinuity at $q(t) = 0$ and $q(t) = q_d$ while $\frac{dM(q)}{dq}$ in eq. (4.20) is continuous at these q values.

Figure 4.7 shows the circuit response of the new model. The SPICE netlist file of the new model is given in Table A.2 (Appendix A). Using the sine input voltage source and varying the voltage amplitude in three steps, the results show the ϕ-q curve, the I-V characteristics, the memristance and the state variable transients. We consider the input voltage as $0.75V$, $1V$ and $1.2V$, shown respectively, by Figures 4.7a1-a3, b1-b2 and c1-c3. Figure 4.7c2 shows the hard switching case, i.e the scenario occuring when a substantial amount of input voltage is applied to the memristor [12].

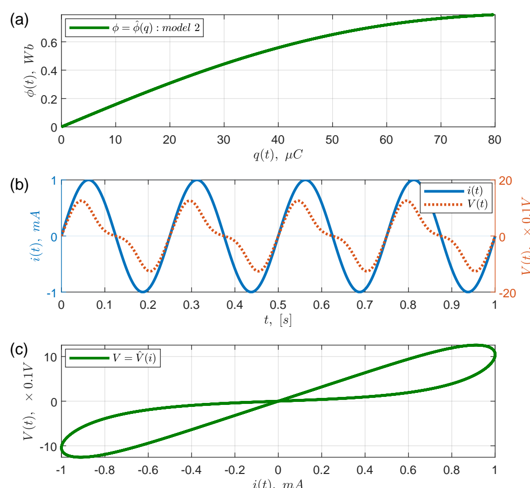

Figure 4.6: Characteristics of the memristor model given in eq. (4.20) by using a sine current input $i(t) = I_0\ sin(\omega t)$. The result is obtained for $R_{off} = 16K\Omega$, $R_{on} = 100\Omega$, $I_0 = 1mA$, $f = 4Hz$ and $q_d = 100\mu C$. (a) ϕ-q curve, (b) current and voltage transients and (c) I-V characteristics.

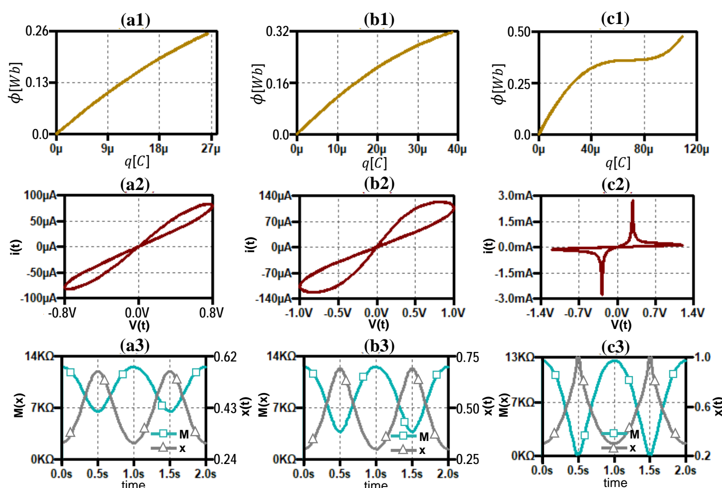

Figure 4.7: SPICE simulation results of the new memristance function (Table A.2). Values of parameters used: $R_{on} = 100\Omega$, $R_{off} = 16K\Omega$, $f = 1Hz$ and $q_d = 100\mu C$. (**a1-a3**) for $V_{\text{amp}} = 0.75V$: ϕ-q curve, I-V graph, Memristance and state variable transition, respectively. (**b1-b3**) for $V_{\text{amp}} = 1.0V$: ϕ-q curve, I-V graph, Memristance and state variable transition, respectively. (**c1-c3**) for $V_{\text{amp}} = 1.2V$: ϕ-q curve, I-V graph, Memristance and state variable transition, respectively.

4.5/ Conclusion

The work is based on the model of a charge-controlled memristor, hence it started with the description of its ϕ-q curve which showed the flux dependency on the charge. In addition, memristor is normally modeled from its constitutive relationship between flux and charge because pinched hysteresis loop only describes its circuit response. New model of memristor is presented and due to its desirable continuity for all charge $q(t)$ flowing through the memristor, it is essentially vital in the study of memristor dynamics involved in cells communication for a nonlinear network (to be presented in the subsequent chapters). Furthermore, the new model is tested in SPICE circuit simulator and it possesses the well-known signatures of a memristor.

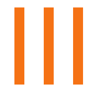

III

MAIN CONTRIBUTION (2)

5

CNN - Memristor dynamics in Nonlinear Network

This chapter presents thorough analysis on the dynamics of charge-controlled memristor between pixel cells, as a foundation enabling to study and anticipate the behaviour of the memristor used as neighbourhood connection in a cellular nonlinear or neural network.

5.1/ Introduction

Since its inception [133, 134], cellular nonlinear networks (CNNs) have given birth to widely accepted techniques in image and signal processing owing to their parallel computation capability and real-time processing. CNN is basically an array of similar elemental units called cells with each cell connected to its adjacent neighbouring cells. As can be seen in Fig. 5.1, the general formation of a two-dimensional CNN is applicable to image processing with the cells interacting to one another either directly due to adjacency (for adjacent cells) or indirectly (for nonadjacent cells) due to the 'propagation effects of the continuous-time dynamics of the network [134]'.

The neighbourhood connections, as shown by the cross-line segments, enhance the mutual interaction among the cells such that each cell address can be written as $C(i, j)$, where: $i = 1,\ 2,\ ,3\ ...,\ x$ and $j = 1,\ 2,\ ,3\ ...,\ y$ with each cell having a neighbourhood of $(2r + 1)^2$, where $r = 1,\ 2,\ ,3\ ...,\ \mathbb{N}$ is the neighbourhood radius and $\mathbb{N}$ is a natural number. Note that CNN communicates locally, in other words, communication between cells is only possible between close cells, this fact lets it differ from a biological CNN.

Each cell of the CNN in Fig. 5.1 represents an image pixel such that the input image is mapped into a similar output image and the network converges to a steady state after having passed through the transient state excited by the input image. In [133], the cell constituents are proposed to be one linear capacitor, two linear resistors, one independent voltage source, one independent current source and at-most $2n$ linear voltage con-

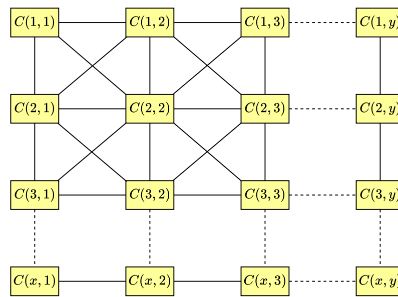

Figure 5.1: CNN – general formation.

trolled current sources, where n is the number of neighbour cells. However, the equivalent circuit is also proposed such that each cell constitutes one linear capacitor in parallel with one voltage controlled resistor R_v [133]. Thus, the formation resembles biological neuron with the exception that CNN allows only close neighbourhood communications.

The dynamics and the equilibrium states are determined by the voltage controlled resistor R_v. Commonly, R_v has three equilibrium states, out of which two are stable states while the other is unstable. Moreover, depending on the cell input, the system can have less than three equilibrium states. Depending upon the system initial condition and after the transient, the system tends to one of the stable equilibrium state. The setup is also realized with the cell composition reported using a nonlinear resistance such as Fitzhug-Nagumo in parallel with a linear capacitor [135–139].

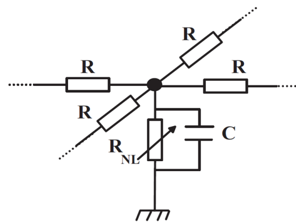

Figure 5.2: 2D CNNs prior to the inclusion of memristor [137].

Memristor-based CNNs have been reported [57, 140] in which a flux-controlled memristor is used in the cell's constituent and using memristor bridge as a synapse [59, 70]. Using memristor for CNN neighbourhood connection is also reported in [48, 141], applicable to image processing such as edge detection. The interesting features of memristors, such as connection flexibility, nano-scaleability, memory capability, conductance modulation etc, are essential properties affirming the reliability of memristor in neuromorphic networks, especially as synaptic function. In the following, we present the application of memristor in a 2D cellular nonlinear network with the cells comparable to pixels in an image processing purpose. Conventionally, the network is made of discrete cells, each containing one linear capacitor C and one nonlinear resistor R_{NL}, while they are coupled together by linear resistors R to form 2D electrical lattice [137], see Fig. 5.2. The linear resistor in the coupling mode is to be replaced by memristor. The approach is accom-

panied by the study of memristor behaviour on the overall system response, such as the effect of initial charge q_0 (corresponding to the memory effect of the memristor) on the system dynamics. Here are some of the advantages of the proposed memristor-based network:

- Reduction in size of the complete built-up due to the nano-nature of the memristor.
- Higher pixel density for the same image size.
- Hence, improving of sharpness.
- Lower power consumption.
- Fault tolerance.
- Connection flexibility.
- Exploring a new technique for information processing and analysis.

5.2/ POSSIBILITIES OF THE MEMRISTOR-BASED 2D CNN

There are three possibilities to implement memristor in the circuit schematic of Fig. 5.2, viz:

1). ***The first possibility is to consider using memristor as a coupler i.e to replace the linear resistance R while retaining the other elements unchanged*, Fig. 5.3a.**

2). ***The second possible approach is to use memristor in place of the nonlinear resistor R_{NL} while keeping all other elements unchanged*, Fig. 5.3b.**

3). ***The third possibility is to use memristor in place of both R and R_{NL} while retaining other elements unchanged*, Fig. 5.3c.**

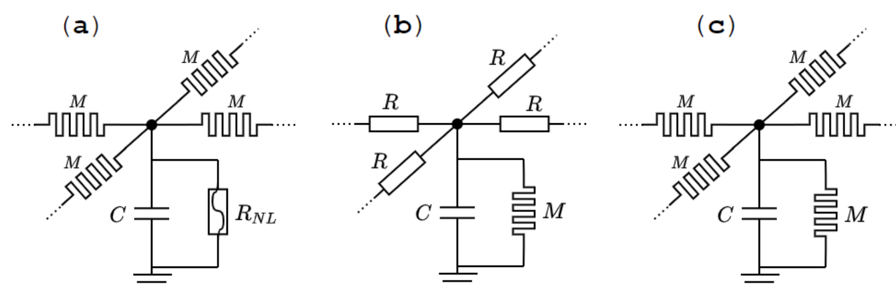

Figure 5.3: Three possibilities of memristor based 2D CNN. (a) Using memristor for coupling, thus replacing the linear resistor, (b) Using memristor in the cell unit by replacing the nonlinear resistor and (c) Using memristor in place of both R and R_{NL} in the system.

This work focuses specifically on Fig. 5.3a where the memristor M is used to replace the coupling linear resistor R.

5.3/ RC CELLULAR NONLINEAR NETWORK

Figure 5.4 shows the RC network, whereby all the elements of the network are nominal resistors and capacitors. Figure 5.4a shows the implementation of a 2D RC cellular nonlinear network. It is a system that entails bidirectional communication between any two adjacent cells coupled together by linear resistors R. To quantitatively understand the behaviour of the system, we consider two cells: Cell-1 and Cell-2, each of them constituted of one linear resistor R_m and R_s respectively, and one capacitor C_m and C_s respectively, coupled by linear resistor R. The interaction between the two cells can be visualized by allowing one cell to serve as a source (or master) and the other one as a recipient (or slave), with their constituent elements distinguished by the subscript letters m and s, respectively.

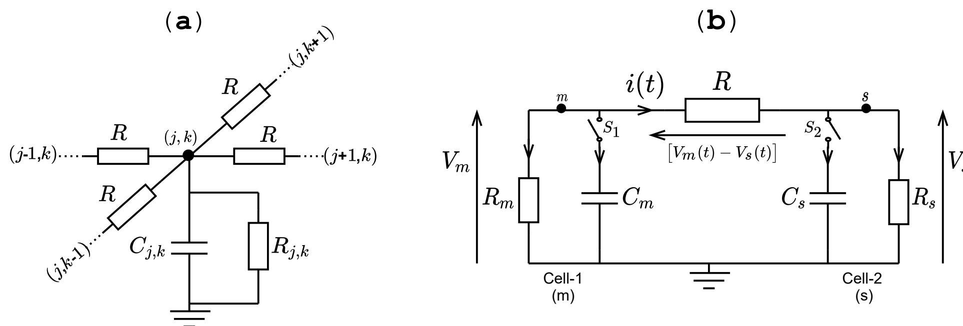

Figure 5.4: RC network. (a) 2D RC CNN (b) Case study: system of two cells.

Figure 5.4b is a bidirectional communication between Cell-1 and Cell-2 via a linear resistor R. It is however important to note that the terms master (m) and slave (s) here specify which of the two cells is more active that decides the direction of the flowing current $i(t)$ through the coupling resistor R. Hence, either of the cells can serve as a master or a slave depending on which among them is acting as the source of information. It is not master and slave in the sense of unidirectional coupled system. In fact if Cell-2 becomes the master, then the voltage across the coupling resistor R becomes $[V_s(t) - V_m(t)]$ and the current $i(t)$ flows toward Cell-1. The aim is to observe the interaction of Cell-1 and Cell-2 via the coupling resistor R, which in comparison, could help to a better understanding of the memristor behaviour in the coupling mode.

The idea is to observe the phase portraits, the evolution of the voltages $V_m(t)$ and $V_s(t)$, the flowing current $i(t)$ and the charge $q(t)$. Switches S_1 and S_2 are closed simultaneously and current $i(t)$ flows from master cell to slave cell, as shown by the arrow direction. By

the application of Kirchhoff's laws, we get the following set of equations:

$$i(t) = -C_m \frac{dV_m}{dt} - \frac{V_m}{R_m}, \tag{5.1}$$

$$i(t) = C_s \frac{dV_s}{dt} + \frac{V_s}{R_s}, \tag{5.2}$$

$$i(t) = \frac{V_m - V_s}{R}. \tag{5.3}$$

5.3.1/ VOLTAGE AND CURRENT EVOLUTION: $V_m(t)$, $V_s(t)$ AND $i(t)$

The voltages $V_m(t)$ and $V_s(t)$ refer to the instantaneous values invoked by closing the switches S_1 and S_2 simultaneously. Initially, some information is stored in the master cell as V_{m_0} and for the slave cell as V_{s_0}. To visualize the evolution of $V_m(t)$, $V_s(t)$ and $i(t)$, three approaches are considered, namely: Analytical solution, SPICE simulation using PSPICE and Numerical solution using MatLab built-in function (e.g ODE23t). The idea is to compare the analytical solution with the ones obtained from SPICE and MatLab simulations.

To begin, Fig. 5.4 is simulated in SPICE and the results are given in Figs. 5.5 and 5.6. Additionally, the second approach is also done by simulating equations (5.1), (5.2) and (5.3) in Matlab using ode23t and the results (also are given in Figs. 5.5 and 5.6) are in agreement with the ones obtained from SPICE. The analytical result is obtained as follows.

Substituting (5.2) into (5.1), we get:

$$C_m \frac{dV_m(t)}{dt} + C_s \frac{dV_s(t)}{dt} + \frac{V_m}{R_m} + \frac{V_s}{R_s} = 0, \Rightarrow \frac{d}{dt}(C_m V_m + C_s V_s) + \frac{C_m V_m}{R_m C_m} + \frac{C_s V_s}{R_s C_s} = 0.$$

Suppose the cells have identical time constant $\tau_1 = R_m C_m = R_s C_s$, thus:

$$\frac{d}{dt}(C_m V_m + C_s V_s) + \frac{C_m V_m + C_s V_s}{\tau_1} = 0, \Rightarrow$$

$$C_m V_m + C_s V_s = (C_m V_m + C_s V_s)_0 \; e^{\frac{-t}{\tau_1}} = \lambda_1 e^{\frac{-t}{\tau_1}},$$

where: $\lambda_1 = (C_m V_m + C_s V_s)_0 = C_m V_{m_0} + C_s V_{s_0}$ is a constant determined by the initial values at time $t = 0$, thus:

$$C_m V_m + C_s V_s = \lambda_1 \; e^{-\frac{t}{\tau_1}} \; . \tag{5.4}$$

From eq. (5.4):

$$V_s = \frac{\lambda_1}{C_s} \; e^{-\frac{t}{\tau_1}} - \frac{C_m}{C_s} V_m. \tag{5.5}$$

Equation (5.5) gives $V_s(t)$ for any given $V_m(t)$. Substituting (5.5) into (5.3), we get:

$$i(t) = \frac{C_s V_m - \lambda_1 \, e^{-\frac{t}{\tau_1}} + C_m V_m}{R \, C_s} \quad \Rightarrow$$

$$i(t) = \frac{(C_m + C_s) \, V_m - \lambda_1 \, e^{-\frac{t}{\tau_1}}}{R \, C_s}. \tag{5.6}$$

At time $t = 0, \; i(0) \neq 0, \; V_m(t = 0) = V_{m_0}, \; V_s(t = 0) = V_{s_0}$. Using the expression of λ_1 in (5.6) we get:

$$i(t) = \frac{C_m V_m - C_m V_{m_0} e^{-\frac{t}{\tau_1}} + C_s V_m - C_s V_{s_0} e^{-\frac{t}{\tau_1}}}{R \, C_s} \quad \Rightarrow$$

$$i(0) = \frac{C_m V_{m_0} - C_m V_{m_0} + C_s V_{m_0} - C_s V_{s_0}}{R \, C_s},$$

$$= \frac{V_{m_0} - V_{s_0}}{R} \text{ as expected, (see eq.(5.3)).}$$

Let $C_o = C_m + C_s$, substituting (5.6) into (5.1), we get:

$$\frac{C_o}{R \, C_s} V_m - \frac{\lambda_1 \, e^{-\frac{t}{\tau_1}}}{R \, C_s} + \frac{V_m}{R_m} + C_m \frac{dV_m}{dt} = 0 \quad \Rightarrow$$

$$\frac{dV_m}{dt} + \frac{V_m}{C_m} \left[\frac{C_o}{R \, C_s} + \frac{1}{R_m} \right] = \frac{\lambda_1}{R \, C_s C_m} \, e^{-\frac{t}{\tau_1}}.$$

Let $R_o = R_m + R_s$ and $\tau_2 = \frac{C_m}{\frac{C_o}{R \, C_s} + \frac{1}{R_m}} = \frac{R}{R_o + R} \, \tau_1 \quad \Rightarrow$

$$\frac{dV_m}{dt} + \frac{V_m}{\tau_2} = \frac{\lambda_1}{R \, C_s C_m} \, e^{-\frac{t}{\tau_1}}. \tag{5.7}$$

$\therefore$ The solution of (5.7) becomes:

$$V_m = \xi(t) \, e^{-\frac{t}{\tau_2}}, \tag{5.8}$$

where $\xi(t)$ is a function to be determined. Using (5.8) in (5.7), we get:

$$\frac{dV_m}{dt} = \frac{d}{dt} \left(\xi(t) \, e^{-\frac{t}{\tau_2}} \right) = e^{-\frac{t}{\tau_2}} \, \frac{d\xi(t)}{dt} + \xi(t) \left(-\frac{1}{\tau_2} \right) e^{-\frac{t}{\tau_2}},$$

and equation (5.7) becomes:

$$e^{-\frac{t}{\tau_2}} \, \frac{d\xi(t)}{dt} + \xi(t) \left(-\frac{1}{\tau_2} \right) e^{-\frac{t}{\tau_2}} + \frac{\xi(t) \, e^{-\frac{t}{\tau_2}}}{\tau_2} = \frac{\lambda_1}{R \, C_s C_m} \, e^{-\frac{t}{\tau_1}},$$

$$\frac{d\xi(t)}{dt} = \frac{\lambda_1}{R\,C_s C_m}\; e^{\frac{t}{\tau_2}-\frac{t}{\tau_1}} \;\Rightarrow$$

$$\xi(t) = \frac{\lambda_1}{R\,C_s C_m\left(\frac{1}{\tau_2}-\frac{1}{\tau_1}\right)}\; e^{\frac{t}{\tau_2}-\frac{t}{\tau_1}} + \lambda_2,$$

where λ_2 is a constant to be determined from V_{m_0} and V_{s_0}. Substituting $\xi(t)$ into (5.8), thus:

$$V_m = \frac{\lambda_1}{R\,C_s C_m\left(\frac{1}{\tau_2}-\frac{1}{\tau_1}\right)}\; e^{-\frac{t}{\tau_1}} + \lambda_2\, e^{-\frac{t}{\tau_2}}.$$

Let $\frac{1}{\tau_3} = \left(\frac{1}{\tau_2}-\frac{1}{\tau_1}\right) = \frac{R_o+R}{R\,\tau_1} - \frac{1}{\tau_1} \;\Rightarrow\; \tau_3 = \frac{R}{R_o}\,\tau_1$. Therefore:

$$V_m = \frac{\tau_3\,\lambda_1}{R\,C_s C_m} e^{-\frac{t}{\tau_1}} + \lambda_2\, e^{-\frac{t}{\tau_2}}.$$

Also by using the simple expressions of τ_3 and λ_1, the expression of V_m can be rewritten as follows:

$$V_m = \frac{R\,\tau_1}{R_o}\;\frac{(C_m V_{m_0} + C_s V_{s_0})}{R\,C_s C_m}\; e^{-\frac{t}{\tau_1}} + \lambda_2\, e^{-\frac{t}{\tau_2}}, \text{ with } \tau_1 = C_s R_s \;\Rightarrow$$

$$V_m = \frac{R_s}{R_o}\;\frac{(C_m V_{m_0} + C_s V_{s_0})}{C_m}\; e^{-\frac{t}{\tau_1}} + \lambda_2\, e^{-\frac{t}{\tau_2}}.$$

The initial conditions are considered to determine the constant λ_2. Hence, at $t = 0$, $V_m = V_{m_0}$ and $V_s = V_{s_0} \Rightarrow$

$$\lambda_2 = V_{m_0} - \frac{R_s}{R_o}.\frac{(C_m V_{m_0} + C_s V_{s_0})}{C_m}, \text{ after simplification we get:}$$

$$\lambda_2 = \frac{R_m}{R_o}\;(V_{m_0} - V_{s_0}).$$

Thus, the expression of $V_m(t)$ becomes:

$$V_m = \frac{R_s}{R_o}.\frac{(C_m V_{m_0} + C_s V_{s_0})}{C_m}\; e^{-\frac{t}{\tau_1}} + \frac{R_m}{R_o}\;(V_{m_0} - V_{s_0})\; e^{-\frac{t}{\tau_2}} \;\Rightarrow$$

$$V_m(t) = \left[\frac{R_s}{R_o} V_{m_0} + \frac{R_m}{R_o} V_{s0}\right] e^{-\frac{t}{\tau_1}} + \frac{R_m}{R_o}(V_{m_0} - V_{s_0})\; e^{-\frac{t}{\tau_2}}. \tag{5.9}$$

Equation (5.5) can be rewritten as:

$V_s = \left(\frac{R_s}{R_m}\, V_{m_0} + V_{s_0}\right) e^{-\frac{t}{\tau_1}} - \frac{R_s}{R_m}\, V_m$, using V_m from (5.9), we get:

$$V_s(t) = \frac{R_s\, V_{m_0}}{R_o}\left(e^{-\frac{t}{\tau_1}} - e^{-\frac{t}{\tau_2}}\right) + \frac{V_{s_0}}{R_o}\left(R_m\, e^{-\frac{t}{\tau_1}} + R_s\, e^{-\frac{t}{\tau_2}}\right) \tag{5.10}$$

Therefore, $i(t)$ is obtained from (5.3): $i(t) = \frac{V_m(t) - V_s(t)}{R} \;\Rightarrow$

$$i(t) = \frac{V_{m_0} - V_{s_0}}{R}\, e^{-\frac{t}{\tau_2}}. \tag{5.11}$$

5.3.2/ Charge $q(t)$ evolution

The charge flowing from the master cell to slave cell starting at $t = 0$ increases until it reaches saturation, meaning that both cells attain same potential level. Note that calling $q(t)$ this flowed charge imposes $q(0) = 0$. To observe the curve $q(t)$ versus t, the following derivations are made. From (5.1) and (5.2):

$\frac{dV_m}{dt} = -\frac{V_m}{\tau_1} - \frac{\dot{q}}{C_m}$ and $\frac{dV_s}{dt} = -\frac{V_s}{\tau_1} + \frac{\dot{q}}{C_s}$, subtracting the second equation from the first, we get:

$$\frac{dV_m}{dt} - \frac{dV_s}{dt} = -\frac{1}{\tau_1}(V_m - V_s) - \left(\frac{1}{C_m} + \frac{1}{C_s}\right)\dot{q}\,.$$

Also from (5.3): $V_m(t) - V_s(t) = R\,\dot{q} \;\;\Rightarrow$

$$\frac{dV_m}{dt} - \frac{dV_s}{dt} = -\frac{R}{\tau_1}\dot{q} - \left(\frac{1}{C_m} + \frac{1}{C_s}\right)\dot{q}\,,$$

$$\frac{dV_m}{dt} - \frac{dV_s}{dt} = -\left(\frac{R}{\tau_1} + \frac{1}{C_m} + \frac{1}{C_s}\right)\frac{dq}{dt}. \tag{5.12}$$

Assuming at $t = 0$, $q(t = 0) = q_0$, $V_m(t = 0) = V_{m_0}$ and $V_s(t = 0) = V_{s_0}$, then equation (5.12) becomes:

$$\int_{V_{m_0}}^{V_m(t)} dV_m - \int_{V_{s_0}}^{V_s(t)} dV_s = -\left(\frac{R}{\tau_1} + \frac{1}{C_m} + \frac{1}{C_s}\right)\int_{q_0}^{q(t)} dq \;\Rightarrow$$

$$V_m - V_s = V_{m_0} - V_{s_0} - \left(\frac{R}{\tau_1} + \frac{R_m}{\tau_1} + \frac{R_s}{\tau_1}\right)(q - q_0).$$

Using eq. (5.3) again, we get:

$$R\,\dot{q} = V_{m_0} - V_{s_0} - \frac{R + R_o}{\tau_1}(q - q_0) \;\;\Rightarrow$$

$$\frac{dq}{dt} + \frac{q}{\tau_2} = \frac{1}{R}(V_{m_0} - V_{s_0}) + \frac{q_0}{\tau_2}. \tag{5.13}$$

The solution of (5.13) is:

$$q(t) = \theta(t)\, e^{-\frac{t}{\tau_2}} + q_0, \tag{5.14}$$

where $\theta(t)$ is a function to be determined. Substituting (5.14) into (5.13), we get:

$$-\frac{\theta(t)}{\tau_2}\, e^{-\frac{t}{\tau_2}} + e^{-\frac{t}{\tau_2}}\frac{d\theta(t)}{dt} + \frac{\theta(t)}{\tau_2}\, e^{-\frac{t}{\tau_2}} + \frac{q_0}{\tau_2} = \frac{1}{R}(V_{m_0} - V_{s_0}) + \frac{q_0}{\tau_2} \quad \Rightarrow \quad \frac{d\theta(t)}{dt} = \frac{1}{R}(V_{m_0} - V_{s_0})\, e^{\frac{t}{\tau_2}},$$

from which, $\theta(t) = \frac{\tau_2}{R}(V_{m_0} - V_{s_0})\, e^{\frac{t}{\tau_2}} + \lambda_3$, where λ_3 is a constant. Then, using $\theta(t)$ in (5.14) gives:

$$q(t) = \frac{\tau_2}{R}(V_{m_0} - V_{s_0}) + \lambda_3\, e^{-\frac{t}{\tau_2}} + q_0.$$

At a time $t = 0$, $q(t) = q_0 \;\Rightarrow\; \lambda_3 = -\frac{\tau_2}{R}(V_{m_0} - V_{s_0})$. Then, $q(t)$ is finally obtained to be:

$$q(t) = \frac{\tau_2}{R}(V_{m_0} - V_{s_0})\left[1 - e^{-\frac{t}{\tau_2}}\right] + q_0, \tag{5.15}$$

which can directly confirms that $i(t)$ is given by equation (5.11).

5.3.3/ Phase portraits: RC network

We rewrite equation (5.12) as:

$$\frac{d}{dt}(V_m - V_s) = -\left(\frac{R}{\tau_1} + \frac{R_m}{\tau_1} + \frac{R_s}{\tau_1}\right)\frac{dq}{dt}.$$

Using equation (5.3), then:

$$\frac{d}{dt}\left(R\frac{dq}{dt}\right) = -\frac{R + R_o}{\tau_1}\frac{dq}{dt} \quad \Rightarrow$$

$$\frac{d^2 q}{dt^2} + \frac{1}{\tau_2}\frac{dq}{dt} = 0. \tag{5.16}$$

Setting $\mathscr{X} = q$, $\mathscr{Y} = \dot{\mathscr{X}} = \frac{dq}{dt}$ and $\dot{\mathscr{Y}} = \frac{d\mathscr{Y}}{dt} = \frac{d^2\mathscr{X}}{dt^2}$:

$$\begin{cases} \dfrac{d\mathscr{X}}{dt} = \mathscr{Y}, \\ \dfrac{d\mathscr{Y}}{dt} = -\dfrac{1}{\tau_2}\mathscr{Y}. \end{cases} \tag{5.17}$$

From the equation set (5.17):

$$\frac{d\mathscr{Y}}{d\mathscr{X}} = -\frac{1}{\tau_2} \quad \Rightarrow \quad \int d\mathscr{Y} = -\frac{1}{\tau_2}\int d\mathscr{X},$$

$$\mathscr{Y} = -\frac{1}{\tau_2}\mathscr{X} + \mathscr{H}, \tag{5.18}$$

where $\mathscr{H}$ is a conservative quantity giving by the initial conditions $\mathscr{X}_0$ and $\mathscr{Y}_0$. $\mathscr{X}_0$ is known to be q_0, while the initial condition of $\mathscr{Y}_0$ is obtained from equation (5.3) as: $\mathscr{Y}_0 = \frac{V_{m_0} - V_{s_0}}{R}$. Therefore, $\mathscr{H}$ is given by:

$$\mathscr{H} = \frac{V_{m_0} - V_{s_0}}{R} + \frac{q_0}{\tau_2}.$$

With $\mathscr{Y} = \frac{d\mathscr{X}}{dt}$, then equation (5.18) becomes:

$$\frac{d\mathscr{X}}{\mathscr{X} - \tau_2\mathscr{H}} = -\frac{dt}{\tau_2} \quad \Rightarrow$$

$$\ln(\mathscr{X} - \tau_2\mathscr{H}) = -\frac{t}{\tau_2} + \ln\mathscr{D},$$

where $\mathscr{D}$ is a constant of integration. At time $t = 0$, $\mathscr{X} = \mathscr{X}_0 = q_0$ and the constant of integration is obtained to be:

$$\mathscr{D} = \mathscr{X}_0 - \tau_2\mathscr{H}.$$

The simplification gives:

$$\frac{\mathscr{X} - \tau_2\mathscr{H}}{q_0 - \tau_2\mathscr{H}} = e^{-\frac{t}{\tau_2}} \quad \Rightarrow$$

$$\mathscr{X} = (q_0 - \tau_2\mathscr{H})e^{-\frac{t}{\tau_2}} + \tau_2\mathscr{H}. \tag{5.19}$$

It is interesting that equation (5.19) is exactly the same as equation (5.15).

5.3.4/ Remarks on the RC network

The time evolution of the charge $q(t)$ is shown in Fig. 5.5. The charge $q(t)$ increases from $q(0) = q_0$ until $V_m(t) = V_s(t)$, meanwhile the current $i(t)$ decreases until $V_m(t) = V_s(t)$ at about $t = 20ms$ where it is zero at this time because $V_m(t) - V_s(t) = 0V$. The time evolutions of $V_m(t)$ and $V_s(t)$, respectively, are obtained using equations (5.9) and (5.10) and they are shown in Fig. 5.6 with the analytical heading. Furthermore, the results of SPICE and MatLab simulations are obtained, also shown in Fig. 5.6. The three results are compared and show perfect agreement with one another. The values of parameters are $R = 10K\Omega$, $R_m = R_s = 100K\Omega$, $C_m = C_s = 1\mu F$, $V_{m_0} = 1V$ and $V_{s_0} = 0V$. The voltage evolution decays to zero due to the resistive nature of the cells.

Figure 5.7 shows the phase portraits result for $R = 10K\Omega$, $R_m = R_s = 100K\Omega$, $C_m = C_s = 1\mu F$, $q_0 = 0$, $\tau_1 = 0.1[sec.]$, $R_o = 200K\Omega$, $C_o = 2\mu F$, $R = 10K\Omega$, $\lambda_1 = 1\mu C$, that is, the same values of parameters used in Figs. 5.5 and 5.6. The initial voltage V_{m_0} is varied in ten steps between $0V$ and $1V$, meanwhile V_{s_0} is fixed at $0V$, hence we showed ten

trajectories. For each case, the corresponding initial conditions $\mathscr{H} = \mathscr{Y}_0 = \frac{V_{m_0} - V_{s_0}}{R}$ is determined, and $\mathscr{Y}$ and $\mathscr{X}$ are obtained from (5.18) and (5.19) respectively. The phase portraits show evolution of the flowing charge from the master cell to the slave one. When $V_{m_0} = 1$, the trajectory is given by the longest curve in which the result matched perfectly to the one shown in Fig. 5.5. The other trajectories are simply to show the variation effect of V_{m_0}. The line $\mathscr{Y} = 0$ is the equilibrium state. For each initial conditions, $\mathscr{Y}$ evolves from $\mathscr{Y}_0$ and stabilizes at $\mathscr{Y} = 0$ (or in other words, $V_{m_0} - V_{s_0} = 0$).

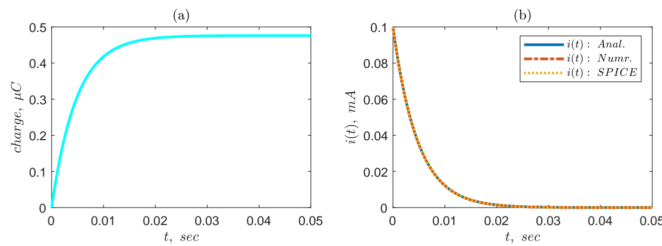

Figure 5.5: Response of the RC network. (a) Charge $q(t)$ evolution given by equation (5.15). (b) The current $i(t)$ flowing through the coupling resistor R, that is from master to slave. $V_{m_0} = 1V$, $V_{s_0} = 0V$, $q_0 = 0$, $R_m = R_s = 100K\Omega$, $C_m = C_s = 1\mu F$ and $R = 10K\Omega$. The current $i(t)$ is zero when $V_m(t) = V_s(t)$ and the difference $V_m(t) - V_s(t)$ becomes zero eventually.

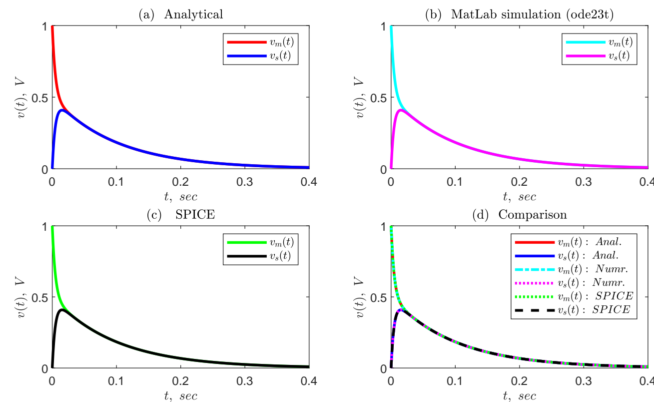

Figure 5.6: Response of the RC network. The time evolution of $V_m(t)$ and $V_s(t)$ according to the three approaches: (a) Analytical solution (b) Numerical solution (c) SPICE simulation (d) Comparison of the three methods showing a strong agreement. $V_{m_0} = 1V$, $V_{s_0} = 0V$, $R_m = R_s = 100k\Omega$, $C_m = C_s = 1\mu F$ and $R = 10k\Omega$.

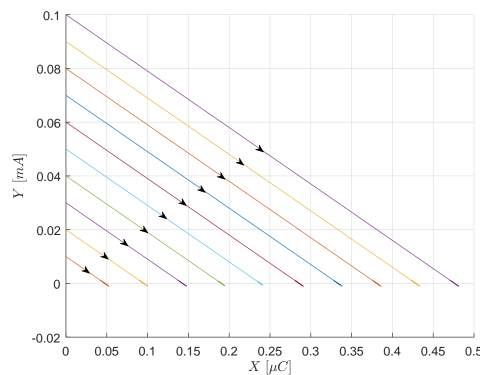

Figure 5.7: Phase portraits of the RC network showing the evolution of the flowing charge through coupling linear resistor until $V_{m_0} = V_{s_0}$ i.e $V_{m_0} - V_{s_0} = 0$ which is given by the line $\mathscr{Y} = 0$. The longest trajectory is for $V_{m_0} = 1V$ and it is interesting that the magnitudes of the flowing charge and current are exactly the same with the ones observed in Figs. 5.5a and b respectively.

5.4/ Memristor in the coupling mode

The first possible scenario is to consider using memristors in the coupling mode as shown in Fig. 5.3**a**. It is however interesting to understand the memristor behaviour and its contribution in the system. Memristor is studied in the coupling mode between two neuron cells where the synchronization phenomena is investigated numerically and theoretically [142–145]. Unidirectional coupling and bidirectional or mutual coupling are the commonly used coupling modes for nonlinear chaotic systems [146]. The synchronization and chaos between two neuron cells are also investigated by using unidirectional and bidirectional coupling [144].

In a first step to implement a 2D memristor based cellular nonlinear network for signal and image processing purposes or for modeling a neural network with memristors as synapses, we rather focus here on the interaction of memristor between pixel cells by considering a system of two-cells in order to assess the behavior of the memristor quantitatively and qualitatively. The idea is to transfer information from one cell to another via a memristor in order to observe its reaction to the proposition. The cells are interconnected bidirectionally, such that they can serve as source or recipient of information from one another. We derive analytically a second order nonlinear differential equation characterizing the interaction of memristor between the two cells bidirectionally. The system is studied in the phase plane allowing to visualize the system dynamics.

Memristive devices are asymmetrical components [22], meaning that they respond differently to the direction of electric current flowing through it, by offering different resistance levels. The variation of memristance (in other words, memristor asymmetry) with respect to the direction of the flowing current affects its reliability in some potential applications where sensitivity in direction is taken into consideration, for example, the memristive grid for neuromorphic application and image processing, because it affects the propagation effects within the cell. This aspect is taken into account by considering the possibility of using a memristor fuse. In Fig. 5.8, we show two cells representation having some localized information. By invoking the circuit, some information may diffuse from one cell to another according to the established potential difference across each cell. One cell is considered as the master that sends information to the receiver cell called the slave through memristor in the direction of red arrow.

Figure 5.8: Two cells symbolic representation coupled together by a memristor. Although the system communicates bidirectionally, however the small red arrow shows transmission preference from master to slave in order to facilitate the description of the study.

The implementation of memristors in the coupling mode is considered in two perspec-

tives:

1. **Linear resistor R in the cell unit (before considering R_{NL})**: This approach mainly focuses on the study of memristor behaviour in the coupling mode that could eventually help to anticipate its contribution in the target design.

2. **Nonlinear resistor R_{NL} (e.g. Fitzhugh-Nagumo) in the cell unit**: The aim is to implement a memristor based 2D CNN with each cell consisting of two elements, linear capacitor and nonlinear resistor, and the cells are connected via a memristor to form 2D arrays of nonlinear electrical lattice reliable for image processing purpose. This aspect is presented in chapter 6.

N.B: Two cells are considered during the analysis of each case. Secondly, the terms master and slave should not be confused, these are not definite terms, it is simply adopted to conveniently describe the study beforehand.

5.5/ LINEAR RESISTORS R IN THE CELL UNIT

This is the simplest case of the first scenario by using nominal resistors R in cell units in place of nonlinear resistors R_{NL}. This will give a better insight in understanding the effect of the memristor in the network before using R_{NL}. The task composes of four methods:

(1). Analytical solution

(2). Numerical solution

(3). Circuit simulation in SPICE

(4). Experiment (pending ...)

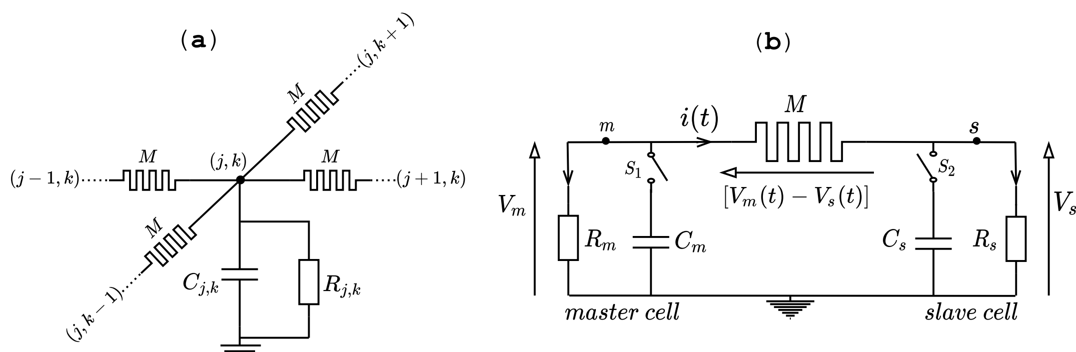

Figure 5.9: 2D cellular nonlinear network. (**a**) Target implementation of the memristor based 2D−CNN using memristors in the coupling mode. (**b**) Circuit schematic of two cells: master (m) and slave (s) cells. Each of them comprises one capacitor and one resistor coupled by a memristor M.

5.5.1/ Analytical description of a specific case: System of two cells

Figure 5.9a shows the target implementation of the memristor-based 2D CNN by using memristors in the coupling mode. For a quantitative study of the system response, a subset of the system (shown in Fig. 5.9b) is considered. It is made up of two unit cells each comprising one linear capacitor and one linear resistor. At time $t = 0$, switches S_1 and S_2, initially open, are closed, then information diffuses from one cell to the other, say from the master one to the slave one, via a memristor as shown by the direction of flowing current. Therefore, the memristor serves as the communication link between the cells. The system becomes saturated when $V_m(t) = V_s(t)$ and at that time $i(t) = 0$ because the cells are at the same potential. Eventually, the time evolution of the cells given by $V_m(t)$ and $V_s(t)$ decays to zero due to the resistive nature of the cells.

The outlined methodologies i.e theory, simulation by SPICE and numerical solution, are to be followed. Consequently, the time evolutions of $V_m(t)$, $V_s(t)$ and $q(t)$ are to be observed. From Fig. 5.9b, application of Kirchhoff's laws gives the following system of equations:

$$i(t) = -C_m \frac{dV_m(t)}{dt} - \frac{V_m(t)}{R_m} , \tag{5.20}$$

$$i(t) = C_s \frac{dV_s(t)}{dt} + \frac{V_s(t)}{R_s} , \tag{5.21}$$

$$V_m(t) - V_s(t) = M(q)\, \dot{q}(t) , \tag{5.22}$$

$$i(t) = \dot{q}(t), \tag{5.23}$$

where $M(q)$ is the memristance defined, respectively, in the first and second models, as:

$$M(q) = \begin{cases} R_{off}, & \text{if } q(t) \leq 0 \\ R_{off} - \dfrac{\delta R}{q_d}\, q, & \text{if } 0 \leq q(t) \leq q_d \\ R_{on}, & \text{if } q(t) \geq q_d \end{cases} \tag{5.24}$$

and

$$M(q) = \begin{cases} R_{off}, & \text{if } q(t) \leq 0 \\ R_{off} - \dfrac{3\,\delta R}{q_d^2}\, q^2 + \dfrac{2\,\delta R}{q_d^3}\, q^3, & \text{if } 0 \leq q(t) \leq q_d \\ R_{on}. & \text{if } q(t) \geq q_d \end{cases} \tag{5.25}$$

Notice that equations (5.20) and (5.21) in section 5.3 are similar to equations (5.1) and (5.2) because the cells elements are similar, i.e a linear resistor and a capacitor.

5.5.2/ Expressions for the evolution of $V_m(t)$ and $V_s(t)$

From equations (5.20) and (5.21), one can see that:

$$\frac{d}{dt}(C_m V_m + C_s V_s) + \frac{C_m V_m}{R_m C_m} + \frac{C_s V_s}{R_s C_s} = 0. \tag{5.26}$$

The aim is to focus on the memristor behaviour. So, even if it would be possible to consider different parameter values for R_m, R_s, C_m and C_s in the further calculations, we simplify for the sake of clarity our study by taking the cells to be identical such that the time constant $\tau_c = R_m C_m = R_s C_s$ is the same for both cells. Then (5.26) simplifies to:

$$C_m V_m + C_s V_s = \lambda\, e^{-\frac{t}{\tau_c}}\ , \tag{5.27}$$

and V_s is expressed to be:

$$V_s = \frac{\lambda}{C_s}\, e^{-\frac{t}{\tau_c}} - \frac{C_m}{C_s} V_m\ . \tag{5.28}$$

Where $\lambda = C_m V_{m_0} + C_s V_{s_0}$ is a constant fixed by the initial conditions. Once again, equations (5.20) and (5.21) respectively could be rewritten as:

$$R_m\ i(t) = -R_m C_m \frac{dV_m}{dt} - V_m, \tag{5.29}$$

$$R_s\ i(t) = R_s C_s \frac{dV_s}{dt} + V_s. \tag{5.30}$$

With $i(t) = \frac{dq}{dt} = \dot{q}(t)$, by adding (5.29) and (5.30), it becomes:

$$-\tau_c \frac{dV_m}{dt} + \tau_c \frac{dV_s}{dt} - V_m + V_s = (R_m + R_s)\dot{q},$$

$$\frac{dV_m}{dt} - \frac{dV_s}{dt} = -\frac{R_0}{\tau_c}\dot{q} - \frac{1}{\tau_c}(V_m - V_s),$$

where $R_0 = R_m + R_s$. Using $V_m - V_s = M(q)\,\dot{q}$ given in (5.22), then:

$$\frac{dV_m}{dt} - \frac{dV_s}{dt} = -\frac{R_0}{\tau_c}\frac{dq}{dt} - \frac{1}{\tau_c}\left(M(q)\,\frac{dq}{dt}\right). \tag{5.31}$$

Equation (5.31) can be solved in 2 ways. Firstly, the equation can be integrated directly and then solved simultaneously with (5.27) in order to find explicit expressions of $V_m(t)$ and $V_s(t)$ as functions of the charge $q(t)$ flowing through the memristor. Secondly, the equation is solved using (5.22) for the study of system dynamics presented in section 5.6.

Going by the first approach, taking into account the initial conditions V_{m_0}, V_{s_0} and q_0, and

integrating (5.31) as:

$$\int_{V_{m_0}}^{V_m} dV'_m - \int_{V_{s_0}}^{V_s} dV'_s = -\frac{R_0}{\tau_c}\int_{q_0}^{q} dq' - \frac{1}{\tau_c}\int_{q_0}^{q} (M(q')\, dq') \;\Rightarrow$$

$$V_m - V_s = (V_{m_0} - V_{s_0}) - \frac{R_0}{\tau_c}(q - q_0) - \frac{\eth}{\tau_c}, \tag{5.32}$$

where:

$$\eth = \int_{q_0}^{q} M(q')\, \mathrm{d}q'. \tag{5.33}$$

Multiplying (5.32) by C_s, thus:

$$C_s V_m - C_s V_s = C_s(V_{m_0} - V_{s_0}) - \frac{C_s R_0}{\tau_c}(q - q_0) - \frac{C_s}{\tau_c}\eth, \tag{5.34}$$

By adding (5.27) and (5.34), it becomes:

$$C_0 V_m = \lambda\, e^{-\frac{t}{\tau_c}} + C_s(V_{m_0} - V_{s_0}) - \frac{C_s R_0}{\tau_c}(q - q_0) - \frac{C_s}{\tau_c}\eth \;\Rightarrow$$

$$V_m = \frac{\lambda}{C_0}\, e^{-\frac{t}{\tau_c}} + \frac{C_s}{C_0}(V_{m_0} - V_{s_0}) - \frac{C_s R_0}{\tau_c C_0}(q - q_0) - \frac{C_s}{\tau_c C_0}\,\eth. \tag{5.35}$$

Where $C_0 = C_m + C_s$. Substituting (5.35) in (5.28), we obtain the expression of $V_s(t)$ as:

$$V_s = \frac{\lambda}{C_s}\, e^{-\frac{t}{\tau_c}} - \frac{C_m}{C_s}\left[\frac{\lambda}{C_0}\, e^{-\frac{t}{\tau_c}} + \frac{C_s}{C_0}(V_{m_0} - V_{s_0}) - \frac{C_s R_0}{\tau_c C_0}(q - q_0) - \frac{C_s}{\tau_c C_0}\,\eth\right],$$

$$V_s = \left(1 - \frac{C_m}{C_0}\right)\frac{\lambda}{C_s}\, e^{-\frac{t}{\tau_c}} - \frac{C_m}{C_0}(V_{m_0} - V_{s_0}) + \frac{C_m R_0}{\tau_c C_0}(q - q_0) + \frac{C_m}{\tau_c C_0}\,\eth \;\Rightarrow$$

$$V_s = \frac{\lambda}{C_0}\, e^{-\frac{t}{\tau_c}} - \frac{C_m}{C_0}(V_{m_0} - V_{s_0}) + \frac{C_m R_0}{\tau_c C_0}(q - q_0) + \frac{C_m}{\tau_c C_0}\,\eth. \tag{5.36}$$

The initial state of the memristor with memristance $M(q)$ whose expression is given in (5.24) or (5.25), is given by the parameter q_0, for which according to q_0, there are 12 possible cases to consider. These cases are enumerated in section 5.6. However, here we introduced the first five cases describing the forward propagation (i.e from master to slave) of charge through the memristor. This will allow to observe the system evolution using the memristance function given by (5.24). Additionally, ð (given by eq. (5.33)) changes according to boundary conditions that model the effect of a window function. Hence, the cases highlight some instances of ð depending on q_0.

1. ***Case 1***: $if\ q_0 \le q(t) \le 0$:

$$\begin{aligned} \eth &= \int_{q_0}^{q} R_{off}\, dq' \\ &= R_{off}\,(q - q_0)\,. \end{aligned} \tag{5.37}$$

2. **Case 2**: $if\ q_0 < 0 < q(t) < q_d$:

$$\begin{aligned}\eth &= \int_{q_0}^{0} R_{off}\, dq' + \int_{0}^{q} \left(R_{off} - \delta R\, \frac{q'}{q_d}\right) dq' \\ &= R_{off}\,(q - q_0) - \delta R\, \frac{q^2}{2q_d}\,. \end{aligned} \tag{5.38}$$

3. **Case 3**: $if\ q_0 < 0 < q_d < q(t)$:

$$\begin{aligned}\eth &= \int_{q_0}^{0} R_{off}\, dq' + \int_{0}^{q_d} \left(R_{off} - \delta R\, \frac{q'}{q_d}\right) dq' + \int_{q_d}^{q} R_{on}\, dq' \\ &= -R_{off}\, q_0 + R_{off}\, q_d - \frac{\delta R}{2q_d}\, q_d^2 + R_{on}\,(q - q_d), \\ &= \frac{1}{2}\delta R\, q_d - R_{off}\, q_0 + R_{on}\, q. \end{aligned} \tag{5.39}$$

4. **Case 4**: $if\ 0 < q_0 < q(t) < q_d$:

$$\begin{aligned}\eth &= \int_{q_0}^{q} \left(R_{off} - \delta R\, \frac{q'}{q_d}\right) dq' \\ &= R_{off}\,(q - q_0) - \frac{\delta R}{2q_d}\,(q^2 - q_0^2)\,. \end{aligned} \tag{5.40}$$

5. **Case 5**: $if\ q_d < q_0 < q(t)$:

$$\begin{aligned}\eth &= \int_{q_0}^{q} R_{on}\, dq' \\ &= R_{on}\,(q - q_0)\,. \end{aligned} \tag{5.41}$$

The fact that the bilayer of TiO_2 material we consider for HP memristor, is used in normal conditions $\left(0 < x < 1 \text{ with } x = \frac{w}{D}\right)$ leads that the memristor is more described by cases 2, 3 and 4, whereas cases 1 and 5 are undesirable conditions related to the current rating of the device. Therefore, for the study purpose, cases 1 and 5 are avoided by modeling the effect of window function. By so doing, it will ensure that $q(t) \in [0, q_d]$.

Once the dynamics of the charge flowing into the memristor $M(q)$ is known, equations (5.35) and (5.36) allow to completely determine $V_m(t)$ and $V_s(t)$. Let us know look for the dynamics of $q(t)$.

5.5.3/ Charge $q(t)$ evolution for memristor coupling mode: using the $M(q)$ model (5.24)

This section presents the time evolution of the charge $q(t)$ flowing from one cell to another, focusing specifically on the model of memristor given by equation (5.24). Here, the

second method for solving equation (5.31) is considered.

Given the eq. (5.31), as:

$$\frac{dV_m}{dt} - \frac{dV_s}{dt} = -\frac{R_0}{\tau_c}\frac{dq}{dt} - \frac{1}{\tau_c}\left(M(q)\ \frac{dq}{dt}\right),$$

which can be rewritten as:

$$\frac{d}{dt}(V_m - V_s) = -\frac{R_o}{\tau_c}\frac{dq}{dt} - \frac{1}{\tau_c}\left(M(q)\ \frac{dq}{dt}\right).$$

Substituting $V_m(t) - V_s(t) = M(q)\ \dot{q}(t)$ from eq. (5.22) and rearranging, we get:

$$R_0\ \frac{dq}{dt} + M(q)\ \frac{dq}{dt} + \tau_c\frac{d}{dt}\left(M(q)\ \frac{dq}{dt}\right) = 0\ \Rightarrow$$

$$(R_0 + M(q))\ \frac{dq}{dt} + \tau_c\frac{d}{dt}\left[M(q)\ \frac{dq}{dt}\right] = 0. \tag{5.42}$$

The time derivative of the product term in (5.42) gives the following equation:

$$(R_0 + M(q))\ \frac{dq}{dt} + \tau_c\ \frac{d}{dt}[M(q)]\ \frac{dq}{dt} + \tau_c\ M(q)\ \frac{d^2q}{dt^2} = 0.$$

Using the identity: $\frac{dM(q)}{dt} = \frac{dM(q)}{dq} \times \frac{dq}{dt}$, then:

$$(R_0 + M(q))\ \frac{dq}{dt} + \tau_c\ \frac{dM(q)}{dq}\ \left(\frac{dq}{dt}\right)^2 + \tau_c\ M(q)\ \frac{d^2q}{dt^2} = 0. \tag{5.43}$$

Equation (5.43) requires a continuous first derivative of $M(q)$ with respect to charge q. Using the first model of $M(q)$ given by eq. (5.24), we see that: $\frac{dM(q)}{dq} = -\frac{\delta R}{q_d}$ in $[0, q_d]$, but 0 for $q \leq 0$ and $q \geq q_d$. However, the model of $M(q)$ given by eq. (5.25) has a continuous first derivative of $M(q)$ with respect to q, hence it is suitable to use for the solution of equation (5.43). Therefore equation (5.43) is treated extensively in section 5.6 using the model (5.25).

To use the model (5.24), we rather consider equation (5.32) given by:

$$V_m - V_s = (V_{m_0} - V_{s_0}) - \frac{R_0}{\tau_c}(q - q_0) - \frac{\eth}{\tau_c}.$$

As $V_m - V_s = M(q)\ \dot{q}$ given by eq. (5.22), and substituting for $M(q)\ \dot{q}$ with $\left(R_{off} - \delta R\frac{q}{q_d}\right)\ \dot{q}$, then:

$$\left(R_{off} - \delta R\frac{q}{q_d}\right)\ \frac{dq}{dt} = (V_{m_0} - V_{s_0}) - \frac{R_0}{\tau_c}(q - q_0) - \frac{\eth}{\tau_c}. \tag{5.44}$$

Hence, (5.44) can be solved according to $\eth$. To further solve (5.44) analytically, the defi-

nition of $\eth$ in ***case 4*** [eq. (5.40)] is considered, such that both q_0 and $q(t)$ are in $[0, q_d]$.

$$\left(R_{off} - \delta R \frac{q}{q_d}\right) \frac{dq}{dt} = (V_{m_0} - V_{s_0}) - \frac{R_0}{\tau_c}(q - q_0) - \frac{1}{\tau_c}\left(R_{off}(q - q_0) - \frac{\delta R}{2\, q_d}(q^2 - q_0^2)\right) \Rightarrow$$

$$\left(R_{off} - \delta R \frac{q}{q_d}\right) \frac{dq}{dt} = (V_{m_0} - V_{s_0}) - \frac{R_t}{\tau_c}(q - q_0) + \frac{\delta R}{2\tau_c\, q_d}(q^2 - q_0^2),$$

$$\frac{2\tau_c\, q_d}{\delta R}\left(R_{off} - \delta R \frac{q}{q_d}\right) \frac{dq}{dt} = (q^2 - q_0^2) - \frac{2q_d\, R_t}{\delta R}(q - q_0) + \frac{2\tau_c\, q_d}{\delta R}(V_{m_0} - V_{s_0}).$$

Let $q\prime = q - q_0$, then $dq\prime = dq$ and $q^2 = (q\prime + q_0)^2 \;\Rightarrow$

$$q^2 - q_0^2 = q\prime^2 + 2q_0\, q\prime.$$

Using the the new variable $q\prime$, then

$$\frac{2\tau_c\, q_d}{\delta R}\left(R_{off} - \delta R\, \frac{q\prime + q_0}{q_d}\right) \frac{dq\prime}{dt} = q\prime^2 + 2q_0\, q\prime - \frac{2q_d\, R_t}{\delta R}\, q\prime + \frac{2\tau_c\, q_d}{\delta R}(V_{m_0} - V_{s_0}) \Rightarrow$$

$$\begin{aligned} \frac{2\tau_c\, q_d}{\delta R}\left(M(q_0) - \frac{\delta R}{q_d} q\prime\right) \frac{dq\prime}{dt} &= q\prime^2 - 2\left[\frac{q_d\, R_t}{\delta R} - q_0\right] q\prime + \frac{2\tau_c q_d}{\delta R}(V_{m_0} - V_{s_0}), \\ &= (q\prime - \alpha)(q\prime - \beta), \\ &= P(q\prime), \end{aligned} \tag{5.45}$$

where $M(q_0) = \left(R_{off} - \delta R \frac{q_0}{q_d}\right)$, $P(q\prime)$ is a second degree polynomial, α and β are the roots of $P(q\prime)$ given by the characteristic equation:

$$q\prime^2 - 2\left[\frac{q_d\, R_t}{\delta R} - q_0\right] q\prime + \frac{2\tau_c q_d}{\delta R}(V_{m_0} - V_{s_0}) = 0,$$

such that: $0 < \beta < \alpha$ if initially $(V_{m_0} - V_{s_0}) > 0$. Therefore, (5.45) becomes

$$\left(M(q_0) - \frac{\delta R}{q_d} q\prime\right) \frac{dq\prime}{P(q\prime)} = \frac{\delta R}{2\tau_c\, q_d}\, dt, \tag{5.46}$$

OR

$$\left[\frac{\kappa_1}{q\prime - \alpha} + \frac{\kappa_2}{q\prime - \beta}\right] dq\prime = \frac{\delta R}{2\tau_c q_d}\, dt. \tag{5.47}$$

κ_1 and κ_2 are constants determined by coefficient comparison method. Therefore, equations (5.46) and (5.47) give the expressions

$$\kappa_1(q\prime - \beta) + \kappa_2(q\prime - \alpha) \;\equiv\; M(q_0) - \frac{\delta R}{q_d} q\prime \;\Rightarrow$$

$$\kappa_1 + \kappa_2 = -\frac{\delta R}{q_d} \tag{5.48a}$$

$$-\kappa_1\beta - \kappa_2\alpha = M(q_0) \tag{5.48b}$$

from eq. (5.48a) : $$\kappa_2 = -\kappa_1 - \frac{\delta R}{q_d} \tag{5.48c}$$

Putting (5.48c) into (5.48b), then:

$$-\kappa_1\beta - \alpha\left(-\kappa_1 - \frac{\delta R}{q_d}\right) = M(q_0) \;\Rightarrow$$

$$\kappa_1 = \frac{1}{(\alpha-\beta)}\left(M(q_0) - \frac{\delta R}{q_d}\alpha\right).$$

Substituting κ_1 into (5.48c), gives:

$$\kappa_2 = -\frac{1}{(\alpha-\beta)}\left[M(q_0) - \frac{\delta R}{q_d}\alpha\right] - \frac{\delta R}{q_d} \;\Rightarrow$$

$$\kappa_2 = -\frac{1}{\alpha-\beta}\left(M(q_0) - \frac{\delta R}{q_d}\beta\right).$$

By integrating (5.47):

$$\int_{q_0}^{q} \frac{\kappa_1}{q-q_0-\alpha}\,dq + \int_{q_0}^{q} \frac{\kappa_2}{q-q_0-\beta}\,dq = \frac{\delta R}{2\tau_c q_d}\int_0^t dt\,,$$

$$\kappa_1\,\ln\left(\frac{q-q_0-\alpha}{-\alpha}\right) + \kappa_2\,\ln\left(\frac{q-q_0-\beta}{-\beta}\right) = \frac{\delta R\,t}{2\tau_c q_d} \;\Rightarrow$$

$$\kappa_1\,\ln\left(\frac{\alpha+q_0-q}{\alpha}\right) + \kappa_2\,\ln\left(\frac{\beta+q_0-q}{\beta}\right) = \frac{\delta R\,t}{2\tau_c q_d}\,, \tag{5.49}$$

or equivalently expressed as:

$$\left[\frac{\alpha+q_0-q}{\alpha}\right]^{\kappa_1}.\left[\frac{\beta+q_0-q}{\beta}\right]^{\kappa_2} = e^{\frac{\delta R\,t}{2\tau_c q_d}}\,. \tag{5.50}$$

When the time t increases from $t = 0$, q also increases from q_0, so dq at the left of eq. (5.47) is positive, which implies $P(q\prime) > 0$. Consequently, $q(t)$ will not be able to pass greater than $q_0+\beta$, and we have to stop the integration at $q_0+\beta$ at the maximum. Then $q-q_0-\alpha$ and $q-q_0-\beta$ are both always negative.

Therefore, (5.50) links the time t and the charge through until the time t when $q(t)$ reaches $q_0+\beta$. Then, the right hand side member of (5.45) is zero, and $V_m(t) = V_s(t)$, whereas their sum will still be decreasing according to eq. (5.27). In fact, this time is infinite. $V_m(t)$

and $V_s(t)$ will wait an infinite time to be exactly the same, that is $V_m(+\infty) = V_s(+\infty) = 0$. At this time, the current $\left(\text{i.e } \dfrac{dq}{dt}\right)$ is zero too.
Note that the effect of q_0 in β is too trivial. So β is independent of q_0, and hence $P(q\prime)$ as well. The roots of $P(q\prime)$, i.e α and β, are unstable under certain condition, for example initial condition of $V_m(t)$ and $V_s(t)$. Therefore, it is interesting to compare the initial potential barrier $(V_{m_0} - V_{s_0})$ between the cells with respect to the ratio $\dfrac{q_0}{q_0+\beta}$. The idea is to observe whether the amplitude of variations between q_0 and $q_0+\beta$ will grow and become more interesting. Then with $q_0 = 30\mu C$, this comparison is given in table 5.1 and the corresponding curve is given in Fig. 5.10.

$(V_{m_0} - V_{s_0})$ *in Volts*	$\dfrac{q_0}{q_0+\beta}$
0	1
1	$\frac{30}{30.47} = 0.985$
2	$\frac{30}{30.15} = 0.969$
5	$\frac{30}{32.37} = 0.927$
10	$\frac{30}{34.74} = 0.864$
20	$\frac{30}{39.50} = 0.759$
30	$\frac{30}{44.28} = 0.678$
40	$\frac{30}{49.07} = 0.611$
50	$\frac{30}{53.89} = 0.557$

Table 5.1: Variation of the initial voltage difference and the corresponding charge ratio. These measurements are taken with: $q_0 = 30\mu C$, $R_{off} = 16k\Omega$, $R_{on} = 100\Omega$, $C_m = C_s = 1\mu F$ and $R_m = R_s = 100k\Omega$.

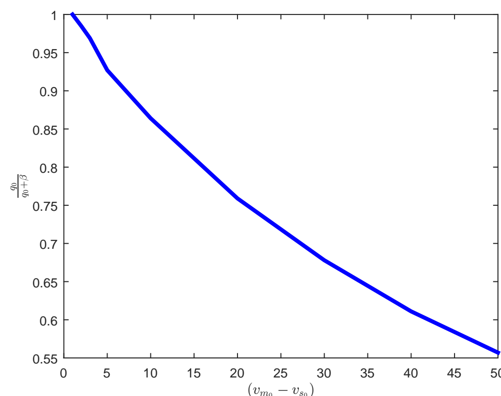

Figure 5.10: Plot of data from table 5.1.

Choosing $V_{m_0} - V_{s_0} = 20V$, we get $q_0 + \beta = 39.50\mu C$. Then when t varies from 0 to infinity (∞), $q(t)$ will vary from q_0 to $q_0 + \beta$. Note that it is impossible for $q(t)$ to be greater than

$q_0 + \beta$ according to equation (5.50). It means that the first root of $P(q)$ is met, that is $q_0 + \beta$, as a stable equilibrium point. One can realize that at q_0, $P(q_0)$ is positive and $P(q)$ will stay positive until $q_0 + \beta$, then the right hand side member of (5.46) is positive, so $\frac{dq}{dt}$ is positive as $\left(R_{off} - \delta R\ \frac{q(t)}{q_d}\right)$ is positive. When $q(t)$ reaches $q_0 + \beta$, $\frac{dq}{dt}$ becomes zero and stops to increase. Even if accidentally $q(t)$ exceeds $q_0 + \beta$, then $P(q)$ becomes negative, and then $\frac{dq}{dt}$ becomes also negative and deceases to $q_0 + \beta$. So, this equilibrium state is stable: everything forces $q(t)$ to tend definitively towards $q_0 + \beta$.

Then, consider equation (5.50), let us begin with $q(t) = q_0$ and of course at this stage $t = 0 \ \Rightarrow$

$$\left(\frac{\alpha}{\alpha}\right)^{\kappa_1} . \left(\frac{\beta}{\beta}\right)^{\kappa_2} = e^{\delta R\ \frac{t}{2\tau_c q_d}} = 1 \ : \ \text{Satisfied.}$$

Let increment q slightly with δq so that: $q = q_0 + n\ \delta q$, where $n = 0,\ 1,\ 2,\ ...\ + N$ where N is a nonzero positive integer. Note that for $n = 0$ corresponds to $q = q_0$ and $t = 0$. It implies that:

$$\begin{array}{ccc}
\left[\dfrac{\alpha + q_0 - 0.\delta q}{\alpha}\right]^{\kappa_1} \left[\dfrac{\beta + q_0 - 0.\delta q}{\beta}\right]^{\kappa_2} & = & e^{\delta R \frac{t_0}{2\tau_c q_d}} \\
\left[\dfrac{\alpha + q_0 - 1.\delta q}{\alpha}\right]^{\kappa_1} \left[\dfrac{\beta + q_0 - 1.\delta q}{\beta}\right]^{\kappa_2} & = & e^{\delta R \frac{t_1}{2\tau_c q_d}} \\
\left[\dfrac{\alpha + q_0 - 2.\delta q}{\alpha}\right]^{\kappa_1} \left[\dfrac{\beta + q_0 - 2.\delta q}{\beta}\right]^{\kappa_2} & = & e^{\delta R \frac{t_2}{2\tau_c q_d}} \\
\vdots \qquad\qquad \vdots & \cdots & \vdots \\
\left[\dfrac{\alpha + q_0 - N.\delta q}{\alpha}\right]^{\kappa_1} \left[\dfrac{\beta + q_0 - N.\delta q}{\beta}\right]^{\kappa_2} & = & e^{\delta R \frac{t_N}{2\tau_c q_d}}
\end{array} \tag{5.51}$$

To go closer to $q_0 + \beta$ as possible, we choose the increment: $\delta q = \frac{\beta}{N}$, such that n will now become more specific. Hence, it follows that:

$$q(t) = q_0 + \frac{n}{N}\beta. \tag{5.52}$$

The time evolution of $q(t)$ is given in Fig. 5.11a. Having known $q(t)$ from (5.52), then ð is calculated from (5.40) and the voltage $V_m(t)$ and $V_s(t)$ are calculated using the derived expressions given by (5.35) and (5.36) respectively, and the system evolution is given in Fig. 5.11b.

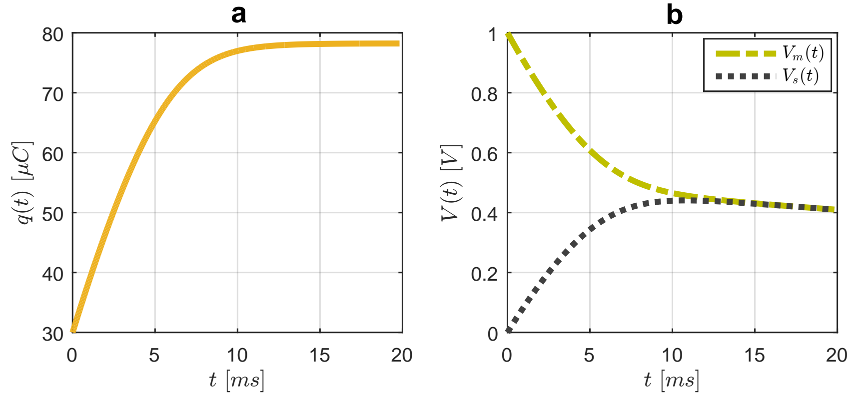

Figure 5.11: Analytical results showing the evolution of $V_m(t)$, $V_s(t)$ and $q(t)$ for Memristor coupling mode according to the analytical description (5.50) of the circuit schematic in Fig. 5.9. $R_m = R_s = 100K\Omega$, $C_m = C_s = 1\mu F$, $V(C_m) = V_{m_0} = 1V$ and $V(C_s) = V_{s_0} = 0V$. Memristor parameters: $R_{off} = 16K\Omega$, $R_{on} = 100\Omega$, $D = 10^{-8}m$, $\mu_v = 10^{-14}m^2/V.s$ and $q_0 = 0.3\ q_d$. (**a**) $q(t)$ evolution, (**b**) $V_m(t)$ and $V_s(t)$ evolution.

SPICE circuit simulation and Numerical solution by MatLab

The SPICE netlist file of memristor given in Table A.1 is used for the SPICE circuit simulation. Furthermore, in either case, the values of the parameters given by HP lab are used in order to suitably compare the results: $R_{off} = 16K\Omega$, $R_{on} = 100\Omega$, $\mu_v = 10fm^2/V.s.$ and $D = 10nm$, which gives $q_d = 100\mu C$. The SPICE simulation data are imported and the results are compared with ones from analytical and numerical solutions, see Fig. 5.12.

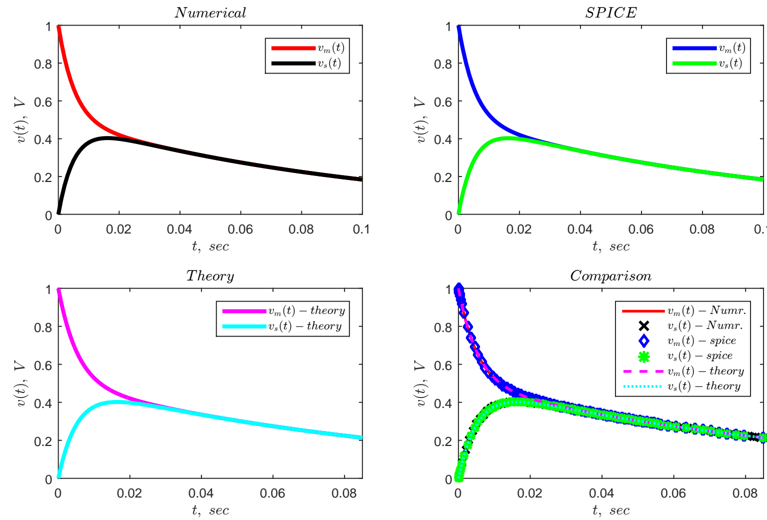

Figure 5.12: Comparison - Memristor coupling mode with linear resistors in the cell unit: $V_m(t)$ and $V_s(t)$ versus time for the three approaches. $R_m = R_s = 100K\Omega$, $C_m = C_s = 1\mu F$, $V(C_m) = V_{m_0} = 1V$ and $V(C_s) = V_{s_0} = 0V$. Memristor parameters: $R_{off} = 16K\Omega$, $R_{on} = 100\Omega$, $D = 10^{-8}m$, $\mu_v = 10^{-14}m^2/V.s$, $R_{init} = 11K\Omega$ and $q_0 = 0.3\ q_d$.

Equations (5.20)-(5.22) are solved numerically by MatLab using its built-in function - ODE function. The initial state of a memristor is a direct consequence of its ability to remember the history of electricity passed through it. With the memristance $M(x) = R_{off} - \delta Rx$, we suppose that the initial state of the memristor is x_0 and the corresponding memristance is $M_0 = 11K\Omega$, then: $x_0 = \dfrac{R_{off} - M_0}{\delta R} \approx 0.31$. For a charge-controlled memristor,

x_0 corresponds to the initial charge q_0 i.e $x_o = \dfrac{q_0}{q_d} \approx 30\mu C$. Figure 5.12 shows the result comparison, showing strong agreement in all the obtained results.

5.5.3.1/ EFFECT OF INITIAL CHARGE q_0 ON SYSTEM DYNAMICS

Recall that q_0 is a parameter representing the memory effect of a charge-controlled memristor. It is obvious that q_0 is not fixed at all time and it does depend on the quantity of electricity passed previously through the device. For unformed memristor device, q_0 is practically zero. However, for a formed memristor device, q_0 is nonzero due to the memory effect of the memristive device. This makes it possible to play with q_0 in the vicinity of q_d. Notice that with $q(t) = q_0 + \beta$ and β is independent of q_0, it implies that for a fixed β: $q(t)$ is affected by q_0. Hence, the higher the q_0, the higher the $q(t)$ and vice-versa. Moreover, this analogy will consequently reflect in the current flowing through the device because $i(t) = \dot{q}$.

Although memristor preserves its previous history, it is very difficult to know the exact initial charge q_0 having flowed through it before the beginning of the charge transfer at $t = 0$ [23]. Knowing its initial value is however important in analysis because the device will start from that state whenever it becomes active again. Therefore, q_0 is a parameter depending on the previous history of the memristor and the initial memristance of ideal charge-controlled memristor is a function of it [41]. There are many possible cases of q_0 to consider, including $q_0 < 0$ or $q_0 > q_d$. However, this section considers only the case where q_0 is always between 0 and q_d such that: $0 < q_0 < q_d$, corresponding to $M(q)$ given by:

$$M(q) = R_{off} - \delta R\, \frac{q}{q_d}. \tag{5.53}$$

For a physical memristor device, the necessary and sufficient condition for $M(q) \geq 0$, is given by: $0 \leq q(t) \leq q_d$. Choosing arbitrary values of q_0 between 0 and q_d is enough to study the memory effect of the memristor on the evolution of $V_m(t)$ and $V_s(t)$ towards the saturation of the system. Considering three possible instances of q_0 i.e $q_0 = 0.1q_d$, $q_0 = 0.3q_d$ and $q_0 = 0.9q_d$, then $V_m(t)$ and $V_s(t)$ are obtained from (5.35) and (5.36) respectively, and the results are given in Fig. 5.13. The continuous and dotted blue traces refer to $V_m(t)$ and $V_s(t)$ for $q_0 = 0.9q_d$ respectively. Similarly, the traces in red and black are for $q_0 = 0.3q_d$ and $q_0 = 0.1q_d$ respectively.

The time constant of the system is affected by the initial memristance: the higher is q_0, the lower is the initial memristance, hence the lower is the time constant and vice versa. This conclusion is drawn by looking at the respective responses of the cells under different initial conditions as depicted by Fig. 5.13. Therefore, the effect of initial memristance on

the dynamics of the system is sensitive and it must be taken into consideration. This time lapse can also explain the concept of different read/write timing in a memristor based memory applications.

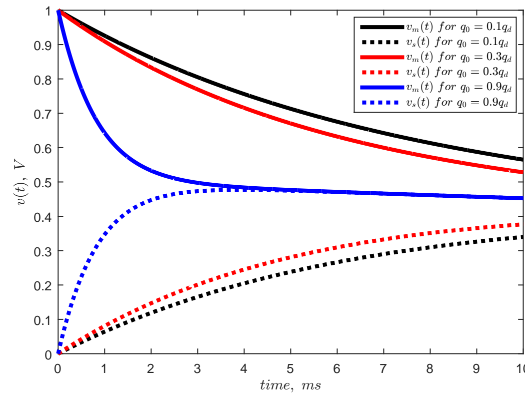

Figure 5.13: Evolution of $V_m(t)$ and $V_s(t)$ showing the effect of initial memristance given by different q_0 instantiations i.e $q_0 = 0.1q_d$, $q_0 = 0.3q_d$ and $q_0 = 0.9q_d$ resectively. At $t = 0$, $V_m(t = 0) = V_{m_0} = 1V$, $V_s(t = 0) = V_{s_0} = 0V$, meanwhile $R_m = R_s = 100K\Omega$, $C_m = C_s = 1\mu F$, $R_{off} = 16K\Omega$, $R_{on} = 100\Omega$ and memristor technology parameters as suggested in [12].

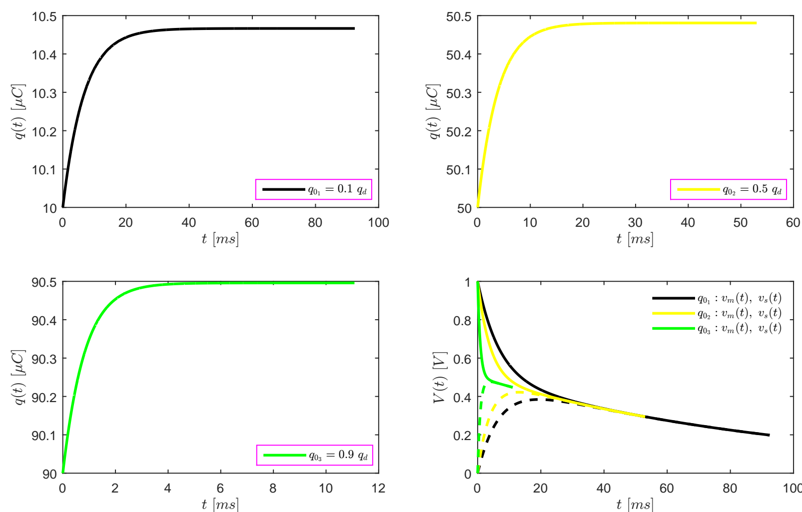

Figure 5.14: Time evolution of $V_m(t)$ and $V_s(t)$ and the corresponding charge $q(t)$ for $q_0 = [0.1q_d,\ 0.5q_d,\ 0.9q_d]$.

5.5.3.2/ Variation of $(V_{m_0} - V_{s_0})$ or specifically V_{m_0}

So far $V_{m_0} = 1V$ and $V_{s_0} = 0V$ are considered, so that the difference $V_{m_0} - V_{s_0} = 1V$. However, it is interesting to observe the effect of different potentials for a fixed q_0, say $30\mu C$ for example. The idea is to observe the memristance transition effects from such initial state when the device is subjected to different input potentials. Therefore, we considered $(V_{m_0} - V_{s_0} = 5V,\ 10,\ 10V,\ 20V$ and $50V)$, the results are given in Fig. 5.15.

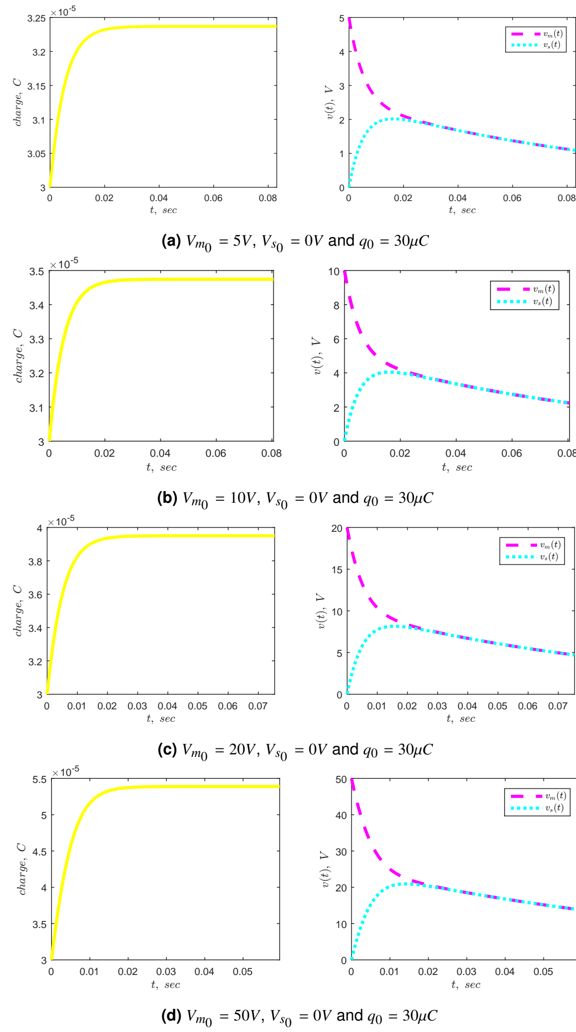

(a) $V_{m_0} = 5V$, $V_{s_0} = 0V$ and $q_0 = 30\mu C$

(b) $V_{m_0} = 10V$, $V_{s_0} = 0V$ and $q_0 = 30\mu C$

(c) $V_{m_0} = 20V$, $V_{s_0} = 0V$ and $q_0 = 30\mu C$

(d) $V_{m_0} = 50V$, $V_{s_0} = 0V$ and $q_0 = 30\mu C$

Figure 5.15: Variation of $V_{m_0} - V_{s_0}$ for a fixed (q_0). Expectantly, $q(t)$ slightly increases with increases in $(V_{m_0} - V_{s_0})$. The simulation time is determined by $q(t)$ and $(V_{m_0} - V_{s_0})$. Similarly, $V_m(t)$ and $V_s(t)$ fit the output data as shown in the plot window of each case.

5.6/ MEMRISTOR DYNAMICS INVOLVED IN CELLS COMMUNICATION

This section focuses on the diffusive effect phenomenon involved in the cells communication via a memristor. Since information is launched from one cell to another through a memristor, hence it is important to study the dynamics at which these cells are communicating. Notice that the dynamic mechanism in this context, is the charge flowing through the memristor until the cells are saturated (i.e $V_m(t) = V_s(t)$ in the case of two cells system). We used the second way of solving equation (5.31) to get equation (5.43) which can be used to study the dynamics of the system.

Given the equation (5.43) as:

$$(R_0 + M(q))\,\frac{dq}{dt} + \tau_c\,\frac{dM(q)}{dq}\left(\frac{dq}{dt}\right)^2 + \tau_c\,M(q)\,\frac{d^2q}{dt^2} = 0. \tag{5.54}$$

Equation (5.54) is a second order nonlinear differential equation, where $M(q)$ is the charge-controlled memristance defined by equations (5.24) and (5.25). However, equation (5.54) requires a continuous first derivative of $M(q)$ with respect to q. The expression of $M(q)$ given in (5.24), is not differentiable at $q(t) = 0$ or q_d, as shown in Fig. 4.5a. Therefore, equation (5.24) does not allow to determine the solution of (5.54) for all possible values of $q(t)$ due to discontinuities at $q(t) = 0$ and $q(t) = q_d$, thus, it is not a good candidate to apply for eq. (5.54). On the other hand, the new model of $M(q)$ given by eq. (5.25) is determined to be continuous and with a continuous first derivative with respect to q (see Fig. 4.5a), thus, becomes suitable to be used in equation (5.54). Notwithstanding, the function $M(q)$ by (5.24) can only be used in (5.54) provided the condition $0 < q(t) < q_d$ is met, for all time. But it is emphasized that $q(t)$ can extend outside this limit, which is exactly why we propose to rather use the new model.

5.6.1/ EVOLUTION OF $q(t)$ IN PHASE PORTRAITS:– SYSTEM SOLUTION USING THE NEW MODEL

Equation (5.54) is to be studied in the phase plane allowing to observe the time evolution of the charge $q(t)$. The system is normalised by considering $X = \dfrac{q}{q_d}$. Moreover, X_0 corresponds to the normalised form of q_0, initial charge having already flowed into the memristor before $t = 0$, namely, $X_0 = \dfrac{q_0}{q_d}$. Thus

$$M(X) = \begin{cases} R_{off}, & if\ X \leq 0 \\ R_{off} - 3\,\delta R\,X^2 + 2\,\delta R\,X^3, & if\ 0 \leq X \leq 1 \\ R_{on}, & if\ X \geq 1 \end{cases} \tag{5.55}$$

Therefore, with $\tau = \frac{t}{\tau_c}$ normalized time, equation (5.54) is rewritten as:

$$(R_0 + M(X))\ \frac{q_d}{\tau_c}\frac{dX}{d\tau} + \frac{\tau_c}{q_d}\frac{dM(X)}{dX}\left(\frac{q_d}{\tau_c}\frac{dX}{d\tau}\right)^2 + \tau_c\ M(X)\ \frac{q_d}{\tau_c^2}\frac{d^2X}{d\tau^2} = 0 \quad \Rightarrow$$

$$[R_0 + M(X)]\ \frac{dX}{d\tau} + \frac{dM(X)}{dX}\left[\frac{dX}{d\tau}\right]^2 + M(X)\ \frac{d^2X}{d\tau^2} = 0. \quad (5.56)$$

Setting $Y = \frac{dX}{d\tau} = \dot{X}$ and $\dot{Y} = \frac{d^2X}{d\tau^2} = \ddot{X}$, where X and Y are normalized quantities of charge and current respectively. Thus (5.56) can be expressed as:

$$[R_0 + M(X)]\ \ Y + \frac{dM(X)}{dX}\ Y^2 + M(X)\ \dot{Y} = 0. \quad (5.57)$$

Furthermore, the system can be more normalized by writing (5.55) in normalised form as $M(X) = \delta R \mathcal{M}(X)$, with the normalised memristance $\mathcal{M}(X)$ given by:

$$\mathcal{M}(X) = \begin{cases} \frac{R_{off}}{\delta R}, & if\ X \leq 0 \\ \frac{R_{off}}{\delta R} - 3\ X^2 + 2\ X^3, & if\ 0 \leq X \leq 1 \\ \frac{R_{on}}{\delta R}, & if\ X \geq 1 \end{cases} \quad (5.58)$$

which gives the complete normalized form of (5.57), as:

$$\left(\frac{R_0}{\delta R} + \mathcal{M}\right)\ Y + \frac{d\mathcal{M}}{dX}\ Y^2 + \mathcal{M}\ \dot{Y} = 0. \quad (5.59)$$

Equation (5.59) is better studied in the plane (X, Y). The dot notation in X and Y means the derivative with respect to τ.

From (5.58) and (5.59), the system is simplified to:

$if\ \ X \leq 0,\ \ \mathcal{M}(X) = \frac{R_{off}}{\delta R}$, then (5.59) becomes

$$\left(\frac{R_0}{\delta R} + \frac{R_{off}}{\delta R}\right) Y + \frac{R_{off}}{\delta R}\ \dot{Y} = 0,$$

$$R_t\ Y + R_{off}\ \dot{Y} = 0 \quad \Rightarrow$$

$$\dot{Y} = -\frac{R_t}{R_{off}} Y,$$

where $R_t = R_0 + R_{off}$. Setting $\gamma_1 = \frac{R_t}{2\delta R}$ and $\gamma_2 = \frac{R_{off}}{2\delta R}$, then $\frac{R_t}{R_{off}} = \frac{\gamma_1}{\gamma_2}$.

∴

$$\begin{cases} \dot{Y} = -\frac{\gamma_1}{\gamma_2} Y, \\ \dot{X} = Y. \end{cases} \tag{5.60}$$

From (5.60), thus:

$\frac{dY}{dX} = -\frac{\gamma_1}{\gamma_2}$, with the first integration to give:

$$Y = -\frac{\gamma_1}{\gamma_2} X + \text{constant}, \tag{5.61}$$

or in a more descriptive way as:

$$H(X, Y) = Y + \frac{\gamma_1}{\gamma_2} X + \mathscr{C}_1 = H_L(X, Y). \tag{5.62}$$

Where $\mathscr{C}_1$ is a term for continuity at $X(\tau) = 0$ as the system continues with the second definition of $\mathscr{M}$ and $H_L(X, Y)$ is a constant determined by initial conditions: X_0, V_{m_0}, V_{s_0} and Y_0, with:

$$Y_0 = \frac{\tau_c \left(V_{m_0} - V_{s_0}\right)}{q_d.\delta R.\mathscr{M}(X_0)},$$

obtained from (5.22) given that $i(t) = \frac{dq}{dt} = \frac{q_d}{\tau_c} Y$. By extension, $H(X, Y)$ corresponds to a conservative quantity similar to the Hamiltonian in mechanics. Therefore, for any initial conditions X_0 and Y_0, $H(X, Y) = h$ can be deduced. $H_L(X, Y)$ gives the h value to the left of the system i.e $X \leq 0$.

$if \;\; 0 \leq X \leq 1, \;\; \mathscr{M}(X) = \frac{R_{off}}{\delta R} - 3X^2 + 2X^3$, then (5.59) becomes:

$$\left(\frac{R_t}{\delta R} - 3\, X^2 + 2\, X^3\right)\, Y + 6(X^2 - X)\, Y^2 + \left(\frac{R_{off}}{\delta R} - 3\, X^2 + 2\, X^3\right)\dot{Y} = 0.$$

Note that $\frac{R_t}{\delta R} = 2\gamma_1$ and $\frac{R_{off}}{\delta R} = 2\gamma_2$, then

$$\left(X^3 - \frac{3}{2}\, X^2 + \gamma_1\right) Y + 3(X^2 - X)\, Y^2 + \left(X^3 - \frac{3}{2}\, X^2 + \gamma_2\right)\dot{Y} = 0 \quad \Rightarrow$$

$$\begin{cases} \dot{Y} = -\frac{\left(X^3 - \frac{3}{2}X^2 + \gamma_1\right) Y + 3(X^2 - X)Y^2}{X^3 - \frac{3}{2}X^2 + \gamma_2} \\ \dot{X} = Y \end{cases} \tag{5.63}$$

Notice that both X and Y are normalised, hence have no unit. Equation (5.63) gives the following Hamiltonian system:

$\frac{dY}{dX} = -\frac{(X^3 - \frac{3}{2}X^2 + \gamma_1) + 3(X^2 - X)Y}{X^3 - \frac{3}{2}X^2 + \gamma_2},$

$(X^3 - \frac{3}{2}X^2 + \gamma_2)\ \frac{dY}{dX} + 3(X^2 - X)\ Y = -(X^3 - \frac{3}{2}X^2 + \gamma_1)\ \Rightarrow$

$\frac{d}{dX}\left((X^3 - \frac{3}{2}X^2 + \gamma_2)\ Y\right) = -(X^3 - \frac{3}{2}X^2 + \gamma_1)$, and integrating gives:

$\int d\left((X^3 - \frac{3}{2}X^2 + \gamma_2)Y\right) = -\int \left(X^3 - \frac{3}{2}X^2 + \gamma_1\right) dX$,

$(X^3 - \frac{3}{2}X^2 + \gamma_2)Y = -\left(\frac{1}{4}X^4 - \frac{1}{2}X^3 + \gamma_1 X\right) + \text{constant}\ \Rightarrow$

$$H(X,Y) = \left(X^3 - \frac{3}{2}X^2 + \gamma_2\right) Y + \frac{1}{4}X^4 - \frac{1}{2}X^3 + \gamma_1 X = h. \tag{5.64}$$

$if\ \ X \geq 1,\ \ \mathscr{M}(X) = \frac{R_{on}}{\delta R}$, then (5.59) becomes:

$(R_0 + R_{on})\ Y + R_{on}\ \dot{Y} = 0,$

$R_u\ Y + R_{on}\ \dot{Y} = 0\ \Rightarrow$

$$\dot{Y} = -\frac{R_u}{R_{on}}\ Y,$$

where $R_u = R_0 + R_{on}$. Similarly, by setting:

$$\frac{R_u}{R_{on}} = \frac{R_t - \delta R}{R_{off} - \delta R} = \frac{\frac{R_t}{\delta R} - 1}{\frac{R_{off}}{\delta R} - 1} = \frac{2\gamma_1 - 1}{2\gamma_2 - 1}\ \Rightarrow$$

$$\begin{cases} \dot{Y} = -\dfrac{2\gamma_1 - 1}{2\gamma_2 - 1} Y \\ \dot{X} = Y \end{cases} \tag{5.65}$$

From (5.65), one can see that:

$\frac{dY}{dX} = -\frac{2\gamma_1 - 1}{2\gamma_2 - 1}$, which by integrating gives:

$Y = -\frac{\gamma_1 - \frac{1}{2}}{\gamma_2 - \frac{1}{2}} X + \text{constant}\ \ \Rightarrow,$

$$\left(\gamma_2 - \frac{1}{2}\right) Y + \left(\gamma_1 - \frac{1}{2}\right) X = \text{constant},$$

Considering the continuity at $X = 1$ and the fact that h is invariant quantity, the equation is

given in a more descriptive form as:

$$H(X,Y) = \left(\gamma_2 - \frac{1}{2}\right)Y + \left(\gamma_1 - \frac{1}{2}\right)X + \mathscr{C}_2 = H_R(X,Y). \tag{5.66}$$

Similarly, $H_R(X,Y)$ is the h value at the right of the system, i.e $X \geq 1$ and $\mathscr{C}_2$ is the continuity term at $X(\tau) = 1$. To finalize the expressions for (5.62) and (5.66), the following conditions are required:

$$\text{Continuity of } H(X,Y) \text{ at } X(\tau) = 0: \quad H_L(X=0,Y) = H(X=0,Y) = h \tag{5.67a}$$

$$\text{Continuity of } H(X,Y) \text{ at } X(\tau) = 1: \quad H(X=1,Y) = H_R(X=1,Y) = h \tag{5.67b}$$

Applying the condition (5.67a) to (5.62) and (5.64), and substituting $X = 0$, then:

$Y + \mathscr{C}_1 = \gamma_2\, Y \;\; \Rightarrow \;\mathscr{C}_1 = (\gamma_2 - 1)\, Y$.

Hence, from $(5.64)\Big|_{X=0}$: $Y = \dfrac{h}{\gamma_2}$. Thus: $\mathscr{C}_1 = \left(1 - \dfrac{1}{\gamma_2}\right) h$. With $H_L(X,Y) = h$ and $\mathscr{C}_1$, equation (5.62) becomes:

$h = Y + \dfrac{\gamma_1}{\gamma_2}X + \left(1 - \dfrac{1}{\gamma_2}\right)h$, which admits the conservative quantity:

$$H_L(X,Y) = \gamma_2 Y + \gamma_1 X = h. \tag{5.68}$$

Applying the condition (5.67b) to (5.64) and (5.66), and substituting $X = 1$, then:

$\left(\gamma_2 - \dfrac{1}{2}\right)Y + \gamma_1 - \dfrac{1}{4} = \left(\gamma_2 - \dfrac{1}{2}\right)Y + \left(\gamma_1 - \dfrac{1}{2}\right) + \mathscr{C}_2 \;\Rightarrow$

$$\mathscr{C}_2 = \frac{1}{4}.$$

Using the expression of $\mathscr{C}_2$, (5.66) becomes:

$$H_R(X,Y) = \left(\gamma_2 - \frac{1}{2}\right)Y + \left(\gamma_1 - \frac{1}{2}\right)X + \frac{1}{4} = h. \tag{5.69}$$

SOLVING FOR $X(\tau)$

To get the phase plane (X, Y), the expression of $X(\tau)$ is to be obtained from (5.68), (5.64) and (5.69) for $X \leq 0$, $0 \leq X \leq 1$ and $X \geq 1$ respectively, by substituting $Y = \dfrac{dX}{d\tau}$, along with the given initial states X_{0_1}, X_{0_2} and X_{0_3}. Why X_{0_1}, X_{0_2} and X_{0_3}? These are terms describing all the possible instances of X_0. It is important to note that the state X_0 is not fixed (in other word, it's unknown) and it strongly depends on the history of the device, which could be either in one of the 3 regions. Similar scenario for q_0 was briefly explored in section 5.5.3.1, however using the expression of $M(q)$ given by eq. (5.24) which is only valid for $X \in [0,\ 1]$. Now in this context and with the help of the modified $M(X)$ model, X_0 is deeply taken into account.

$X(\tau) \in [-\infty,\ 0]$:

Equation (5.68) is solved to give:

$$\frac{dX}{d\tau} = -\frac{\gamma_1}{\gamma_2}\left(X - \frac{h}{\gamma_1}\right),$$

$$\frac{dX}{X - \frac{h}{\gamma_1}} = -\frac{\gamma_1}{\gamma_2} d\tau,$$

$$\ln\left(X - \frac{h}{\gamma_1}\right) = -\frac{\gamma_1}{\gamma_2}\tau + \ln K_1 \quad \Rightarrow$$

$$X - \frac{h}{\gamma_1} = K_1\, e^{-\frac{\gamma_1}{\gamma_2}\tau}.$$

At $\tau = 0$, $X(\tau = 0) = X_{0_1}$ which is the initial state when the system is described by (5.68), then $K_1 = X_{0_1} - \dfrac{h}{\gamma_1} \quad \Rightarrow$

$$X(\tau) = \left(X_{0_1} - \frac{h}{\gamma_1}\right) e^{-\frac{\gamma_1}{\gamma_2}\tau} + \frac{h}{\gamma_1}. \tag{5.70}$$

N.B: $X_{0_1} \leq X(\tau) \leq 0$. The normalised time for this case can be expressed from (5.70), as:

$$\ln\left(\frac{X(\tau) - \frac{h}{\gamma_1}}{X_{0_1} - \frac{h}{\gamma_1}}\right) = -\frac{\gamma_1}{\gamma_2}\ \tau \ \Rightarrow$$

$$\tau = -\frac{\gamma_2}{\gamma_1}\ \ln\left(\frac{X(\tau) - \frac{h}{\gamma_1}}{X_{0_1} - \frac{h}{\gamma_1}}\right), \qquad \tau \in [-\infty,\ \tau_1]. \tag{5.71}$$

Where τ_1 is the time when $X(\tau) = 0$, and is given by:

$$\tau_1 = -\frac{\gamma_2}{\gamma_1} \ln\left(-\frac{h}{\gamma_1 X_{0_1} - h}\right) \Rightarrow$$

$$\tau_1 = -\frac{\gamma_2}{\gamma_1} \ln\left(\frac{h}{h - \gamma_1 X_{0_1}}\right). \tag{5.72}$$

Furthermore, at $\tau = \tau_1$, $X(\tau)$ continued with the second description of the system given by equation (5.64).

$X(\tau) \in [0,\ 1]$:

The solution is derived from (5.64), as:

$$Y = \frac{\mathrm{d}X}{\mathrm{d}\tau} = \frac{h - \left(\frac{1}{4}X^4 - \frac{1}{2}X^3 + \gamma_1 X\right)}{\left(X^3 - \frac{3}{2}X^2 + \gamma_2\right)} \Rightarrow$$

$$\frac{X^3 - \frac{3}{2}X^2 + \gamma_2}{X^4 - 2X^3 + 4\gamma_1 X - 4h}\mathrm{d}X = -\frac{\mathrm{d}\tau}{4}, \tag{5.73}$$

where:

$$\tau = \tau_1 - 4\int_{X_{0_2}}^{X} \frac{P_3(X')}{P_4(X')}\,\mathrm{d}X', \qquad \tau \in [\tau_1,\ \tau_2] \tag{5.74}$$

In addition, $P_3(X) = X^3 - \frac{3}{2}X^2 + \gamma_2$, $P_4(X) = X^4 - 2X^3 + 4\gamma_1 X - 4h$, τ_2 is the time when $X(\tau) = 1$ and X_{0_2} is the initial state if the system is described by (5.64). Note that $0 \le X_{0_2} \le X(\tau)$. However due to continuity at $X(\tau_1) = 0$, we could have $X(\tau_1) \le X_{0_2}$. In addition to the study of phase portraits for equation (5.74), it is important to look for the existence of real roots of $P_4(X)$ and singularity points of the system.

The ***equilibrium points of the system*** are met when $\frac{dY}{d\tau} = 0$ and $\frac{dX}{d\tau} = Y = 0$, in other words $V_m(t) = V_s(t)$. The equilibrium points of the system (5.63), and focus on equation (5.74), we see directly that $Y = 0$ is enough to have $\frac{dX}{d\tau} = 0$ and $\frac{dY}{d\tau} = 0$. Then every point $(X, Y = 0)$ is possibly an equilibrium point. Notice that $\frac{dP_4(X)}{dX} = P_4'(X)$ is proportional to:

$$X^3 - \frac{3}{2}X^2 + \gamma_1 = 0, \tag{5.75}$$

having atleast one real root X_e corresponding to the value of $X(\tau)$ at the equilibrium point $Y = 0$. Then if we have 3 real roots for $X^3 - \frac{3}{2}X^2 + \gamma_1 = 0$, the curve $P_4(X)$ will have 3 maxima or minima and it will help to factor $P_4(X)$ for all its possible roots. Figure 5.16 shows some graphical representation of $P_4(X)$ according to the value of h. It will be interesting to have the general solution of equation (5.75) in terms of γ_1. Therefore, the

equation is solved along with a brief review on the formation of cubic formula for solving cubic equation which would enable to factor $P_3(X)$ and $P_4(X)$ for any given γ_1, γ_2 and h values. Equation (5.75) resembles the general monic cubic equation given by:

$$X^3 + aX^2 + bX + c = 0, \qquad a, b, c \in \mathbb{C}.$$

The equation is reduced to a perfect cubic by posing a new variable $\tilde{\chi} = X + \frac{a}{3}$ and the second degree term is eliminated. Thus leaving behind a depressed form of the equation, as:

$$\tilde{\chi}^3 + P\,\tilde{\chi} + Q = 0, \qquad P, Q \in \mathbb{C}, \tag{5.76}$$

where:

$$X = \tilde{\chi} - \frac{a}{3}, \;\; P = b - \frac{a^2}{3} \text{ and } Q = c + \frac{2a^3}{27} - \frac{ba}{3}.$$

Equation (5.76) is an associated form of the previous one having the same solution. Therefore, with $\tilde{\chi} = \tilde{u} - \tilde{v}$, equation (5.76) is equivalent to the algebra identity:

$$(\tilde{u} - \tilde{v})^3 + 3\tilde{u}\tilde{v}(\tilde{u} - \tilde{v}) - (\tilde{u}^3 - \tilde{v}^3) = 0, \qquad \tilde{u}, \tilde{v} \in \mathbb{C}$$

with:

$$\tilde{u}\tilde{v} = \frac{P}{3}$$
$$\tilde{u}^3 - \tilde{v}^3 = -Q$$

These equations are solved simultaneously, for example with $\tilde{u} = \frac{P}{3\tilde{v}}$, then the second equation becomes $\left(\frac{P}{3\tilde{v}}\right)^3 - \tilde{v}^3 = -Q \;\Rightarrow$

$$(\tilde{v}^3)^2 - Q(\tilde{v}^3) - \frac{P^3}{27} = 0.$$

This is a quadratic equation in $\tilde{v}^3$ and it gives 2 possible solutions of $\tilde{v}^3$. Thus by quadratic formula, it becomes:

$$\tilde{v} = \sqrt[3]{\frac{Q}{2} + \sqrt{\Delta}} \text{ or } \tilde{v} = \sqrt[3]{\frac{Q}{2} - \sqrt{\Delta}},$$

where Δ is the discriminant and is given by:

$$\Delta = \frac{Q^2}{4} + \frac{P^3}{27}.$$

Therefore, knowing $\tilde{v}$:

$$\tilde{u} = \frac{P}{3\tilde{v}}.$$

So far we have only got the particular solution. Therefore, to generalize the formulation,

Euler's identity $e^{j\theta}$ is considered for which the complex solution is taken into consideration. Recall that $e^{jn\pi} = 1$ for any even number n. Then for $n = 2$, let us define a cube root of unity as ω, so that $\omega^3 = e^{j2\pi} = 1$, then:

$$\omega = e^{j\frac{2\pi}{3}} = -\frac{1}{2} + \frac{\sqrt{3}}{2}j.$$

It follows that $(\omega^2)^3 = 1$, implying that 1, ω and ω^2 are all cube roots of unity. In general, given one of the roots $\tilde{v}$ as a particular solution, then the other two roots are $\tilde{v}\omega$ and $\tilde{v}\omega^2$. Hence, picking a particular solution $\tilde{v}$, then $\tilde{u} = \frac{P}{3\tilde{v}}$ and the three possible solutions of the depressed cubic equation are:

$$\tilde{\chi}_1 = \tilde{u} - \tilde{v}, \;\; \tilde{\chi}_2 = \tilde{u}\omega^2 - \tilde{v}\omega \;\; \text{and} \;\; \tilde{\chi}_3 = \tilde{u}\omega - \tilde{v}\omega^2.$$

The complete solution of a monic cubic equation is obtained from: $X = \tilde{\chi} - \frac{a}{3} \Rightarrow$,

$$X_1 = \tilde{u} - \tilde{v} - \frac{a}{3}, \;\; X_2 = \tilde{u}\omega^2 - \tilde{v}\omega - \frac{a}{3} \;\; \text{and} \;\; X_3 = \tilde{u}\omega - \tilde{v}\omega^2 - \frac{a}{3}. \tag{5.77}$$

N.B: For $\Delta < 0$, one has to find the cube root of complex number, for example $\sqrt[3]{c + j\,d}$ ... using De Moivre's theorem, which stated that

$$(c + j\,d)^n = r^n(cos\; n\theta + j\; sin\; n\theta)$$

where r and θ are modulus and argument. However our system requires to solve for $\sqrt[3]{j}$ due to the fact that the coefficient of the first degree term is zero, i.e $b = 0$ (see eq. (5.75)). Therefore, posing $j = 0 + j = r(cos\theta + jsin\theta) \;\; \Rightarrow$ modulus $r = 1$ and argument $\theta = \frac{\pi}{2}$. Moreover, it is known that $j^n = cos\,\frac{n\pi}{2} + j\; sin\,\frac{n\pi}{2}$. Since 2π describes a complete clock circle, thus choosing $2\pi n$, with n representing three consecutive integers (say for e.g -1, 0 and 1) to give the cube roots. Then with cube root of j as $j^{\frac{1}{3}}$ and using De Moivre's theorem, the cube roots are obtained as:

$$j^{\frac{1}{3}} = cos\frac{\frac{\pi}{2} + 2\pi n}{3} + jsin\frac{\frac{\pi}{2} + 2\pi n}{3}, \qquad n \in [-1, 0, 1]$$

Upon simplification:

$$j^{\frac{1}{3}} = \begin{cases} -j, & if\; n = -1 \\ \frac{\sqrt{3}}{2} + j\frac{1}{2}, & if\; n = 0 \\ -\frac{\sqrt{3}}{2} + j\frac{1}{2}, & if\; n = 1 \end{cases}$$

Although these give all the cube roots and satisfy $\sqrt[3]{j}$, it is however simpler to see that: $j = cos\,\frac{\pi}{2} + jsin\,\frac{\pi}{2} \;\; \Rightarrow \;\; j^{\frac{1}{3}} = cos\,\frac{\pi}{6} + jsin\,\frac{\pi}{6} = \frac{\sqrt{3}}{2} + j\frac{1}{2}$. This corresponds to the above case

with $n = 0$. Moreover, it ensures proper permutation of the general solution as outlined. Given equation (5.75) and by comparison, the coefficients are:

$$a = -\frac{3}{2}, \quad b = 0 \text{ and } c = \gamma_1,$$

which gives:

$$X_e = \tilde{\chi} + \frac{1}{2}, \quad P_e = -\frac{3}{4} \text{ and } Q_e = \gamma_1 - \frac{1}{4}.$$

Note that the subscript *e* in X_e, P_e and Q_e refers to the case "study of equilibrium point" given by (5.75). Substituting for P_e and Q_e, thus:

$$\Delta_e = \frac{Q_e^2}{4} + \frac{P_e^3}{27} = \frac{2\gamma_1^2 - \gamma_1}{8} \text{ and } \tilde{v}_e = \sqrt[3]{\frac{Q_e}{2} + \sqrt{\Delta_e}} = \frac{\sqrt[3]{4\gamma_1 - 1 + \sqrt{16\gamma_1^2 - 8\gamma_1}}}{2}.$$

Let us assign $\mathscr{A} := 4\gamma_1 - 1$, then $\mathscr{A}^2 - 1 = 16\gamma_1^2 - 8\gamma_1 \quad \Rightarrow$

$$\tilde{v}_e = \frac{\sqrt[3]{\mathscr{A} + \sqrt{\mathscr{A}^2 - 1}}}{2}.$$

Meanwhile:

$$\tilde{u}_e = \frac{P_e}{3\tilde{v}_e} = -\frac{1}{2\sqrt[3]{\mathscr{A} + \sqrt{\mathscr{A}^2 - 1}}}.$$

The complete solution of the original equation (5.75) is given by:

$$X_{e_1} = \tilde{u}_e - \tilde{v}_e + \frac{1}{2}, \quad X_{e_2} = \tilde{u}_e\omega^2 - \tilde{v}_e\omega + \frac{1}{2} \text{ and } X_{e_3} = \tilde{u}_e\omega - \tilde{v}_e\omega^2 + \frac{1}{2}. \tag{5.78}$$

The values of parameters in Fig. 5.9 are considered as: $R_{off} = 16K\Omega$, $R_{on} = 100\Omega$, $\delta R = R_{off} - R_{on} = 15.9K\Omega$, $R_m = R_s = 100K\Omega$ and $C_m = C_s = 1\mu F$. Therefore, $R_0 = R_m + R_s = 200K\Omega$ and $R_t = R_0 + R_{off} = 216K\Omega$. Then:

$$\gamma_1 = \frac{R_t}{2\delta R} = 6.792, \quad \gamma_2 = \frac{R_{off}}{2\delta R} = 0.503, \quad P_e = -\frac{3}{4}, \quad Q_e = 6.542,$$

$$\Delta_e = 10.6853, \quad \mathscr{A} = 26.168, \quad \tilde{v}_e = 1.8701 \text{ and } \tilde{u}_e = -0.1337.$$

$\therefore$

$$X_{e_1} = \tilde{u}_e - \tilde{v}_e + \frac{1}{2} = -1.5037$$
$$X_{e_2} = \tilde{u}_e\omega^2 - \tilde{v}_e\omega + \frac{1}{2} = 1.5019 - j1.5037$$
$$X_{e_3} = \tilde{u}_e\omega - \tilde{v}_e\omega^2 + \frac{1}{2} = 1.5019 + j1.5037$$

Having known X_e , the value of h at this condition is h_e and is to be obtained from (5.64). Thus:

$$h_e = H(X = X_e, Y = 0) = H(X_e, 0) \quad \Rightarrow$$
$$h_e = \frac{1}{4}X_e^4 - \frac{1}{2}X_e^3 + \gamma_1 X_e. \tag{5.79}$$

Hence giving $X_e = -1.5037$, then $h_e = -7.2349$.

The ***singularity points of the system*** are where the derivative $\frac{dY}{d\tau}$ does not exist, i.e $\frac{dY}{d\tau} = \infty \quad \Rightarrow$

$$X^3 - \frac{3}{2}X^2 + \gamma_2 = 0, \tag{5.80}$$

having atleast one real root X_s corresponding to the singular line, for any given γ_2. Following similar approach, we obtain the general solution of (5.80) as:

$$X_{s_1} = \tilde{u}_s - \tilde{v}_s + \frac{1}{2}, \quad X_{s_2} = \tilde{u}_s\omega^2 - \tilde{v}_s\omega + \frac{1}{2} \text{ and } X_{s_3} = \tilde{u}_s\omega - \tilde{v}_s\omega^2 + \frac{1}{2}.$$

Here the coefficients are: $a = -\frac{3}{2}$, $b = 0$ and $c = \gamma_2$, which gives

$$P_s = b - \frac{a^2}{3} = -\frac{3}{4}, \; Q_s = c + \frac{2a^3}{27} - \frac{ba}{3} = \gamma_2 - \frac{1}{4},$$

With $\Delta_s = \frac{Q_s^2}{4} + \frac{P_s^3}{27} = \frac{2\gamma_2^2 - \gamma_2}{8}, \quad \tilde{v}_s = \sqrt[3]{\frac{Q_s}{2} + \sqrt{\Delta_s}} = \frac{\sqrt[3]{\mathscr{B} + \sqrt{\mathscr{B}^2 - 1}}}{2}$, and

$$\tilde{u}_s = \frac{P_s}{3\tilde{v}_s} = -\frac{1}{2\sqrt[3]{\mathscr{B} + \sqrt{\mathscr{B}^2 - 1}}}$$

Where $\mathscr{B} = 4\gamma_2 - 1$. Using the values of the circuit parameters, then $\gamma_2 = 0.503$ and the other variables are:

$$Q_s = 0.253, \; \Delta_s = 3.772 \times 10^{-4}, \; \tilde{v}_s = 0.5264 \text{ and } \tilde{u}_s = -0.4748 \; \Rightarrow$$

$$X_{s_1} = \tilde{u}_s - \tilde{v}_s + \frac{1}{2} = -0.5012$$
$$X_{s_2} = \tilde{u}_s\omega^2 - \tilde{v}_s\omega + \frac{1}{2} = 1.0006 - j0.0446$$
$$X_{s_3} = \tilde{u}_s\omega - \tilde{v}_s\omega^2 + \frac{1}{2} = 1.0006 + j0.0446$$

Similarly, the h value at the singular line is h_s and is given by:

$$h_s = H(X = X_s, Y = Y_s) = H(X_s, Y_s) \quad \Rightarrow$$

$$h_s = \left(X_s^3 - \frac{3}{2}X_s^2 + \gamma_2\right)Y_s + \frac{1}{4}X_s^4 - \frac{1}{2}X_s^3 + \gamma_1 X_s. \tag{5.81}$$

With $X_s = -0.5012$, then $Y_s = 0$ and $h_s = 1.7848$. Therefore $X_e < X_s$ and $h_e < h_s$.

AN EXAMPLE FOR CALCULATING THE ROOTS OF $P_4(X)$:

The general solution of the quartic polynomial $P_4(X)$, can be obtained by reducing the function to its associated cubic function, which could consequently be solve using Cardano's method described above. Therefore, given the equation

$$X^4 - 2X^3 + 4\gamma_1 X - 4h = 0, \tag{5.82}$$

then posing from the first two terms $\tilde{x} = X - \frac{1}{2}$ in order to eliminate the third degree term, thus

$$\tilde{x}^4 - \frac{3}{2}\tilde{x}^2 + (4\gamma_1 - 1)\tilde{x} + 2\gamma_1 - 4h - \frac{3}{16} = 0.$$

Hence corresponding to the depressed quartic equation for which the third degree term is out, that is:

$$\tilde{x}^4 + \tilde{p}\tilde{x}^2 + \tilde{q}\tilde{x} + \tilde{r} = 0, \qquad \tilde{p}, \tilde{q}, \tilde{r} \in \mathbb{C}, \tag{5.83}$$

where:

$$\tilde{p} = -\frac{3}{2}, \;\; \tilde{q} = 4\gamma_1 - 1 \;\text{ and }\; \tilde{r} = 2\gamma_1 - 4h - \frac{3}{16}.$$

Henceforth the depressed quartic equation is solved in terms of $\tilde{p}$, $\tilde{q}$ and $\tilde{r}$, and thereafter substituted to find the solution of the given original equation, by using $X = \tilde{x} + \frac{1}{2}$. Let us introduce a new variable $\tilde{k}$ so that

$$(\tilde{x}^2 + \tilde{k})^2 - 2\tilde{k}\tilde{x}^2 - \tilde{k}^2 = \tilde{x}^4, \qquad \tilde{k} \in \mathbb{C}$$

Then (5.83) becomes:

$$(\tilde{x}^2 + \tilde{k})^2 = (2\tilde{k} - \tilde{p})\tilde{x}^2 - \tilde{q}\tilde{x} + (\tilde{k}^2 - \tilde{r}) \tag{5.84a}$$

$$= (\tilde{\alpha}\tilde{x} + \tilde{\beta})^2 \tag{5.84b}$$

$$= \tilde{\alpha}^2\tilde{x} + 2\tilde{\alpha}\tilde{\beta}\tilde{x} + \tilde{\beta}^2$$

Note that $\tilde{k}$ is chosen so that the right hand side of equation (5.84a) is a perfect square, and hence become (5.84b). $\tilde{\alpha}, \tilde{\beta}$ and $\tilde{k}$ are obtained by coefficient comparison method:

$$\tilde{\alpha} = \sqrt{2\tilde{k} - \tilde{p}}, \quad \tilde{\beta} = -\frac{\tilde{q}}{2\tilde{\alpha}} = -\frac{\tilde{q}}{2\sqrt{2\tilde{k} - \tilde{p}}} \quad \text{and} \quad \tilde{\beta}^2 = \tilde{k}^2 - \tilde{r}$$

Moreover, the sufficient condition needed to solve for $\tilde{k}$ is obtained from the two expressions of $\tilde{\beta}$ and it becomes:

$$\tilde{k}^2 - \tilde{r} = \left(-\frac{\tilde{q}}{2\sqrt{2\tilde{k} - \tilde{p}}}\right)^2,$$

and is simplified to give

$$\tilde{k}^3 - \frac{\tilde{p}}{2}\tilde{k}^2 - \tilde{r}\,\tilde{k} + \frac{\tilde{p}\tilde{r}}{2} - \frac{\tilde{q}^2}{8} = 0. \tag{5.85}$$

Equation (5.85) is a cubic function in $\tilde{k}$ to be solved using the previous derived Cardano's method. Thus:

$$\tilde{y}^3 + P\tilde{y} + Q = 0,$$

where:

$$\tilde{y} = \tilde{k} - \frac{\tilde{p}}{6}, \quad P = -\tilde{r} - \frac{\tilde{p}^2}{12}, \quad \text{and} \quad Q = \frac{\tilde{p}\tilde{r}}{3} - \frac{\tilde{q}^2}{8} - \frac{\tilde{p}^3}{108}.$$

Hence the remaining parameters are obtained as:

$$\Delta_1 = \frac{Q^2}{4} + \frac{P^3}{27}, \quad \tilde{V} = \sqrt[3]{\frac{Q}{2} + \sqrt{\Delta_1}} \quad \text{and} \quad \tilde{U} = \frac{P}{3\tilde{V}}.$$

With $\tilde{k} = \tilde{y} + \frac{\tilde{p}}{6}$, and $\omega = -\frac{1}{2} + \frac{\sqrt{3}}{2}j$, the three possible solutions of (5.85) are:

$$\begin{aligned}
\tilde{k}_1 &= \tilde{U} - \tilde{V} + \frac{\tilde{p}}{6} \\
\tilde{k}_2 &= \tilde{U}\omega^2 - \tilde{V}\omega + \frac{\tilde{p}}{6} \\
\tilde{k}_3 &= \tilde{U}\omega - \tilde{V}\omega^2 + \frac{\tilde{p}}{6}
\end{aligned}$$

Any of the 3 solutions of $\tilde{k}$ (i.e $\tilde{k}_1$-$\tilde{k}_3$) will satisfy equation (5.84b), as such one solution is enough to find the solution of (5.82). Therefore, from (5.84b) we get 2 quadratic equations in $\tilde{x}$, as:

$$\tilde{x}^2 + \tilde{k} = \pm(\tilde{\alpha}\tilde{x} + \tilde{\beta}) \implies$$

$$\tilde{x}^2 - \tilde{\alpha}\tilde{x} + \tilde{k} - \tilde{\beta} = 0 \tag{5.86a}$$

$$\tilde{x}^2 + \tilde{\alpha}\tilde{x} + \tilde{k} + \tilde{\beta} = 0 \tag{5.86b}$$

Equation (5.86) is solved to give the 4 possible solutions of the depressed quartic equation (5.83). From equation (5.86a) and (5.86b) respectively, we get:

$$\tilde{x}_1 = \frac{\tilde{\alpha} + \sqrt{\Delta_2}}{2}, \quad \tilde{x}_2 = \frac{\tilde{\alpha} - \sqrt{\Delta_2}}{2}, \text{ where: } \Delta_2 = \tilde{\alpha}^2 - 4(\tilde{k} - \tilde{\beta}) \text{ and}$$
$$\tilde{x}_3 = \frac{-\tilde{\alpha} + \sqrt{\Delta_3}}{2}, \quad \tilde{x}_4 = \frac{-\tilde{\alpha} - \sqrt{\Delta_3}}{2}, \text{ where: } \Delta_3 = \tilde{\alpha}^2 - 4(\tilde{k} + \tilde{\beta}).$$

Finally, the solution of the original equation (5.82) is obtained from $X = \tilde{x} + \frac{1}{2}$. With $\gamma_1 = 6.792$, $h = 6.682$ and $\tilde{k} = \tilde{k}_1$ then

$$\tilde{p} = -1.500, \quad \tilde{q} = 26.168, \quad \tilde{r} = -13.331 \text{ and } \tilde{k} = 3.041.$$

Similarly, all the subsequent variables are calculated and the solutions are:

$$\left.\begin{aligned} X_1 &= \tilde{x}_1 + \frac{1}{2} = 1.8768 + j2.4284 \\ X_2 &= \tilde{x}_2 + \frac{1}{2} = 1.8768 - j2.4284 \\ X_3 &= \tilde{x}_3 + \frac{1}{2} = 1.0222 \\ X_4 &= \tilde{x}_4 + \frac{1}{2} = -2.7758 \end{aligned}\right\} \text{example of case to determine the roots of } P_4(X) = 0$$

The equivalent simplified expressions for the two real roots of (5.82) are:

$$\begin{aligned} X_{r_1} &= \frac{1}{2}\left(1 + \sqrt{3 - U_r + 2\frac{(4\gamma_1 - 1)}{\sqrt{U_r}}} - \sqrt{U_r}\right), \\ X_{r_2} &= \frac{1}{2}\left(1 - \sqrt{3 - U_r + 2\frac{(4\gamma_1 - 1)}{\sqrt{U_r}}} - \sqrt{U_r}\right), \end{aligned} \tag{5.87}$$

where:

$$U_r = 1 + 2\sqrt[3]{\sqrt{\Delta_r} - Q_r} - 2\sqrt[3]{\sqrt{\Delta_r} + Q_r}; \ \Delta_r = Q_r^2 + \frac{8}{27}P_r^3, \ P_r = 2h - \gamma_1 \text{ and } Q_r = h - \gamma_1^2.$$

Equation (5.74) is to be solved analytically depending on the given values for γ_1, γ_2 and h. Therefore, for $h \in [-\infty, +\infty]$, four possible analytical solutions of (5.74) appear, as outlined in the following.

1). *for* $h \in [-\infty, h_e]$ **:** $P_4(X)$ has no real root. The solution of (5.74) becomes:

$$d\tau = (-4)\frac{X^3 - \frac{3}{2}X^2 + \gamma_2}{(X^2 + \beta_1 X + \beta_2)(X^2 + \beta_3 X + \beta_4)}dX,$$

where:

$$\beta_1 = 1 - \sqrt{1 + 2\sigma}; \ \ \beta_3 = 1 + \sqrt{1 + 2\sigma},$$
$$\beta_2 = \sigma - \frac{2\gamma_1 + \sigma}{\sqrt{1 + 2\sigma}}; \ \ \beta_4 = \sigma + \frac{2\gamma_1 + \sigma}{\sqrt{1 + 2\sigma}}.$$

With:

$$-\sigma^3 + (2\gamma_1 - 4h)\sigma + 2(\gamma_1^2 - h) = 0,$$
$$\tau = \tau_1 - 4\int_{X_{0_2}}^{X}\left(\frac{b_0 + b_1 X}{X^2 + \beta_1 X + \beta_2} + \frac{b_2 + b_3 X}{X^2 + \beta_3 X + \beta_4}\right)dX,$$

where

$$b_0 = \frac{\frac{5}{2}\beta_2 + \gamma_2}{\beta_4 - \beta_2}; \ \ b_2 = \frac{\gamma_2 + \frac{5}{2}\beta_4}{\beta_2 - \beta_4},$$
$$b_1 = \frac{\beta_2(\beta_2 - \beta_4) + \frac{5}{2}(\beta_1\beta_4 - \beta_2\beta_3) + \gamma_2(\beta_1 - \beta_3)}{(\beta_4 - \beta_2)^2},$$
$$b_3 = \frac{\beta_4(\beta_4 - \beta_2) + \frac{5}{2}(\beta_2\beta_3 - \beta_1\beta_4) + \gamma_2(\beta_2 - \beta_1)}{(\beta_4 - \beta_2)^2},$$

and then:

$$\begin{aligned}\tau \ = \ & \tau_1 - 4\Bigg[\ln\left[(X^2 + \beta_1 X + \beta_2)^{\frac{b_1}{2}}(X^2 + \beta_3 X + \beta_4)^{\frac{b_3}{2}}\right] \\ & + \frac{2b_0 + b_1\beta_1}{\sqrt{4\beta_2 - \beta_1^2}}\,arctan\left(\frac{2}{\sqrt{4\beta_2 - \beta_1^2}}\left[X + \frac{\beta_1}{2}\right]\right) \\ & + \frac{2b_2 + b_3\beta_3}{\sqrt{4\beta_4 - \beta_3^2}}\,arctan\left(\frac{2}{\sqrt{4\beta_4 - \beta_3^2}}\left[X + \frac{\beta_3}{2}\right]\right)\Bigg]. \end{aligned} \quad (5.88)$$

2). *for* $h = h_e$**:** $P_4(X)$ has a double real root called X_e and equation (5.74) is solved as follows:

$$d\tau = (-4)\left[\frac{e_0}{X - X_e} + \frac{e_1}{(X - X_e)^2} + \frac{e_3 X + e_4}{X^2 + \tilde{a}_1 X + \tilde{a}_2}\right]dX$$

where:

$$e_1 = \frac{X_e^3 - \frac{3}{2}X_e^2 + \gamma_2}{X_e^2 + \tilde{a}_1 X_e + \tilde{a}_2},$$
$$e_3 = \frac{(\tilde{a}_1 + 2X_e)[\gamma_2 + \tilde{a}_2(\frac{3}{2} + \tilde{a}_1)] - [\tilde{a}_2 - \tilde{a}_1(\frac{3}{2} + \tilde{a}_1)](X_e^2 - \tilde{a}_2)}{(\tilde{a}_1 + 2X_e)(2\tilde{a}_2 X_e + \tilde{a}_1\tilde{a}_2) + (X_e^2 - \tilde{a}_2)(2X_e\tilde{a}_1 - \tilde{a}_2 + \tilde{a}_1^2 + X_e^2)},$$
$$e_4 = \frac{(2X_e\tilde{a}_1 - \tilde{a}_2 + \tilde{a}_1^2 + X_e^2)[\gamma_2 + \tilde{a}_2(\frac{3}{2} + \tilde{a}_1)] - (2\tilde{a}_2 X_e + \tilde{a}_1\tilde{a}_2)[\tilde{a}_1(\frac{3}{2} + \tilde{a}_1) - \tilde{a}_2]}{(\tilde{a}_1 + 2X_e)(2\tilde{a}_2 X_e + \tilde{a}_1\tilde{a}_2) + (X_e^2 - \tilde{a}_2)(2X_e\tilde{a}_1 - \tilde{a}_2 + \tilde{a}_1^2 + X_e^2)},$$

and

$$e_0 = \alpha_3 - e_3, \ \ \tilde{a}_1 = -\frac{4h}{X_e^2} \text{ and } \tilde{a}_2 = 2X_e - 2.$$

$\therefore$

$$\tau = \tau_1 - 4\left[e_0 \ln(X - X_e) - \frac{e_1}{X - X_e} + \frac{2e_4 - \tilde{a}_1 e_3}{\sqrt{4\tilde{a}_2 - \tilde{a}_1^2}} \, arctan\left(\frac{2}{\sqrt{4\tilde{a}_2 - \tilde{a}_1^2}}\left[X + \frac{\tilde{a}_1}{2}\right]\right)\right]. \quad (5.89)$$

3). *for* $h = h_s$: $P_3(X)$ and $P_4(X)$ have a same real root. Equation (5.74) becomes:

$$-\frac{d\tau}{4} = \frac{P_{2S}(X)}{P_{3S}(X)} dX,$$

and $P_{3S}(X)$ has another real root called X_{s_a}. We get:

$$\mathrm{d}\tau = (-4)\left[\frac{e_9}{X - X_{s_a}} + \frac{e_{10}X + e_{11}}{X^2 + \lambda_2 X + \lambda_8}\right] \mathrm{d}X,$$

where:

$$X_{s_a} < X_e < X_s < 0 \, ; \quad H(X_{s_a}, Y_{s_a}) = h_s \ \ \Rightarrow$$

$$\tau = \tau_1 - 4\left[e_9 \ln(X - X_{s_a}) + \frac{2e_{11} - \lambda_2 e_{10}}{\sqrt{4\lambda_8 - \lambda_2^2}} \, arctan\left(\frac{2}{\sqrt{4\lambda_8 - \lambda_2^2}}\left[X + \frac{\lambda_2}{2}\right]\right)\right]. \quad (5.90)$$

4). *for* $h \in]h_e, h_s[\cup]h_s, +\infty[$: $P_4(X)$ has 2 distinct real roots X_{a_1} and X_{a_2}, meanwhile the 2 others are complex ones. Then equation (5.74) becomes:

$$\mathrm{d}\tau = (-4)\left[\frac{e_{18}}{X - X_{a_1}} + \frac{e_{19}}{X - X_{a_2}} + \frac{e_{20} + e_{21}X}{X^2 + \lambda_1 X + \lambda_2}\right] \mathrm{d}X.$$

With $X_{a_1} < X_e < X_{a_2}$,

$$e_{18} = \frac{X_{a_1}^3 - \frac{3}{2}X_{a_1}^2 + \gamma_2}{(X_{a_1} - X_{a_2})(X_{a_1}^2 + \lambda_1 X_{a_1} + \lambda_2)} \ ; \quad e_{19} = \frac{X_{a_2}^3 - \frac{3}{2}X_{a_2}^2 + \gamma_2}{(X_{a_2} - X_{a_1})(X_{a_2}^2 + \lambda_1 X_{a_2} + \lambda_2)},$$

$$e_{20} = e_{11}(X_{a_1} + X_{a_2} - \frac{3}{2} - e_{19}(\lambda_1 - X_{a_1}) - e_{18}(\lambda_1 - X_{a_2}))$$

$\therefore$

$$\tau = \tau_1 - 4\ln\left[(X - X_{a_1})^{e_{18}}(X - X_{a_2})^{e_{19}}(X^2 + \lambda_1 X + \lambda_2)^{\frac{e_{11}}{2}}\right]$$
$$+ (-4)\frac{2e_{20} - \lambda_1 e_{21}}{\sqrt{4\lambda_2 - \lambda_1^2}} \, arctan\left[\frac{2}{\sqrt{4\lambda_2 - \lambda_1^2}}\left(X + \frac{\lambda_1}{2}\right)\right]. \quad (5.91)$$

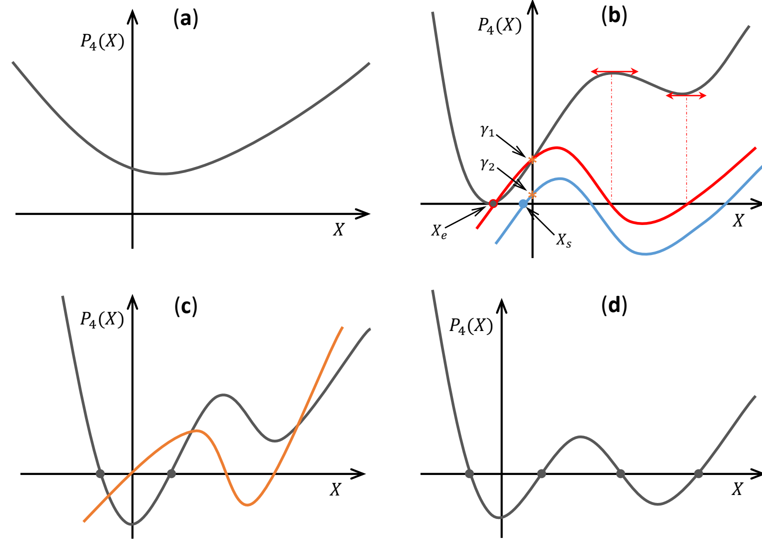

Figure 5.16: Illustration of some roots for $P_4(X)$ according to a value of h. (**a**) No real root, (**b**) double real root, the cubic functions are respectively for $X^3 - \frac{3}{2}X + \gamma_1$ and $X^3 - \frac{3}{2}X + \gamma_2$, (**c**) 2 distinct real roots and (**d**) 4 real roots.

Adopted solution:

Although it is mathematically consistent to consider all the aforementioned h possibilities regarding the solutions of (5.74), however we focus in the following to the fourth possibility because it involves all physically possible h values. The solution of equation (5.74) is now written in a new way:

$$\int_{\tau_1}^{\tau} d\tau = (-4)\int_{X_{0_2}}^{X}\left(\frac{\tilde{\alpha}_1}{X'-X_1}+\frac{\tilde{\alpha}_2}{X'-X_2}+\frac{\tilde{\alpha}_3+\tilde{\alpha}_4 X'}{X'^2+\tilde{\beta}_1 X'+\tilde{\beta}_2}\right)dX' \quad \Rightarrow$$

$$\tau = \tau_1 - 4\left|\ln\left[(X'-X_1)^{\tilde{\alpha}_1}(X'-X_2)^{\tilde{\alpha}_2}\right]+\ln\left[X'^2+\tilde{\beta}_1 X'+\tilde{\beta}_2\right]^{\frac{\tilde{\alpha}_4}{2}} + \frac{2\tilde{\alpha}_3-\tilde{\alpha}_4\tilde{\beta}_1}{\sqrt{4\tilde{\beta}_2-\tilde{\beta}_1^2}}\ arctan\left[\frac{2}{\sqrt{4\tilde{\beta}_2-\tilde{\beta}_1^2}}\left(X'+\frac{\tilde{\beta}_1}{2}\right)\right]\right|_{X_{0_2}}^{X}$$

$\therefore$

$$\tau = \tau_1 - 4\left[\ln\left(\left[\frac{X-X_1}{X_{0_2}-X_1}\right]^{\tilde{\alpha}_1}\left[\frac{X-X_2}{X_{0_2}-X_2}\right]^{\tilde{\alpha}_2}\right)+\ln\left(\frac{X^2+\tilde{\beta}_1 X+\tilde{\beta}_2}{X_{0_2}^2+\tilde{\beta}_1 X_{0_2}+\tilde{\beta}_2}\right)^{\frac{\tilde{\alpha}_4}{2}} + \frac{2\tilde{\alpha}_3-\tilde{\alpha}_4\tilde{\beta}_1}{\sqrt{4\tilde{\beta}_2-\tilde{\beta}_1^2}}\left(\arctan\frac{2\left(X+\frac{\tilde{\beta}_1}{2}\right)}{\sqrt{4\tilde{\beta}_2-\tilde{\beta}_1^2}}-\arctan\frac{2\left(X_{0_2}+\frac{\tilde{\beta}_1}{2}\right)}{\sqrt{4\tilde{\beta}_2-\tilde{\beta}_1^2}}\right)\right],\quad \tau\in[\tau_1,\ \tau_2] \tag{5.92}$$

where:

$$\tilde{\beta}_1 = X_1 + X_2 - 2,\ \ \tilde{\beta}_2 = \frac{-4h}{X_1 X_2},$$

$$\tilde{\alpha}_1 = \frac{X_1^3 - \frac{3}{2}X_1^2 + \gamma_2}{(X_1 - X_2)(X_1^2 + \tilde{\beta}_1 X_1 + \tilde{\beta}_2)},$$

$$\tilde{\alpha}_2 = \frac{X_2^3 - \frac{3}{2}X_2^2 + \gamma_2}{(X_2 - X_1)(X_2^2 + \tilde{\beta}_1 X_2 + \tilde{\beta}_2)},$$

$$\tilde{\alpha}_3 = \frac{\gamma_2 + \tilde{\alpha}_1 \tilde{\beta}_2 X_2 + \tilde{\alpha}_2 \tilde{\beta}_2 X_1}{X_1 X_2},$$

and

$$\tilde{\alpha}_4 = 1 - \tilde{\alpha}_1 - \tilde{\alpha}_2.$$

X_1 and X_2 are the two real roots of $P_4(X)$ given by (5.87), while the other two roots are complex conjugate numbers. Recall that τ_1 is eventually the time where $X(\tau) = 0$, therefore at $X(\tau) = 1$, $\tau = \tau_2$ and is obtained from (5.92), as:

$$\begin{aligned} \tau_2 \quad = \quad & \tau_1 - 4\left[\ln\left(\left[\frac{1 - X_1}{X_{0_2} - X_1} \right]^{\tilde{\alpha}_1} \left[\frac{1 - X_2}{X_{0_2} - X_2} \right]^{\tilde{\alpha}_2} \right) + \ln\left(\frac{1 + \tilde{\beta}_1 + \tilde{\beta}_2}{X_{0_2}^2 + \tilde{\beta}_1 X_{0_2} + \tilde{\beta}_2} \right)^{\frac{\tilde{\alpha}_4}{2}} \right. \\ & \left. + \frac{2\tilde{\alpha}_3 - \tilde{\alpha}_4 \tilde{\beta}_1}{\sqrt{4\tilde{\beta}_2 - \tilde{\beta}_1^2}} \left(\arctan \frac{2 + \tilde{\beta}_1}{\sqrt{4\tilde{\beta}_2 - \tilde{\beta}_1^2}} - \arctan \frac{2\left(X_{0_2} + \frac{\tilde{\beta}_1}{2}\right)}{\sqrt{4\tilde{\beta}_2 - \tilde{\beta}_1^2}} \right) \right], \end{aligned} \tag{5.93}$$

Finally, when the initial condition $X(\tau = 0) = X_0$ is already greater than 1, we consider the following.

$X(\tau) \in [1, +\infty]$:

From (5.69):

$$\left(\gamma_2 - \frac{1}{2}\right)\frac{dX}{d\tau} = h - \left(\gamma_1 - \frac{1}{2}\right)X - \frac{1}{4},$$

$$\int_{X_{0_3}}^{X} \frac{\mathrm{d}X'}{X - \frac{h - \frac{1}{4}}{\gamma_1 - \frac{1}{2}}} = -\frac{2\gamma_1 - 1}{2\gamma_2 - 1} \int_{\tau_2}^{\tau} \mathrm{d}\tau \;\Rightarrow$$

$$X(\tau) = \frac{h - \frac{1}{4}}{\gamma_1 - \frac{1}{2}} + \left(X_{0_3} - \frac{h - \frac{1}{4}}{\gamma_1 - \frac{1}{2}}\right) e^{-\frac{2\gamma_1 - 1}{2\gamma_2 - 1}(\tau - \tau_2)}, \tag{5.94}$$

where X_{0_3} is the initial state when the system is described by (5.69). The expression of the normalized time τ for this region is obtained from (5.94), as:

$$\tau = \tau_2 - \frac{2\gamma_2 - 1}{2\gamma_1 - 1} \ln\left[\frac{X - \frac{4h-1}{4\gamma_1 - 2}}{X_{0_3} - \frac{4h-1}{4\gamma_1 - 2}} \right], \qquad \tau \in [\tau_2, +\infty] \tag{5.95}$$

Note that $1 \leq X_{0_3} \leq X(\tau)$ and owing to continuity at $X(\tau) = 1$, it is possible to have $X(\tau_2) \leq X_{0_3}$. So h being a constant depending on initial conditions, it is kept even across the boundaries $X = 0$ and $X = 1$. For each special initial conditions, the system (5.60), (5.63) and (5.65) involves in keeping constant the quantity $H(X, Y)$ with the specific h value depending on these initial conditions. The initial state of the memristor with memristance $M(q)$ is given by the parameters q_0, V_{m_0} and V_{s_0} which determines X_0 and Y_0. The phase portraits of the system dynamics are described by equations (5.60), (5.63) and (5.65), and can be studied in two separate cases, according to the sign of the initial normalised current Y_0.

It is important to note that X_{0_1}, X_{0_2} and X_{0_3} are encapsulated in X_0 as it was manifested throughout the cases A1-B6 as outlined underneath. Furthermore, for $X_{0_1} < 0$, $X_{0_2} = 0$ and $X_{0_3} = 1$, the system is analogously described by case A3. Thus by so doing, the system takes into account the unknown boundary position corresponding to X_0 which reflects the memory effect of the device from its previous usage.

With the memristance $\mathscr{M}(X)$ given by (5.58) and recall that ð is defined in equation (5.33), the equivalent normalised expression of ð is as follows:

$$\xi = \int_{X_0}^{X} \mathscr{M}(X')\, \mathrm{d}X', \tag{5.96}$$

where ξ is the normalised form of ð given by $\xi = \dfrac{ð}{\delta R\, q_d}$, thus ð is known provided X is known.

1. **(A).:** If $Y_0 > 0$, the time evolution of the normalized charge $X(\tau)$ will be directed toward the right, and corresponds to six possible behaviours (some of them are shown in Fig. 5.17).

A1. $X_0 \leq X < 0$, (black line for example).

$$\begin{aligned} \xi &= \int_{X_0}^{X} \frac{R_{off}}{\delta R}\, \mathrm{d}X', \\ &= \frac{R_{off}}{\delta R}\, (X - X_0). \end{aligned}$$

A2. $X_0 < 0$ and $X(t \to \infty) < 1$, (orange and green curves for example).

$$\begin{aligned} \xi &= \int_{X_0}^{0} \frac{R_{off}}{\delta R} \mathrm{d}X' + \int_{0}^{X} \Big(\frac{R_{off}}{\delta R} - 3X'^2 + 2X'^3\Big) \mathrm{d}X', \\ &= \frac{R_{off}}{\delta R}\, (X - X_0) - X^3 + \frac{1}{2} X^4. \end{aligned}$$

A3. $X_0 < 0$ and $X(t \to \infty) > 1$, (the magenta line and the blue one for example).

$$\begin{aligned} \xi &= \int_{X_0}^{0} \frac{R_{off}}{\delta R} \mathrm{d}X' + \int_{0}^{1} \Big(\frac{R_{off}}{\delta R} - 3X'^2 + 2X'^3\Big)\mathrm{d}X' + \int_{1}^{X} \frac{R_{on}}{\delta R}\mathrm{d}X', \\ &= \frac{R_{on}}{\delta R} X - \frac{R_{off}}{\delta R} X_0 + \frac{1}{2}. \end{aligned} \tag{5.97}$$

A4. $0 < X_0 \leq X < 1$, this case being included in case A2, only the starting state is changed.

$$\begin{aligned} \xi &= +\int_{X_0}^{X} \Big(\frac{R_{off}}{\delta R} - 3X'^2 + 2X'^3\Big)\mathrm{d}X', \\ &= \frac{R_{off}}{\delta R} (X - X_0) - (X^3 - X_0^3) + \frac{1}{2}(X^4 - X_0^4). \end{aligned}$$

A5. $0 < X_0$ and $X(t \to \infty) > 1$.

$$\begin{aligned} \xi &= \int_{X_0}^{1} \Big(\frac{R_{off}}{\delta R} - 3X'^2 + 2X'^3\Big)\mathrm{d}X' + \int_{1}^{X} \frac{R_{on}}{\delta R}\mathrm{d}X', \\ &= \frac{R_{on}}{\delta R} X - \frac{R_{off}}{\delta R} X_0 + X_0^3 - \frac{1}{2}X_0^4 + \frac{1}{2}. \end{aligned}$$

A6. $1 < X_0 \leq X$.

$$\begin{aligned} \xi &= \int_{X_0}^{X} \frac{R_{on}}{\delta R}\mathrm{d}X', \\ &= \frac{R_{on}}{\delta R}(X - X_0). \end{aligned}$$

Note that cases A5 and A6 are included in case A3, with only a change of the initial conditions, that is, the starting point.

The first case corresponds simply to time evolution of the charge given by (5.70). It is described by the black line, where h=1.528. For case A2, as depicted for example by the green curve in Fig. 5.17, with $h = 6.122$, $X(\tau)$ evolves first according to (5.70) from initial state ($X_0 = -0.5$, $Y_0 = 18.922$), reaches $X(\tau) = 0$ in $\tau_1 = 32.68ms$ given after (5.92), then is described by (5.92) until it reaches ($X_1 = 0.943$, $Y = 0$) when $t \to +\infty$. For the third case, as depicted in Fig. 5.17 by the blue line for example, with $h = 6.682$ with initial conditions ($X_0 = -0.5$, $Y_0 = 20.036$), $X(\tau)$ is described by (5.70) until $\tau_1 = 30.43ms$, then by (5.92) until $\tau_2 = 94.30ms$ corresponding to $X(\tau) = 1$ in (5.92), then by (5.94) until the equilibrium state ($X(\tau) = 1.022$, $Y = 0$).

Notice that each trajectory describes how the system evolves to reach the equilibrium point $Y = 0$ for any given initial condition. As expected, the slopes for $X \leq 0$ and $X \geq 1$, corresponding to the high and low resistance state of the memristor device respectively, are the same for any given initial condition. Thus, the curves in the

regions $X \le 0$ and $X \ge 1$ evolve in parallel with respect to one another.

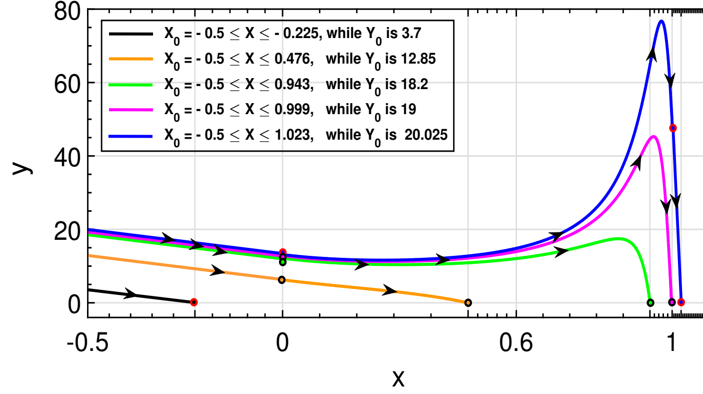

Figure 5.17: Phase portraits for $Y_0 > 0$, describing the system dynamics from left to right, toward the equilibrium points with $Y = 0$. Each trajectory corresponds to a specific initial condition of the system. The trajectory in black is for ($X_0 \le X < 0$), the ones in orange, green and pink are for ($X_0 < 0$ and $X(t \to \infty) < 1$) and the one in blue is for ($X_0 < 0$ and $X(t \to \infty) > 1$).

2. (B).**:** For $Y_0 < 0$, the phase portraits are given in Fig. 5.18, which is rather a different evolution pattern due to memristor asymmetry, with a time evolution of $X(\tau)$ toward the left. Similarly, six possible behaviours can be observed, depending on the starting point, see Fig. 5.18, where some examples of trajectories are given.

B1. $1 < X \le X_0$ (blue and pink lines).

$$\begin{aligned}\xi &= -\int_{X_0}^{X} \frac{R_{on}}{\delta R} \mathrm{d}X', \\ &= \frac{R_{on}}{\delta R}(X - X_0).\end{aligned}$$

B2. $X_0 > 1$ and $0 < X(t \to \infty) < 1$ (green line).

$$\begin{aligned}\xi &= \int_{X_0}^{1} \frac{R_{on}}{\delta R} \mathrm{d}X' + \int_{1}^{X} \Big(\frac{R_{off}}{\delta R} - 3X'^2 + 2X'^3\Big) \mathrm{d}X', \\ &= \frac{R_{off}}{\delta R} X - X^3 + \frac{1}{2} X^4 - \frac{R_{on}}{\delta R} X_0 - \frac{1}{2}.\end{aligned}$$

B3. $X_0 > 1$ and $X(t \to \infty) < 0$ (not represented).

$$\begin{aligned}\xi &= \int_{X_0}^{1} \frac{R_{on}}{\delta R} \mathrm{d}X' + \int_{1}^{0} \Big(\frac{R_{off}}{\delta R} - 3X'^2 + 2X'^3\Big) \mathrm{d}X' + \int_{0}^{X} \frac{R_{off}}{\delta R} \mathrm{d}X', \\ &= \frac{R_{off}}{\delta R} X - \frac{R_{on}}{\delta R} X_0 - \frac{1}{2}.\end{aligned}$$

B4. $0 < X \leq X_0 < 1$ (orange line).

$$\begin{aligned}\xi &= -\int_{X_0}^{X}\Big(\frac{R_{off}}{\delta R} - 3X'^2 + 2X'^3\Big)\mathrm{d}X' \\ &= \frac{R_{off}}{\delta R}(X_0 - X) - (X_0^3 - X^3) + \frac{1}{2}(X_0^4 - X^4).\end{aligned}$$

B5. $X_0 < 1$ and $X(t \to \infty) < 0$ (black line).

$$\begin{aligned}\xi &= \int_{X_0}^{0}\Big(\frac{R_{off}}{\delta R} - 3X'^2 + 2X'^3\Big)\mathrm{d}X' + \int_{0}^{X}\frac{R_{off}}{\delta R}\mathrm{d}X', \\ &= \frac{R_{off}}{\delta R}(X - X_0) + X_0^3 - \frac{1}{2}X_0^4.\end{aligned}$$

B6. $X \leq X_0 < 0$ (included in black line).

$$\begin{aligned}\xi &= -\int_{X_0}^{X}\frac{R_{off}}{\delta R}\mathrm{d}X', \\ &= \frac{R_{off}}{\delta R}(X_0 - X).\end{aligned}$$

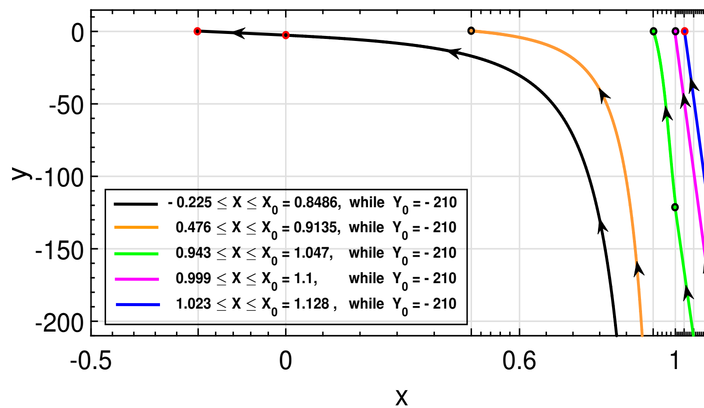

Figure 5.18: Phase portraits for $Y_0 < 0$ describing the system dynamics from right to left, toward equilibrium states with $Y = 0$. The trajectories in blue and pink are for $(1 < X \leq X_0)$, the one in green is for $(X_0 > 1$ and $0 < X(t \to \infty) < 1)$, in orange is for $(0 < X \leq X_0 < 1)$ and in black is for $(X_0 < 1$ and $X(t \to \infty) < 0)$.

Note that for any case, that is from A1 to B6, to observe the time evolution of $V_m(t)$ and $V_s(t)$, the expression of $\eth$ must be obtained according to (5.33). The expression of $M(q)$ according to (5.55) is valid for all the aforementioned cases owing to its continuity at $q(t) = 0$ and $q(t) = q_d$.

5.6.2/ CASE A3 RESULTS COMPARISON: ANALYTICAL, SPICE AND NUMERICAL

To compare the results according to the three methods, case A3 is considered because it involves all the possibilities of $X(\tau)$. All the results are obtained using the values of parameters: ionic mobility $\mu_v = 10^{-14}m^2/V.s$, device width $D = 10nm$, $q_d = 100\mu C$, $q_0 = 30\mu C$, lower conductive region $R_{off} = 16K\Omega$ and higher conductive region $R_{on} = 100\Omega$. The cell elements are: $R_m = R_s = 100K\Omega$, $C_m = C_s = 1\mu F$, thus giving $\gamma_1 = 6.792$ and $\gamma_2 = 0.503$. For any given h, the parameters of the system (5.60)-(5.94) are calculated accordingly and the phase portraits are given in Figs. 5.17 and 5.18. The result takes into account the forth or back flow toward the equilibrium point $Y = 0$. Typical memristor device is known to be asymmetric [22], thus as depicted by the lack of symmetry portrayed in Figures 5.17 and 5.18.

Furthermore, the voltage evolution of the cells according to the ***analytical method*** is given in Fig. 5.19a, compared with the ones obtained from SPICE and numerical solution given by Matlab. The initial conditions of the cells are $V_{m_0} = 17V$, $V_{s_0} = -15V$ and $q_0 = -50\mu C$. The analytical expressions for the evolution of $V_m(t)$ and $V_s(t)$ are given by (5.35) and (5.36) respectively, with $\eth$ calculated from (5.97). In this example, we have $h = 6.682$, $X_1 = 1.022$, $X_2 = -2.776$ and the other two roots of $P_4(X)$ are complex conjugate pairs. Based on the analytical description of the system, X_1 is sufficient to study the system dynamics.

When X reaches X_1, the right hand side member of (5.44) is zero, which implies $V_m(t) = V_s(t)$, whereas their sum will still decrease according to (5.27) emphasizing that the first root of $P_4(X)$ is met and corresponds to a stable equilibrium point.

The setup is simulated in ***SPICE*** using the netlist file in Table 5.2, which is the modified form of the one given in Table A.1, so it becomes suitable for case A3. The SPICE simulation results are given in Fig. 5.19b. Moreover, the result according to the ***numerical method*** is obtained by direct solution of equations (5.20)-(5.22) through Matlab numerically, using its built-in ODE function. The memristance function in (5.58) is used in (5.22) after denormalization and the system evolution is given in Fig. 5.19c.

According to these methods, namely: analytical solution, SPICE simulation and numerical solution, the results are visualized separately and thereafter compared, which shows strong agreement with one another, see Fig. 5.19.

Table 5.2: Modified memristor SPICE netlist file

```
.SUBCKT memristor pl mn PARAMS: Ron=100 Roff=16K D=10N uv=10F q0=-50u
.PARAM qd={D^2/(uv*Ron)}
* Xo=q0/qd; the initial state of the device
* State equation  *
Gx 0 x value={ I(Emem)/qd}
Cx x 0 1 IC={Xo}
Raux x 0 1T
* Port equation *
Emem pl mn value={if (V(x)<=0, I(Emem)*Roff, if (V(x)<1,  I(Emem)*(Roff-3*(
  Roff-Ron)*V(x)^2-2*(Roff-Ron)*V(x)^3), else( I(Emem)*Ron)))}
.ENDS memristor
```

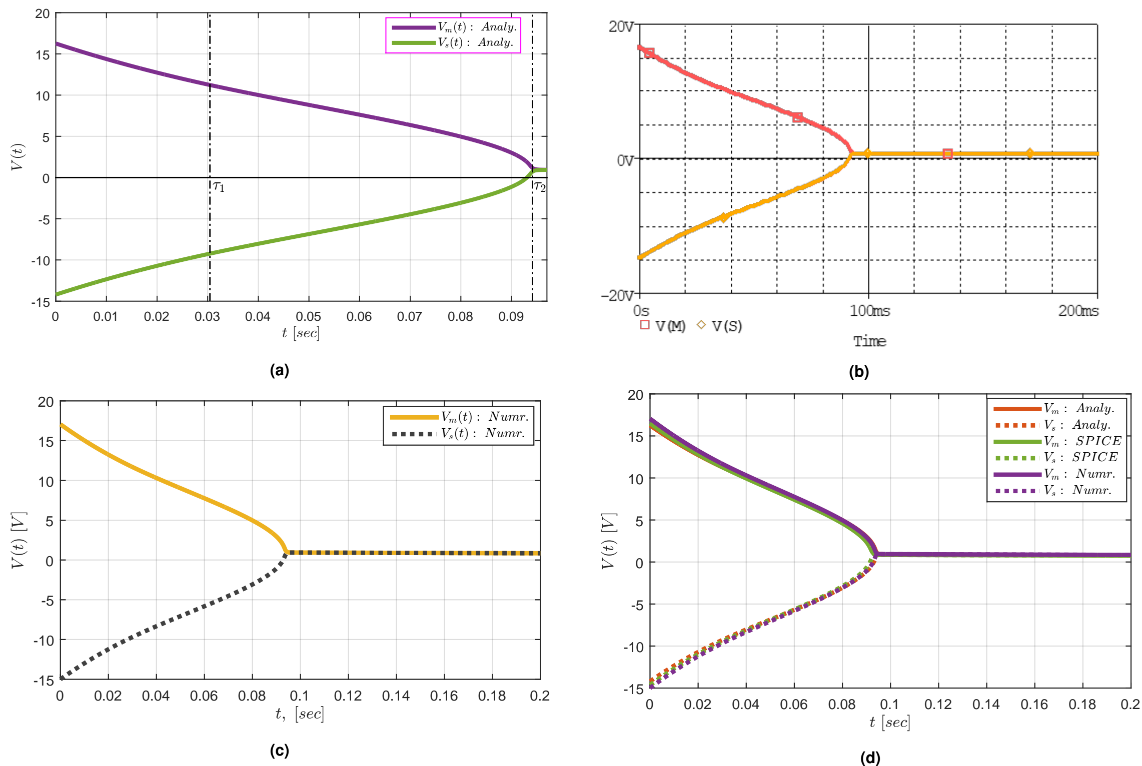

Figure 5.19: Time evolution of $V_m(t)$ and $V_s(t)$ according to: (a) Analytical description, (b) SPICE circuit simulation, (c) Numerical solution with MatLab and (d) Comparison of the three methods. Here $V_{m_0} = 17V$, $V_{s_0} = -15V$, $q_0 = -50\mu C$, which corresponds to case A3 (blue line in Fig. 5.17) and $h = 6.682$.

5.6.3/ System solution with HP model

The expression of $M(q)$ defined in (5.24) is considered, however only valid for $0 < q < q_d$. With $M(q) = R_{off} - \frac{\delta R}{q_d} q = R_{off} - \delta R\, X$ and with $M = \delta R \mathscr{M}$, then:

$$\mathscr{M}(X) = \frac{R_{off}}{\delta R} - X \text{ and } \frac{d\mathscr{M}}{dX} = -1.$$

Thus, equation (5.59) becomes successively:

$$\left(\frac{R_0}{\delta R}+\frac{R_{off}}{\delta R}-X\right)Y-Y^2+\left(\frac{R_{off}}{\delta R}-X\right)\dot{Y}=0,$$

$$\left(\frac{R_t}{\delta R}-X\right)Y-Y^2+\left(\frac{R_{off}}{\delta R}-X\right)\dot{Y}=0.$$

$$(2\gamma_1-X)Y-Y^2+(2\gamma_2-X)\dot{Y}=0 \quad\Rightarrow$$

$$\begin{cases}\dot{Y}=\dfrac{Y^2-(2\gamma_1-X)Y}{(2\gamma_2-X)},\\ \dot{X}=Y.\end{cases} \tag{5.98}$$

Where $\gamma_1=\dfrac{R_t}{2\,\delta R}$ and $\gamma_2=\dfrac{R_{off}}{2\,\delta R}$ as defined previously. From (5.98):

$$(2\gamma_2-X)\frac{dY}{dX}-Y=-(2\gamma_1-X),$$

$$\frac{d}{dX}\Big[(2\gamma_2-X)Y\Big]=-(2\gamma_1-X) \;\Rightarrow$$

$$(2\gamma_2-X)Y+2\gamma_1X-\frac{1}{2}\,X^2=H_n. \tag{5.99}$$

H_n is the Hamiltonian constant. With $Y=\dfrac{dX}{d\tau}$, (5.99) can be rewritten as:

$$(2\gamma_2-X)\frac{dX}{d\tau}+2\gamma_1X-\frac{1}{2}\,X^2=H_n\,,$$

$$-(X-2\gamma_2)\frac{dX}{d\tau}=\frac{1}{2}(X^2-4\gamma_1X+2H_n) \;\Rightarrow$$

$$\frac{X-2\gamma_2}{X^2-4\gamma_1X+2H_n}\,dX=-\frac{1}{2}d\tau. \tag{5.100}$$

The solution of eq. (5.100) is derived to be:

$$\int_{X_0}^{X}\left[\frac{\iota_1}{X'-\nu_1}+\frac{\iota_2}{X'-\nu_2}\right]dX'=-\frac{1}{2}\int_0^{\tau}d\tau' \quad\Rightarrow$$

$$\tau=-2\left[\iota_1\,\ln\left(\frac{X-\nu_1}{X_0-\nu_1}\right)+\iota_2\,\ln\left(\frac{X-\nu_2}{X_0-\nu_2}\right)\right], \tag{5.101}$$

where X_0 is the initial state corresponding X_{0_2} in equation (5.92), meanwhile ν_1 and ν_2 are the roots of the quadratic denominator:

$$X^2-4\gamma_1X+2H_n=0,$$

and where ι_1 and ι_2 are constants determined as follows:

$$\iota_1(X-\nu_2)+\iota_2(X-\nu_1)=X-2\gamma_2,$$

from which, by comparing coefficients, we get the equations set:

$$\iota_1 + \iota_2 = 1 \tag{5.102a}$$

$$\iota_1\ \nu_2 + \iota_2\ \nu_1 = 2\gamma_2 \tag{5.102b}$$

Solving equation (5.102) simultaneously, gives:

$$\iota_1 = \frac{\nu_1 - 2\gamma_2}{\nu_1 - \nu_2} \quad \text{and} \quad \iota_2 = \frac{2\gamma_2 - \nu_2}{\nu_1 - \nu_2}.$$

5.7/ MEMRISTOR ASYMMETRY

The model of TiO_2 memristor is given by:

$$\frac{dx}{dt} = \frac{i(t)}{q_d}, \tag{5.103a}$$

$$V(t) = M(x)\ i(t), \tag{5.103b}$$

$$M(x) = R_{off} - \delta R\ x. \tag{5.103c}$$

Equation (5.103) characterizes a bipolar memristor where the resistance switching depends on the voltage polarity [147–149]. However there are other reported memristors exhibiting symmetry in polarity, such as unipolar, nonpolar and complementary resistive switching memristors [44,150–152]. Here, the resistance switching between R_{off} and R_{on} (and vice-versa) can be completed in the same voltage polarity. As such, uni-polar memristors are important elements in memory arrays and logic circuit implementation [153].

Memory circuit element being intrinsically asymmetric [22], TiO_2 memristor cross-bar is used to visualize the nature of current flowing through the device with respect to the polarities of the applied voltage. Figure 5.20a and 5.20b show a virgin memristor and the equivalent symbol respectively. Figures 5.20c and 5.20d show two identical memristors M_1 and M_2 connected in parallel across a voltage source V with terminals for a direct polarization for M_1 but reversed in the case of M_2, both memristors having the same initial condition. The schematic is shown in a way to illustrate the trending of the mobile charge carriers under the influence of external bias. The currents through M_1 and M_2 are measured as I_1 and I_2 respectively, and $V(t) = I_1(t)M_1 = I_2(t)M_2$. Although the memristors are identical, Fig. 5.20e shows that $|I_1| \neq |I_2|$, hence the conductivity differs if the polarity is reversed, even though with same initial condition and voltage excitation. Thus, it is showed that the device offers low resistance path with the orientation of M_1 and high resistance path for that of M_2.

The schematic is shown in Fig. 5.20a, where initially the width of TiO_2 altogether is D, the width of the doped ($TiO_{2\text{-}e}$) region is w and the undoped one is $(D\text{-}w)$. Figure 5.20c shows that the positive charges in the doped region are repelled by the positive terminal of the power supply, thereby making the width of the doped region to expand, such that: $w \to D$, as illustrated by the width trending w_p. If the terminals of the applied voltage are reversed (Fig. 5.20d), the negative terminal from the power supply attracts the positive charges in the doped region, thereby causing the contraction of the doped region, such that: $w \to 0$ with the width trending illustrated as w_n.

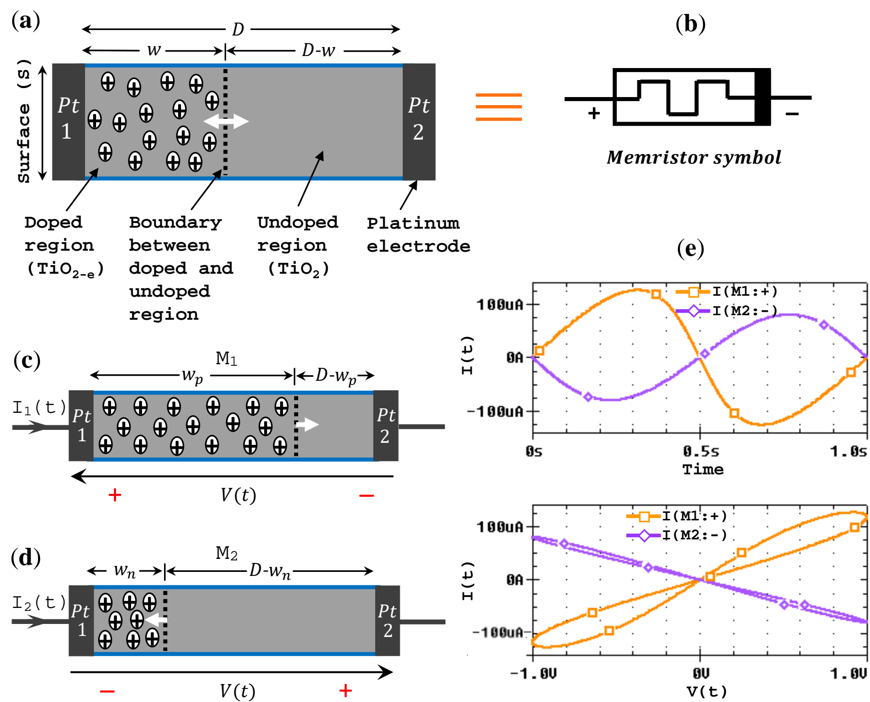

Figure 5.20: Concentration of the dopants in relation to charge carrier mobility with respect to the polarity of input signal. **(a)** Virgin memristor, **(b)** symbolic representation, **(c)** application of positive bias causes the expansion of the doped region through the bulk of the device, **(d)** application of negative bias causes the contraction of the doped region [107]. Respectively, the overall process affects the device conducting channel widths w_p and w_n, and it gives the trend on how w approaches 0 or D, **(e)** the currents I_1 and I_2 through M_1 and M_2 respectively, and the corresponding I-V curves for $V(t) = V_o\ sin(\omega t)$, $V_o = 1V$, $R_{off} = 16K\Omega$ and $R_{on} = 100\Omega$. Reversing the polarity of the memristor also affects the absolute value of the following current. The I-V curve of the current $I_2(t)$ falls in the second and fourth quadrants due to the reversed polarity of the input voltage $V(t)$.

Figure 5.20e shows the comparison of the current flowing through M_1 and M_2 with respect to the applied voltage source. The result is obtained using a sine input voltage source and a window function by ([107]). The current $I_1(t)$ and $I_2(t)$ have different absolute values. The current-voltage graph of $I_2(t)$ falls in the second and fourth quadrants due to the reversed terminals of $V(t)$.

It follows that the conductivity of a memristor can be compared to diode in terms of terminal polarity. However, unlike diode, memristor conducts electricity in both directions but the conductivity increases if its higher polarity terminal is connected to the positive terminal of the applied voltage source and decreases if its lower polarity terminal is connected to the positive terminal of the applied input voltage source.

In a nano scale device, even small voltages can generate large electric field required to cause current to flow through the device. The smaller the device, the higher the electric field is developed and hence more current flows through the device [12]. Electroforming process forms the oxygen vacancies which cause a high conducting channel ($TiO_{2\text{-}e}$) shunting the bulk of the insulation film TiO_2 [106, 154]. Depending on the nature of the bipolar input source, the conducting channel is affected by the variation of the tunneling barrier width (D-w). Therefore, the device conductivity can be described by Simmons tunneling barrier model [155–157], devoted to the conduction of a material in a given medium. Depending on the magnitude of the input source, the boundary moves back and forth proportionally to the concentration of the dopant, thus, setting the resistance of the memristor. Note that in Fig. 5.20a, in reality the boundary can never be outside of the interval

$[0, D]$, because there is always doped and undoped material present, in other word, the doped region can only expand or contract but never ceases to exist.

5.8/ MEMRISTOR ASYMMETRY FROM CIRCUIT POINT OF VIEW

To vividly visualize the effect of memristor asymmetry, we consider two identical RC cells shown in Fig. 5.21. The cells are labeled as cell-1 and cell-2 having potentials V_1 and V_2 respectively, coupled together by a memristor M with its orientation as shown. Two tests are carried out, namely:

a. Cond-1: $V_1 > V_2$,

b. Cond-2: $V_1 < V_2$,

which allows to observe the interaction of the memristor bidirectionally. In the former, the direction of $i(t)$ is as shown in Fig. 5.21a, meanwhile in the latter the direction is reversed, see Fig. 5.21b. We will take into account the history of the memristor, that is, $q(t) = \int_{-\infty}^{t} i(\tau)d\tau = q_0 + \int_{0}^{t} i(\tau)d\tau$, with q_0 as the amount of charge already flowed through device from its last usage, thus it becomes the initial charge at time $t = 0$. Considering the same memristor M with the same previous history, characterized by the initial charge q_0, in Cond-1, placed in one way as shown in Fig. 5.21, and in Cond-2, on the opposite way.

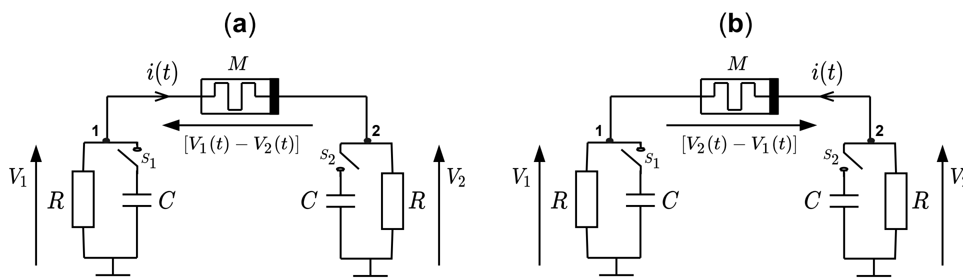

Figure 5.21: Memristor asymmetry from circuit point of view: two charged RC cells coupled together by a memristor. The circuit is invoked at time $t = 0$ by switchs S_1 and S_2. The cells are at different potentials so that the current $i(t)$ will flow through the memristor. The test is done for $V_1 > V_2$ and then $V_1 < V_2$. For example $V_1 = 1V$, $V_2 = 0V$ and then $V_1 = 0V$, $V_2 = 1V$. The voltage across the memristor is $V_m(t)$. (**a**) Cond-1 and $V_m(t) = V_1(t) - V_2(t)$. (**b**) Cond-2 and $V_m(t) = V_2(t) - V_1(t)$.

Figure 5.21 is simulated in SPICE using the memristor model by ([111]), which can easily be implemented experimentally. The setup is activated by closing the switches S_1 and S_2 simultaneously. For each Cond-1 and Cond-2, we considered the initial charge $q_0 = 38\mu C$, meanwhile the low and high resistance limits of the memristor are 100Ω and $16K\Omega$ respectively, ([12]). Given the initial conditions of the cells, that is for Cond-1: $V_{1_0} = 1V$, $V_{2_0} = 0V$ while for Cond-2: $V_{1_0} = 0V$, $V_{2_0} = 1V$, the result is shown in Fig. 5.22. It is however important to note that the initial voltages can have any numerical values. Figure 5.22a shows the memristance transition for Cond-1 and Cond-2, illustrated respectively, by the solid and dash curves. Figure 5.22b shows the corresponding time evolution of $V_1(t)$ and $V_2(t)$. The results show that Cond-1 and Cond-2 lead to quite different scenarios.

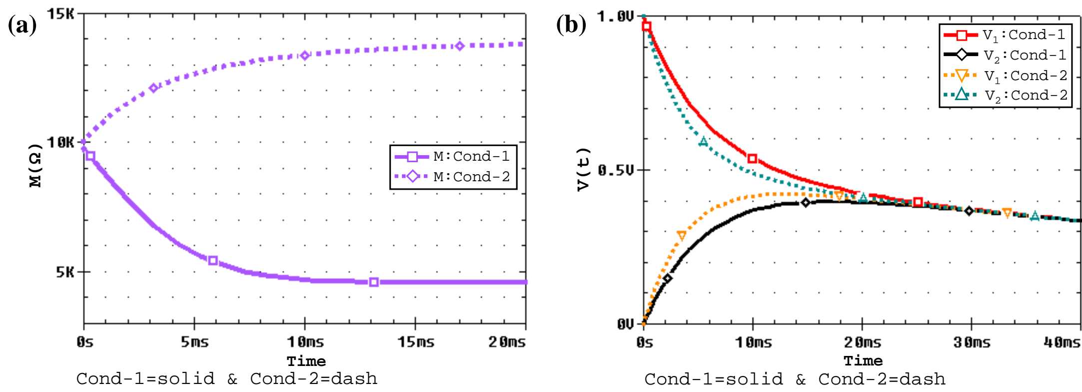

Figure 5.22: The interaction of the cells according to Cond-1 (solid curves) and Cond-2 (dash curves) for $q_0 = 38\mu C$, $R_{on} = 100\Omega$, $R_{off} = 16K\Omega$ with $V_{1_0} = 1V$, $V_{2_0} = 0V$ for Cond-1 and $V_{1_0} = 0V$, $V_{2_0} = 1V$ for Cond-2. **(a)** Memristance transition, **(b)** time evolution of $V_1(t)$ and $V_2(t)$.

In Cond-1, the memristance decreases corresponding to the expansion of the doped region, meanwhile, for Cond-2, the memristance increases corresponding to the contraction of the doped region. In both Cond-1 and Cond-2, the memristance transition eventually flattens as the cells stabilize, i.e at a time when $V_1(t) = V_2(t)$. The memristance transition depends on the initial conditions of the cells. For example, Fig. 5.23 shows the case where the initial conditions of the cells are changed with two different initial charges as $q_{0_1} = 46\mu C$ and $q_{0_2} = 31\mu C$. Figures 5.23a and 5.23b respectively, show the memristance transition and the corresponding voltage evolution of the cells. Secondly, Fig. 5.24 shows the effect of changing the initial voltage. The initial charge is maintained at $q_0 = 33.8\mu C$ while the initial voltage is varied in two steps: $V_{0_a} = 1V$ and then $V_{0_b} = 1.5V$. Hence, given that $V_{0_b} > V_{0_a}$, the memristance transits faster especially for Cond-1.

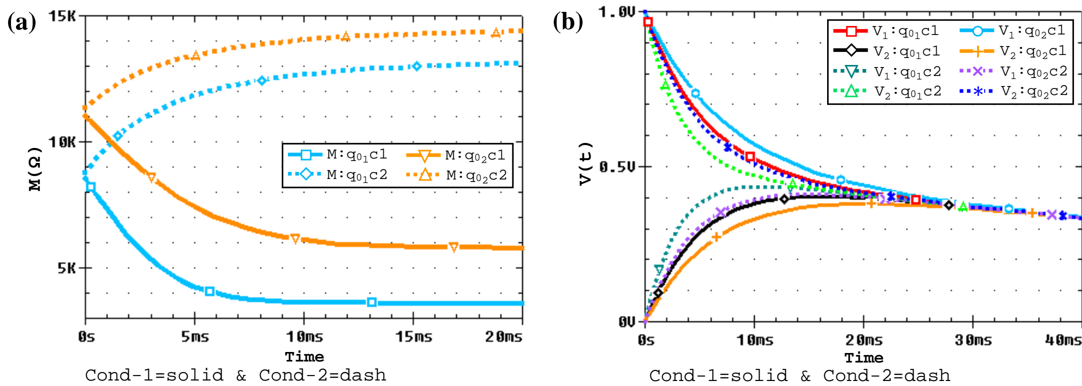

Figure 5.23: System evolution using two different initial charges $q_{0_1} = 46\mu C$ and $q_{0_2} = 31\mu C$ with $V_{1_0} = 1V$, $V_{2_0} = 0V$ for Cond-1 (solid curves) and $V_{1_0} = 0V$, $V_{2_0} = 1V$ for Cond-2 (dash curves). **(a)** Memristance transition showing the variation effect of the initial charge, **(b)** the corresponding evolution of $V_1(t)$ and $V_2(t)$.

Furthermore, Figs. 5.22b and 5.24b show that the orientation of the memristor according to Cond-1 or Cond-2 affects the time taken for the system to stabilize. Let $V_m(t)$ represents the voltage across memristor, hence $V_m(t) = V_1(t) - V_2(t)$ for Cond-1 and $V_m(t) = V_2(t) - V_1(t)$ for Cond-2 as shown in Fig. 5.21a and 5.21b respectively. No current flows through the memristor when $V_1(t) = V_2(t)$ because the voltage across the memrisor is also zero even though $V_1(t) = V_2(t) \neq 0$, see Fig. 5.25. The combined evolution of $V_1(t)$ and $V_2(t)$ eventually stabilizes to zero due

to the resistive nature of the cells. Figure 5.26 compares the flowing charge through the memristor and the corresponding memristance evolution.

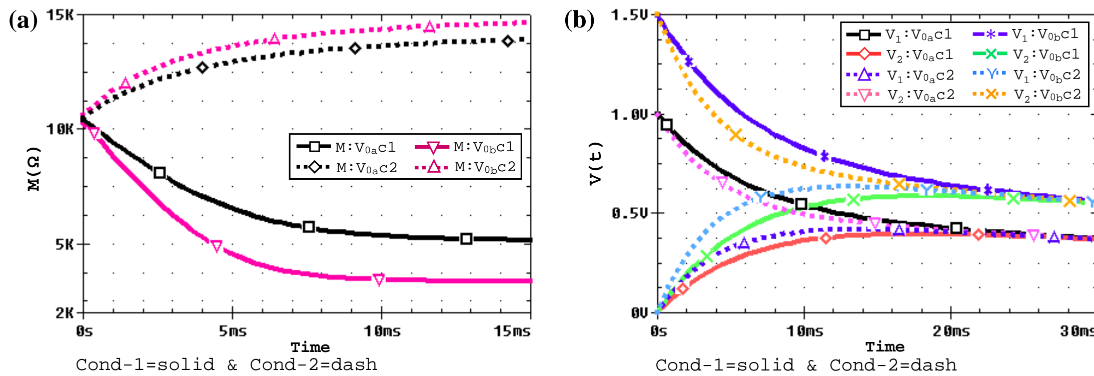

Figure 5.24: The effect of changing the initial voltage. $V_{0_a} = 1V$ and $V_{0_b} = 1.5V$ are the initial conditions of the cells and the initial charge $q_0 = 33.8\mu C$. For the black curve, $V_{1_0} = V_{0_a}$ and $V_{2_0} = 0V$ (solid) (and then $V_{1_0} = 0V$ and $V_{2_o} = V_{0_a}$ (dash)), meanwhile for the magenta one, $V_{1_0} = V_{0_b}$ and $V_{2_0} = 0V$ (solid) (and then $V_{1_0} = 0V$ and $V_{2_0} = V_{0_b}$ (dash)). **(a)** Memristance transition, **(b)** Voltage evolution.

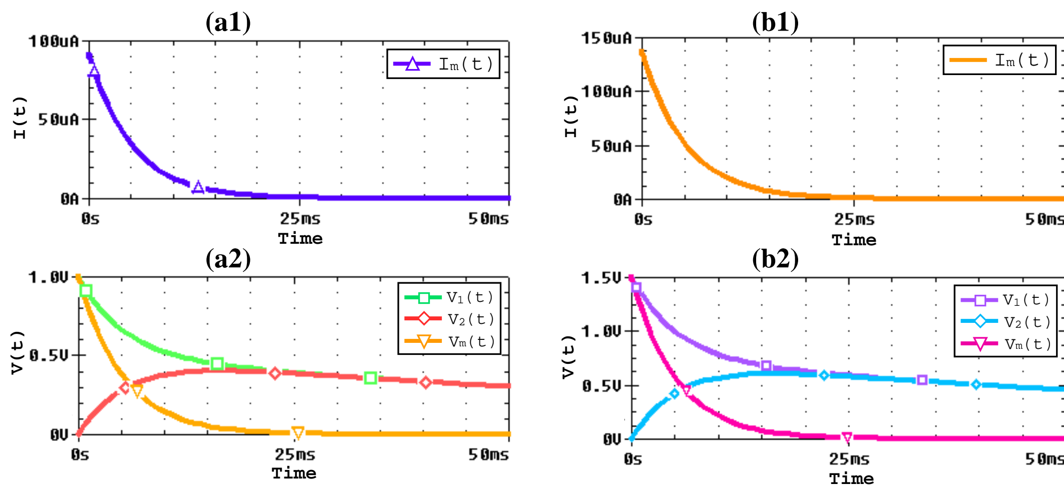

Figure 5.25: The current flowing through the memristor, evolution of $V_1(t)$ and $V_2(t)$ for cells 1 and 2 respectively, and the voltage across the memristor $V_m(t)$. No current flows through the memristor when $V_1(t) = V_2(t)$ and the voltage across the memristor is also zero. $V_1(t)$ and $V_2(t)$ eventually decay to zero due to the resistive nature of the cells. (**a1** & **a2**) $V_{0_a} = 1V$ and (**b1** & **b2**) $V_{0_b} = 1.5V$.

Furthermore, the asymmetry effect can be observed using the analytical solution given by section 5.6, and is shown in Fig. 5.27. Note that the difference $V_1 - V_2$ becomes $V_2 - V_1$ if the system is described by Cond-2. Therefore, depending on X_0, Y evolves positively according to Cond-1 and negatively according to Cond-2. Recall that the value of X_0 is not known, however its possible occurrence is taken into consideration by Fig. 5.27. Each trajectory begins with the corresponding value of Y_0. Therefore, depending on X_0, different evolution patterns are observed in the phase portraits. The phase portraits show the families of curves for different initial conditions. The results are obtained for $R_{on} = 100\Omega$ and $R_{off} = 16K\Omega$. Note that the memristance is unchanged for $X \leq 0$ and $X \geq 1$ and is respectively given by R_{off} and R_{on} as depicted by the parallel evolution of the curves outside the interval $[0, 1]$. Therefore, different possibilities are considered, that

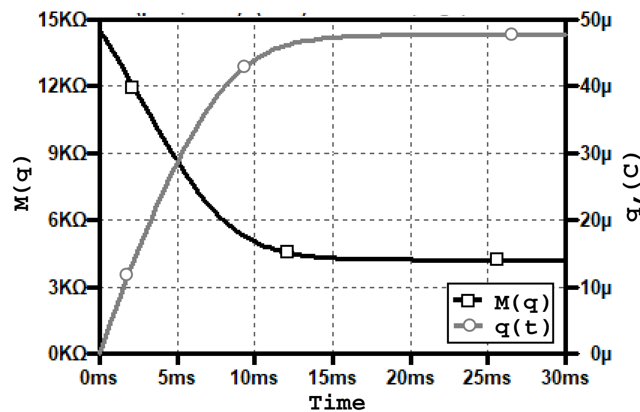

Figure 5.26: Cond-1: the flowing charge and the corresponding memristance evolution. $V_{1_0} = 2V$, $V_{2_0} = 0V$, $R = 100K\Omega$, $C = 1\mu C$, $R_{off} = 16K\Omega$, $R_{on} = 100\Omega$ and $q_d = 100\mu C$.

take into account the case where $X_0 = 0$ or 1 and beyond. The lack of symmetry is highly observable as the curves evolve from left to right for $Y > 0$ and then from right to left for $Y < 0$ for Cond-1 and Cond-2 respectively.

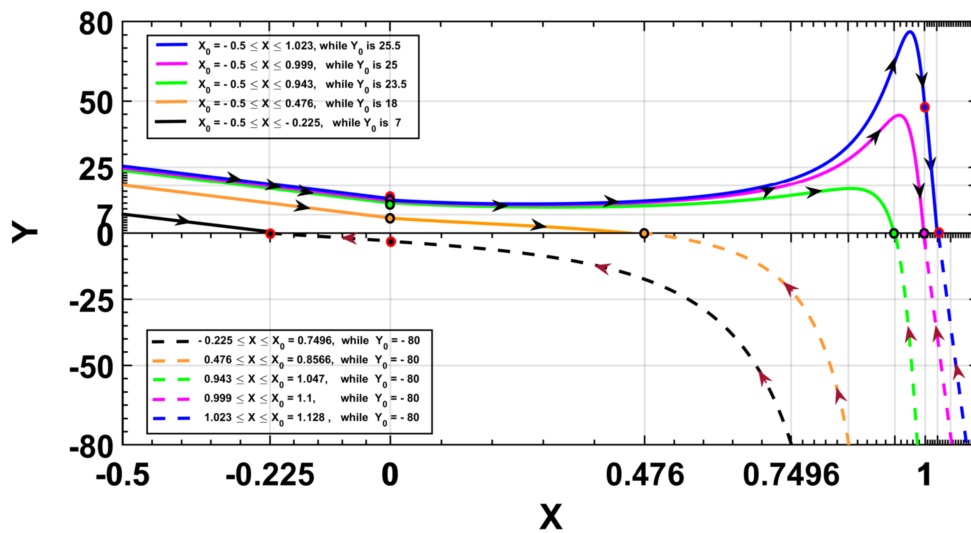

Figure 5.27: Phase portraits for cases A1 to B6, showing the charge evolution from left to right for $Y_0 > 0$ and from right to left for $Y_0 < 0$ under different initial conditions. For $X \leq 0$ and $X \geq 1$ the memristance is constant, hence the curves happen to be parallel emphasizing a constant slope at the regions. The lack of symmetry is noticeable within the bulk of the device.

5.8.1/ Memristor fuse

To achieve memristive effect with symmetry, a memristor fuse is proposed. The lack of bilaterality manifested in a memristor device is challenging in terms of its usage for certain applications, such as communication link in bidirectional applications [137]. As observed in Fig. 5.22, using memristor to link two possible sources of information com-

municating together bidirectionally is not advisable owing to its resistance dependency on the amount and direction of the flowing current. To convert it, memristor fuse is proposed and then demonstrated in [158–160]. It is basically formed by connecting two memristors anti-serially in order to avoid the lack of bilaterality [161]. Memristor fuse is reported to be useful in memristive grid network for CNN neighborhood connection and image processing [160–165]. In general [166], there are four possible ways to form series connections of two memristors with respect to their polarities, see Fig. 5.28a.

As shown in Fig. 5.28a, cases 1 and 2 refer to a serial connection of two memristors and the memristive effect is retained for these branches. Meanwhile, cases 3 and 4 are identical in structure and refer to anti-serial connection of two memristors, thus form a memristor fuse. The memristive effect for branches in cases 3 and 4 could be suppressed [107], see Fig. 5.28b. However, case 3 of Fig. 5.28a is the commonly adopted formation of a memristor fuse [160]. Note that cases 1 and 2 resembles Figs. 5.20a and 5.20b respectively, with the exception that two memristors are involved.

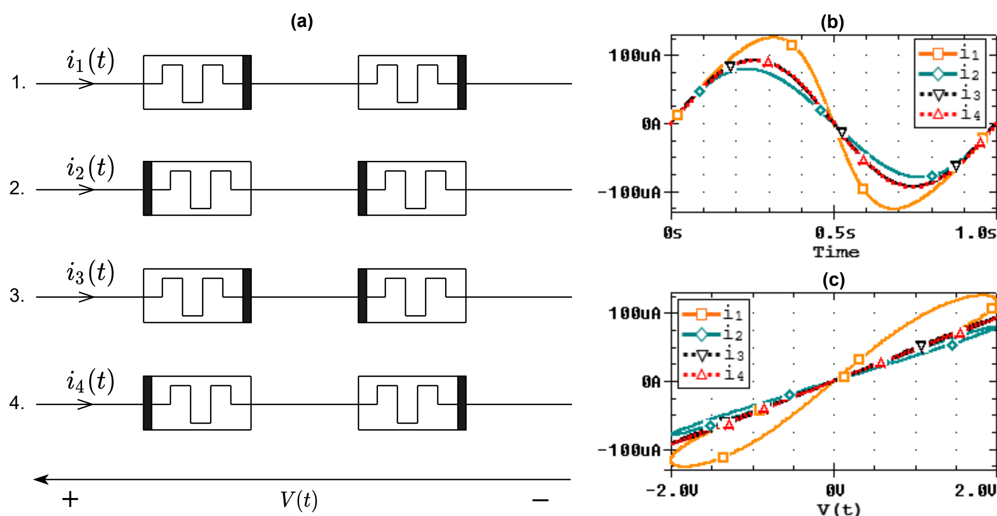

Figure 5.28: Four possible series connections of two memristors with respect to the input source. Memristive effect is retained for cases 1 and 2 whereas it is balanced for cases 3 and 4 [107]. Although cases 3 and 4 both formed a memristor fuse, case 3 is commonly considered as memristor fuse formation [160].

It is important to note that the resistance of the memristor fuse is the sum of the resistance of each of the individual memristor, because the equivalent memristance is additive in a serially connected memristor. In addition, this could be a disadvantage to the desired amount of current and it also affects the dynamic features of memristor to the extent that the current-voltage graph is merely linear, hence the formation resembles normal resistor. Therefore, the resistance limits of the memristor fuse must be the same as for one memristor if acting alone.

Pinched hysteresis loop is one of the most distinguished fingerprints of a memristor [24, 26] and is a reflection of its memory effect. As pointed out in [10, 23], without the memory, memristor is nothing different from a resistor. Verification test is performed to

compare memristor fuse with a standalone memristor as demonstrated in Fig. 5.29a. M_p and M_n are set with their polarity reversed in parallel with a memristor fuse M_f, all connected across the same voltage source $V(t)$. Therefore, for the same resistance limits, the memristance of a memristor fuse is higher than the memristance of a standalone memristor, as can be observed from the respective slopes of Fig. 5.29b.

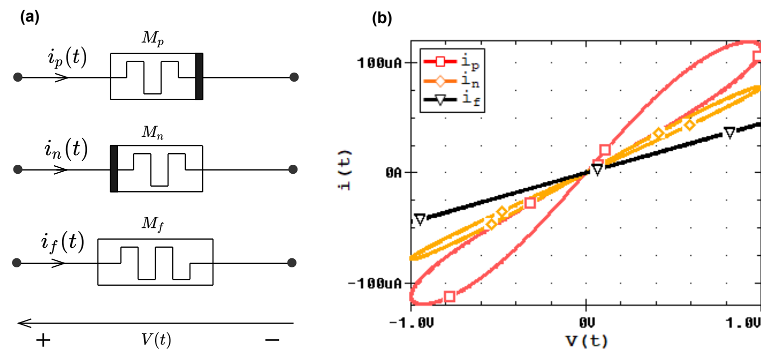

Figure 5.29: Circuit response comparison of a memristor fuse with standalone memristors. **(a)** Circuit schematic with a sine input voltage source. M_p is the memristor with positive polarity preference, M_n with negative polarity preference and M_f is the memristor fuse, **(b)** current-voltage characteristics for M_p (red), M_n (orange) and M_f (black).

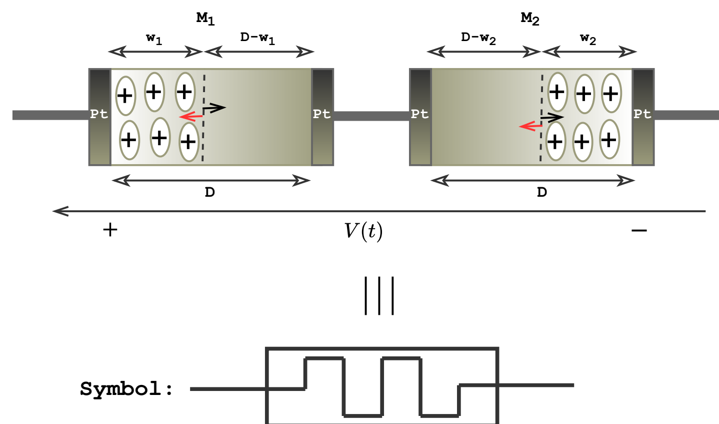

Figure 5.30: Schematic of a memristor fuse formed by 2 TiO_2 memristors M_1 and M_2. The positive spot signifies the positive oxygen vacancies, which serve as the higher conducting part of each memristors. w_1 and w_2 represent the instantaneous width of the doped region, meanwhile the black and red arrows describe the trending expansion and contraction of the doped region, respectively. Hence, for any input voltage, say $V(t)$, an increase in the width w_1 corresponds to a decrease in w_2 and vice versa.

Figure 5.30 shows the schematic of a memristor fuse formed by anti-series connection of two memristors M_1 and M_2 with the instantaneous dopant width denoted by w_1 and w_2 respectively. During positive bias, w_1 expands meanwhile w_2 contracts and during negative bias, w_1 contracts while w_2 expands. As w_1 tends to D, w_2 tends to 0 and the converse gives the other way round. Moreover, w_1 and w_2 could be represented in normalized forms as x_1 and x_2, where $x_1 = \frac{w_1}{D}$ and $x_2 = \frac{w_2}{D}$. Then the drift speeds of the respective

dopant are expressed as:

$$\frac{dx_1(t)}{dt} = \frac{1}{q_{d_1}} i(t), \tag{5.104a}$$

$$\frac{dx_2(t)}{dt} = -\frac{1}{q_{d_2}} i(t), \tag{5.104b}$$

where q_{d_1} and q_{d_2} are the values of q_d for the memristors M_1 and M_2 respectively. The same current flows through a series connection of two memristors, hence $i(t)$ is the same for both M_1 and M_2. From equation (5.104) and considering the expression of the memristance given by eq. (5.24) rather than the one given in eq. (5.25) because it is simpler and already investigated in [166], the rates of change of the instantaneous memristance of M_1 and M_2 are, respectively, obtained to be:

$$\frac{dM_1(t)}{dt} = -\frac{\delta R}{q_{d_1}} i(t), \text{ for } x_1 \in [0,1] \tag{5.105a}$$

$$\frac{dM_2(t)}{dt} = \frac{\delta R}{q_{d_2}} i(t), \text{ for } x_2 \in [0,1] \tag{5.105b}$$

Although the current $i(t)$ flowing through them is the same, however the rate of change of memristance for one differs from the other. Therefore, from (5.105a) and (5.105b), the rate of change of M_1 with respect to that of M_2 is given by:

$$\frac{dM_1(t)}{dt} = -\frac{q_{d_2}}{q_{d_1}} \frac{dM_2(t)}{dt} = -\varrho \frac{dM_2(t)}{dt}, \tag{5.106}$$

where $\varrho = \frac{q_{d_2}}{q_{d_1}} = \frac{\varrho_1}{\varrho_2}$ is called the mismatch factor [166] describing the increase of M_1 with respect to the decrease of M_2 and vice versa. Meanwhile $\varrho_1 = \frac{q_d}{q_{d_1}}$ and $\varrho_2 = \frac{q_d}{q_{d_2}}$, are parameters characterizing the mismatch factor ϱ with respect to the universal value of q_d. Note that $q_{d_1} \neq q_{d_2}$, each possibly able to depend on the dimension (D), the mobility of charge carriers and the value of the lowest resistance (R_{on}) for M_1 and M_2 respectively. Thus the mismatch factor is determined by the mobilities and velocities of charge carriers in both memristors. Given the initial memristance of M_1 and M_2 as M_{1_0} and M_{2_0} respectively, then integrating (5.106) gives:

$$M_1(t) = -\varrho M_2(t) + \delta M_0, \text{ if } x_1 \text{ and } x_2 \in [0,1] \tag{5.107}$$

where $\delta M_0 = M_{1_0} + \varrho M_{2_0}$. As the net memristance is additive in a series connection of memristors, the instantaneous memristance of the memristor fuse $M_f(t)$ is given by: $M_f(t) = M_1(t) + M_2(t)$, thus:

$$M_f(t) = (1-\varrho) M_2(t) + \delta M_0 = \frac{\varrho - 1}{\varrho} M_1(t) + \frac{\delta M_0}{\varrho}. \tag{5.108}$$

Equation (5.108) shows that the instantaneous memristance of the memristor fuse depends strongly on the mismatch factor (ϱ). In the following we present some interesting results comparing the responses of M_1, M_2 and M_f, in remaining in $[0, 1]$ for both x_1 and x_2.

Let us first consider a single memristor with linear model: $\frac{dx}{dt} = \frac{i(t)}{q_d}$ and $M(x) = R_{off} - \delta R x$, then $i(t) = \frac{V(t)}{M(x)}$, where $V(t)$ is the input voltage applied to the memristor. Therefore, using a constant input voltage V, then the relationship can be expressed as

$$\int_{x_o}^{x} (R_{off} - \delta R x')dx' = \frac{1}{q_d} \int_0^t V dt' \quad \Rightarrow$$

$$R_{off}(x - x_o) - \frac{\delta R}{2}(x^2 - x_o^2) = \frac{V}{q_d} t. \tag{5.109}$$

Note that at time $t = 0$, $x = x_o$ and when $x = 1$, $t = t_F$. Thus t_F is obtained from eq. (5.109) as:

$$t_F = \frac{q_d}{V}\left[R_{off} - \frac{\delta R}{2} - R_{off} x_o + \frac{\delta R}{2} x_o^2\right]. \tag{5.110}$$

Setting $\tilde{x} = x - x_o \;\Rightarrow\; x^2 - x_o^2 = \tilde{x}^2 + 2x_o\tilde{x}$. Therefore, equation (5.109) becomes:

$$\frac{\delta R}{2}\tilde{x}^2 - (R_{off} - \delta R x_o)\tilde{x} + \frac{V}{q_d} t = 0, \tag{5.111}$$

having determinant $\Delta = (R_{off} - \delta R x_o)^2 - \frac{2\delta R.V}{q_d} t > 0$ for $t \in [0, t_F]$ because it is smallest at time t_F, when it is calculated to be:

$$\Delta = (R_{off} - \delta R x_o)^2 - \frac{2\delta R.V}{q_d}\frac{q_d}{V}\left[R_{off} - \frac{\delta R}{2} - R_{off} x_o + \frac{\delta R}{2} x_o^2\right] = R_{on}^2.$$

Solving equation (5.111) gives

$$\tilde{x} = \frac{(R_{off} - \delta R x_o) \pm \sqrt{(R_{off} - \delta R x_o)^2 - \frac{2\delta R.V}{q_d} t}}{\delta R}. \tag{5.112}$$

With $x = \tilde{x} + x_o$ and $M = (R_{off} - \delta R.x)$, then the only feasible solution of $M_1(t)$ is:

$$M = \sqrt{(R_{off} - \delta R x_o)^2 - \frac{2\delta R.V}{q_d} t}, \text{ for } t \in [0, t_F] \text{ and } M = R_{on} \text{ for } t \geq t_F. \tag{5.113}$$

Using a square wave input voltage $V = \pm 2V$, $q_d = 100\mu C$, the time $t_F = 0.4025s$. The period T of the square wave input voltage is chosen such that $t_F > T/2$, allowing to use the total field of memristor variations. If $q_{d_1} = q_{d_2}$, $\varrho = 1$, then from equation (5.108), $M_f(t) = \delta M_0 = M_{1_0} + M_{2_0}$, that is a constant. However, $M_f(t)$ is time-varying function, hence it is necessary to have $q_{d_1} \neq q_{d_2}$ in order to exploit the real behaviour of $M_f(t)$.

Figure 5.31 shows the memristance transition of the memristors $M_1(t)$, $M_2(t)$ and the memristor-fuse $M_f(t)$ using the mismatch factor $\varrho = 2$ (i.e $q_{d_2} = 2q_{d_1}$). The results show that the increase in one memristor corresponds to the decrease of the other one and vice versa, meanwhile the memristance of the memristor fuse transits uniformly.

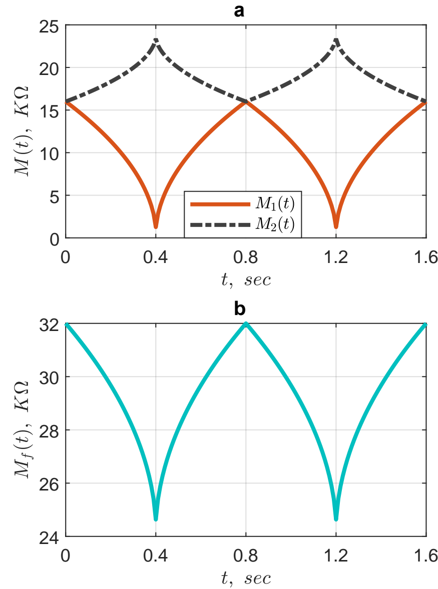

Figure 5.31: Analytical results of the memristor fuse showing the memristance transitions for $M_1(t)$, $M_2(t)$ and the memristor fuse $M_f(t)$. $\varrho = 2$, $q_{d_1} = 100\mu C$, $q_{d_2} = 200\mu C$, $R_{off} = 16K\Omega$ and $R_{on} = 100\Omega$. (**a**) memristance transitions for the memristors M_1 and M_2 (**b**) memristance of the memristor fuse M_f.

Using the nonlinear model

With $g(x) = x(1-x)$, then

$$\frac{dx}{dt} = \frac{1}{q_d}x(1-x) \text{ and } M(x) = R_{off} - \delta R x.$$

Similarly, with input voltage V, then $i(t) = \dfrac{V}{M(x)}$, which implies that

$$\int_{x_o}^{x} \frac{R_{off} - \delta R x^*}{x^*(1-x^*)} dx^* = \frac{1}{q_d} \int_0^t V dt^*.$$

Similarly, V is a constant input voltage, thus the solution is:

$$R_{off} \ln \frac{x}{x_o} - R_{on} \ln \frac{1-x}{1-x_o} = \frac{1}{q_d} V.t \tag{5.114}$$

Equation (5.114) shows that if we use the window function, first we cannot even determine the behaviour of the memristor when the voltage across it is a constant.

Using the cubic model of the memristor

Here, the relationship is expressed for a single memristor:

$$\frac{dx}{dt} = \frac{1}{q_d} i(t) \text{ and } M(x) = R_{off} - 3\delta R x^2 + 2\delta R x^3. \tag{5.115}$$

With $i(t) = \frac{V}{M(x)}$ and for V as a constant input voltage, then

$$\int_{x_o}^{x} (R_{off} - 3\delta R x'^2 + 2\delta R x'^3) dx' = \frac{1}{q_d} \int_0^t V dt' \quad \Rightarrow$$

$$\frac{\delta R}{2} x^4 - \delta R x^3 + R_{off} x + d_o - \frac{1}{q_d} V.t = 0, \tag{5.116}$$

where $d_o = -\frac{\delta R}{2} x_o^4 + \delta R x_o^3 - R_{off} x_o$ and $d_o = 0$ if $x_o = 0$. Here, the parameter t_1 for the cubic model is called t_{1_n} and is obtained from equation (5.116) when $x = 1$, thus:

$$t_{1_n} = \frac{q_d}{V} \left(R_{off} - \frac{\delta R}{2} + d_o \right). \tag{5.117}$$

Using the general formulation for solving the quartic polynomial, equation (5.116) can be solved to find the real solution which can be used to determine $M(x)$. Therefore equation (5.116) is rewritten as:

$$x^4 - 2x^3 + \frac{2R_{off}}{\delta R} x + B = 0, \tag{5.118}$$

where $B = \frac{2d_o}{\delta R} - \frac{2}{q_d \delta R} V.t$. Setting from the first two terms that $X = x - \frac{1}{2}$ allowing to eliminate the third degree term, hence

$$X^4 + pX^2 + qX + r = 0, \tag{5.119}$$

where $p = -\frac{3}{2}$, $q = \frac{R_{off}+R_{on}}{\delta R}$ and $r = -\frac{3}{16} + \frac{R_{off}}{\delta R} + B$. Using a new variable k and the identity: $(X^2 + k)^2 - 2kX^2 - k^2 = X^4$, then equation (5.119) becomes:

$$\begin{aligned} (X^2 + k)^2 &= (2k - p)X^2 - qX + (k^2 - r) \\ &= (aX + b)^2 \\ &= a^2 X^2 + 2abX + b^2 \end{aligned} \tag{5.120}$$

By coefficient comparison: $a = \sqrt{2k - p}$, $b = -\frac{q}{2a} = -\frac{q}{2\sqrt{2k-p}}$ and $b^2 = k^2 - r$, from which:

$$k^3 - \frac{p}{2} k^2 - rk + \frac{pr}{2} - \frac{q^2}{8} = 0 \quad \Rightarrow$$

$$y^3 + Py + Q = 0,$$

where $y = k - \frac{p}{6}$, $P = -r - \frac{p^2}{12}$ and $Q = \frac{pr}{2} - \frac{q^2}{8} - \frac{p^3}{108}$.

Therefore, $\Delta_1 = \frac{Q^2}{4} + \frac{P^3}{27}$, $v = \sqrt[3]{\frac{Q}{2} + \sqrt{\Delta_1}}$ and $u = \frac{P}{3v}$. With $k = y + \frac{p}{6}$ and $\omega = -\frac{1}{2} + \frac{\sqrt{3}}{2}j$, then the solutions of k are:

$$
\begin{aligned}
k_1 &= u - v + \frac{p}{6}, \\
k_2 &= u\omega^2 - v\omega + \frac{p}{6}, \\
k_3 &= u\omega - v\omega^2 + \frac{p}{6}.
\end{aligned}
$$

Hence, from equation (5.120): $X^2 + k = \pm(aX + b)$ which gives the four possible solutions as:

$$X_1 = \frac{a + \sqrt{\Delta_2}}{2}, \quad X_2 = \frac{a - \sqrt{\Delta_2}}{2} \quad \text{with} \quad \Delta_2 = a^2 - 4(k - b)$$

and

$$X_3 = \frac{-a + \sqrt{\Delta_3}}{2}, \quad X_4 = \frac{-a - \sqrt{\Delta_3}}{2} \quad \text{with} \quad \Delta_3 = a^2 - 4(k + b).$$

Finally, the solution is $x = X + \frac{1}{2}$ accordingly for x_1, x_2, x_3 and x_4.

For example, Figure 5.32 shows the results using $\varrho = 2$, $q_{d_1} = 100\mu C$, $q_{d_2} = 200\mu C$, $R_{off} = 16K\Omega$, $R_{on} = 100\Omega$, $M_{1_0} = M_{2_0} = R_{off}$, $x_o = 0.1$ and $M(x) = R_{off} - 3\delta R x^2 + 2\delta R x^3$ with $x \in [x_o, x_r]$, where x_r means the root corresponding to the real solution of equation (5.116), then the memristance of the memristor fuse is:

$$M_f(t) = \frac{\varrho - 1}{\varrho}\left(R_{off} - 3\delta R x_r^2 + 2\delta R x_r^3\right) + \frac{\delta M_0}{\varrho}. \tag{5.121}$$

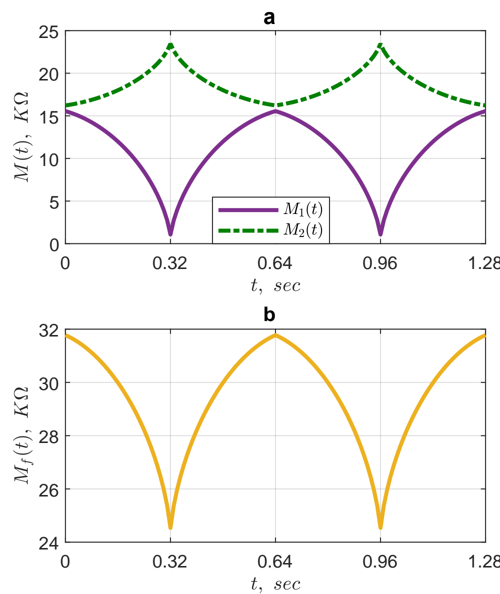

Figure 5.32: Analytical result of the memristor fuse using the new model. $\varrho = 2$, $q_{d_1} = 100\mu C$, $q_{d_2} = 200\mu C$, $R_{off} = 16K\Omega$ and $R_{on} = 100\Omega$. (**a**) memristance of M_1 and M_2, (**b**) memristance of the memristor fuse M_f.

We consider this memristor fuse, consisting in M_1 and M_2 in series, and substituted to a fixed voltage V, such as $V = V_1 + V_2$, with V_1 the voltage across M_1 and V_2 across M_2, the same current $i(t)$ flowing through M_1 and M_2, as shown in Fig. 5.33.

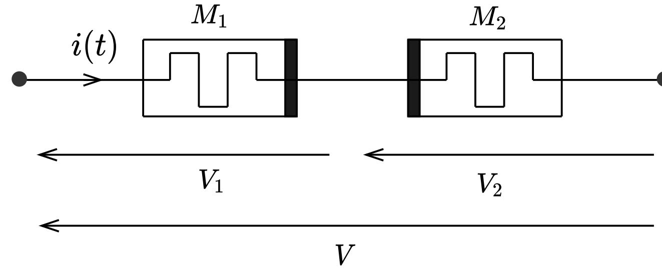

Figure 5.33: Exploring the responses of the two memristors in the memristor fuse.

From Kirchhoff's laws, we get:

$$V = V_1 + V_2 = [M_1(t) + M_2(t)].i(t) = M_f(t).i(t),$$

whose derivative versus time is:

$$M_f(t)\frac{di(t)}{dt} + \frac{dM_f(t)}{dt}i(t) = 0.$$

Using equation (5.108) and (5.105), we get:

$\frac{V}{i(t)}.\frac{di(t)}{dt} + \delta R.i(t)^2\left[\frac{1}{q_{d_2}} - \frac{1}{q_{d_1}}\right] = 0$, that is:

$$-\frac{1}{i(t)^3}\frac{di(t)}{dt} = \frac{\delta R}{V}\left(\frac{1}{q_{d_2}} - \frac{1}{q_{d_1}}\right).$$

This equation is to be integrated from $t = 0$, when $i(t = 0) = i_0 = \frac{V}{M_{1_0}+M_{2_0}}$ to give:

$$\frac{1}{i(t)^2} - \frac{1}{i_0^2} = \frac{\delta R.t}{V}\left(\frac{1}{q_{d_2}} - \frac{1}{q_{d_1}}\right)$$

or:

$$i(t) = \frac{V}{\sqrt{(M_{1_0} + M_{2_0})^2 + V.\delta R.t\left(\frac{1}{q_{d_2}} - \frac{1}{q_{d_1}}\right)}}.$$

If $q_{d_2} > q_{d_1}$, $i(t)$ is increasing with time and if $q_{d_2} < q_{d_1}$, $i(t)$ is decreasing. Note however that this expression is correct as long as either $M_1(t)$ or $M_2(t)$ stays inside the interval $[R_{on}, R_{off}]$, that is for $x_1 = \frac{w_1}{D_1} \in [0, 1]$ and $x_2 = \frac{w_2}{D_2} \in [0, 1]$.

Considering for example $q_{d_2} > q_{d_1}$, leading to the stronger condition: $t \leq t_{lim}$ such that:

$$\frac{\delta R.V}{q_{d_1}} \int_0^{t_{lim}} \frac{dt^*}{\sqrt{(M_{1_0} + M_{2_0})^2 - V.\delta R.t^* \left(\frac{1}{q_{d_1}} - \frac{1}{q_{d_2}}\right)}} \leq M_{1_0} - R_{on}.$$

It is required that the expression in the root stays positive strictly, so:

$$t < \frac{(M_{1_0} + M_{2_0})^2}{V.\delta R \left(\frac{1}{q_{d_1}} - \frac{1}{q_{d_2}}\right)},$$

and also $t < t_{lim}$. By calculations we know that:

$$\left(-2\sqrt{b - ax}\right)' = \frac{a}{\sqrt{b - ax}} \text{ if } x < \frac{b}{a}.$$

Then:

$$\int_0^{t_{lim}} \frac{dt^*}{\sqrt{(M_{1_0} + M_{2_0})^2 - V.\delta R.t^* \left(\frac{1}{q_{d_1}} - \frac{1}{q_{d_2}}\right)}} = \frac{-2}{V\delta R \left(\frac{1}{q_{d_1}} - \frac{1}{q_{d_2}}\right)} \left[\sqrt{(M_{1_0} + M_{2_0})^2 - V.\delta R.t \left(\frac{1}{q_{d_1}} - \frac{1}{q_{d_2}}\right)} \right]_0^{t_{lim}}$$

$\Rightarrow$

$$\frac{-2}{V\delta R \left(\frac{1}{q_{d_1}} - \frac{1}{q_{d_2}}\right)} \left[\sqrt{(M_{1_0} + M_{2_0})^2 - V.\delta R.t_{lim} \left(\frac{1}{q_{d_1}} - \frac{1}{q_{d_2}}\right)} - (M_{1_0} + M_{2_0}) \right] \leq \left(\frac{M_{1_0} - R_{on}}{\delta RV}\right) q_{d_1},$$

$$\frac{2}{\left(\frac{1}{q_{d_1}} - \frac{1}{q_{d_2}}\right)} \left[(M_{1_0} + M_{2_0}) - \sqrt{(M_{1_0} + M_{2_0})^2 - V.\delta R.t_{lim} \left(\frac{1}{q_{d_1}} - \frac{1}{q_{d_2}}\right)} \right] \leq (M_{1_0} - R_{on})\, q_{d_1},$$

$$\frac{2(M_{1_0} + M_{2_0})\, q_{d_2} q_{d_1}}{(q_{d_2} - q_{d_1})} \left[1 - \sqrt{1 - \frac{V.\delta R.t_{lim}(q_{d_2} - q_{d_1})}{q_{d_1} q_{d_2} \left(M_{1_0} + M_{2_0}\right)^2}} \right] \leq (M_{1_0} - R_{on})\, q_{d_1},$$

$$1 - \sqrt{1 - \frac{V.\delta R.t_{lim}(q_{d_2} - q_{d_1})}{q_{d_1} q_{d_2} \left(M_{1_0} + M_{2_0}\right)^2}} \leq \frac{(M_{1_0} - R_{on})\,(q_{d_2} - q_{d_1})}{2(M_{1_0} + M_{2_0}).q_{d_2}},$$

$$1 - \frac{(M_{1_0} - R_{on})\,(q_{d_2} - q_{d_1})}{2(M_{1_0} + M_{2_0}).q_{d_2}} \leq \sqrt{1 - \frac{V.\delta R.t_{lim}(q_{d_2} - q_{d_1})}{q_{d_1} q_{d_2} \left(M_{1_0} + M_{2_0}\right)^2}},$$

$$\left(1 - \frac{(M_{1_0} - R_{on})\,(q_{d_2} - q_{d_1})}{2(M_{1_0} + M_{2_0}).q_{d_2}}\right)^2 \leq 1 - \frac{V.\delta R.t_{lim}(q_{d_2} - q_{d_1})}{q_{d_1} q_{d_2} \left(M_{1_0} + M_{2_0}\right)^2},$$

$$\frac{V.\delta R.t_{lim}(q_{d_2} - q_{d_1})}{q_{d_1} q_{d_2} \left(M_{1_0} + M_{2_0}\right)^2} \leq -\frac{\left(M_{1_0} - R_{on}\right)^2 \left(q_{d_2} - q_{d_1}\right)^2}{4\left(M_{1_0} + M_{2_0}\right)^2 .q_{d_2}^2} + \frac{(M_{1_0} - R_{on})\,(q_{d_2} - q_{d_1})}{(M_{1_0} + M_{2_0})\,.q_{d_2}},$$

$$\frac{V.\delta R.t_{lim}}{q_{d_1}\left(M_{1_0} + M_{2_0}\right)} \leq (M_{1_0} - R_{on}) - \frac{\left(M_{1_0} - R_{on}\right)^2 (q_{d_2} - q_{d_1})}{4\left(M_{1_0} + M_{2_0}\right) .q_{d_2}},$$

$$t_{lim} \leq \frac{(M_{1_0} - R_{on})(M_{1_0} + M_{2_0})q_{d_1}}{V\delta R} - \frac{(M_{1_0} - R_{on})^2 (q_{d_2} - q_{d_1})}{V\delta R} \frac{q_{d_1}}{q_{d_2}} \Rightarrow$$

$$t \leq t_{lim} = \frac{q_{d_1}}{V\delta R}\left[(M_{1_0} - R_{on})(M_{2_0} + R_{on})\right] + \frac{q_{d_1}^2}{q_{d_2}} \frac{(M_{1_0} - R_{on})^2}{V\delta R}. \tag{5.122}$$

As shown in Fig. 5.33, the current $i(t) = \frac{dq}{dt} = \dot{q}$ flowing through M_1 and M_2 is the same, and the schematic forms memristor fuse with $V = M_f(q).i = M_f(q).\dot{q}$. We would like to express here $M_f(q)$ with respect to the charge q flowing through M_1 and M_2 by means of current $i = \dot{q}$. As presented in this chapter, the memristor M_1 can be studied with the cubic model (for $0 \leq q \leq q_d$)

$$M_1(q) = R_{off} - 3\delta R \frac{q^2}{q_{d_1}^2} + 2\delta R \frac{q^3}{q_{d_1}^3},$$

when the current is represented toward right, that is, from unmarked side to marked side (see section 2.4). However, for memrisor M_2, the current is rather directed from marked side to unmarked side, that is $M(q)$ is to be replaced by another $M_2(q)$ expression, that is, intuitively (Figure 5.34):

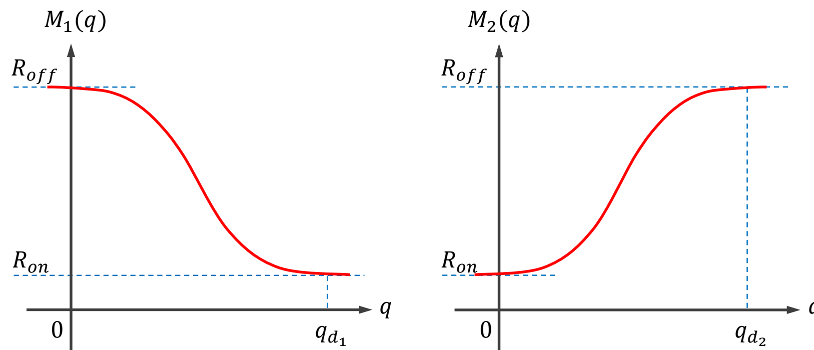

Figure 5.34: Memristance of M_1 and M_2 with respect to the flowing charge. It is clear that the increase in memristance of M_1 correspond to decrease in the one for M_2 and vice-versa.

Following the method of section 4.4 to find the new model, it is straightforward to write:

$$M_2(q) = \begin{cases} R_{on}, & for\ q \leq 0 \\ R_{on} + bq + cq^2 + dq^3, & for\ 0 \leq q \leq q_{d_2} \\ R_{off}. & for\ q \geq q_{d_2} \end{cases} \tag{5.123}$$

Requesting the continuity for the first derivative $\frac{dM_2(q)}{dq}$, we find: $b = 0$, $c = \frac{3\delta R}{q_{d_2}^2}$, $d = \frac{-2\delta R}{q_{d_2}^3}$, leading to:

$$M_2(q) = \begin{cases} R_{on}, & if\ q \leq 0 \\ R_{on} + 3\delta R \frac{q^2}{q_{d_2}^2} - 2\delta R \frac{q^3}{q_{d_2}^3}, & if\ 0 \leq q \leq q_{d_2} \\ R_{off}. & if\ q \geq q_{d_2} \end{cases} \tag{5.124}$$

Coming back to memristor fuse memristance, it follows if we assume that both M_1 and M_2 start with the same initial charge q_0 and for example $q_{d_2} > q_{d_1}$,

- if $q \leq 0$:

$$M_f(q) = R_{off} + R_{on},$$

- if $0 \leq q \leq q_{d_1} < q_{d_2}$:

$$M_f(q) = R_{off} + R_{on} + 3\delta R q^2 \left(\frac{1}{q_{d_2}^2} - \frac{1}{q_{d_1}^2} \right) - 2\delta R q^3 \left(\frac{1}{q_{d_2}^3} - \frac{1}{q_{d_1}^3} \right),$$

- if $q_{d_1} \leq q \leq q_{d_2}$:

$$M_f(q) = 2R_{on} + 3\delta R \frac{q^2}{q_{d_2}^2} - 2\delta R \frac{q^3}{q_{d_2}^3},$$

- if $q \geq q_{d_2}$:

$$M_f(q) = R_{off} + R_{on}.$$

Of course, the memristor effect disappears if the memristors are the same (i.e $q_{d_1} = q_{d_2}$), which we will exclude in the following.

Submitted to a fixed voltage V, the dynamics of $M_f(q)$ is such that:

$$V = M_f(q)\ i(t) = M_f(q)\ \dot{q},$$

whose derivative versus time gives:

$$0 = \frac{dM_f(q)}{dq} . \dot{q}^2 + M_f(q)\ \ddot{q}.$$

Staying in $[0, q_{d_1}]$ for the sake of simplicity, this equation writes:

$$\begin{aligned}\left[6\delta R\ q \left(\frac{1}{q_{d_2}^2} - \frac{1}{q_{d_1}^2} \right) - 6\delta R\ q^2 \left(\frac{1}{q_{d_2}^3} - \frac{1}{q_{d_1}^3} \right) \right] \dot{q}^2 &= - \left[R_{off} + R_{on} + 3\delta R q^2 \left(\frac{1}{q_{d_2}^2} - \frac{1}{q_{d_1}^2} \right) - 2\delta R q^3 \left(\frac{1}{q_{d_2}^3} - \frac{1}{q_{d_1}^3} \right) \right] \ddot{q}, \\ &= -\frac{V}{\dot{q}} . \ddot{q},\end{aligned}$$

where $\frac{V}{\dot{q}} = M_f(q)$. With the mismatch factor $\varrho = \frac{q_{d_2}}{q_{d_1}}$, the equation becomes:

$$\frac{d^2 q}{dt^2} = \frac{6\delta R}{q_{d_1} V} \left[\left(\frac{1}{\varrho^3} - 1 \right) \frac{q^2}{q_{d_1}^2} - \left(\frac{1}{\varrho^2} - 1 \right) \frac{q}{q_{d_1}} \right] \left(\frac{dq}{dt} \right)^3 . \tag{5.125}$$

Equation (5.125) can be expressed in normalized form by considering $X = \frac{q}{q_{d_1}}$ and $\tau = \frac{t}{\tau_x}$, that is:

$$\frac{d^2 X}{d\tau^2} = \frac{6\ \delta R\ q_{d_1}}{\tau_x} \left[\left(\frac{1}{\varrho^3} - 1 \right) X^2 - \left(\frac{1}{\varrho^2} - 1 \right) X \right] \left(\frac{dX}{d\tau} \right)^3 .$$

Finally, calling $Y = \frac{dX}{d\tau}$, this equation become:

$$\frac{dY}{d\tau} = \frac{6\ \delta R\ q_{d_1}}{\tau_x} \left[\left(\frac{1}{\varrho^3} - 1 \right) X^2 - \left(\frac{1}{\varrho^2} - 1 \right) X \right] Y^3 \quad \Rightarrow$$

$$\begin{cases} \frac{dX}{d\tau} = Y, \\ \frac{dY}{d\tau} = \frac{6\ \delta R\ q_{d_1}}{\tau_x}\left[\left(\frac{1}{\varrho^3}-1\right)X^2-\left(\frac{1}{\varrho^2}-1\right)X\right]Y^3. \end{cases} \tag{5.126}$$

Equation (5.126) is simplified to give:

$$\frac{dY}{dX} = \frac{6\ \delta R\ q_{d_1}}{\tau_x}\left[\left(\frac{1}{\varrho^3}-1\right)X^2-\left(\frac{1}{\varrho^2}-1\right)X\right]Y^2 \quad \Rightarrow$$

$$Y = -\frac{1}{\frac{6\ \delta R\ q_{d_1}}{\tau_x}\left[\left(\frac{1}{\varrho^3}-1\right)\frac{X^3}{3}-\left(\frac{1}{\varrho^2}-1\right)\frac{X^2}{2}\right]+K},$$

where K is a constant of integration. Substituting $Y = \frac{dX}{d\tau}$, we get:

$$\left\langle \frac{6\ \delta R\ q_{d_1}}{\tau_x}\left[\left(\frac{1}{\varrho^3}-1\right)\frac{X^3}{3}-\left(\frac{1}{\varrho^2}-1\right)\frac{X^2}{2}\right]+K\right\rangle dX = -d\tau \quad \Rightarrow$$

$$\frac{6\ \delta R\ q_{d_1}}{\tau_x}\left[\left(\frac{1}{\varrho^3}-1\right)\frac{X^4}{12}-\left(\frac{1}{\varrho^2}-1\right)\frac{X^3}{6}\right]+KX-\mathscr{B} = \tau_0-\tau, \tag{5.127}$$

where τ_0 is the initial normalized time and $\mathscr{B}$ represents the expression:

$$\mathscr{B} = \frac{6\ \delta R\ q_{d_1}}{\tau_x}\left[\left(\frac{1}{\varrho^3}-1\right)\frac{X_0^4}{12}-\left(\frac{1}{\varrho^2}-1\right)\frac{X_0^3}{6}\right]+KX_0.$$

5.9/ MEMRISTOR FUSE IN THE COUPLING MODE

Figure 5.35 shows the 2 RC cells network using memristor fuse in the coupling mode. In the following, we compare the responses of the memristor according to the circuit in Fig. 5.21 and the ones for memristor fuse given by Fig. 5.35. Then, we present the analytical solution of the network using memristor fuse.

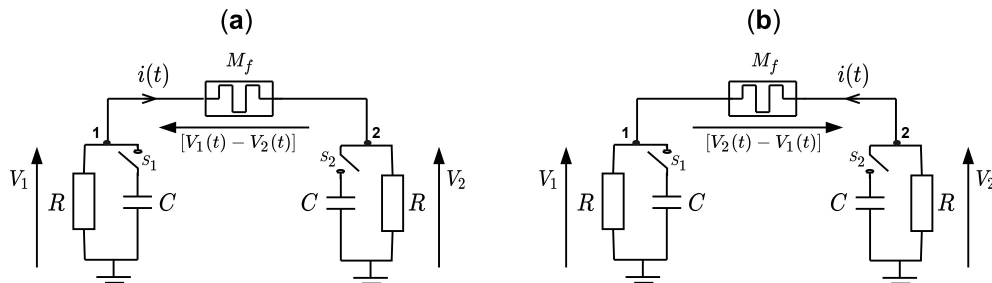

Figure 5.35: Memristor fuse in the coupling mode. (a) Cond-1 (for $V_1 > V_2$) and (b) Cond-2 (for $V_1 < V_2$).

Figure 5.36 shows the comparison of the circuit response for memristor and memristor fuse using the setup of Fig. 5.21. Recall that for Cond-1, $V_{1_0} > V_{2_0}$ and for Cond-2, $V_{2_0} > V_{1_0}$. Then for Cond-1: $V_{1_0} = 1V$ and $V_{2_0} = 0V$ while for Cond-2: $V_{1_0} = 0V$ and $V_{2_0} = 1V$ with $q_0 = 45.58\mu C$, $C = 1\mu F$ and $R = 100K\Omega$ in each case. Furthermore, M_{c1} and M_{c2} represent memristor according to Cond-1 and Cond-2 respectively. Similarly, M_{f1} and M_{f2} represent memristor fuse according to Cond-1 and Cond-2 respectively. The system evolves and eventually stabilizes when $V_1(t) = V_2(t)$,

see Fig. 5.36.

Figure 5.36a shows the evolution of $V_1(t)$ and $V_2(t)$ for M_{c1}, M_{c2}, M_{f1} and M_{f2}. The results of M_{c1} and M_{c2} show a shift difference during the transient state while there is no such shift between the curves of M_{f1} and M_{f2}, showing that memristor fuse behaves equally in both Cond-1 and Cond-2. Figure 5.36b shows the currents through the memristor as i_{c1} and i_{c2} according to Cond-1 and Cond-2 respectively, and then through memristor fuse as i_{f1} and i_{f2} according to Cond-1 and Cond-2 respectively. Furthermore, the results show that no current is flowing through the memristor when $V_1(t) = V_2(t)$ as similarly observed in the analytical result of Fig. 5.27. The difference in the starting currents is due to the resistance according to each case, see Fig. 5.36c. The results show the differences in the memristor responses according to Cond-1 and Cond-2, but the memristor fuse behaves indifferent in both conditions.

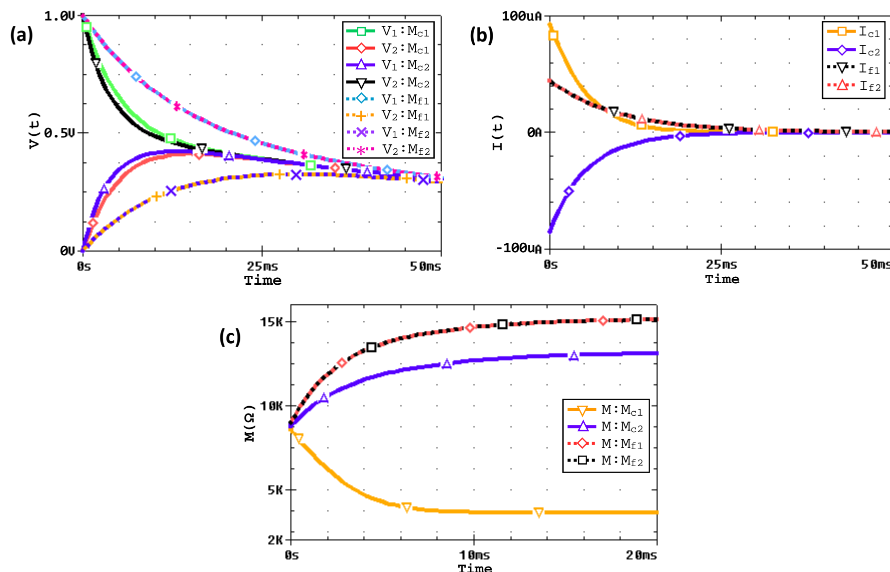

Figure 5.36: Comparing the system evolution using the circuit of **Figure 5.21** by considering memristor (M) and then memristor-fuse (M_f). Mc1 and Mc2 correspond respectively to a single memristor used according to Cond-1 and Cond-2, while Mf1 and Mf2 correspond respectively to a memristor fuse used according to Cond-1 and Cond-2. The results show the response for each case until the system stabilized: **(A)** the voltage evolution as $V_1(t)$ and $V_2(t)$, **(B)** the flowing currents through the memristor (I_{c1} and I_{c2} for Cond-1 and Cond-2 respectively) and memristor fuse (I_{f1} and I_{f2} for Cond-1 and Cond-2 respectively), **(C)** memristance transition. Given the same initial condition, the results show that memristor fuse conducts equally in both directions. For Mc1, Mc2, Mf1 and Mf2: c1, c2, f1 and f2 are subscripts denoting Cond-1 and Cond-2 accordingly.

5.9.1/ ANALYTICAL INTERPRETATION OF MEMRISTOR FUSE IN NONLINEAR NETWORK

The following presents the analytical interpretation of Fig. 5.35. However we consider only Fig. 5.35a because the cells are identical with the difference only in initial conditions. Closing the switches S_1 and S_2 simultaneously at $t = 0$, then Kirchhoff's laws gives the following set of

equations:

$$i(t) = -C\frac{dV_1}{dt} - \frac{V_1}{R}, \tag{5.128}$$

$$i(t) = C\frac{dV_2}{dt} + \frac{V_2}{R}, \tag{5.129}$$

$$i(t) = \frac{dq}{dt}, \tag{5.130}$$

and

$$V_1 - V_2 = M_f\frac{dq}{dt}, \tag{5.131}$$

where M_f is the memristor fuse given by equation (5.108). Equations (5.128)-(5.131) are similar to (5.20)-(5.23). Therefore, we can rewrite equation (5.54) as:

$$(2R + M_f(q))\,\frac{dq}{dt} + \tau_c\,\frac{dM_f(q)}{dq}\,\left(\frac{dq}{dt}\right)^2 + \tau_c\,M_f(q)\,\frac{d^2q}{dt^2} = 0. \tag{5.132}$$

Similarly, using $\tau = \frac{t}{\tau_c}$ as the normalized time, then equation (5.132) becomes:

$$(2R + M_f(q))\,\frac{dq}{d\tau} + \frac{dM_f(q)}{dq}\,\left(\frac{dq}{d\tau}\right)^2 + M_f(q)\,\frac{d^2q}{d\tau^2} = 0. \tag{5.133}$$

Equation (5.133) requires a continuous first derivative of $M_f(q)$ with respect to the flowing charge through the memristor fuse, hence we consider the new memristance function in (5.133) because it has a continuous first derivative of $M_f(q)$ with respect to q. Therefore, $M_1(q) = R_{off} - 3\delta R\varrho_1^2\,\frac{q^2}{q_d^2} + 2\delta R\varrho_1^3\,\frac{q^3}{q_d^3}$ recalling that $q_{d_1} = \frac{q_d}{\varrho_1}$ and $q_{d_2} = \frac{q_d}{\varrho_2}$, and $M_f(q)$ expressed from equation (5.108) as:

$$M_f(q) = \frac{\varrho - 1}{\varrho}\left(R_{off} - 3\delta R\varrho_1^2\,\frac{q^2}{q_d^2} + 2\delta R\varrho_1^3\,\frac{q^3}{q_d^3}\right) + \frac{\delta M_0}{\varrho}, \tag{5.134}$$

and

$$\frac{dM_f(q)}{dq} = \frac{\varrho - 1}{\varrho}\left(-6\delta R\varrho_1^2\,\frac{q}{q_d^2} + 6\delta R\varrho_1^3\,\frac{q^2}{q_d^3}\right). \tag{5.135}$$

Equations (5.134) and (5.135) can be expressed in normalized form by considering $X = \frac{q}{q_d}$ as the normalized charge and $\mathscr{M}_f(X) = \frac{M_f(X)}{\delta R}$ as the normalized memristance of the memristor fuse. Therefore, equations (5.134) and (5.135) respectively, become:

$$\mathscr{M}_f(X) = \frac{\varrho - 1}{\varrho}\left(\frac{R_{off}}{\delta R} - 3\varrho_1^2\,X^2 + 2\varrho_1^3\,X^3\right) + \frac{\delta M_0}{\varrho\,\delta R}, \tag{5.136}$$

and

$$\frac{d\mathscr{M}_f(X)}{dX} = \frac{\varrho - 1}{\varrho}\left(-6\varrho_1^2\,X + 6\varrho_1^3\,X^2\right). \tag{5.137}$$

Similarly, the equivalent normalized form of equation (5.133) becomes:

$$\left(\frac{2R}{\delta R}+\mathscr{M}_f(X)\right)\frac{dX}{d\tau}+\frac{d\mathscr{M}_f(X)}{dX}\left(\frac{dX}{d\tau}\right)^2+\mathscr{M}_f(X)\,\frac{d^2X}{d\tau^2}=0. \tag{5.138}$$

Setting $Y=\dfrac{dX}{d\tau}$, equation (5.138) is to be studied in the phase plane (X,Y). Therefore, equation (5.138) becomes:

$$\left(\frac{2R}{\delta R}+\mathscr{M}_f(X)\right)Y+\frac{d\mathscr{M}_f(X)}{dX}Y^2+\mathscr{M}_f(X)\,\frac{dY}{d\tau}=0. \tag{5.139}$$

Substituting equations (5.136) and (5.137) into equation (5.139), we get:

$$\begin{aligned}&\left[\frac{2R}{\delta R}+\frac{\varrho-1}{\varrho}\left(2\varrho_{1}^{3}\,X^3-3\varrho_{1}^{2}\,X^2+\frac{R_{off}}{\delta R}\right)+\frac{\delta M_0}{\varrho\,\delta R}\right]Y+\frac{\varrho-1}{\varrho}\left(6\varrho_{1}^{3}\,X^2-6\varrho_{1}^{2}\,X\right)\,Y^2\\&+\left[\frac{\varrho-1}{\varrho}\left(2\varrho_{1}^{3}\,X^3-3\varrho_{1}^{2}\,X^2+\frac{R_{off}}{\delta R}\right)+\frac{\delta M_0}{\varrho\,\delta R}\right]\frac{dY}{d\tau}=0\;\Rightarrow\end{aligned}$$

$$\begin{cases}\dfrac{dX}{d\tau}=Y,\\[2mm]\dfrac{dY}{d\tau}=\dfrac{-\left[\frac{\varrho-1}{\varrho}\left(2\varrho_{1}^{3}\,X^3-3\varrho_{1}^{2}\,X^2+\frac{R_{off}}{\delta R}\right)+\frac{2R}{\delta R}+\frac{\delta M_0}{\varrho\,\delta R}\right]Y-\frac{\varrho-1}{\varrho}\left(6\varrho_{1}^{3}\,X^2-6\varrho_{1}^{2}\,X\right)Y^2}{\left[\frac{\varrho-1}{\varrho}\left(2\varrho_{1}^{3}\,X^3-3\varrho_{1}^{2}\,X^2+\frac{R_{off}}{\delta R}\right)+\frac{\delta M_0}{\varrho\,\delta R}\right]}.\end{cases} \tag{5.140}$$

From equation (5.140), we get:

$$\begin{aligned}&\left(\frac{\varrho-1}{\varrho}\left(2\varrho_{1}^{3}\,X^3-3\varrho_{1}^{2}\,X^2+\frac{R_{off}}{\delta R}\right)+\frac{\delta M_0}{\varrho\,\delta R}\right)\frac{dY}{dX}+\frac{\varrho-1}{\varrho}\left(6\varrho_{1}^{3}\,X^2-6\varrho_{1}^{2}\,X\right)Y=\\&-\left[\frac{\varrho-1}{\varrho}\left(2\varrho_{1}^{3}\,X^3-3\varrho_{1}^{2}\,X^2+\frac{R_{off}}{\delta R}\right)+\frac{2R}{\delta R}+\frac{\delta M_0}{\varrho\,\delta R}\right].\end{aligned} \tag{5.141}$$

Equation (5.141) can be rewritten as:

$$\begin{aligned}&\frac{d}{dX}\left[\left(\frac{\varrho-1}{\varrho}\left(2\varrho_{1}^{3}\,X^3-3\varrho_{1}^{2}\,X^2+\frac{R_{off}}{\delta R}\right)+\frac{\delta M_0}{\varrho\,\delta R}\right)Y\right]=\\&-\left[\frac{\varrho-1}{\varrho}\left(2\varrho_{1}^{3}\,X^3-3\varrho_{1}^{2}\,X^2+\frac{R_{off}}{\delta R}\right)+\frac{2R}{\delta R}+\frac{\delta M_0}{\varrho\,\delta R}\right],\end{aligned}$$

and its integration gives the following:

$$\begin{aligned}&\int d\left[\left(\frac{\varrho-1}{\varrho}\left(2\varrho_{1}^{3}\,X^3-3\varrho_{1}^{2}\,X^2+\frac{R_{off}}{\delta R}\right)+\frac{\delta M_0}{\varrho\,\delta R}\right)Y\right]=\\&-\int\left[\frac{\varrho-1}{\varrho}\left(2\varrho_{1}^{3}\,X^3-3\varrho_{1}^{2}\,X^2+\frac{R_{off}}{\delta R}\right)+\frac{2R}{\delta R}+\frac{\delta M_0}{\varrho\,\delta R}\right]dX\;\Rightarrow\end{aligned}$$

$$H(X,Y)=\left[\frac{\varrho-1}{\varrho}\left(2\varrho_{1}^{3}\,X^3-3\varrho_{1}^{2}\,X^2+\frac{R_{off}}{\delta R}\right)+\frac{\delta M_0}{\varrho\,\delta R}\right]Y+\frac{\varrho-1}{\varrho}\left(\frac{\varrho_{1}^{3}}{2}X^4-\varrho_{1}^{2}\,X^3+\frac{R_{off}}{\delta R}X\right)+\left(\frac{2R}{\delta R}+\frac{\delta M_0}{\varrho\,\delta R}\right)X, \tag{5.142}$$

where $H(X,Y)$ is a conservative expression depending on the initial conditions of the system.

Using $Y = \frac{dX}{d\tau}$, then equation (5.142) becomes:

$$\frac{dX}{d\tau} = \frac{H - \frac{\varrho-1}{\varrho}\left(\frac{\varrho_1^3}{2}X^4 - \varrho_1^2\, X^3 + \frac{R_{off}}{\delta R}X\right) - \left(\frac{2R}{\delta R} + \frac{\delta M_0}{\varrho\ \delta R}\right)X}{\frac{\varrho-1}{\varrho}\left(2\varrho_1^3\, X^3 - 3\varrho_1^2\, X^2 + \frac{R_{off}}{\delta R}\right) + \frac{\delta M_0}{\varrho\ \delta R}}, \tag{5.143}$$

which can be solved to obtain an analytical solution of X.

Using the parameters values: $R_{off} = 16K\Omega$, $R_{on} = 100\Omega$, $\delta R = R_{off} - R_{on} = 15900\Omega$, $R = 100K\Omega$, $C = 1\mu F$, $\tau_c = RC = 0.1s$, $q_{d_1} = 120\mu C$, $q_{d_2} = 180\mu C$, $q_d = 200\mu C$, which gives $\varrho_1 = \frac{q_d}{q_{d_1}} = 1.67$, $\varrho_2 = \frac{q_d}{q_{d_2}} = 1.11$ and $\varrho = \frac{\varrho_1}{\varrho_2} = 1.50$. Recall that $M_1(q) = R_{off} - 3\delta R\varrho_1^2 \frac{q^2}{q_d^2} + 2\delta R\varrho_1^3 \frac{q^3}{q_d^3}$, with $q_0 = 60\mu C$, we get $M_{1_0} = 8000\Omega$, $M_{2_0} = 12000\Omega$ and $\delta M_0 = M_{1_0} + \varrho M_{2_0} = 26000\Omega$. The initial voltage are: $V_{1_0} = 2V$ and $V_{2_0} = 0V$. For any value of X_0, the initial memristance of the memristor fuse $\mathscr{M}_f(X_0)$ is obtained directly from equation (5.136) and the initial condition Y_0 is obtained from equation (5.131) as:

$$Y_0 = \frac{\tau_c}{q_d}\frac{(V_{1_0} - V_{2_0})}{\delta R\mathscr{M}_f(X_0)}.$$

Figure 5.37 shows the phase portraits result of the analytical solution with memristor fuse in the coupling mode. In comparison to Fig. 5.27, the result in Fig. 5.37 showed a desirable symmetry which is very promising in our application owing to its bidirectional nature.

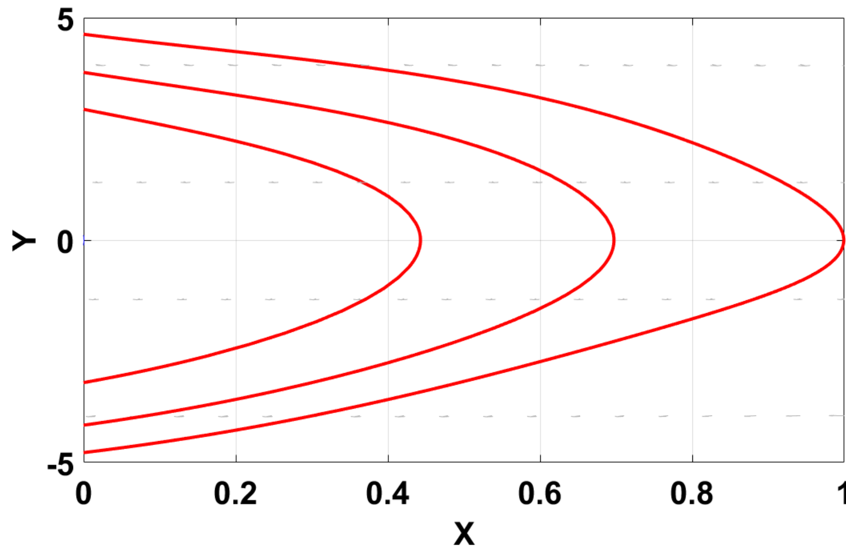

Figure 5.37: Phase portraits of the analytical solution with memristor fuse in the coupling mode. The results showed a rather better symmetry than a standalone memristor.

5.10/ Conclusion

A brief background of CNN is introduced and we outlined the three possible formations of the memristor based 2D cellular nonlinear or neural networks. The conductivity of a memristor device resembles that of a chemical synapse, hence we consider the first scenario where memristor is used in the cells neighborhood connections due to its connection flexibility and resemblance in

using memristors as synaptic links between real neurons.

Here we considered the part of the network consisting of two cells coupled together by a memristor, thus allowing to study, qualitatively and quantitatively, the interaction of the memristor within the network. The behaviour of the memristor is investigated bidirectionally by allowing one cell to act as the master while the other one acts as slave and then conversely. It is shown analytically and from the circuit point of view that the conductivity of a memristor device depends on the polarity of the applied input signal, thus affecting the mobility of its charge carrier and is due to the intrinsic nature of the device. It is inevitable nature of a memristor device irrespective of its device technology. Hence, memristive effect changes according to the connection mode and the amount of current flowing through it, showing that memristor is not bilateral circuit element as verified by our circuits.

Memrisor fuse is promising as memristive grid network in CNN neighborhood connection. We introduced the concept of memristor fuse in the coupling mode along with a theoretical foundation useful for its analytical study. This particular study is ongoing and it will soon be submitted to a journal for publication.

6

MEMRISTOR COUPLED 2 CELLS WITH CUBIC RESISTANCE

Memristor based 2D CNN is introduced whereby each elemental cell corresponds to Fitzhugh Nagumo cell applicable to signal processing. Similarly, the analysis starts with the system of two cells and then the generalized 2D network reliable to process any number of cells.

6.1/ NONLINEAR RESISTOR R_{NL} IN THE CELL UNIT

Figure 6.1 shows the two-dimensional cellular nonlinear network using memristor in the neighborhood connections. Each of the cell unit consists of one linear capacitor C and one nonlinear resistor R_{NL}, with an adjacent coupling made of memristor M. Hence, it form $M \times N$ arrays of cells and the potential at each junction at row (m) and column (n) is respectively denoted by $V_{m,n}$. Nonlinear resistance, such as Fitzhugh−Nagumo is used in modeling the R_{NL}. For any junction (say (m,n) for example), the voltage is given by $V_{m,n}$ and the nonlinear current function I_{NL} is given by:

$$I_{NL_{(m,n)}} = f(V_{m,n}) = \frac{V_{m,n}}{R_o} \frac{(V_{m,n} - V_a)(V_{m,n} - V_b)}{V_a V_b}, \tag{6.1}$$

whereas the nonlinear resistance at node (m,n) is $R_{NL_{(V_{m,n})}}$ and is given by:

$$R_{NL_{(V_{m,n})}} = \frac{V_{m,n}}{I_{NL_{(m,n)}}} = \frac{R_o V_a V_b}{(V_{m,n} - V_a)(V_{m,n} - V_b)}, \tag{6.2}$$

and the corresponding potential energy $W(V_{m,n})$ is given by:

$$W(V_{m,n}) = \frac{1}{4}V_{m,n}^4 - \frac{V_a + V_b}{3}V_{m,n}^3 + \frac{V_a V_b}{2}V_{m,n}^2 + \mathscr{A}, \tag{6.3}$$

where $\mathscr{A}$ is a constant of integration. Meanwhile, the parameters V_a and V_b are the roots of the nonlinear resistance R_{NL}, as used previously in Fitzhugh Nagumo model and R_o is the linear approximation of R_{NL}, see Fig. 6.2a. Unlike RC cells where each cell always stabilizes at 0, here the cell can stabilize at a point of lowest potential energy corresponding to $V_n = 0$ and $V_n = V_b$ (see Fig. 6.2b) and these are the two possible equilibrium states. Therefore: 0, V_a and V_b are constant voltages corresponding to the characteristic roots of the cubic function $f(V_n)$ at any nodal potential

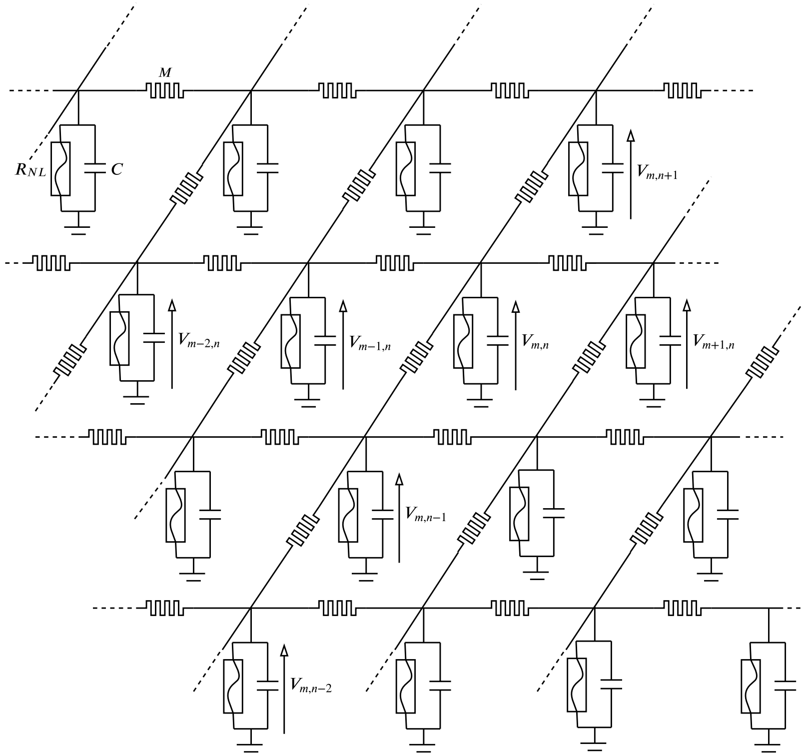

Figure 6.1: Memristor-based 2D CNN – Display of 16 cells with memristors in the coupling mode, that is, adjacent neighbourhood connections.

$V_{m,n}$ under consideration, such that:

$$0 < V_a < V_b.$$

Hence, with V_a being unstable potential state, it implies 0 and V_b are the only two stable potential energy states. It can be seen from Fig. 6.2b, for:

$$\begin{cases} V_b - 2V_a > 0 & \Rightarrow \quad \textit{the cell stabilizes at } V_b. \\ V_b - 2V_a < 0 & \Rightarrow \quad \textit{the cell stabilizes at } 0. \end{cases}$$

Depending on the threshold value of the source signal, each cell stabilizes to one of the two stable roots (i.e 0 or V_b) of its R_{NL} and the stability is determined by the unstable root V_a. Hence, to explore this phenomenon qualitatively and to observe the interaction of memristor in the system, we consider the subset of the network made up of two cells coupled by a memristor (specifically a charge-controlled memristor). An information is launched from one cell (known as the master) to the other cell (known as the slave) via a memristor as demonstrated in Fig. 6.3.

The cells are identical such that $C = C_m = C_s$ as expected in a 2D-network of pixel cells, hence the system evolution is determined by their respective node voltages. The underlined task involves to determine:

- **i.** *the voltage ($V_m(t)$ and $V_s(t)$) evolution*,
- **ii.** *the charge ($q(t)$) evolution – memristor coupling mode by our analytical cubic model $M(q)$*,

with respect to the eight system's control parameters: C, q_0, V_a, V_b, R_o, R_{off}, R_{on} and q_d. Similarly,

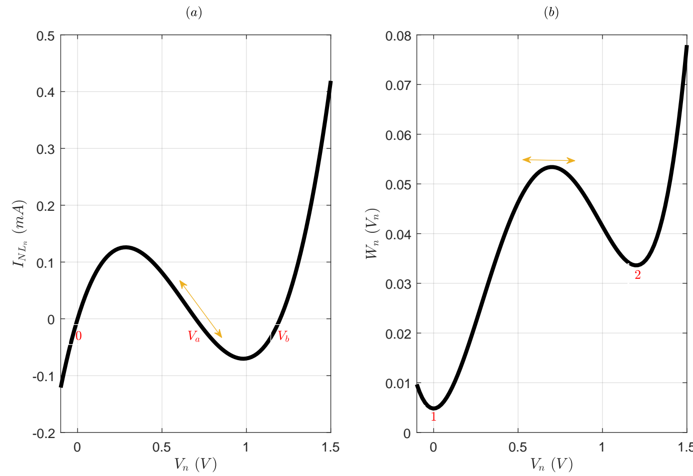

Figure 6.2: Nonlinear resistance response. (a) I-V characteristic. (b) The corresponding potential energy showing the stable equilibrium state at $V_n = 0$ and $V_n = V_b$. $R_0 = 1023\Omega$ and the roots of the nonlinear resistance are $0V$, $V_a = 0.7V$ and $V_b = 1.2$.

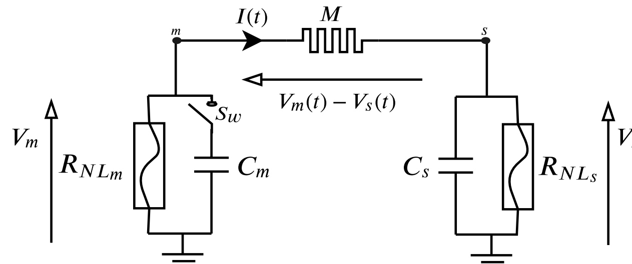

Figure 6.3: Two cells coupled by a memristor. The interaction of the cells via memristor is studied by launching information from one cell (known as the master) to other (known as the slave), whose elements are labeled with subscript letters m and s respectively.

the solution is to be found according to three approaches, namely: Analytical solution, Numerical solution and SPICE simulation. The idea is to observe the significance of the memristor in the design and to find out whether all the three methods would agree with one another perfectly.

6.2/ Analytical study

By closing the switch s_w, then the time evolutions of the master and slave cells are $V_m(t)$ and $V_s(t)$ respectively, and the current $I(t) = \frac{dq}{dt}$ flows through the memristor until $V_m(t) = V_s(t) =$ constant. Then, the application of Kirchhoff's law gives the following system description:

$$\frac{dq}{dt} = -C_m \frac{dV_m(t)}{dt} - I_{NL_m}(t) \,, \tag{6.4}$$

$$\frac{dq}{dt} = C_s \frac{dV_s(t)}{dt} + I_{NL_s}(t) \,, \tag{6.5}$$

$$\frac{dq}{dt} = \frac{V_m(t) - V_s(t)}{M(q)} \,, \tag{6.6}$$

$$\begin{cases} I_{NL_m}(t) = f(V_m(t)) = \dfrac{V_m(t)}{R_{NL,m}} = \dfrac{V_m(t)}{R_o}\dfrac{(V_m(t)-V_a)(V_m(t)-V_b)}{V_aV_b}, \\ R_{NL_m}(t) = \dfrac{V_m(t)}{I_{NL_m}(t)} = \dfrac{R_oV_aV_b}{(V_m(t)-V_a)(V_m(t)-V_b)}, \end{cases} \tag{6.7}$$

$$\begin{cases} I_{NL_s}(t) = f(V_s(t)) = \dfrac{V_s(t)}{R_{NL_s}(t)} = \dfrac{V_s(t)}{R_o}\dfrac{(V_s(t)-V_a)(V_s(t)-V_b)}{V_aV_b}, \\ R_{NL_s}(t) = \dfrac{V_s(t)}{I_{NL_s}(t)} = \dfrac{R_oV_aV_b}{(V_s(t)-V_a)(V_s(t)-V_b)}, \end{cases} \tag{6.8}$$

and $M(q)$ is in first step given by:

$$M(q) = \alpha - \beta_1 q, \qquad 0 < q(t) < q_d, \tag{6.9}$$

and in a second step, it is given by:

$$M(q) = \alpha - \beta_2 q^2 + \gamma q^3, \qquad 0 \le q(t) \le q_d. \tag{6.10}$$

Where:

$\alpha = R_{off}$, parameter of the memristor, giving its resistance when the undoped region occupies all its width w, $\beta_1 = \dfrac{R_{off} - R_{on}}{q_d} = \dfrac{\delta R}{q_d}$, where R_{on} corresponds to the memristor resistance when the doped region occupies all the width D, and q_d is the charge parameter linked to the vacancy mobility in the memristor, $\beta_2 = \dfrac{3\delta R}{q_d^2}$ and $\gamma = \dfrac{2\delta R}{q_d^3}$. Note that in both equations (6.9) and (6.10): $M(q) = R_{off}$ if $q(t) \le 0$ and $M(q) = R_{on}$ if $q(t) \ge q_d$.

Setting $R'_o = R_o.V_a.V_b$ (in $\Omega.V^2$) for the sake of calculations simplicity, then equations (6.4)-(6.6) are, respectively, rewritten as follows:

$$\frac{dq}{dt} = -C\frac{dV_m}{dt} - \frac{V_m(V_m-V_a)(V_m-V_b)}{R'_o}, \tag{6.11}$$

$$\frac{dq}{dt} = C\frac{dV_s}{dt} + \frac{V_s(V_s-V_a)(V_s-V_b)}{R'_o}, \tag{6.12}$$

$$\frac{dq}{dt} = \frac{V_m - V_s}{M(q)}, \tag{6.13}$$

This system of 3 equations is rather to be expressed:

$$\frac{dq}{dt} = \frac{V_m - V_s}{M(q)}, \tag{6.14a}$$

$$\frac{dV_m}{dt} = -\frac{V_m - V_s}{C.M(q)} - \frac{V_m(V_m-V_a)(V_m-V_b)}{R'_oC}, \tag{6.14b}$$

$$\frac{dV_s}{dt} = \frac{V_m - V_s}{C.M(q)} - \frac{V_s(V_s-V_a)(V_s-V_b)}{R'_oC}, \tag{6.14c}$$

The system (q, V_m, V_s) in equations (6.14a)-(6.14c) deserves to be studied in a 6D-phase portrait Poincaré analysis. However, we would like to get, rather and mainly, the behaviour of $q(t)$ versus time t. In fact, it is to show that the initial value q_0 is a fundamental parameter able to dramatically change the time evolution of the system (q, V_m, V_s).

Let us define: $x = \dfrac{V_m - V_s}{2}$ and $y = \dfrac{V_m + V_s}{2}$, respectively differential and common modes of (mas-

ter/slave) pair, such that $V_m = x + y$ and $V_s = y - x$. The initial set of equations (6.14a)-(6.14c) becomes:

$$\begin{aligned} \frac{dq}{dt} &= \frac{2x}{M(q)}, \\ \frac{dx}{dt} + \frac{dy}{dt} &= -\frac{2x}{C.M(q)} - f(x+y), \\ \frac{dy}{dt} - \frac{dx}{dt} &= \frac{2x}{C.M(q)} - f(y-x), \end{aligned}$$

with the cubic function $f(\theta) = \frac{\theta(\theta - a)(\theta - b)}{R'_o C}$, where $a = V_a$ and $b = V_b$. It implies that:

$$\frac{dx}{dt} = -\frac{2x}{CM(q)} - \frac{f(x+y) - f(y-x)}{2}, \tag{6.15a}$$

$$\frac{dy}{dt} = -\frac{f(x+y) + f(y-x)}{2}, \tag{6.15b}$$

$$\frac{dq}{dt} = \frac{2x}{M(q)}. \tag{6.15c}$$

We find that:

$$\begin{aligned} f(x+y) &= \frac{(x+y)(x+y-a)(x+y-b)}{R'_o C} \\ &= \frac{x^3 + y^3 + 3x^2y + 3xy^2 - (a+b)x^2 - (a+b)y^2 - 2(a+b)xy + abx + aby}{R'_o C}, \end{aligned}$$

and

$$\begin{aligned} f(y-x) &= \frac{(y-x)(y-x-a)(y-x-b)}{R'_o C} \\ &= \frac{-x^3 + y^3 + 3x^2y - 3xy^2 - (a+b)y^2 - (a+b)x^2 + 2(a+b)xy + aby - abx}{R'_o C}. \end{aligned}$$

Note that $f(y - x)$ could rather be got from $f(x + y)$ in replacing x by $(-x)$. Furthermore,

$$\frac{f(x+y) + f(y-x)}{2} = \frac{1}{R'_o C}\left[y^3 + 3x^2y - (a+b)y^2 - (a+b)x^2 + aby\right] \text{ (only even powers of } x\text{)},$$

and

$$\frac{f(x+y) - f(y-x)}{2} = \frac{1}{R'_o C}\left[x^3 + 3xy^2 - 2(a+b)xy + abx\right] \text{ (only odd powers of } x\text{)}.$$

Then we get the following set of differential coupled equations:

$$\frac{dq}{dt} = \frac{2x}{M(q)}, \tag{6.16a}$$

$$\frac{dx}{dt} = -\frac{2x}{CM(q)} - \frac{1}{R'_o C}\left[x^3 + 3xy^2 - 2(a+b)xy + abx\right], \tag{6.16b}$$

$$\frac{dy}{dt} = -\frac{1}{R'_o C}\left[y^3 + 3x^2y - (a+b)y^2 - (a+b)x^2 + aby\right]. \tag{6.16c}$$

Equation (6.16c) shows that the dynamics of the common mode is completely managed by the cubic nonlinear resistance, with parameter $R'_o C$, while the memristor only behaves by means of x^2

in the right hand-side of the equation. It is quite normal that only the differential mode takes into account the memristor, as the voltage across it depends on $V_m - V_s$, that is the differential mode.

Focusing first on (6.16c), we remark that the right hand-side corresponds to:

$$\frac{(y^3 - (a+b)y^2 + aby) + x^2(3y - (a+b))}{R_o'C},$$

that is: $f(y) + \dfrac{x^2}{R_o'C}(3y - (a+b))$.

x, differential mode, will tend to zero, starting from $\frac{V_{m_0} - V_{s_0}}{2}$, less than 1 in main conditions. y will too decay to zero, starting from $\frac{V_{m0}+V_{s0}}{2}$ which is not very different from $\frac{V_a+V_b}{3} \simeq \frac{3V_a}{3}$ in main conditions with $V_a \sim \frac{V_b}{2}$.

So, in a first approximation, $x = \alpha e^{-\frac{t}{T_0}}$ with $\alpha = \frac{V_{m0}}{2}$, one can approximate the right hand-side of (6.16c) to keep only:

$$\frac{dy}{dt} = -\frac{1}{R_o'C}\left[y^3 - (a+b)y^2 + \left(3\alpha^2 e^{-\frac{2t}{T_0}} + ab\right)y - (a+b)\alpha^2 e^{-\frac{2t}{T_0}}\right]. \tag{6.17}$$

Figure 6.4 shows the comparison result of equations (6.16c) and (6.17) for both the two possible stability states. The result is obtained for $C = 1\mu F$, $R_o = 10K\Omega$, $T_0 = 5ms$, $V_{m_0} = 1.5V$, $V_{s_0} = 0V$ and $V_b = 1.2V$. Meanwhile $V_a = 0.12V$ and $0.9V$ for Figures 6.4**a** and **b** respectively.

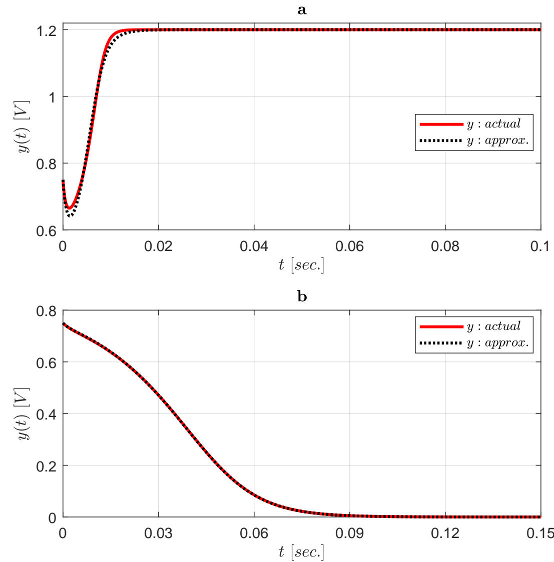

Figure 6.4: Comparison of the evolution of $y(t)$ and its approximation, (**a**) $V_a = 0.12V$ and the steady state at V_b and (**b**) $V_a = 0.9V$ and the steady state at 0.

Then, we can study the remaining set of 2 equations, focusing on the memristor role:

$$\frac{dq}{dt} = \frac{2x}{M(q)},$$
$$\frac{dx}{dt} = -\frac{2x}{CM(q)} - \frac{1}{R_o'C}\left[x^3 + 3xy^2 - 2(a+b)xy + abx\right],$$

Let us remark that:

$$\frac{x^3+3xy^2-2(a+b)xy+abx}{R_o'C} = \frac{x^3-(a+b)x^2+abx}{R_o'C} + \frac{(a+b)x^2-2(a+b)xy+3xy^2}{R_o'C},$$
$$= f(x) + \frac{x}{R_o'C}\left((a+b)x-2(a+b)y+3y^2\right).$$

With still the rough assumption $3y \simeq a+b$, the last term is $\frac{x}{R_o'C}(a+b)(x-y)$, which is proportional to V_s and then neglectible for the first part of the system dynamic. We get then the 2 equations set:

$$\begin{cases} \frac{dq}{dt} = \frac{2x}{M(q)}, \\ \frac{dx}{dt} = \frac{-2x}{CM(q)} - f(x) = \frac{-2x}{CM(q)} - \frac{x(x-V_a)(x-V_b)}{R_o'V_aV_b}, \end{cases} \tag{6.18}$$

showing the competition between the role of Fitzhugh cubic resistance and the one of the memristor in the differential mode dynamics.

Figure 6.5 show the time evolution of the system $V_m(t)$, $V_s(t)$, the differential mode (x) and the common mode (y). The results are obtained using $R_o = 10K\Omega$, $C = 1\mu F$, $V_{m_0} = 1.5V$, $V_{s_0} = 0V$, $V_b = 1.2V$ and $V_a = 0.12V$. The system always stabilizes at 0 or V_b, that is, at the time when $V_m(t) = V_s(t)$ and the differential mode is always 0. The common mode always stabilizes at the system steady state 0 or V_b which is determined by V_a. Figure 6.6 shows the variation of V_a and its effect on the system steady state. The role of V_a is analyzed extensively in the following section 6.3.

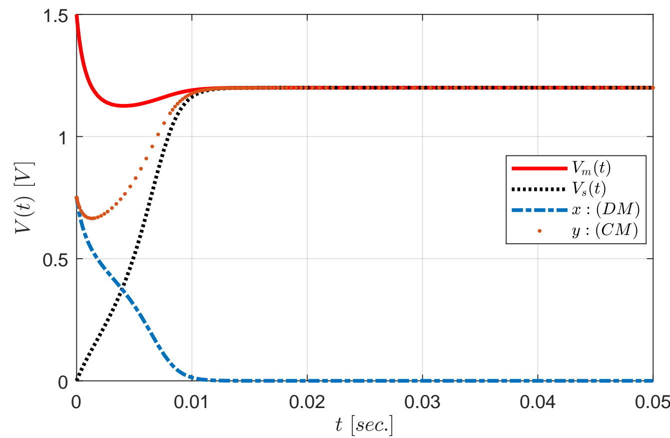

Figure 6.5: System evolution $V_m(t)$, $V_s(t)$, x and y. $R_o = 10K\Omega$, $C = 1\mu F$, $V_{m_0} = 1.5V$, $V_{s_0} = 0V$, $V_b = 1.2V$ and $V_a = 0.12V$.

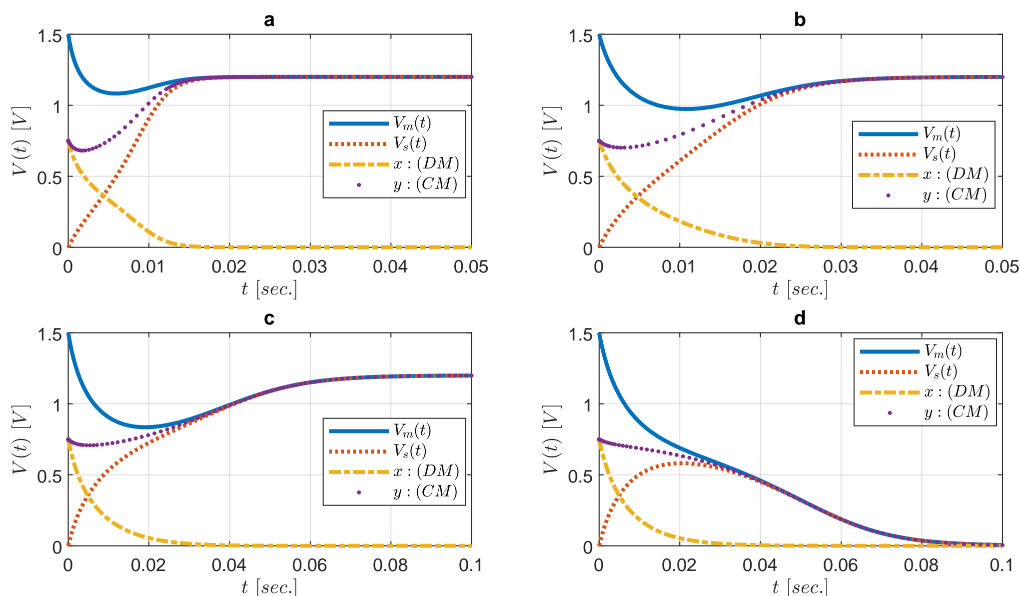

Figure 6.6: System evolution showing the variation of V_a. $R_o = 10K\Omega$, $C = 1\mu F$, $V_{m_0} = 1.5V$, $V_{s_0} = 0V$, $V_b = 1.2V$, (**a**) $V_a = 0.2V$, (**b**) $V_a = 0.4V$, (**c**) $V_a = 0.6V$ and (**d**) $V_a = 0.8V$.

6.3/ NUMERICAL SOLUTION – WITH MATLAB

Here, equations (6.11)-(6.13) are directly simulated in Matlab using its built-in function (ODE solver), such as ODE45. The result is obtained for different values of V_a and V_b with respect to different initial conditions of V_m and V_s, known as V_{m_0} and V_{s_0} respectively, as given in Fig. 6.7 and the subsequent figures.

6.3.1/ CORRELATING V_m, V_s, V_a AND V_b

Recall that the master cell (cell m) is at higher potential than the slave one (cell s), therefore, the dynamics and saturation of the system are preferentially towards cell s. With V_a being unstable potential whose value is decided by the consequence effect of V_m or V_s, so that the system potential field can be chosen such as:

$$0 \leq V_s < V_a < V_b \leq V_m, \tag{6.19}$$

with the assumption $V_s \to 0$ while 0 and V_b are the only two stable states. However, equation (6.19) is not absolutely compulsory because V_m and V_s can be both $> V_a$ or $< V_a$. Additionally, it is possible to have $V_m \leq V_b$ but this will not have significant effect on the stability of the system due to the fact that even if V_m is higher or lower than V_b, the system will eventually stabilize at 0 or V_b depending upon the value of V_a. Thus, solving the model equations (6.11)-(6.13) numerically, it shows only two stable states 0 or V_b, even if $V_a < V_m < V_b$ (or $> V_b$).

Considering V_a to take fractional value of V_b, for example $V_a = \Upsilon V_b$ such that: $0 < \Upsilon < 1$ and setting $V_{s_0} = 0$, then three possible values of V_{m_0} are considered, viz:

- $V_{m_0} = V_b$, given by the first column of Fig. 6.7 i.e **a1**-**a7**.
- $V_{m_0} < V_b$, given by the second column of Fig. 6.7 i.e **b1**-**b7**.

- $V_{m_0} > V_b$, given by the third column of Fig. 6.7 i.e **c1**-**c7**.

Figure 6.7 shows the results for $\Upsilon = [0.25,\ 0.45,\ 0.49,\ 0.5,\ 0.51,\ 0.55$ and $0.75]$ and it shows consistency except in the vicinity where:

$$\Upsilon = 0.5 \quad \text{i.e} \ \ V_a = \frac{V_b}{2}.$$

Recall that if $V_b - 2V_a > 0$ (or $V_b - 2V_a < 0$) the system stabilizes at V_b (or 0) respectively. However, $\Upsilon = 0.5$ implies that $V_b - 2V_a = 0$. In this case, the system stability state depends on the values of parameters, for example, the memristance value ($R_{on} \sim R_{off}$), V_m, V_s, q_0 and R_0. Therefore, the stability is indefinite and could be at 0 or V_b as summarized below:

i. *Value of* R_0: The results in Fig. 6.7 were obtained for $R_0 = 10K\Omega$ and the results take into account the values of V_a around $\frac{V_b}{2}$, i.e $\Upsilon = 0.49$, 0.5 and 0.51 for Figs. 6.7**a3**-**c3**, **a4**-**c4** and **a5**-**c5** respectively, in order to observe what will likely be the response if the value of V_a is about to give $V_b - 2V_a = 0$ (i.e half the value of V_b). However, using $R_0 = 2883\Omega$, the evolution and stability of Figs. 6.7**b2** and **a4** at $V_a = \frac{V_b}{2}$ become different, see also Figs. 6.8**b2** and **a4**. Notice that only R_0 is changed. Hence, the only difference between Fig. 6.7 and 6.8 is the value of R_0. Table 6.1 shows the difference $V_b - 2V_a$ when V_a varies in $[0, V_b]$, allowing for easy study of Fig. 6.7.

N°/Line.	Υ	(**a1**-**a7**) $V_b - 2V_a\ (V)$	(**b1**-**b7**) $V_b - 2V_a\ (V)$	**c1**-**c7** $V_b - 2V_a\ (V)$
1	0.25	0.5	0.65	0.5
2	0.45	0.1	0.13	0.1
3	0.49	0.02	0.026	0.02
4	0.5	0	0	0
5	0.51	0.02	-0.026	-0.02
6	0.55	-0.1	-0.13	-0.1
7	0.75	-0.5	-0.65	-0.5

Table 6.1: Table of values of Fig. 6.7 for the difference $V_b - 2V_a$ as a deterministic factor of system stability. $V_{s_0} = 0V$ and $V_a = \Upsilon V_b$. (**a1**-**a7**) $V_b = 1V$ and $V_{m_0} = 1V$, (**b1**-**b7**) $V_b = 1.3V$ and $V_{m_0} = 1V$ and (**c1**-**c7**) $V_b = 1V$ and $V_{m_0} = 1.3V$.

ii. *Value of* V_{m_0} *and* V_{s_0}: Changing the values of the cells initial conditions (i.e V_{m_0} and V_{s_0}) can cause the cells to change their stable states especially when V_a is around $\frac{V_b}{2}$. Compare Figs. 6.7**a1**-**a7** and 6.7**c1**-**c7** where only V_{m_0} is changed, i.e $V_{m_0} = 1V$ and $V_{m_0} = 1.3V$ respectively. It is further observed that the trend of the system stability is the similar even if both the initial conditions of V_{m_0} and V_{s_0} are non zero.

iii. Figure 6.9 shows the effect of changing initial condition of the memristor on the system evolution and stability. It also takes into account the variations of R_0. The initial memristance of the memristor is given by the initial charge q_0. Four different initial charges are considered as: $q_{0_1} = 20\mu C$, $q_{0_2} = 40\mu C$, $q_{0_3} = 60\mu C$ and $q_{0_4} = 80\mu C$, as indicated respectively, by the subscripts numbers **1**-**4** in Fig. 6.9A, B and C. Notice that only one parameter is varied at a time. Figure 6.9A: $R_0 = 1023\Omega$ while q_0 varied, Fig. 6.9B: $R_0 = 2833\Omega$ while q_0 varies and Fig. 6.9C: $R_0 = 10K\Omega$ while q_0 varies. In each case, $V_a = 0.7V$, $V_b = 1.3V$, $V_{m_0} = 1.5V$ and

$V_{s_0} = 0V$. Even though V_a plays significant role on the system steady state, the results show that other parameters (e.g R_o and q_0) affect the dynamics and steady state of the system.

iv. The results of Fig. 6.10 are for values of V_m and V_b compatible to SPICE results, thus it allows for easy comparison of the three methods. The result is obtained for $R_0 = 2833\Omega$, $V_b = 1.5V$ and $V_{m_0} = 2V$. Similarly, V_a varies according to $\Upsilon = [0.25,\ 0.45,\ 0.49,\ 0.5,\ 0.51,\ 0.55,\ 0.75,\ 0.9]$ with the corresponding results given by Figs. 6.10**a**, **b**, **c**, **d**, **e**, **f**, **g** and **h**, respectively. Furthermore, the difference $V_b - 2V_a$ is calculated and tabulated in Table 6.2.

Figure 6.10	**a**	**b**	**c**	**d**	**e**	**f**	**g**	**h**
Υ	0.25	0.45	0.49	0.5	0.51	0.55	0.75	0.9
$V_b - 2V_a$ (V)	0.75	0.15	0.03	0	-0.03	-0.15	-0.75	-1.20

Table 6.2: Table of $V_b - 2V_a$ for Fig. 6.10. $V_{s_0} = 0V$, $V_a = \Upsilon V_b$, $V_b = 1.5V$ and $V_{m_0} = 2V$.

v. The results of Figs. 6.7-6.10 show that the parameters V_a, R_0 and q_0 have significant effect on the system evolution and the steady state. The inflexion nature of the curves is the manifestation of the nonlinear resistance and it is due to the fact that substantial amount of voltage is required to activate all of its three branches.

Figures 6.7-6.10 show that the differential mode (DM) and the common mode (CM) are clearly seen on all these cases, showing that the dynamics of these 2 modes can be effectively studied separately as done in section 6.2. As illustrated in Fig. 6.7, initially $V_m(t)$ and $V_s(t)$ evolve in differential mode (DM) and then the combined evolution in common mode (CM). We observed similar evolution of $V_m(t)$ and $V_s(t)$ in Figs. 6.8-6.10.

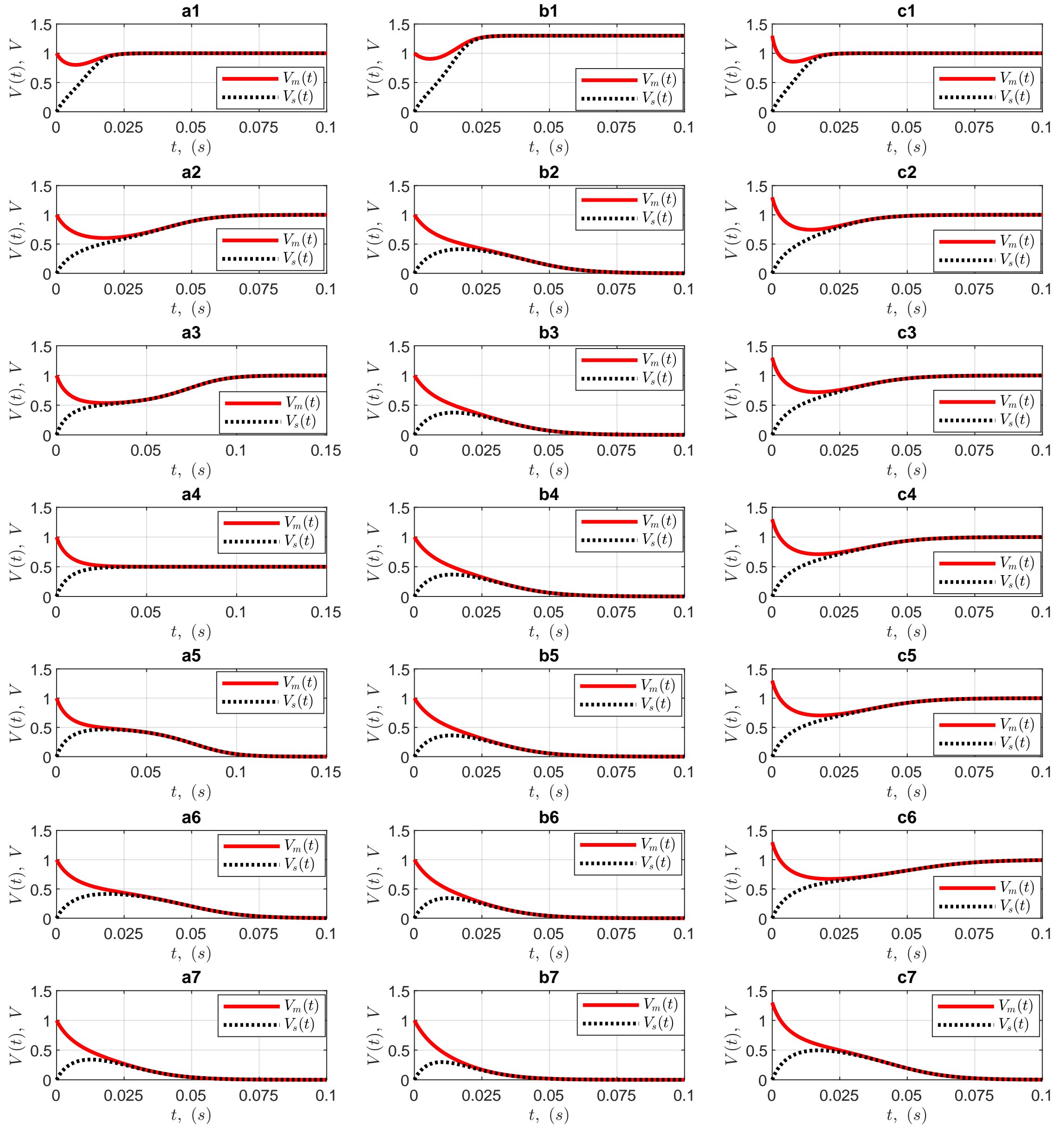

Figure 6.7: Results for $R_0 = 10K\Omega$, $q_0 = 0.3q_d$, $V_s = 0V$ and $\Upsilon = [0.25,\ 0.45,\ 0.49,\ 0.5,\ 0.51,\ 0.55$ and $0.75]$ respectively indicated by the subscripts (**1-7**) down across the rows, showing the variations of V_a for three different values of V_m and V_b. The values of the other parameters are $R_{on} = 100\Omega$, $R_{off} = 16K\Omega$ and $C_m = C_s = 1\mu F$. (**a1**-**a7**) < First column > is for $V_m = V_b = 1V$ and V_a varies down across the column. (**b1**-**b7**) < Second column > is for $V_m < V_b$, here $V_m = 1V$, $V_b = 1.3V$. (**c1**-**c7**) < Third column > is for $V_m > V_b$ i.e $V_m = 1.3V$ and $V_b = 1V$. Down across the raw of each column, is the variation of V_a with respect to V_b according to Υ. With the exception of the fourth row (**a4**-**c4**) where $V_a = \frac{V_b}{2}$ and its vicinity, the results show that for $V_a < \frac{V_b}{2}$ the system stabilizes at V_b and for $V_a > \frac{V_b}{2}$ the system stabilizes at zero 0. However, for $V_a = \frac{V_b}{2}$ the values of parameters [i.e V_m, V_s, R_0, q_0, V_a, V_b and the memristive effect (R_{off} and R_{on})] decides the stability state and it is always 0 or V_b. The effect of changing parameters values on the system stability state can be clearly seen across the columns (**a4**-**c4**) where $V_a = \frac{V_b}{2}$. Note that figure (**a4**) can stabilize at 0 or V_b simply by changing the values of q_0, V_m or R_0.

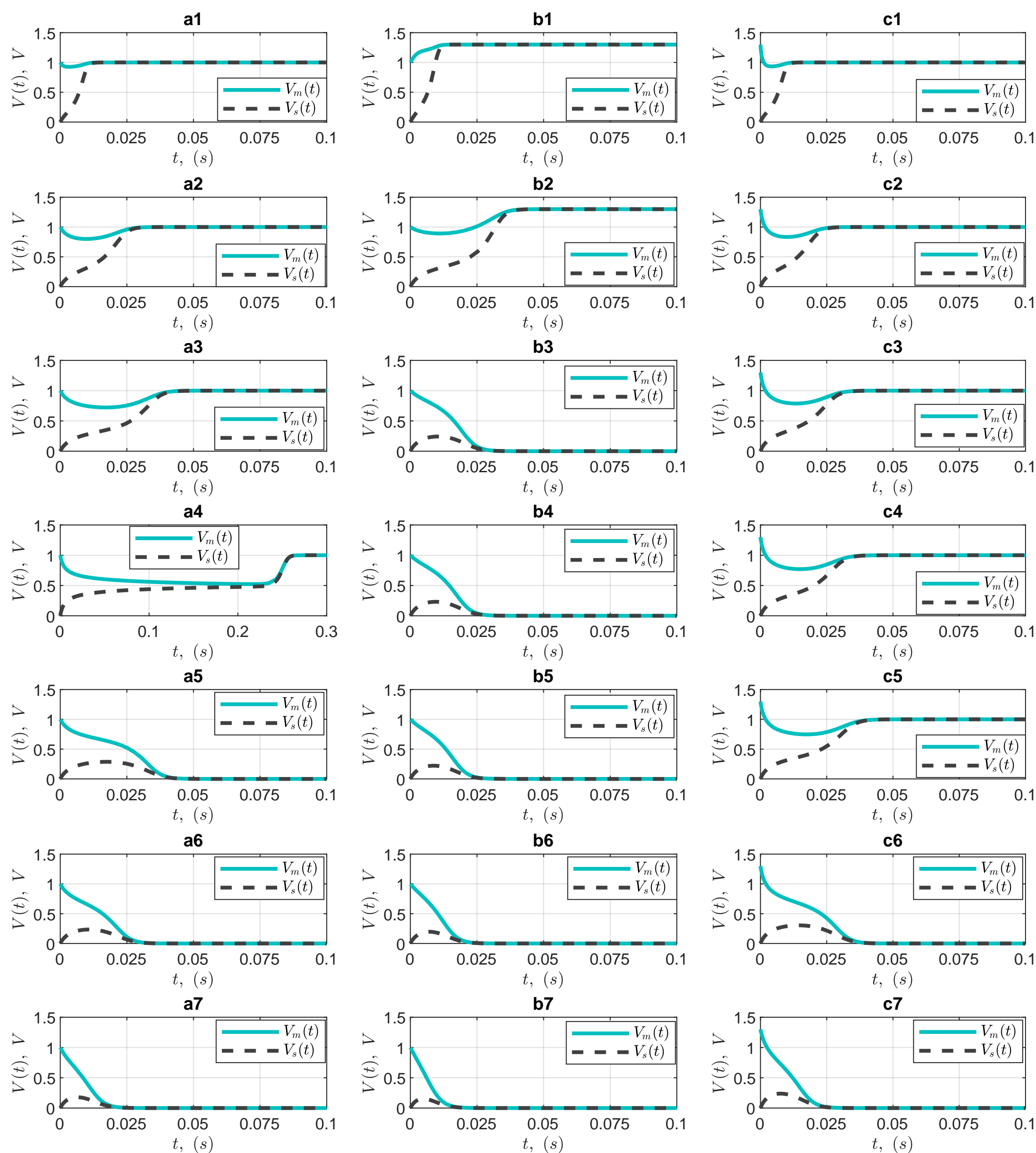

Figure 6.8: Results for $R_0 = 2833\Omega$, $\Upsilon = [0.25,\ 0.45,\ 0.49,\ 0.5,\ 0.51,\ 0.55,\ 0.75]$ and $V_s = 0V$. (**a1**-**a7**) $V_{m_0} = V_b = 1V$. (**b1**-**b7**) $V_{m_0} < V_b$ i.e $V_{m_0} = 1V$ and $V_b = 1.3V$. (**c1**-**c7**) $V_{m_0} > V_b$ i.e $V_{m_0} = 1.3V$ and $V_b = 1V$. Down across the rows is the variation of V_a within $[0,\ V_b]$. Here, the values of parameters are similar to the ones in Fig. 6.7 with only the change in the value of R_0. It shows different evolution and stability for Figs. **b2** and **a4**.

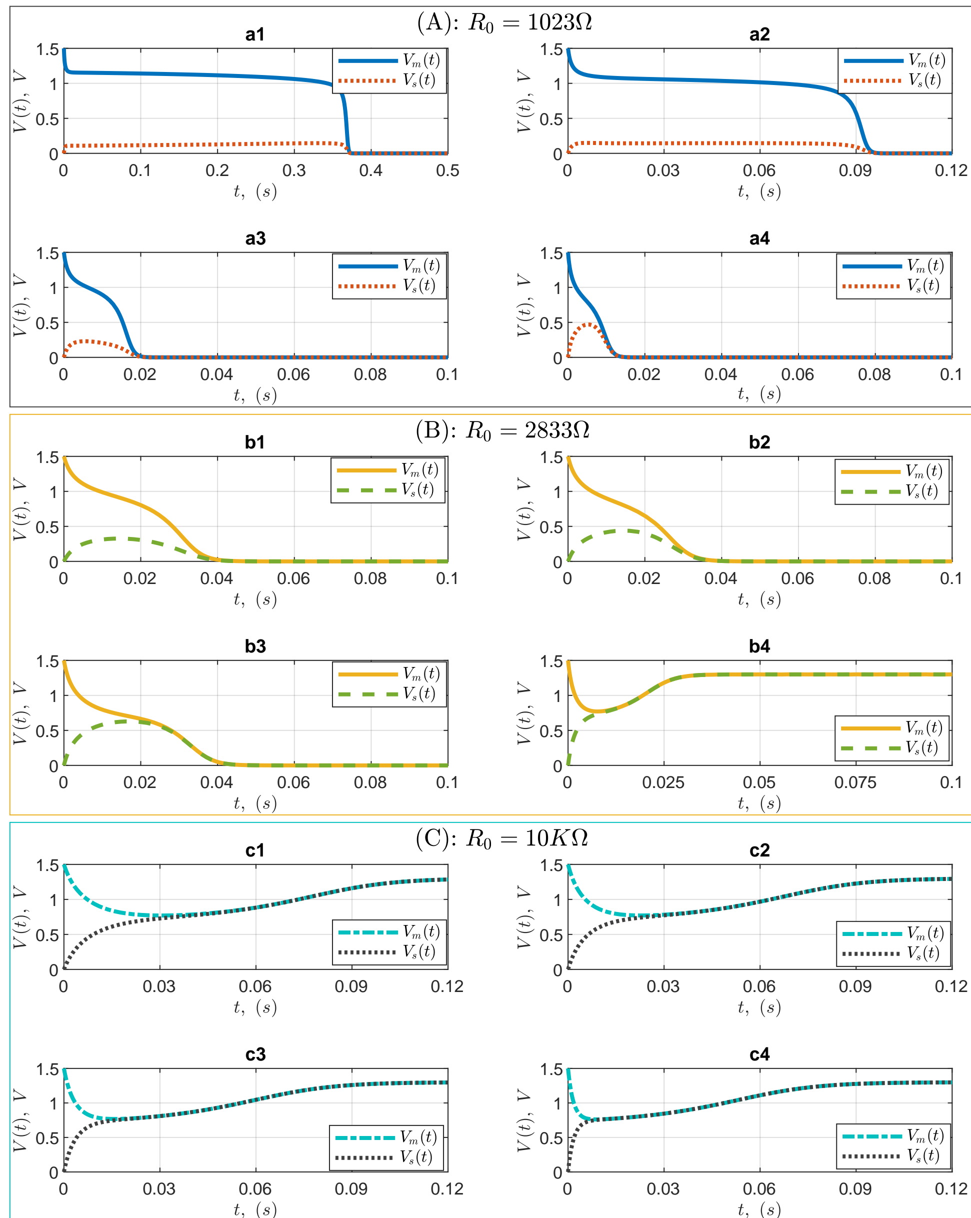

Figure 6.9: Effect of initial memristance given by the initial charge q_0 on the system evolution and the steady state. Four different initial charges are considered as: $q_{0_1} = 20\mu C$, $q_{0_2} = 40\mu C$, $q_{0_3} = 60\mu C$ and $q_{0_4} = 80\mu C$, as indicated respectively by the subscripts numbers **1**-**4** in figures **a**, **b** and **c**. In each case, $V_a = 0.7V$, $V_b = 1.3V$, $V_{m_0} = 1.5V$ and $V_{s_0} = 0V$. (A) $R_0 = 1023\Omega$, (B) $R_0 = 2833\Omega$ and (C) $R_0 = 10K\Omega$. It shows that values of q_0 and R_0 have an effect on the evolution and steady state of the system.

6.4/ SPICE SIMULATION

The SPICE component of R_{NL} is needed in order to simulate the circuit of Fig. 6.3 in a SPICE circuit simulator (for example PSPICE, LTSPICE etc). The schematic representation of R_{NL} is given in Fig. 6.11, having its current-voltage relationship resembling the analytical cubic function $f(V_n)$. Thus, the I_{NL_n}-V_n plane have three distinct slopes each defined by the inverse of its branch resistance. The activation of the respective branches is achieved by the diodes D_1, D_2 and D_3, however monitored by the values of the resistances R_1-R_5 in conjunction with V_n.

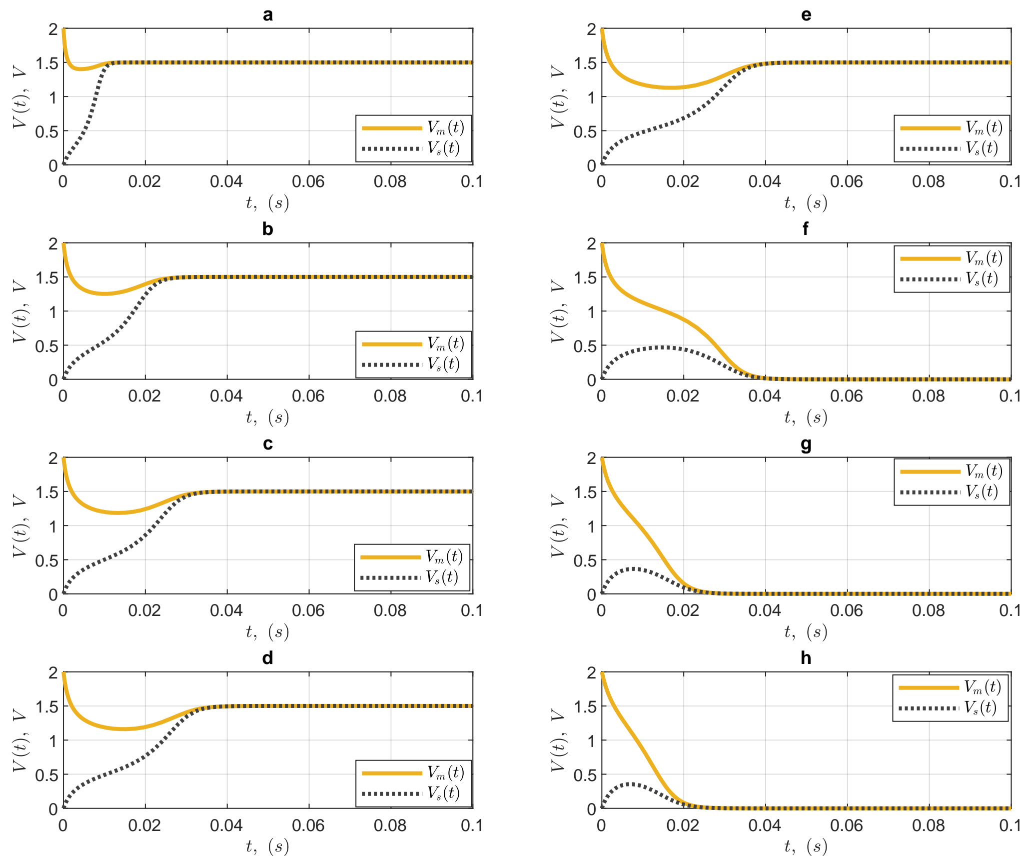

Figure 6.10: Results obtained for parameters values comparable to SPICE showing the variations of $V_a \in [0, V_b]$. $R_0 = 2833\Omega$, $V_s = 0V$ and $\Upsilon = [0.25,\ 0.45,\ 0.49,\ 0.5,\ 0.51,\ 0.55,\ 0.75,\ 0.9]$ shown respectively by figures **a**, **b**, **c**, **d**, **e**, **f**, **g** and **h**. These results are based on reasonable values of parameters that can easily be compared with the one in SPICE simulations. For example, $V_b = 1.5$ is chosen to take into account threshold value of the diodes D_2 and D_3 (see Fig. 6.11), meanwhile $V_m = 2V$ is to ensure enough bias of the equivalent R_{NL}.

The idea is to create the equivalent two terminal R_{NL} component in SPICE as shown in Fig. 6.11 (right), representing the exact circuit functionality as Fig. 6.11 (left). To do this, the nodes are labeled accordingly as shown in Fig. 6.11. The model of THAT4301 operational amplifier is used in the OpAmp block. Default model of silicon diode is used for D_1, D_2 and D_3. However, other models of diode can be used as well, an example of such models is given in the commented lines of Table B.1 (Appendix B).

Following the SPICE directives, the complete netlist file required for creating the R_{NL} component is given in Table B.1 (Appendix B). The THAT4301 SUBCIRCUIT block is called into the main R_{NL} SUBCIRCUIT and the symbolic two-terminals representation of the generated R_{NL} SPICE component is shown in Fig. 6.11 (right).

6.4.1/ R_{NL} CIRCUIT SCHEMATIC DESCRIPTION

From Fig. 6.11, V_n is the applied voltage at node n which gives rise to the flow of the nonlinear current response I_{NL_n} through the block. Initially, V_n is small and I_{NL_n} varies linearly with respect to V_n, therefore only the first branch is active having a constant resistance designated as R_0 with

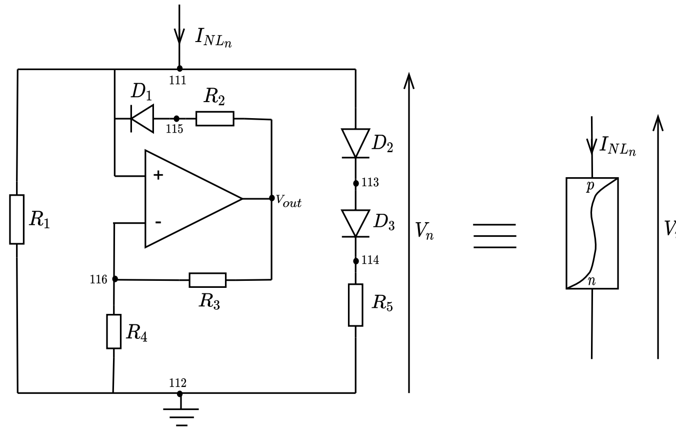

Figure 6.11: Nonlinear resistance circuit and its equivalent SPICE component. Nonlinear resistance circuit schematic representation (left) and the created two-terminals SPICE component of the onlinear resistance (right).

a positive rising slope $\left(\frac{1}{R_1}\right)$ in the I_{NL_n} versus V_n plane. I_{NL_n} will continue to flow through the first branch until the threshold value of D_1 is reached and then the combined threshold value of D_2 and D_3 which activate the second and third branches respectively.

$\therefore\ V_{116} = V_n$, with $I_- = I_+ = 0$ implies that R_3 and R_4 are serially connected. The current through R_4 is:

$$I_{R_4} = \frac{V_{116}}{R_4} = \frac{V_n}{R_4} = I_{R_3}.$$

The voltage drops across R_3 is:

$$R_3 \times \frac{V_n}{R_4},$$

thereby making the potential at node out (i.e V_{out} in Fig. 6.11a) to be:

$$V_{out} = R_3 \frac{V_n}{R_4} + V_n = \left(1 + \frac{R_3}{R_4}\right) V_n. \tag{6.20}$$

For whatever values of R_3 and R_4, it always gives:

$$\left(1 + \frac{R_3}{R_4}\right) > 1.$$

$$\Rightarrow \quad V_{out} > V_n\ , \quad \text{see Fig. 6.12b.}$$

The resistances R_2, R_3 and R_4 are chosen so that:

$$R_3 > R_4 > R_2.$$

As V_n increases and reaches the threshold voltage of the diode D_1, then D_1 becomes active, hence the second branch begins to be conductive and the current flowing through R_2 becomes more significant than the one flowing though R_3 and R_4 due to the current tendency to flow from higher to a lower potential level, hence, it flows reversibly. This shows that the second branch implies a negative resistor which gives rise to the negative slope in the I_{NL_n}-V_n plane.
The condition for this happening can be seen from the relationship between V_{out} and V_n in eq.

(6.20) , thus:

$$V_{out} - V_n > V_{th_{D_1}} \Rightarrow V_n > \frac{R_4}{R_3} V_{th_{D_1}}. \tag{6.21}$$

Equation (6.21) gives the necessary condition required for the activation of the second branch. Therefore, the voltage drops across R_2 is:

$$V_{R_2} = V_n - V_{out} = -\frac{R_3}{R_4} V_n,$$

and the current flowing through R_2 is:

$$I_{R_2} = \frac{V_{R_2}}{R_2} = -\frac{R_3}{R_4\ R_2} V_n.$$

Hence, the second branch forms a dipole that imposes a negative slope in the I_{NL_n} versus V_n plane with a magnitude: $-\frac{R_4\ R_2}{R_3}$.

As V_n increases and becomes higher than the combined threshold voltage of the diodes D_2 and D_3, then the third branch is activated and almost whole of I_{NL_n} flows through R_5 owing to its lowest resistance path. This gives rise to the positive slope in the I_{NL_n}-V_n plane with a value of $\frac{1}{R_5}$.

For example, the schematic is reproduced in Fig. 6.12a with the resistance values defined as:

$$R_1 = 6.8K\Omega,\ R_2 = 2K\Omega,\ R_3 = 7.2K\Omega,\ R_4 = 6.8K\Omega \text{ and } R_5 = 1K\Omega.$$

Meanwhile the complete SPICE circuit analysis is given by Figs. 6.12**b**, **c** and **d**, with results conformed to the outlined description. According to equation (6.20) and for any applied voltage V_n to R_{NL_n}, the magnitude of V_{out} (Fig. 6.12) is determined by the factor $(1 + r_{34})$, where $r_{34} = \frac{R_3}{R_4}$ is the resistance ratio. Note that V_{out} is the voltage at the output node of the operational amplifier. Knowing that $r_{34} \neq 0$, then V_{out} is regulated by the value of r_{34}. Using the above listed values of R_3 and R_4, then $r_{34} = 1.0588$ to four decimals places. For an input voltage $V_{in} = 2V$, it is calculated to give:

$$\begin{aligned} V_{out} &= (1 + r_{34})V_{in} \\ &= 4.1176\ V. \end{aligned}$$

This result is the same as the SPICE simulation result shown in Fig. 6.12**b** i.e $V_{out} = 4.14V$.

Furthermore, the current flowing through each branch can be visualized separately. Figure 6.12**c** shows the branch currents of the R_{NL} and the corresponding DC sweep of the applied input voltage V_{in} in Fig. 6.12**d**, presenting the flowing current in each branch (and I_{NL} as a whole) with respect to the applied input voltage V_{in}. The currents through the first, second and third branches are I_x, I_y and I_z respectively, thus:

$$I_{NL} = I_x + I_y + I_z.$$

The magnitude of the current flowing in each branch with respect to time is shown in Fig. 6.12**c** where the current in the first branch ($I_x \approx 298\mu A$) is small and positive, in the second branch the current ($I_y \approx -730\mu A$) is negative and in the third branch the current ($I_z \approx 710\mu A$) is positive and high, while $I_{nl} \approx 270\mu A$. Moreover, these currents can be obtained by handy calculations as

follows:

$$I_x = \frac{V_{in}}{R_1} = \frac{2}{6.8} \times 10^{-3} = 294\mu A,$$
$$I_y = \frac{V_{in} + V_{th_{D_1}} - V_{out}}{R_2} = \frac{2 + 0.7 - 4.1176}{2} \times 10^{-3} = -708\mu A,$$
$$I_z = \frac{V_{in} - V_{th_{D_2}} - V_{th_{D_3}}}{R_5} = \frac{2 - 0.6 - 0.6}{1} \times 10^{-3} = 800\mu A.$$

These calculated values are the same with the ones in Fig. 6.12 obtained by SPICE simulation. However, the slight difference is due to the threshold value V_{th} of diode which has typical value in the range $[0.6 \sim 0.7V]$ for silicon material. The magnitude of I_{NL} flowing is obtained to be:

$$I_{NL} = \left(\frac{1}{R_1} + \frac{1}{R_5} - \frac{R_3}{R_2\ R_4}\right) V_n + \left(\frac{1}{R_2} - \frac{2}{R_5}\right) V_{th_D}. \tag{6.22}$$

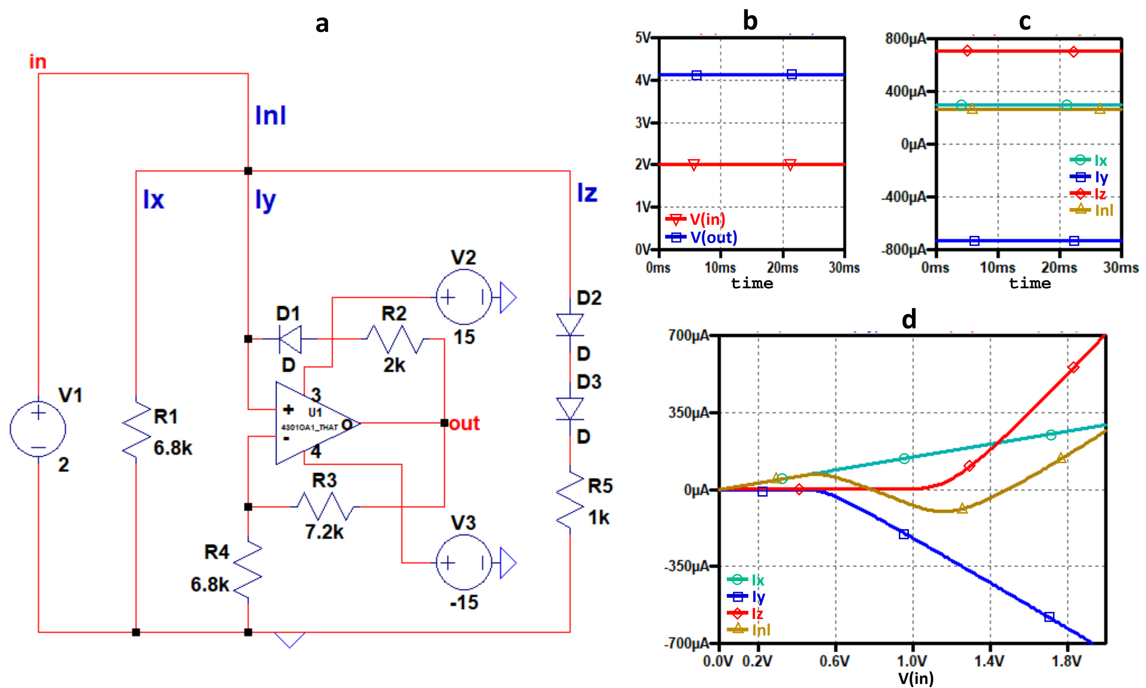

Figure 6.12: Complete circuit analysis of the SPICE R_{NL} component. (**a**) Circuit schematic: $V_{in} = 2V$, $R_1 = 6.8K\Omega$, $R_2 = 2K\Omega$, $R_3 = 7.2K\Omega$, $R_4 = 6.8K\Omega$, $R_5 = 1K\Omega$ and model of THAT4301 OpAmp. (**b**)Voltage V_{in} and V_{out} transient and it shows that $V_{out} > V_{in}$ confirming equation (6.20). This difference in potential forces the current flowing through R_2 to flow negatively. (**c**) Current flowing through the R_{NL}. First branch: I_x is small and positive. Second branch: I_y is negative. Third branch: I_z is high and positive. (**d**) DC sweep of V_{in} for Fig. c. See also Fig. 6.13.

However, to understand Fig. 6.12**d** vividly, it is reproduced in Fig. 6.13 using the SPICE data, hence the results become more descriptive. Figure 6.13a, b, c and d respectively, show the currents I_x, I_y, I_z and I_{NL} (sum of I_x, I_y and I_z).

The three vertical dotted lines mark the activation trends of the three branches, respectively, initiated at a potential labeled as A, B and C. The potentials at these points refer to the threshold values required for the activation of the R_{NL} branches. It shows that, while V_{in} is small, current I_x flows through the resistor R_1 in the first branch, but I_y and I_z are zero until a certain voltage has reached a necessary value required to activate the diode D_1 in the second branch and the diodes

D_2 and D_3 in the third branch. Hence, the second and third branches are not active initially for a small voltage. The current in the second branch I_y is completely negative. It departs from zero level at a voltage of about $0.6V$ corresponding to the threshold value of diode D_1. Then, I_y versus V_{in} falls with a fairly constant negative slope until the combined threshold voltage of D_2 and D_3 is reached at point C of about $1.2V$. Then, the third branch becomes activated, and more current I_z flows because the voltage is high and R_5 is the least resistance. The corresponding nonlinear cubic function (Fig. 6.13d) gives the combined response of the three branches as demarcated by three vertical dotted lines.

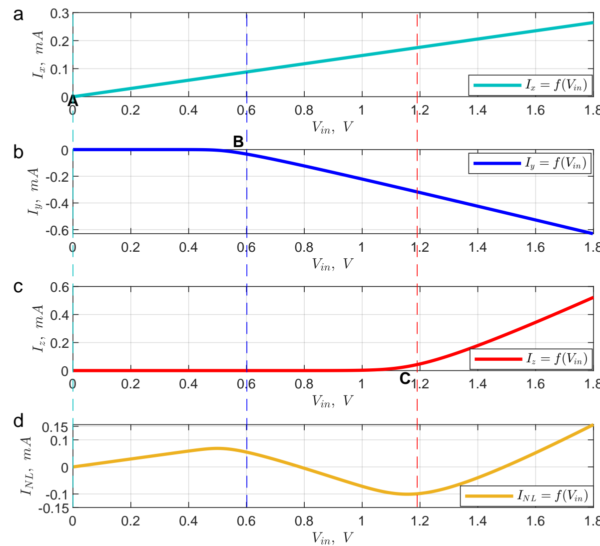

Figure 6.13: Branch currents responses visualization of the R_{NL} circuit schematic. At point A, V_A is the potential when the first branch becomes active. Then, V_{in} increases and reaches the threshold value of diode D_1 at point B (i.e $V_B = 0.6V$), thus activates the second branch. When V_{in} becomes high enough, the combined threshold of diodes D_2 and D_3 is reached at point C (i.e $V_C = 1.2V$) and the third branch is activated. These systematic approaches always manifest itself in the nonlinear resistance response.

6.4.2/ VERIFICATION OF THE R_{NL} SPICE COMPONENT

The created two terminals SPICE component symbol of the R_{NL} is already shown in Fig. 6.11 (right), where the letters p and n refer to higher and lower potential terminals respectively. Using a $2V$ input voltage, the complete circuit analysis of the R_{NL} response is given in Figs. 6.12 and 6.13, and it shows the desired circuit functionality. However, any change in the resistance values has significant effect on the evolution of the cubic function, for example the values of V_a and V_b. This section is to verify the created R_{NL} component before implementing it in the 2D CNN simulation and to observe some other possible factors that are likely to be taken into consideration. The verification test entails using arbitrary values of resistors R_1-R_5 in three steps, namely: small, medium and high values in order to observe the effect of the change in the resistances R_1-R_5 on the characteristics roots V_a and V_b.

1. **Test 1**: This is to observe the functionality of the created R_{NL} component from its cubic response. This test considers Low values of the resistors R_1-R_5 as $R_1 = 1K\Omega$, $R_2 = 2K\Omega$, $R_3 = 3K\Omega$, $R_4 = 1K\Omega$ and $R_5 = 100\Omega$. Figure 6.14a shows the response of the R_{NL} with the characteristic roots 0, $V_a = 0.64V$ and $V_b = 1.28V$.

2. **Test 2**: This test considers medium values of the resistors R_1-R_5, similar to the ones used in the analysis of the circuit schematic in Fig. 6.12a i.e [$R_1 = 6.8K\Omega$, $R_2 = 2K\Omega$, $R_3 = 7.2K\Omega$, $R_4 = 6.8K\Omega$ and $R_5 = 1K\Omega$]. Hence, with these values, Fig. 6.14b shows the response of the R_{NL} component and the roots are 0, $V_a = 0.79V$ and $V_b = 1.49V$, as shown accordingly. These values of V_a and V_b match perfectly with the ones obtained in Fig. 6.12d from its circuit schematic.

3. **Test 3**: This test considers substantial values of the resistors R_1-R_5 as: $R_1 = 10K\Omega$, $R_2 = 2.3K\Omega$, $R_3 = 11.8K\Omega$, $R_4 = 10K\Omega$ and $R_5 = 1K\Omega$. Figure 6.14c shows the response of R_{NL} with $V_a = 0.62V$ and $V_b = 1.68V$. Figure 6.14d compares the variations of V_a and V_b for Figs. 6.14a, b and c. Note that all the results are obtained for the same input and other parameters except for the resistors R_1-R_5.

Table 6.3: Table of values for tests 1-3.

Figure	$R_1(\Omega)$	$R_2(\Omega)$	$R_3(\Omega)$	$R_4(\Omega)$	$R_5(\Omega)$	$V_a(V)$	$V_b(V)$
6.13a	1K	2K	3K	1K	100	0.64	1.28
6.13b	6.8K	2K	7.2K	6.8K	1K	0.79	1.49
6.13c	10K	2.3K	11.8K	10K	1K	0.62	1.68

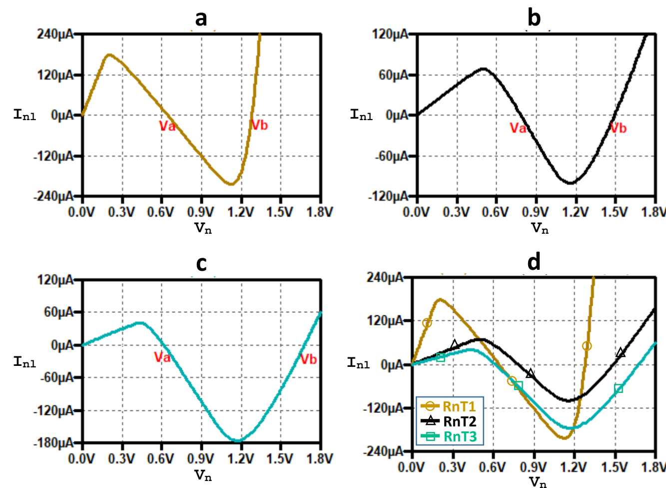

Figure 6.14: Verification of the created R_{NL} SPICE component based on the values of the resistors R_1-R_5. $V_{in} = 1.8V$. (**a**) Test-1: low resistances values, $V_a = 0.64V$ and $V_b = 1.28V$ (**b**) Test-2: medium resistances values, $V_a = 0.79V$ and $V_b = 1.49V$. (**c**) Test-3: high resistances values, $V_a = 0.62V$ and $V_b = 1.68V$. (**d**) Comparing figures **a**, **b** and **c** together.

4. **Test 4**: This is to observe the effect of the applied voltage change on the characteristics roots V_a and V_b. For fixed values of the resistors R_1-R_5, the input voltage does not affect the value of V_a and V_b. However, it does affect the quantity of I_{NL} flowing through R_{NL} due to the voltage increase or decrease for a fixed equivalent resistance value. It is observed with Fig. 6.14b that if V_{in} is high enough, the third branch becomes highly conductive but the values of V_a and V_b remain exactly at $0.79V$ and $1.49V$ respectively, even so V_{in} has changed. This shows that for fixed chosen resistors values, the input voltage does not affect the position of the characteristic roots of the cubic function and this is in compliance with conditions in equations (6.20) and (6.21).

5. **Test 5**: Variable resistances can be used for the resistors R_1-R_5 [139]. It has been shown in **tests** 1-4 that using fixed resistance values the circuit behaves decisively, as such the characteristic roots V_a and V_b remain virtually fixed. However, this might be a disadvantage in the case of a dynamical system in which V_a and V_b are subject to changes. For instance, in binarization where the stimuli are weighted and then decide the stability state.

$$\begin{aligned} R_1 &= [0,\ 10k\Omega]\ (\pm 5\%), \\ R_2 &= [1.8k\Omega,\ 2.3k\Omega]\ (\pm 5\%), \\ R_3 &= [6.8k\Omega,\ 11.8k\Omega]\ (\pm 5\%), \\ R_4 &= [0,\ 10k\Omega]\ (\pm 5\%), \\ R_5 &= [0,\ 1.5k\Omega]\ (\pm 5\%), \end{aligned}$$

6.4.3/ SPICE simulation of the 2-cells system – with Memristor and R_{NL}

Now that once the SPICE R_{NL} component is at disposal, next is to perform the circuit simulation of Fig. 6.3. Similarly, the memristor SPICE component is created using the values of parameters as: $R_{on} = 100\Omega$, $R_{off} = 16K\Omega$, $q_0 = 30\mu C$, $\mu_v = 10^{-14}m^2/V.s$ and $D = 10nm$. Figure 6.15 shows the complete circuit analysis of the two-cells system. V_m and V_s are the voltage across the master and slave cells respectively, defined by the initial condition of capacitors C_m and C_s, hence, the voltage across R_{NL_m} and R_{NL_s} respectively. The result is obtained for: $R_1 = 10K\Omega$, $R_2 = 2.3K\Omega$, $R_3 = 11K\Omega$, $R_4 = 10K\Omega$, $R_5 = 1.3K\Omega$, thus $V_a = 0.68V$ and $V_b = 1.77V$. Hence the stability at V_b is expected because $V_b - 2V_a > 0$.

The initial conditions of the cells are: $V_{m_0} = 2V$ and $V_{s_0} = 0V$. The evolution of $V_m(t)$ towards V_b is faster than the one of $V_s(t)$ because its value is closer to V_b. It is also observed that the activity in R_{NL_m} takes place in the vicinity of its third branch, however all the three branches in R_{NL_s} are activated because cell-s is initially at zero potential. This observation is confirmed by the nature of the flowing currents $I(R_{NL_m})$ and $I(R_{NL_s})$ through the cell-m and cell-s respectively. The current through the memristor $I(Mem)$ shows the effect of changing memristance. At about $20ms$, $V_m(t) = V_s(t) =$ constant and then settled at V_b shortly (about $25ms$). At this point the current in each branch is zero, thus the network is completely stabilized. The inflexion effect in $V_s(t)$ curve manifests the nature of the cubic resistance response, because this can only be seen when the entire branches of the R_{NL} are activated. Hence compare with evolution curve of $V_m(t)$.

6.4.3.1/ SPICE - Correlating V_m, V_s, V_a and V_b

It was shown earlier that the values of the resistances R_1-R_5 play crucial role in the response of the cubic resistance. Therefore it is important to play around with the values of R_1 to R_5 for the purpose of obtaining different values of V_a and V_b and to observe in each case, the corresponding time evolution of the cells.

Note that V_a and V_b are not directly implemented in the SPICE R_{NL} component (see Appendix B.1). However, the role of V_a and V_b can be achieved by choosing desirable values of R_{NL} resistances

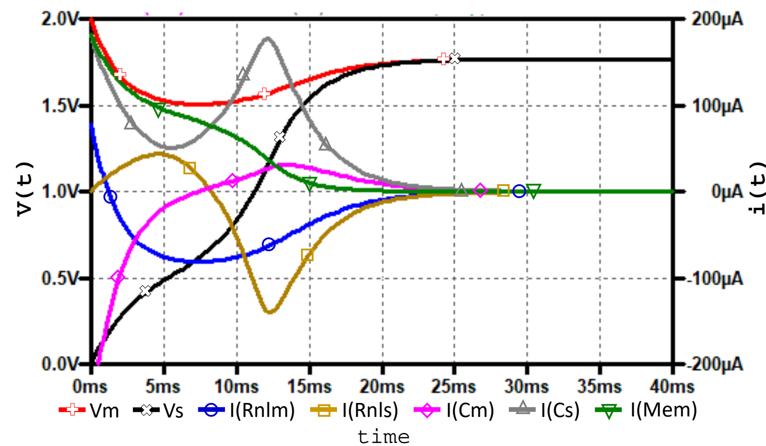

Figure 6.15: Complete circuit analysis of the two-cells network. The result is obtained for: $R_1 = 10K\Omega$, $R_2 = 2.3K\Omega$, $R_3 = 11K\Omega$, $R_4 = 10K\Omega$, $R_5 = 1.3K\Omega$, thus it gives $V_a = 0.68V$ and $V_b = 1.77V$. $C_m = C_s = 1\mu C$, $R_{off} = 16K\Omega$, $R_{on} = 100\Omega$ and $q_d = 100\mu C$. The system stabilizes at V_b because $V_b - 2V_a > 0$. The initial conditions of the cells are: $V_{m_0} = 2V$ and $V_{s_0} = 0V$. At about $20ms$, $V_m(t) = V_s(t)$ = constant and then settled at V_b shortly (about $25ms$). At this point the current in each branch is zero, thus the network is completely stabilized.

(i.e R_1-R_5). Firstly, verification test is performed to check whether the SPICE simulation results would be in agreement with the previous defined convention, which says: for $V_b - 2V_a > 0$, the system stabilizes at V_b, while for $V_b - 2V_a < 0$, the system stabilizes at 0. The test is carried out by considering some sets of values for R_1-R_5, and in each case the values of V_a and V_b are noted.

To study the system behaviour, we consider four different sets of principles which yield four different values of V_a and V_b. These principles are: *low resistances values of* R_1*-*R_5, *medium resistances values of* R_1*-*R_5, *high resistances values of* R_1*-*R_5 and *arbitrary choice of* R_1*-*R_5. In each case, the result is compared with the ones obtained by numerical simulation of equations (6.11)-(6.13).

i). *Low resistances values of* R_1*-*R_5: Small resistance values are used for each of the five resistors. For example: $R_1 = 1K\Omega$, $R_2 = 1K\Omega$, $R_3 = 4.5K\Omega$, $R_1 = 1K\Omega$ and $R_5 = 100\Omega$. It gives $V_a = 0.175V$ and $V_b = 1.493V$. Thus, $V_b - 2V_a > 0$. Similarly, the initial conditions of the master and slave cells are $V_{m_0} = 2V$ and $V_{s_0} = 0V$ respectively, and Fig. 6.16a shows the result,

ii). *Medium resistance values of* R_1*-*R_5: The considered values of the resistors are: $R_1 = 6.8K\Omega$, $R_2 = 2K\Omega$, $R_3 = 7.2K\Omega$, $R_4 = 6.8K\Omega$ and $R_5 = 1K\Omega$, thus the result gives $V_a = 0.79V$ and $V_b = 1.49V$, hence $V_b - 2V_a = -0.09 < 0$. Figure 6.16b shows results and the system stabilizes at V_b. However, the steady state is 0 because $V_b - 2V_a < 0$. One possible reason is that the difference is virtually zero and it was shown earlier that if $V_b - 2V_a = 0$ the stability could be at 0 or V_b.

iii). *High resistance values of* R_1*-*R_5: Substantial values of resistance are used, for example: $R_1 = 10K\Omega$, $R_2 = 2.5K\Omega$, $R_3 = 11K\Omega$, $R_4 = 10K\Omega$ and $R_5 = 1.5K\Omega$, and it gives $V_a = 0.691V$ and $V_b = 1.779V$. Thus $V_b - 2V_a > 0$. Figure 6.16c shows the result with the system stabilized at Vb, expectedly.

iv). *Arbitrary resistance values of* R_1*-*R_5: The values of the resistors are chosen randomly, just as it will behave in the case of variable resistors. $R_1 = 10K\Omega$, $R_2 = 2K\Omega$, $R_3 = 8K\Omega$, $R_4 = 10K\Omega$ and $R_5 = 1K\Omega$. It gives $V_a = 1V$, $V_b = 1.23V$, hence $V_b - 2V_a < 0$. The system

stabilizes at 0 as shown in Fig. 6.16d. Notice here that $R_4 > R_3$, hence the need for R_4 and R_3 to be variable so that the steady state is determined by the external stimulus. For R_4 and R_3 being variable, the system stabilizes at V_b for $R_4 < R_3$ and at 0 for $R_4 > R_3$ respectively.

Table 6.4: Table of values for R_1-R_5, for the two-cells simulations (Fig. 6.16).

Figure	$R_1(\Omega)$	$R_2(\Omega)$	$R_3(\Omega)$	$R_4(\Omega)$	$R_5(\Omega)$	$V_a(V)$	$V_b(V)$	V_b-$2V_a$	Stab.
6.15a	1K	1K	4.5K	1K	100	0.175	1.493	> 0	V_b
6.15b	6.8K	2K	7.2K	6.8K	1K	0.79	1.49	≈ 0	V_b
6.15c	10K	2.5K	11K	10K	1.5K	0.691	1.779	> 0	V_b
6.15d	10K	2K	8K	10K	1K	1.00	1.23	< 0	0

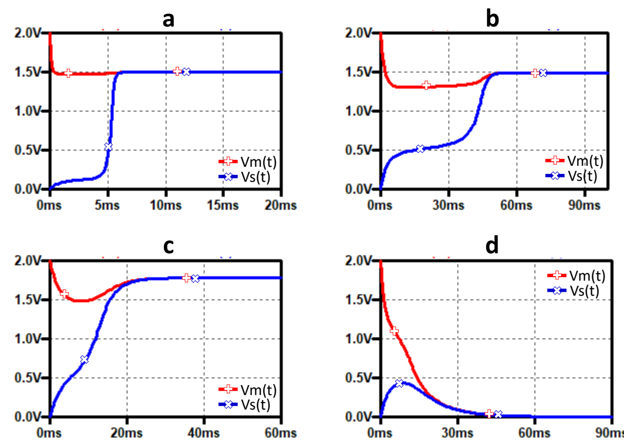

Figure 6.16: Two cells SPICE Simulation for some chosen values of resistances, showing the steady state of the system based on the variations of resistors R_1-R_5. (a) low values of R_1-R_5, (b) medium values of R_1-R_5, (c) high values of R_1-R_5 and (d) arbitrary values of R_1-R_5.

We can give quick remarks based on the obtained results:

a). The SPICE results agreed perfectly with the ones obtained by numerical solution (Matlab).

b). $V_b - 2V_a = 0$ emphasizes the enriched unstability of the characteristic root V_a and the stability of the system is established by the relative potential difference of the cells with respect to the reference potential at the highest stable state (i.e V_b).

c). It is important to note that the values of R_3 and R_4 play significant role in the generated value of V_a and hence, the stability of the system toward 0 or V_b. Because changes in the values of other resistors have less effect. The next analysis considers varying only R_3 and R_4 in order to visualize the system response for different cases.

6.4.3.2/ Effect of R_2, R_3 and R_4 on the system stability decision

The instantaneous values of V_a and V_b are defined by the resistances R_1-R_5, especially R_2, R_3 and R_4. Therefore, one can play around with the values of these resistors to meet any desired specifications. R_2, R_3 and R_4 play significant role in the system stability toward 0 or V_b because V_a

is determined by the potential V_{out} at the output of the OpAmp terminal:

$$V_{out} = \left(1 + \frac{R_3}{R_4}\right) V_n ,$$

Thus, for $R_3 > R_4$, the negative current is high and embeds V_a far away from V_b. On the contrary, for $R_3 < R_4$, the negative current is low and V_a becomes closer to V_b. Figure 6.17 shows some sets of results obtained by varying R_3 and R_4. The results are obtained for fixed values of R_1, R_2 and R_5 as $10K\Omega$, $2K\Omega$ and $1K\Omega$ respectively, meanwhile $R_4 = 10K\Omega$ with R_3 as $12K\Omega$, $11K\Omega$, $10K\Omega$, $9K\Omega$, $8K\Omega$ and $6K\Omega$, given by Figs. 6.17a, b, c, d, e and f respectively.

Table 6.5: Table of values for the variation of R_3 and R_4, for the two-cells simulations (Fig. 6.17).

Figure	$R_1(\Omega)$	$R_2(\Omega)$	$R_3(\Omega)$	$R_4(\Omega)$	$R_5(\Omega)$	R_3 & R_4	Stab.
6.16a	10K	2K	12K	10K	1K	$R_3 > R_4$	V_b
6.16b	"	"	11k	"	"	$R_3 > R_4$	V_b
6.16c	"	"	10K	"	"	$R_3 = R_4$	V_b
6.16d	"	"	9K	"	"	$R_3 < R_4$	V_b
6.16e	"	"	8K	"	"	$R_3 < R_4$	0
6.16f	"	"	6K	"	"	$R_3 < R_4$	0

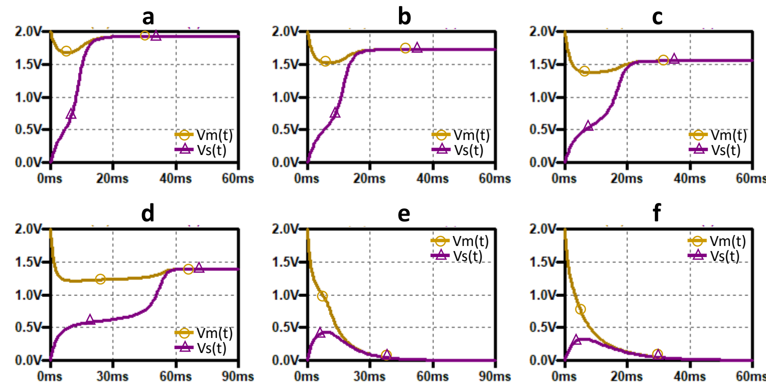

Figure 6.17: Variations effect of R_3 and R_4 on the system steady state, using $R_1 = 10K\Omega$, $R_2 = 2K\Omega$ and $R_5 = 1K\Omega$. For a fixed value of R_2, it shows that the system stabilizes at V_b and 0 for $R_3 > R_4$ and $R_3 < R_4$ respectively. (a) $R_3 = 12K\Omega$, (b) $R_3 = 11K\Omega$, (c) $R_3 = 10K\Omega$, (d) $R_3 = 9K\Omega$, (e) $R_3 = 8K\Omega$ and (f) $R_3 = 6K\Omega$. Note that any change in the value of R_2 can affect the steady state of the system.

Thus, for a fixed value of R_2, the results show that:

- *for $R_3 > R_4$, the system stabilizes at V_b.*
- *for $R_3 < R_4$, the system stabilizes at 0.*
- *for $R_3 = R_4$ the system steady state is determined by R_2 value. Figure 6.17c is for $R_3 = R_4 = 10K\Omega$ with $R_2 = 2K\Omega$. Then, increasing the value of R_2 (e.g $3K\Omega$), the system steady state becomes 0, but decreasing the value of R_2 (e.g $1.5K\Omega$), the system steady state remains at V_b. Similar response is observed in Fig. 6.17d (i.e $R_3 = 9K\Omega$). In fact, when the value of R_3 is closed to R_4's one (i.e $R_3 \approx R_4$), the steady state of the system depends strongly on R_2 value, because the steady state can change for any small change in the value of R_2. Furthermore, even if $R_3 \gg R_4$ (i.e V_b as the likely steady state) or $R_3 \ll R_4$ (i.e 0 as the likely*

steady state), then variations of R_2 can change the steady state of the system from V_b to 0 or 0 to V_b, but not very small variations as in the case where $R_3 \approx R_4$.

- *The steady state of the system is determined by the values of R_2, R_3 and R_4.*

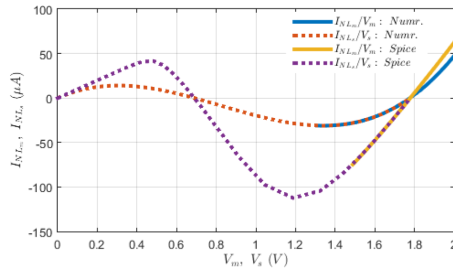

(a) R_{NL} comparison for SPICE and Numerical.

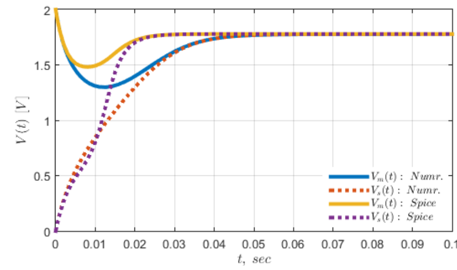

(b) $V_m(t)$ and $V_s(t)$ evolution comparison for SPICE and Numerical.

Figure 6.18: Result comparison for SPICE simulation and numerical solution. Similar behaviour is observed.

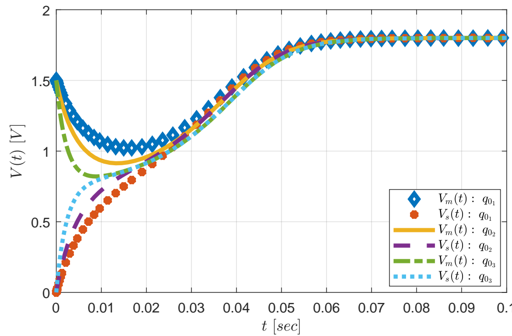

(a) Effect of q_0 in the case $V_b - 2Va > 0$. $V_a = 0.7$, $V_b = 1.8$. The system stabilizes at V_b.

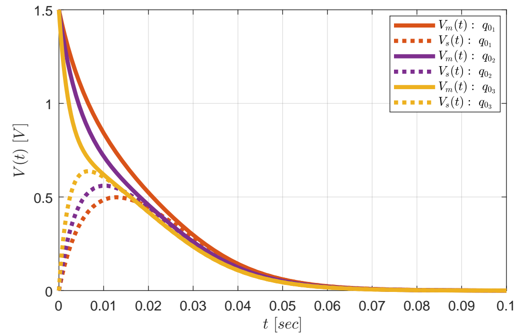

(b) Effect of q_0 in the case $V_b - 2Va < 0$, $V_a = 1.1V$, $V_b = 1.8V$. The system stabilizes at 0.

Figure 6.19: Effect of initial memristance on the evolution of $V_m(t)$ and $V_s(t)$. $q_{0_1} = 25\mu C$, $q_{0_2} = 50\mu C$, $q_{0_3} = 75\mu C$, $R_{on} = 100\Omega$, $R_{off} = 16K\Omega$, $C = 1\mu F$, $R_0 = 10K\Omega$, $V_{m_0} = 1.5V$ and $V_{s_0} = 0V$. In each case the initial memristance $M(q_0)$ affects the system evolution toward the equilibrium state V_b and 0 respectively.

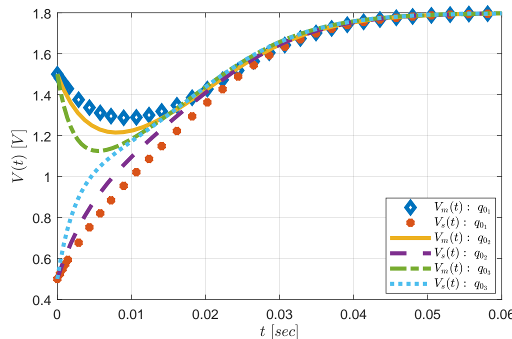

(a) Effect of q_0 in the case $V_b - 2Va > 0$. $V_a = 0.75V$ and $V_b = 1.8V$. The system stabilizes at V_b.

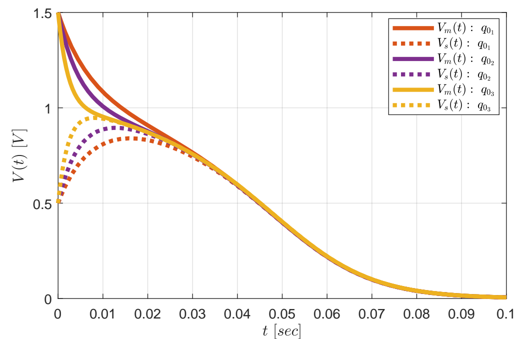

(b) Effect of q_0 in the case $V_b - 2Va < 0$, $V_a = 1V$, $V_b = 1.8V$. The system stabilizes at 0.

Figure 6.20: Effect of initial memristance on the evolution of $V_m(t)$ and $V_s(t)$. $q_{0_1} = 25\mu C$, $q_{0_2} = 50\mu C$, $q_{0_3} = 75\mu C$, $R_{on} = 100\Omega$, $R_{off} = 16K\Omega$, $C = 1\mu F$, $R_0 = 10K\Omega$, $V_{m_0} = 1.5V$ and $V_{s_0} = 0.5V$. Using the same values of parameters except that V_{s_0} is nonzero. Similalrly, the effect of $M(q_0)$ is highly observable.

6.5/ DIFFUSION EFFECTS IN A NONLINEAR ELECTRICAL LATTICE USING MEMRISTIVE COUPLING

This section presents a one dimensional nonlinear diffusive electrical lattice consisting of N identical cells, each made of one linear capacitor C in parallel with a nonlinear resistance R_{NL} and a series memristive coupling as shown in Fig. 6.21.

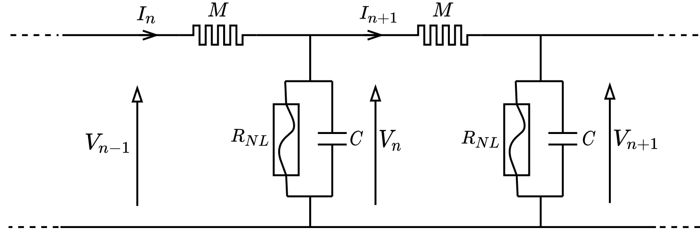

Figure 6.21: Schematic representation of the 1D-nonlinear diffusive electrical network for N number of identical cells. The coupling is made by the memristor, meanwhile each cell is composed of a linear capacitor C in parallel with a nonlinear resistor R_{NL}.

6.6/ DESCRIPTION

From Fig. 6.21, the application of Kirchhoff laws gives the nonlinear discrete equation:

$$
\begin{aligned}
I_n &= C\frac{dV_n}{dt} + I_{NL} + \frac{V_n - V_{n+1}}{M(q)} = \frac{V_{n-1} - V_n}{M(q)}, \\
C\frac{dV_n}{dt} &= -I_{NL} - \frac{V_n - V_{n+1}}{M(q)} + \frac{V_{n-1} - V_n}{M(q)} \quad \Rightarrow \\
\frac{dV_n}{dt} &= \frac{1}{CM(q)}\left(V_{n-1} - 2V_n + V_{n+1}\right) - \frac{f(V_n)}{C},
\end{aligned}
\tag{6.23}
$$

where n is the index signifying a particular cell under consideration, hence equation (6.23) is valid for $2 \leq n \leq N-1$ with N the total number of cells, because for $n = 1$ and $n = N$, the grid points corresponding to V_0 and V_{N+1} are outside of the system domain. Furthermore, V_{n-1}, V_n and V_{n+1} are respectively the voltage at cell $n-1$, n and $n+1$, meanwhile $f(V_n) = I_{NL_n}$ is the nonlinear current function through the R_{NL} of cell n, thus given by:

$$
f(V_n) = \frac{V_n(V_a - V_n)(V_b - V_n)}{R_0 V_a V_b}. \tag{6.24}
$$

Here R_0 is the linear approximation of R_{NL}, V_a and V_b being the constant voltages defining the characteristic roots of the cubic function $f(V_n)$, and we choose now the conditions $2V_a \leq V_b$.

Hence, (6.23) gives the second order finite difference of a diffusion equation introduced by Nagumo et al. [167], introduced for simulating the transmission of information in nerve axon, given by:

$$
\frac{\partial V}{\partial t} = \frac{\partial^2 V}{\partial x^2} + g(V), \tag{6.25}
$$

where $g(V)$ is a cubic function analogous to $f(V_n)$ in equation (6.23).

Furthermore, equation (6.23) contains a second order finite difference scheme of the form:

$$\frac{U_{i-1} - 2U_i + U_{i+1}}{h^2} = \hat{g}(x_i), \qquad i = 1, 2, ..., N-1 \tag{6.26}$$

At the boundary $\frac{dV}{dt} = 0$, no current leaves the network, that is we can apply Neumann boundary condition, such that: $V_1 = V_0$ and $V_{N+1} = V_{N-1}$, and hence we obtained respectively, the finite difference scheme as:

$$\frac{dV_1}{dt} = \frac{1}{CM(q)}(V_2 - V_1) - \frac{V_1(V_a - V_1)(V_b - V_1)}{\tau_c V_a V_b} \tag{6.27a}$$

$$\frac{dV_N}{dt} = \frac{1}{CM(q)}(V_{N-1} - V_N) - \frac{V_N(V_a - V_N)(V_b - V_N)}{\tau_c V_a V_b} \tag{6.27b}$$

where $\tau_c = R_0 C$.

When the voltages are distributed so that the spatial extent is sufficiently large with respect to the pitch of the electrical network (that is to say, V_n varies slightly from one cell to another), one can do the approximation of continuous media:

$$V_{n\pm1} = V \pm \frac{\partial V}{\partial n} + \frac{1}{2}\frac{\partial^2 V}{\partial^2 n} \pm \frac{1}{3!}\frac{\partial^3 V}{\partial^3 n} + ... \tag{6.28}$$

Relating x and n by $x = \delta n$, with δ allowing to return to the true dimensions. In that case:

$$V_{n+1} - 2V_n + V_{n-1} \simeq \delta^2 \frac{\partial^2 V}{\delta x^2} \tag{6.29}$$

The term δ having no physical meaning in electronics, we can pose that $\delta = 1$. From equations (6.23) and (6.29), we get:

$$\frac{\partial V}{\partial t} = \frac{1}{CM(q)}\frac{\partial^2 V}{\partial x^2} - \frac{V(V_a - V)(V_b - V)}{\tau_c V_a V_b} \tag{6.30}$$

Equation (6.30) correspond to the continuous Fitzhugh-Nagumo equation without the recovery term. We can rewrite (6.30) as:

$$\frac{\partial V}{\partial t} = \frac{1}{CM(q)}\frac{\partial^2 V}{\partial x^2} - F(V), \tag{6.31}$$

where:

$$F(V) = \frac{V(V_a - V)(V_b - V)}{\tau_c V_a V_b}. \tag{6.32}$$

If we remove the coupling term in (6.30), we get:

$$\frac{\partial V}{\partial t} = -\frac{V(V_a - V)(V_b - V)}{\tau_c V_a V_b}. \tag{6.33}$$

$\frac{\partial V}{\partial t} = 0$ corresponds to equilibrium states implying that $V = 0$, $V = V_a$ and $V = V_b$. Let V^*, be the value of equilibrium on which the we add a small perturbation ε, so that:

$$\varepsilon(t) = V - V^* \ll 1.$$

Equation (6.33) can be expressed as: $\frac{\partial V}{\partial t} = -F(V)$, so that:

$$\frac{\partial}{\partial t}(\varepsilon + V^*) = -F(V^* + \varepsilon),$$

$$\frac{\partial}{\partial t}(\varepsilon) + \frac{\partial}{\partial t}(V^*) \sim -F(V^*) - \varepsilon \frac{dF(V^*)}{dV},$$

and using the fact that $\frac{\partial}{\partial t}(V^*) = 0$ and $F(V^*) = 0$ at equilibrium, we get at first order ε:

$$\frac{\partial \varepsilon}{\partial t} = -\varepsilon \frac{\mathrm{d}F(V^*)}{\mathrm{d}V} \Rightarrow$$

$$\varepsilon = \varepsilon_0 \, e^{-\frac{\mathrm{d}F(V^*)}{\mathrm{d}V}t}. \tag{6.34}$$

From (6.32), the derivative of $F(V)$ gives:

$$\frac{\mathrm{d}F(V)}{\mathrm{d}V} = -\frac{1}{\tau_c V_a V_b}\left(3V^2 - 2(V_a + V_b)V + V_a V_b\right).$$

As V_a is always less than V_b, we get:
* if $V = 0$:

$$\left.\frac{\mathrm{d}F(V)}{\mathrm{d}V}\right|_0 = \frac{1}{\tau_c} > 0.$$

* if $V = V_a$:

$$\left.\frac{\mathrm{d}F(V)}{\mathrm{d}V}\right|_{V_a} = \frac{V_a - V_b}{\tau_c V_b} < 0.$$

* if $V = V_b$:

$$\left.\frac{\mathrm{d}F(V)}{\mathrm{d}V}\right|_{V_b} = \frac{V_b - V_a}{\tau_c V_a} > 0.$$

Hence, 0 and V_b are the two stable equilibrium states, while V_a is the unstable equilibrium state.

Furthermore, as the equation (6.33) yields:

$$\frac{\partial V}{\partial t} = -\frac{1}{\tau_c} V \left(1 - \frac{V}{V_a}\right)\left(1 - \frac{V}{V_b}\right) = -F(V), \tag{6.35}$$

and considering the nonlinear function $-F(V)$ as a force which is the derivated from a potential energy ($W(V)$), we can write:

$$-\frac{1}{\tau_c} V \left(1 - \frac{V}{V_a}\right)\left(1 - \frac{V}{V_b}\right) = -\frac{dW(V)}{dV} \Rightarrow$$

$$W(V) = \frac{1}{\tau_c V_a V_b}\left[\frac{V^4}{4} - (V_a + V_b)\frac{V^3}{3} + V_a V_b \frac{V^2}{2} + C^{te}\right], \tag{6.36}$$

where C^{te} is a constant of the integration. The minima of $W(V)$ function are 0 and V_b, indeed values of stable equilibrium positions. The values of these minima weigh the attraction of each of the stable state, thus Fitzhugh-Nagumo is a bistable equation.

Coming back to equations system sets (6.23), (6.24) and (6.27), we can take advantage of the main result of Chapter 6, devoted to the case of 2 (R_{NL}, C) cells coupled by a memristor $M(q)$, such as:

- The common mode (CM) between the voltage V_n and its neighbouring cells V_{n-1} and V_{n+1} is almost exclusively led by the dynamics of nonlinear cell (R_{NL}, C):

$$\frac{d}{dt}V_{n,CM} = -\frac{1}{R_o C}V_{n,CM}\left(1 - \frac{V_{n,CM}}{V_a}\right)\left(1 - \frac{V_{n,CM}}{V_b}\right),$$

that is:

$$V_{n,CM}(t).\left(\frac{V_{n,CM}(t) - V_b}{V_{n,CM}(0) - V_b}\right)^{\frac{V_a}{V_b - V_a}} . \left(\frac{V_{n,CM}(0) - V_a}{V_{n,CM}(t) - V_a}\right)^{\frac{V_b}{V_b - V_a}} = V_{n,CM}(0)\ e^{-\frac{t}{R_o C}}. \quad (6.37)$$

This result shows that, according to the initial value of $V_{n,CM}(0)$ with respect to V_a and V_b, the time evolution of the common mode of the voltages in the vicinity of cell n will evolve toward 0 or V_b (toward 0 if $V_{n,CM}(0) < V_a$ and toward V_b if $V_{n,CM}(0) > V_a$).

- The differential mode (DM) between the voltage V_{n-1} (or V_{n+1}) and V_n will be in fact led by a competition between:

  1) the influence of (R_{NL}, C) cell, acting as a binarization process toward 0 or V_b, according respectively to the case $V_{n,DM}(0) < V_a$ or $V_{n,DM}(0) > V_a$,

  2) the influence of the memristor with its history, coupling the neighbouring sites.

  In image processing applications, this network is specially interesting. By weighing the role of both processes, we can give the priority to a process of pure binarization on one hand, if the memristor has large impedance with respect to R_o, or to a process of edge detection, if the memristor has small impedance with respect to R_o. In addition, its history will play a stabilizing role in preventing any singularity in image succession.

6.7/ Conclusion

The schematic of the memristor based 2D cellular nonlinear network is presented, with the cells constituting cubic resistance such as Fitzhugh-Nagumo. Using the system of two cells coupled by a memristor, the response of the network is analyzed according to analytical solution, numerical solution and SPICE simulation with the aid of the created SPICE R_{NL} component. The analytical solution is not finished yet, however the system evolution agrees with ones obtained by numerical solution and SPICE simulation. We observed the dynamic and the steady state response of the cells along with the roles of memristor and the cubic resistance.

Unlike the RC cells where the voltage evolution of the cells always tends to 0, here the cells always stabilize at one of the two stable states, namely, 0 and V_b. The effect of parameter variation (specifically V_a and q_0) on the dynamic and steady state response of the system, shows that the network can implement image processing techniques such as mathematical morphology (dilation and erosion) for signal filtering and edge detection. Furthermore, the introduced 1D diffusive network is promising for binarization circuit and noise removal.

IV

General Conclusion

7

GENERAL CONCLUSION AND PERSPECTIVES

7.1/ GENERAL CONCLUSION

The memristor is a new circuit element with ongoing philosophical criticism for being called the fourth basic passive circuit element alongside resistor, capacitor, and inductor. First, we presented the review on the four basic passive circuit elements and then followed by in-depth analysis of memristor including its modeling, philosophical argument, device technologies and applications. We explored some subtleties related to intrinsic asymmetry of a memristor worthy to be considered especially in using memristor as a memristive grid network for CNN neighborhood connection. We presented the detailed ϕ-q description and derived a new model of memristor which is particularly interesting because of two main reasons: 1) it does not require a window function whose physical meaning is not intuitive and 2) it has a continuous first derivative with respect to charge, thus allowing us to solve a specific system analytically for all flowing charges through the memristor.

We presented a memristor based 2D nonlinear network essentially for information (signal and image) processing. As the first step before studying such a memristor based network, we considered the system of only two cells, namely master and slave coupled together by a memristor, which allows us to observe the interactional behaviour and contribution of the memristor within the network, both qualitatively and quantitatively. The response of the system was analyzed by following three methodologies: analytical, numerical, and analog simulations. The results according to these methods were obtained for the same memristor parameters values. It was worthwhile to observe that these methods agreed with one another perfectly. The network being a bidirectional coupled system, the terms master and slave are only a convenient way to specify which of the two cells is more active in deciding the direction of the flowing charge through the memristor. They are not master and slave in the sense of unidirectional coupled systems. In this context, we considered first 2 RC cells and then secondly, 2 Fitzhugh-Nagumo cells, but always with a memristor as a coupling component.

Using two initially charged RC cells coupled together by a linear resistor and allowing information to flow from one cell to the other one and vice-versa, we observed of course a perfect symmetry in the response of the network with respect to the dynamics of the flowing charge through the

coupling linear resistance. However, replacing the coupling linear resistance by a memristor, we observed a different scenario due to intrinsic asymmetry of a memristor which is caused by the resistance switching transition between its two limiting values. A charge-controlled memristor model is used, in which we considered the initial charge q_0 having flowed through the memristor in its previous history as a parameter defining the initial memristance. We highlighted the fundamental role of the memristor history, in showing that if all parameters are changed except q_0, the system behavior is however quite different according to q_0. As expected intuitively, the initial charge acts strongly on the dynamics of charge transfer from master to slave cells. We have studied the effect of initial charge q_0 on the system dynamics leading us to get a second order nonlinear differential equation characterizing the flow of charge from one cell to the other. The dynamics of memristor for pixel-to-pixel communication was described with the aid of phase plane analysis in which the memristor asymmetry becomes more apparent.

The behavior of memristor with respect to the polarity reversal effect of the input signal was investigated. We have shown from the circuit point of view and the analytical solution that the conductivity of the memristor depends on the polarity of the applied input signal, thus affecting the mobility of its charge carriers, this property being due to the intrinsic nature of the device. It is an inevitable nature of a bipolar memristor, irrespective of its device technology. Hence, memristive effect changes according to the connection mode and the amount of current flowing through it, showing that the memristor is not a bilateral circuit element like a resistor as verified by our study. To achieve memristive effect with symmetry, a memristor fuse is rather proposed. We have therefore presented the detailed analytical interpretation of the memristor fuse. We also authenticated the memristor fuse prior to applying it in a circuit and the results showed that the memristor fuse behaves like a standalone memristor under high input frequency. Although connecting two memristors anti-serially to form a memristor fuse lets the dynamics of the two state variables system become more intricate, as well as the dynamics of the resistance switching, terminal asymmetry is resolved as confirmed by our results. The symmetry displayed by the memristor-fuse suggests it to be a promising element useful as memristive grid in neighborhood connections and it could become an important concept for the ongoing study of our memristor-based network. We presented the detailed analytical interpretation of memristor fuse between the 2 RC cells and the symmetry is observed in the phase portraits analysis.

The last phase of the work entailed using Fitzhugh-Nagumo cells which is far more intricate than the RC cells where the only stable state is always zero due to the resistive nature of the cells. With Fitzhugh-Nagumo cells we have two stable states. Similarly, we studied the network of 2 Fitzhugh-Nagumo cells coupled together by a memristor analytically, numerically and by SPICE simulation, both methods confirming the two possible stable states. The analytical study was explored to include both common mode and differential mode, the latter reflecting in essence the effect of the voltage across the memristor. The steady state is determined with respect to the unstable state, suggesting that the network can also be used in a binarization scheme, for example to process different gray levels. Furthermore, we extended the concept to include one-dimensional cellular nonlinear electrical lattice using memristive coupling and so show how the network could be used to study the diffusion effect between neuron cells and also to be used to perform signal filtering.

7.2/ Future Perspectives

Due to increasing demand of small and very fast reliable systems nowadays, nano-scalability is one of the challenges facing nano-electronic industries. Memristor has interesting features such as nano-scalability, memory capability, conductance modulation etc., which spark interest globally. Furthermore, these features among many others, suggest memristor to stand a chance in playing a crucial role for generating a new paradigm of signal and image processing and beyond. We outlined 3 potential methods to include memristor in the conventional 2D cellular nonlinear network. In this work, we focused on the first method where memristors are used to replace the series coupling resistance, analogous to the technique of using memristors as synaptic links between electronic neurons. Hence in addition to signal processing, the network can also be used for electronic prosthesis in bio-medical applications. However, the other two methods would be considered in the future because we do think that they are also valid options to include memristor in the network, especially due to the nonlinear nature of the memristor.

Initially, the work targeted four approaches namely: Analytical solution, Numerical solution, Circuit simulation in SPICE and Experiments. The first three approaches were accomplished. However, the restriction rules caused by the coronavirus pandemic necessitate the work to be carried-out remotely, hence no experiment was performed except some pioneer tests. The results obtained by SPICE are promising and could be easily implemented experimentally. We showed detailed analysis of only 2 cells in which the coupling network can be extended to any number of cells under consideration. The experimental aspect of the memristor based 2D nonlinear network will be performed later. In the future, we will implement the network to perform real-time image processing experimentally. Furthermore, we begin to consider signal filtering using the outlined memristor based 1D network, for example for noise removal. This is part of the ongoing studies.

Finally, we are deeply convinced of the huge potential of memristor as a coupling element in neural networks, acting as an electronic synapse. We think that introducing our new model M(q) to describe the instantaneous memristance as a cubic function of the total charge having flowed through the memristor is the good way to analyze in detail the behavior of this passive fourth component in its total environment. It could give the key to understand how it can process the right information transmission in the neural scheme with respect to the voltage applied across it and the current flowing through it.

7.3/ Publications

1. International journals

- Isah, A., Nguetcho, A. S. T., Binczak, S., & Bilbault, J. M. (2019). Dynamics of a charge-controlled memristor in master–slave coupling. Electronics Letters, 56(4), 211-213.
- Isah, A., Nguetcho, A. S. T., Binczak, S., & Bilbault, J. M. (2020). Memristor dynamics involved in cells communication for a 2D non-linear network. IET Signal Processing, 14(7), 427-434.

- Isah, A., Tchakoutio Nguetcho, A. S., Binczak, S., & Bilbault, J. M. (2021). Polarity reversal effect of a memristor from circuit point of view and insights into the memristor-fuse. Frontiers in Communications and Networks, 2, 26.
- Isah, A., Nguetcho, A. S. T., Binczak, S., & Bilbault, J. M. (2021). Comparison of the performance of the memristor models in 2D cellular nonlinear network. Electronics MDPI, Circuit and Signal Processing, 10(13), 1577.
- Isah, A., Nguetcho, A. S. T., Binczak, S., & Bilbault, J. M. Analytical interpretation of memristor fuse in nonlinear network [*to be submiited*]
- Isah, A., Nguetcho, A. S. T., Binczak, S., & Bilbault, J. M. Interaction of two pixel cells via memristor and their competitiveness toward a stable equilibrium state [*to be submitted*]
- Aliyu Isah. Review on the basic circuit elements and memristor interpretation: Analysis, Technology and Applications [*to be submitted*]

2. International conferences

- Isah, A., Nguetcho, A. S. T., BINCZAK, S., & BILBAULT, J. M. (2020, June). Dynamics of a charge transfer through a memristor between two initially charged cells. In The 13th CHAOS 2020 International Conference (p. 56), 9-12 June 2020, Florence, Italy.
- Isah, A., Nguetcho, A. S. T., BINCZAK, S., & BILBAULT, J. M. (2021, June). The interaction of memristor in nonlinear networks for image and signal processing. *The 14th CHAOS 2021 International Conference* 8-11 June, 2021, Athens, Greece.
- Isah, A., Nguetcho, A. S. T., BINCZAK, S., & BILBAULT, J. M. Memristor - the fourth fundamental passive electronic component and its memory interpretation. CETSIS 2021: Symposium on the Teaching of Technologies and Information and Systems Sciences, 8-10 June 2021, Valenciennes, France.
- Isah, A., Nguetcho, A. S. T., BINCZAK, S., & BILBAULT, J. M. Comparison of the coupling effect of the memristor and memristor fuse in 2D cellular nonlinear network. International Symposium Topical Problems of Nonlinear Wave Physics (NWP-2021), 19-22 September 2021, Nizhny Novgorod, Russia.

3. Local conferences, events and symposiums

- Isah, A., Nguetcho, A. S. T., BINCZAK, S., & BILBAULT, J. M. Introduction to memristor and applications. Doctoral day, 14 March 2019, Le Creusot, France.
- Isah, A., Binczak, S., Nguetcho, AST, Dos Santos, S., Troisgros, R., & Bilbault, J.M. Le memristor, qu’est ce que c’est? Fête de la Science, 5-13 October, 2019, Dijon, France.

BIBLIOGRAPHY

[1] Ruben Xing, John Wang, and Qiyang Chen. The contemporary it transformations. *Proceedings of the Northeast Business & Economics Association*, 2010.

[2] Frederick Seitz. On the trail of the transistor. *Nature*, 388(6640):339–340, 1997.

[3] R Stanley Williams. How we found the missing memristor. In *Chaos, CNN, Memristors and Beyond: A Festschrift for Leon Chua With DVD-ROM, composed by Eleonora Bilotta*, pages 483–489. World Scientific, 2013.

[4] Jonathan Swingler. *Reliability Characterisation of Electrical and Electronic Systems*. Elsevier, 2015.

[5] Deyan Lin, Leon Chua, and Shu-Yuen Hui. The first man-made memristor: Circa 1801 [scanning our past]. *Proceedings of the IEEE*, 103(1):131–136, 2014.

[6] Themistoklis Prodromakis. Two centuries of memristors. In *Chaos, CNN, Memristors and Beyond: A Festschrift for Leon Chua With DVD-ROM, composed by Eleonora Bilotta*, pages 508–517. World Scientific, 2013.

[7] Matthias Wuttig and Noboru Yamada. Phase-change materials for rewriteable data storage. *Nature materials*, 6(11):824, 2007.

[8] Takayuki Kato and Keiji Tanaka. Electronic properties of amorphous and crystalline ge2sb2te5 films. *Japanese journal of applied physics*, 44(10R):7340, 2005.

[9] Yuriy V Pershin and Massimiliano Di Ventra. Memory effects in complex materials and nanoscale systems. *Advances in Physics*, 60(2):145–227, 2011.

[10] Leon Chua. Memristor-the missing circuit element. *IEEE Transactions on circuit theory*, 18(5):507–519, 1971.

[11] Leon O Chua and Sung Mo Kang. Memristive devices and systems. *Proceedings of the IEEE*, 64(2):209–223, 1976.

[12] Dmitri B Strukov, Gregory S Snider, Duncan R Stewart, and R Stanley Williams. The missing memristor found. *nature*, 453(7191):80, 2008.

[13] Alex Nugent. Knowm memristor introduction.

[14] Gorm Krogh Johnsen. An introduction to the memristor-a valuable circuit element in bioelectricity and bioimpedance. *Journal of electrical bioimpedance*, 3(1):20–28, 2012.

[15] Michael Irving. Smallest 3d transistors ever made measure a minuscule 2.5 nanometers.

[16] Blaise Mouttet. Memresistors and non-memristive zero-crossing hysteresis curves. *arXiv preprint arXiv:1201.2626*, 2012.

[17] Blaise Mouttet. The memristor and the scientific method, 2012.

[18] Sascha Vongehr and Xiangkang Meng. The missing memristor has not been found. *Scientific reports*, 5:11657, 2015.

[19] Isaac Abraham. The case for rejecting the memristor as a fundamental circuit element. *Scientific reports*, 8(1):10972, 2018.

[20] KANPUR KOTHI MANDHANA. A seminar report on memristor.

[21] Aliyu Isah, Stéphane Binczak, Aurélien Serge Tchakoutio Nguetcho, Serge Dos Santos, Romain Troisgros, and Jean Marie Bilbault. Le memristor, qu'est ce que c'est? 5-13 October 2019.

[22] Massimiliano Di Ventra, Yuriy V Pershin, and Leon O Chua. Putting memory into circuit elements: memristors, memcapacitors, and meminductors [point of view]. *Proceedings of the IEEE*, 97(8):1371–1372, 2009.

[23] CHUA Leon. Everything you wish to know about memristors but are afraid to ask. *Radioengineering*, 24(2):319, 2015.

[24] Shyam Prasad Adhikari, Maheshwar Pd Sah, Hyongsuk Kim, and Leon O Chua. Three fingerprints of memristor. *IEEE Transactions on Circuits and Systems I: Regular Papers*, 60(11):3008–3021, 2013.

[25] Dalibor Biolek, Zdeněk Biolek, Viera Biolková, and Zdeněk Kolka. Some fingerprints of ideal memristors. In *2013 IEEE international symposium on circuits and systems (ISCAS2013)*, pages 201–204. IEEE, 2013.

[26] Leon Chua. If it's pinched it'sa memristor. *Semiconductor Science and Technology*, 29(10):104001, 2014.

[27] Leon Chua. Resistance switching memories are memristors. *Applied Physics A*, 102(4):765–783, 2011.

[28] Hyongsuk Kim, Maheshwar Pd Sah, and Shyam Prasad Adhikari. Pinched hysteresis loops is the fingerprint of memristive devices. *arXiv preprint arXiv:1202.2437*, 2012.

[29] DA Clauss, RM Ralich, and RD Ramsier. Hysteresis in a light bulb: connecting electricity and thermodynamics with simple experiments and simulations. *European Journal of Physics*, 22(4):385, 2001.

[30] Vladislav S Markin, Alexander G Volkov, and Leon Chua. An analytical model of memristors in plants. *Plant signaling & behavior*, 9(10):e972887, 2014.

[31] D Biolek, Z Biolek, and V Biolkova. Pinched hysteretic loops of ideal memristors, memcapacitors and meminductors must be 'self-crossing'. *Electronics letters*, 47(25):1385–1387, 2011.

[32] Kristy A Campbell. Self-directed channel memristor for high temperature operation. *Microelectronics journal*, 59:10–14, 2017.

[33] Zdeněk Biolek, Dalibor Biolek, and Viera Biolková. Computation of the area of memristor pinched hysteresis loop. *IEEE Transactions on Circuits and Systems II: Express Briefs*, 59(9):607–611, 2012.

[34] Zdeněk Biolek, Dalibor Biolek, and Viera Biolkova. Analytical computation of the area of pinched hysteresis loops of ideal mem-elements. *Radioengineering*, 22(1):132–135, 2013.

[35] D Biolek, Z Biolek, and V Biolkova. Interpreting area of pinched memristor hysteresis loop. *Electronics Letters*, 50(2):74–75, 2014.

[36] Yuriy V Pershin and Massimiliano Di Ventra. Comment on 'if it's pinched it's a memristor'. *Semiconductor Science and Technology*, 34(9):098001, 2019.

[37] J Kim, Yuriy V Pershin, M Yin, T Datta, and Massimiliano Di Ventra. An experimental proof that resistance-switching memories are not memristors. *arXiv preprint arXiv:1909.07238*, 2019.

[38] Blaise Mouttet. Pinched hysteresis loops are a fingerprint of square law capacitors, 2012.

[39] Blaise Mouttet. Response to 'pinched hysteresis loops is the fingerprint of memristive devices', 2012.

[40] Dalibor Biolek, Zdenek Biolek, Viera Biolkova, Alon Ascoli, and Ronald Tetzlaff. About vi pinched hysteresis of some non-memristive systems. *Mathematical Problems in Engineering*, 2018, 2018.

[41] Yuriy V Pershin and Massimiliano Di Ventra. A simple test for ideal memristors. *Journal of Physics D: Applied Physics*, 52(1):01LT01, 2018.

[42] Jinsun Kim, Yuriy V Pershin, Ming Yin, Timir Datta, and Massimiliano Di Ventra. An experimental proof that resistance-switching memory cells are not memristors. *Advanced Electronic Materials*, 6(7):2000010, 2020.

[43] Gina C Adam, Brian D Hoskins, Mirko Prezioso, Farnood Merrikh-Bayat, Bhaswar Chakrabarti, and Dmitri B Strukov. 3-d memristor crossbars for analog and neuromorphic computing applications. *IEEE Transactions on Electron Devices*, 64(1):312–318, 2016.

[44] Zhongrui Wang, Saumil Joshi, Sergey E Savel'ev, Hao Jiang, Rivu Midya, Peng Lin, Miao Hu, Ning Ge, John Paul Strachan, Zhiyong Li, et al. Memristors with diffusive dynamics as synaptic emulators for neuromorphic computing. *Nature materials*, 16(1):101–108, 2017.

[45] Kuk-Hwan Kim, Siddharth Gaba, Dana Wheeler, Jose M Cruz-Albrecht, Tahir Hussain, Narayan Srinivasa, and Wei Lu. A functional hybrid memristor crossbar-array/cmos system for data storage and neuromorphic applications. *Nano letters*, 12(1):389–395, 2012.

[46] Siddharth Gaba, Patrick Sheridan, Jiantao Zhou, Shinhyun Choi, and Wei Lu. Stochastic memristive devices for computing and neuromorphic applications. *Nanoscale*, 5(13):5872–5878, 2013.

[47] Yu Chen, Gang Liu, Cheng Wang, Wenbin Zhang, Run-Wei Li, and Luxing Wang. Polymer memristor for information storage and neuromorphic applications. *Materials Horizons*, 1(5):489–506, 2014.

[48] Themistoklis Prodromakis and Chris Toumazou. A review on memristive devices and applications. In *2010 17th IEEE International Conference on Electronics, Circuits and Systems*, pages 934–937. IEEE, 2010.

[49] Pinaki Mazumder, Sung-Mo Kang, and Rainer Waser. Memristors: devices, models, and applications. *Proceedings of the IEEE*, 100(6):1911–1919, 2012.

[50] Roberto Marani, Gennaro Gelao, and Anna Gina Perri. A review on memristor applications. *arXiv preprint arXiv:1506.06899*, 2015.

[51] Bharathwaj Muthuswamy. Implementing memristor based chaotic circuits. *International Journal of Bifurcation and Chaos*, 20(05):1335–1350, 2010.

[52] Ya-Ming Xu, Li-Dan Wang, and Shu-Kai Duan. A memristor-based chaotic system and its field programmable gate array implementation. *Acta Physica Sinica*, 65(12):120503, 2016.

[53] SG Hu, SY Wu, WW Jia, Q Yu, LJ Deng, Yong Qing Fu, Y Liu, and Tu Pei Chen. Review of nanostructured resistive switching memristor and its applications. *Nanoscience and Nanotechnology Letters*, 6(9):729–757, 2014.

[54] Kamran Eshraghian, Kyoung-Rok Cho, Omid Kavehei, Soon-Ku Kang, Derek Abbott, and Sung-Mo Steve Kang. Memristor mos content addressable memory (mcam): Hybrid architecture for future high performance search engines. *IEEE Transactions on Very Large Scale Integration (VLSI) Systems*, 19(8):1407–1417, 2010.

[55] Said Hamdioui, Lei Xie, Hoang Anh Du Nguyen, Mottaqiallah Taouil, Koen Bertels, Henk Corporaal, Hailong Jiao, Francky Catthoor, Dirk Wouters, Linn Eike, et al. Memristor based computation-in-memory architecture for data-intensive applications. In *2015 Design, Automation & Test in Europe Conference & Exhibition (DATE)*, pages 1718–1725. IEEE, 2015.

[56] ShuKai Duan, XiaoFang Hu, LiDan Wang, ChuanDong Li, and Pinaki Mazumder. Memristor-based rram with applications. *Science China Information Sciences*, 55(6):1446–1460, 2012.

[57] Shukai Duan, Xiaofang Hu, Zhekang Dong, Lidan Wang, and Pinaki Mazumder. Memristor-based cellular nonlinear/neural network: design, analysis, and applications. *IEEE transactions on neural networks and learning systems*, 26(6):1202–1213, 2014.

[58] Andy Thomas. Memristor-based neural networks. *Journal of Physics D: Applied Physics*, 46(9):093001, 2013.

[59] Shyam Prasad Adhikari, Changju Yang, Hyongsuk Kim, and Leon O Chua. Memristor bridge synapse-based neural network and its learning. *IEEE Transactions on Neural Networks and Learning Systems*, 23(9):1426–1435, 2012.

[60] Sung Hyun Jo, Ting Chang, Idongesit Ebong, Bhavitavya B Bhadviya, Pinaki Mazumder, and Wei Lu. Nanoscale memristor device as synapse in neuromorphic systems. *Nano letters*, 10(4):1297–1301, 2010.

[61] Bernabé Linares-Barranco and Teresa Serrano-Gotarredona. Memristance can explain spike-time-dependent-plasticity in neural synapses. *Nature precedings*, pages 1–1, 2009.

[62] Greg S Snider. Spike-timing-dependent learning in memristive nanodevices. In *Proceedings of the 2008 IEEE International Symposium on Nanoscale Architectures*, pages 85–92. IEEE Computer Society, 2008.

[63] Myonglae Chu, Byoungho Kim, Sangsu Park, Hyunsang Hwang, Moongu Jeon, Byoung Hun Lee, and Byung-Geun Lee. Neuromorphic hardware system for visual pattern recognition with memristor array and cmos neuron. *IEEE Transactions on Industrial Electronics*, 62(4):2410–2419, 2014.

[64] Chris Yakopcic, Raqibul Hasan, and Tarek M Taha. Flexible memristor based neuromorphic system for implementing multi-layer neural network algorithms. *International Journal of Parallel, Emergent and Distributed Systems*, 33(4):408–429, 2018.

[65] Yuriy V Pershin and Massimiliano Di Ventra. Practical approach to programmable analog circuits with memristors. *IEEE Transactions on Circuits and Systems I: Regular Papers*, 57(8):1857–1864, 2010.

[66] Julien Borghetti, Gregory S Snider, Philip J Kuekes, J Joshua Yang, Duncan R Stewart, and R Stanley Williams. 'memristive'switches enable 'stateful'logic operations via material implication. *Nature*, 464(7290):873–876, 2010.

[67] Sangho Shin, Kyungmin Kim, and Sung-Mo Kang. Memristor applications for programmable analog ics. *IEEE Transactions on Nanotechnology*, 10(2):266–274, 2010.

[68] James Hutchinson, Christof Koch, Jin Luo, and Carver Mead. Computing motion using analog and binary resistive networks. *Computer*, 21(3):52–63, 1988.

[69] İ Cem Göknar, Fatih Öncül, and Elham Minayi. New memristor applications: Am, ask, fsk, and bpsk modulators. *IEEE Antennas and Propagation Magazine*, 55(2):304–313, 2013.

[70] Hyongsuk Kim, Maheshwar Pd Sah, Changju Yang, Tamás Roska, and Leon O Chua. Memristor bridge synapses. *Proceedings of the IEEE*, 100(6):2061–2070, 2011.

[71] Sylvain Saïghi, Christian G Mayr, Teresa Serrano-Gotarredona, Heidemarie Schmidt, Gwendal Lecerf, Jean Tomas, Julie Grollier, Sören Boyn, Adrien F Vincent, Damien Querlioz, et al. Plasticity in memristive devices for spiking neural networks. *Frontiers in neuroscience*, 9:51, 2015.

[72] Gwendal Lecerf, Jean Tomas, Sören Boyn, Stéphanie Girod, Ashwin Mangalore, Julie Grollier, and Sylvain Saïghi. Silicon neuron dedicated to memristive spiking neural networks. In *2014 IEEE International Symposium on Circuits and Systems (ISCAS)*, pages 1568–1571. IEEE, 2014.

[73] Sören Boyn, Julie Grollier, Gwendal Lecerf, Bin Xu, Nicolas Locatelli, Stéphane Fusil, Stéphanie Girod, Cécile Carrétéro, Karin Garcia, Stéphane Xavier, et al. Learning through ferroelectric domain dynamics in solid-state synapses. *Nature communications*, 8(1):1–7, 2017.

[74] Mirko Prezioso, F Merrikh Bayat, Brian Hoskins, K Likharev, and Dmitri Strukov. Self-adaptive spike-time-dependent plasticity of metal-oxide memristors. *Scientific reports*, 6(1):1–6, 2016.

[75] Changhong Wang, Wei He, Yi Tong, and Rong Zhao. Investigation and manipulation of different analog behaviors of memristor as electronic synapse for neuromorphic applications. *Scientific reports*, 6:22970, 2016.

[76] TD Dongale, ND Desai, KV Khot, CK Volos, PN Bhosale, and RK Kamat. An electronic synapse device based on tio2 thin film memristor. *Journal of Nanoelectronics and Optoelectronics*, 13(1):68–75, 2018.

[77] Yi Li, Yingpeng Zhong, Jinjian Zhang, Lei Xu, Qing Wang, Huajun Sun, Hao Tong, Xiaoming Cheng, and Xiangshui Miao. Activity-dependent synaptic plasticity of a chalcogenide electronic synapse for neuromorphic systems. *Scientific reports*, 4:4906, 2014.

[78] Luis A Camuñas-Mesa, Bernabé Linares-Barranco, and Teresa Serrano-Gotarredona. Neuromorphic spiking neural networks and their memristor-cmos hardware implementations. *Materials*, 12(17):2745, 2019.

[79] Valerio Milo, Gerardo Malavena, Christian Monzio Compagnoni, and Daniele Ielmini. Memristive and cmos devices for neuromorphic computing. *Materials*, 13(1):166, 2020.

[80] Rui Wang, Tuo Shi, Xumeng Zhang, Wei Wang, Jinsong Wei, Jian Lu, Xiaolong Zhao, Zuheng Wu, Rongrong Cao, Shibing Long, et al. Bipolar analog memristors as artificial synapses for neuromorphic computing. *Materials*, 11(11):2102, 2018.

[81] Dániel Hajtó, Ádám Rák, and György Cserey. Robust memristor networks for neuromorphic computation applications. *Materials*, 12(21):3573, 2019.

[82] Marta Pedró, Javier Martín-Martínez, Marcos Maestro-Izquierdo, Rosana Rodríguez, and Montserrat Nafría. Self-organizing neural networks based on oxram devices under a fully unsupervised training scheme. *Materials*, 12(21):3482, 2019.

[83] Wookyung Sun, Sujin Choi, Bokyung Kim, and Junhee Park. Three-dimensional (3d) vertical resistive random-access memory (vrram) synapses for neural network systems. *Materials*, 12(20):3451, 2019.

[84] Agustín Cisternas Ferri, Alan Rapoport, Pablo I Fierens, German A Patterson, Enrique Miranda, and Jordi Suñé. On the application of a diffusive memristor compact model to neuromorphic circuits. *Materials*, 12(14):2260, 2019.

[85] Zhengwu Liu, Jianshi Tang, Bin Gao, Xinyi Li, Peng Yao, Yudeng Lin, Dingkun Liu, Bo Hong, He Qian, and Huaqiang Wu. Multichannel parallel processing of neural signals in memristor arrays. *Science advances*, 6(41):eabc4797, 2020.

[86] Peng Yao, Huaqiang Wu, Bin Gao, Jianshi Tang, Qingtian Zhang, Wenqiang Zhang, J Joshua Yang, and He Qian. Fully hardware-implemented memristor convolutional neural network. *Nature*, 577(7792):641–646, 2020.

[87] Yang Lu, Ana Alvarez, Chung-Ho Kao, Jong-Shing Bow, San-Yuan Chen, and I-Wei Chen. An electronic silicon-based memristor with a high switching uniformity. *Nature Electronics*, 2(2):66–74, 2019.

[88] Serge Dos Santos, Ali Masood, Sadataka Furui, and Giuseppe Nardoni. Self-calibration of multiscale hysteresis with memristors in nonlinear time reversal based processes. In *2018 16th Biennial Baltic Electronics Conference (BEC)*, pages 1–4. IEEE, 2018.

[89] Serge Dos Santos and Sadataka Furui. A memristor based ultrasonic transducer: The memosducer. In *2016 IEEE International Ultrasonics Symposium (IUS)*, pages 1–4. IEEE, 2016.

[90] Massimiliano Di Ventra, Yuriy V Pershin, and Leon O Chua. Circuit elements with memory: memristors, memcapacitors, and meminductors. *Proceedings of the IEEE*, 97(10):1717–1724, 2009.

[91] ZhenYu Yin, Heng Tian, GuanHua Chen, and Leon O Chua. What are memristor, memcapacitor, and meminductor? *IEEE Transactions on Circuits and Systems II: Express Briefs*, 62(4):402–406, 2015.

[92] L. Chua. Memristor and memristive systems symposium, Univ.California, Berkeley, CA, USA, 2008.

[93] Guy Z Cohen, Yuriy V Pershin, and Massimiliano Di Ventra. Lagrange formalism of memory circuit elements: Classical and quantum formulations. *Physical Review B*, 85(16):165428, 2012.

[94] Massimiliano Di Ventra and Yuriy V Pershin. Memory materials: a unifying description. *Materials Today*, 14(12):584–591, 2011.

[95] Yu V Pershin, J Martinez-Rincon, and M Di Ventra. Memory circuit elements: from systems to applications. *Journal of Computational and Theoretical Nanoscience*, 8(3):441–448, 2011.

[96] Yuriy V Pershin and Massimiliano Di Ventra. Neuromorphic, digital, and quantum computation with memory circuit elements. *Proceedings of the IEEE*, 100(6):2071–2080, 2011.

[97] Massimiliano Di Ventra and Yuriy V Pershin. Biologically-inspired electronics with memory circuit elements. In *Advances in Neuromorphic Memristor Science and Applications*, pages 15–36. Springer, 2012.

[98] DJ Kim, H Lu, S Ryu, C-W Bark, C-B Eom, EY Tsymbal, and A Gruverman. Ferroelectric tunnel memristor. *Nano letters*, 12(11):5697–5702, 2012.

[99] Zhongqiang Hu, Qian Li, Meiya Li, Qiangwen Wang, Yongdan Zhu, Xiaolian Liu, Xingzhong Zhao, Yun Liu, and Shuxiang Dong. Ferroelectric memristor based on pt/bifeo3/nb-doped srtio3 heterostructure. *Applied Physics Letters*, 102(10):102901, 2013.

[100] Victor Erokhin, Tatiana Berzina, and Marco P Fontana. Hybrid electronic device based on polyaniline-polyethyleneoxide junction. *Journal of applied physics*, 97(6):064501, 2005.

[101] Xiaobin Wang, Yiran Chen, Haiwen Xi, Hai Li, and Dimitar Dimitrov. Spintronic memristor through spin-torque-induced magnetization motion. *IEEE electron device letters*, 30(3):294–297, 2009.

[102] Yu V Pershin and Massimiliano Di Ventra. Spin memristive systems: Spin memory effects in semiconductor spintronics. *Physical Review B*, 78(11):113309, 2008.

[103] Santosh Murali, Jaana S Rajachidambaram, Seung-Yeol Han, Chih-Hung Chang, Gregory S Herman, and John F Conley Jr. Resistive switching in zinc–tin-oxide. *Solid-state electronics*, 79:248–252, 2013.

[104] R. Stanley Williams. Finding the missing memristor.

[105] XiaoFang Hu, ShuKai Duan, LiDan Wang, and XiaoFeng Liao. Memristive crossbar array with applications in image processing. *Science China Information Sciences*, 55(2):461–472, 2012.

[106] Matthew D Pickett, Dmitri B Strukov, Julien L Borghetti, J Joshua Yang, Gregory S Snider, Duncan R Stewart, and R Stanley Williams. Switching dynamics in titanium dioxide memristive devices. *Journal of Applied Physics*, 106(7):074508, 2009.

[107] Yogesh N Joglekar and Stephen J Wolf. The elusive memristor: properties of basic electrical circuits. *European Journal of Physics*, 30(4):661, 2009.

[108] Themistoklis Prodromakis, Boon Pin Peh, Christos Papavassiliou, and Christofer Toumazou. A versatile memristor model with nonlinear dopant kinetics. *IEEE transactions on electron devices*, 58(9):3099–3105, 2011.

[109] Valeriy A Slipko and Yuriy V Pershin. Importance of the window function choice for the predictive modelling of memristors. *IEEE Transactions on Circuits and Systems II: Express Briefs*, 2019.

[110] S Benderli and TA Wey. On spice macromodelling of tio 2 memristors. *Electronics letters*, 45(7):377–379, 2009.

[111] Zdeněk Biolek, Dalibor Biolek, and Viera Biolkova. Spice model of memristor with nonlinear dopant drift. *Radioengineering*, 18(2), 2009.

[112] Shahar Kvatinsky, Eby G Friedman, Avinoam Kolodny, and Uri C Weiser. Team: Threshold adaptive memristor model. *IEEE Transactions on Circuits and Systems I: Regular Papers*, 60(1):211–221, 2012.

[113] TA Anusudha and SRS Prabaharan. A versatile window function for linear ion drift memristor model–a new approach. *AEU-International Journal of Electronics and Communications*, 90:130–139, 2018.

[114] Shahar Kvatinsky, Keren Talisveyberg, Dmitry Fliter, Avinoam Kolodny, Uri C Weiser, and Eby G Friedman. Models of memristors for spice simulations. In *2012 IEEE 27th Convention of Electrical and Electronics Engineers in Israel*, pages 1–5. IEEE, 2012.

[115] Juntang Yu, Xiaomu Mu, Xiangming Xi, and Shuning Wang. A memristor model with piecewise window function. *Radioengineering*, 22(4):969–974, 2013.

[116] Yasuhiro Takahashi, Toshikazu Sekine, and Michio Yokoyama. Spice model of memristive device using tukey window function. *IEICE Electronics Express*, 12(5):20150149–20150149, 2015.

[117] Rabab Farouk Abdel-Kader and Sherif M Abuelenin. Memristor model based on fuzzy window function. In *2015 IEEE International Conference on Fuzzy Systems (FUZZ-IEEE)*, pages 1–5. IEEE, 2015.

[118] Jinxiang Zha, He Huang, and Yujie Liu. A novel window function for memristor model with application in programming analog circuits. *IEEE Transactions on Circuits and Systems II: Express Briefs*, 63(5):423–427, 2015.

[119] Jeetendra Singh and Balwinder Raj. An accurate and generic window function for nonlinear memristor models. *Journal of Computational Electronics*, 18(2):640–647, 2019.

[120] Panayiotis S Georgiou, Sophia N Yaliraki, Emmanuel M Drakakis, and Mauricio Barahona. Window functions and sigmoidal behaviour of memristive systems. *International Journal of Circuit Theory and Applications*, 44(9):1685–1696, 2016.

[121] Yuriy V Pershin and Massimiliano Di Ventra. Spice model of memristive devices with threshold. *arXiv preprint arXiv:1204.2600*, 2012.

[122] Shahar Kvatinsky, Misbah Ramadan, Eby G Friedman, and Avinoam Kolodny. Vteam: A general model for voltage-controlled memristors. *IEEE Transactions on Circuits and Systems II: Express Briefs*, 62(8):786–790, 2015.

[123] Shahar Kvatinsky, Keren Talisveyberg, Dmitry Fliter, Eby G Friedman, Avinoam Kolodny, and Uri C Weiser. Verilog-a for memristor models. *CCIT Technical Report*, 801, 2011.

[124] Dalibor Biolek, Zdenek Biolek, and Viera Biolkova. Spice modeling of memristive, memcapacitative and meminductive systems. In *2009 European Conference on Circuit Theory and Design*, pages 249–252. IEEE, 2009.

[125] Ahmed Gomaa Radwan, M Affan Zidan, and KN Salama. Hp memristor mathematical model for periodic signals and dc. In *2010 53rd IEEE International Midwest Symposium on Circuits and Systems*, pages 861–864. IEEE, 2010.

[126] Ádám Rák and György Cserey. Macromodeling of the memristor in spice. *IEEE Transactions on Computer-Aided Design of Integrated Circuits and Systems*, 29(4):632–636, 2010.

[127] Juraj Valsa, Dalibor Biolek, and Zdeněk Biolek. An analogue model of the memristor. *International Journal of Numerical Modelling: Electronic Networks, Devices and Fields*, 24(4):400–408, 2011.

[128] Carlos Sánchez-López, Jorge Mendoza-Lopez, MA Carrasco-Aguilar, and Carlos Muñiz-Montero. A floating analog memristor emulator circuit. *IEEE Transactions on Circuits and Systems II: Express Briefs*, 61(5):309–313, 2014.

[129] Wang Xiao-Yuan, Andrew L Fitch, Herbert HC Iu, Victor Sreeram, and Qi Wei-Gui. Implementation of an analogue model of a memristor based on a light-dependent resistor. *Chinese Physics B*, 21(10):108501, 2012.

[130] DALIBOR Biolek, VIERA Biolkova, ZDENEK Kolka, and ZDENEK Biolek. Passive fully floating emulator of memristive device for laboratory experiments. *Advances in Electrical and Computer Engineering*, 2015.

[131] Hyongsuk Kim, Maheshwar Pd Sah, Changju Yang, Seongik Cho, and Leon O Chua. Memristor emulator for memristor circuit applications. *IEEE Transactions on Circuits and Systems I: Regular Papers*, 59(10):2422–2431, 2012.

[132] KNOWM. Sdc memristor development history.

[133] Leon O Chua and Lin Yang. Cellular neural networks: Theory. *IEEE Transactions on circuits and systems*, 35(10):1257–1272, 1988.

[134] Leon O Chua and Lin Yang. Cellular neural networks: Applications. *IEEE Transactions on circuits and systems*, 35(10):1273–1290, 1988.

[135] Jean-Christophe Comte, Patrick Marquié, Jean-Marie Bilbault, and Stéphane Binczak. Noise removal using a nonlinear two-dimensional diffusion network. In *Annales des télécommunications*, volume 53, pages 483–487. Springer, 1998.

[136] Patrick Marquié, Stéphane Binczak, Jean-Christophe Comte, Bernard Michaux, and Jean-Marie Bilbault. Diffusion effects in a nonlinear electrical lattice. *Physical Review E*, 57(5):6075, 1998.

[137] Jean-Christophe Comte, Patrick Marquié, and Jean-Marie Bilbault. Contour detection based on nonlinear discrete diffusion in a cellular nonlinear network. *International Journal of Bifurcation and Chaos*, 11(01):179–183, 2001.

[138] Stéphane Binczak, Jean-Marie Bilbault, and Patrick Marquié. Pattern dynamics in a nonlinear electrical lattice. *International Journal of Bifurcation and Chaos*, 13(02):483–492, 2003.

[139] Stéphane Binczak and Jean-Marie Bilbault. Experimental propagation failure in a nonlinear electrical lattice. *International Journal of Bifurcation and Chaos*, 14(05):1819–1830, 2004.

[140] Mauro Di Marco, Mauro Forti, and Luca Pancioni. Complete stability of feedback cnns with dynamic memristors and second-order cells. *International Journal of Circuit Theory and Applications*, 44(11):1959–1981, 2016.

[141] Eero Lehtonen and Mika Laiho. Cnn using memristors for neighborhood connections. In *2010 12th International Workshop on Cellular Nanoscale Networks and their Applications (CNNA 2010)*, pages 1–4. IEEE, 2010.

[142] Alon Ascoli, Valentina Lanza, Fernando Corinto, and Ronald Tetzlaff. Synchronization conditions in simple memristor neural networks. *Journal of the Franklin Institute*, 352(8):3196–3220, 2015.

[143] Fei Xu, Jiqian Zhang, Tingting Fang, Shoufang Huang, and Maosheng Wang. Synchronous dynamics in neural system coupled with memristive synapse. *Nonlinear dynamics*, 92(3):1395–1402, 2018.

[144] Jihong Zhang and Xiaofeng Liao. Synchronization and chaos in coupled memristor-based fitzhugh-nagumo circuits with memristor synapse. *Aeu-international journal of electronics and communications*, 75:82–90, 2017.

[145] Bocheng Bao, Qinfeng Yang, Dong Zhu, Yunzhen Zhang, Quan Xu, and Mo Chen. Initial-induced coexisting and synchronous firing activities in memristor synapse-coupled morris–lecar bi-neuron network. *Nonlinear Dynamics*, 99(3):2339–2354, 2020.

[146] Ch K Volos, IM Kyprianidis, IN Stouboulos, E Tlelo-Cuautle, and S Vaidyanathan. Memristor: A new concept in synchronization of coupled neuromorphic circuits. *Journal of Engineering Science & Technology Review*, 8(2), 2015.

[147] John Paul Strachan, Dmitri B Strukov, Julien Borghetti, J Joshua Yang, Gilberto Medeiros-Ribeiro, and R Stanley Williams. The switching location of a bipolar memristor: chemical, thermal and structural mapping. *Nanotechnology*, 22(25):254015, 2011.

[148] Patryk Krzysteczko, Günter Reiss, and Andy Thomas. Memristive switching of mgo based magnetic tunnel junctions. *Applied Physics Letters*, 95(11):112508, 2009.

[149] JM Teixeira, J Ventura, R Fermento, JP Araujo, JB Sousa, P Wisniowski, and PP Freitas. Electroforming, magnetic and resistive switching in mgo-based tunnel junctions. *Journal of Physics D: Applied Physics*, 42(10):105407, 2009.

[150] Chikako Yoshida, Masaki Kurasawa, Young Min Lee, Masaki Aoki, and Yoshihiro Sugiyama. Unipolar resistive switching in co fe b/ mg o/ co fe b magnetic tunnel junction. *Applied Physics Letters*, 92(11):113508, 2008.

[151] Hsin-Hung Huang, Wen-Chieh Shih, and Chih-Huang Lai. Nonpolar resistive switching in the pt/mgo/pt nonvolatile memory device. *Applied Physics Letters*, 96(19):193505, 2010.

[152] Eike Linn, Roland Rosezin, Carsten Kügeler, and Rainer Waser. Complementary resistive switches for passive nanocrossbar memories. *Nature materials*, 9(5):403–406, 2010.

[153] Lei Yin, Ruiqing Cheng, Zhenxing Wang, Feng Wang, Marshet Getaye Sendeku, Yao Wen, Xueying Zhan, and Jun He. Two-dimensional unipolar memristors with logic and memory functions. *Nano letters*, 20(6):4144–4152, 2020.

[154] J Joshua Yang, Matthew D Pickett, Xuema Li, Douglas AA Ohlberg, Duncan R Stewart, and R Stanley Williams. Memristive switching mechanism for metal/oxide/metal nanodevices. *Nature nanotechnology*, 3(7):429, 2008.

[155] John G Simmons. Electric tunnel effect between dissimilar electrodes separated by a thin insulating film. *Journal of applied physics*, 34(9):2581–2590, 1963.

[156] John G Simmons. Generalized formula for the electric tunnel effect between similar electrodes separated by a thin insulating film. *Journal of applied physics*, 34(6):1793–1803, 1963.

[157] JG Simmons. Conduction in thin dielectric films. *Journal of Physics D: Applied Physics*, 4(5):613, 1971.

[158] Feijun Jiang and Bertram E Shi. The memristive grid outperforms the resistive grid for edge preserving smoothing. In *2009 European Conference on Circuit Theory and Design*, pages 181–184. IEEE, 2009.

[159] Alexander Serb, Ali Khiat, and Themistoklis Prodromakis. Practical demonstration of a memristive fuse. *arXiv preprint arXiv:1609.02410*, 2016.

[160] Andras Gelencser, Themistoklis Prodromakis, Christofer Toumazou, and Tamas Roska. A biomimetic model of the outer plexiform layer by incorporating memristive devices. *Physical Review E*, 85(4):041918, 2012.

[161] Melih Yildirim, Yunus Babacan, and Firat Kacar. Memristive retinomorphic grid architecture removing noise and preserving edge. *AEU-International Journal of Electronics and Communications*, 97:38–44, 2018.

[162] Changju Yang and Hyongsuk Kim. Linearized programming of memristors for artificial neuro-sensor signal processing. *Sensors*, 16(8):1320, 2016.

[163] Chuan Kai Kenneth Lim, A Gelencser, and T Prodromakis. Computing image and motion with 3-d memristive grids. In *Handbook of Memristor Networks*, pages 1177–1210. Springer, 2019.

[164] Arturo Sarmiento-Reyes and Yojanes Rodríguez-Velásquez. Maze-solving with a memristive grid of charge-controlled memristors. In *2018 IEEE 9th Latin American Symposium on Circuits & Systems (LASCAS)*, pages 1–4. IEEE, 2018.

[165] Yuriy V Pershin and Massimiliano Di Ventra. Solving mazes with memristors: A massively parallel approach. *Physical Review E*, 84(4):046703, 2011.

[166] Mohamed E Fouda, Moustafa A Khatib, Ahmed G Mosad, and Ahmed G Radwan. Generalized analysis of symmetric and asymmetric memristive two-gate relaxation oscillators. *IEEE Transactions on Circuits and Systems I: Regular Papers*, 60(10):2701–2708, 2013.

[167] Jinichi Nagumo, Suguru Arimoto, and Shuji Yoshizawa. An active pulse transmission line simulating nerve axon. *Proceedings of the IRE*, 50(10):2061–2070, 1962.

List of Figures

1.1 Memristance analogy to water flow through a pipe of varying diameter: where d is a diameter such that: $d_1 \gg d_2$. 5

1.2 2D cellular nonlinear networks (CNN). C is a linear capacitor and R_{NL} is a nonlinear resistance. (**a**) Coupling using linear resistance R and (**b**) coupling using memristor M. 7

2.1 Display of some basic electronic components. 9

2.2 Symmetrical view of the four basic circuit elements and their correlations with the four circuit variables. 10

2.3 Different configurations of resistors. (a) Electronic symbol of resistor, surface mount resistor (or chip resistor) and other configurations depending upon applications. (b) Some examples of variable resistors. (c) Nonlinear resistors. 12

2.4 Geometry viewpoint of a resistor made up of uniformly conductive wire: A and L are the cross-sectional area and the length of the material respectively. 13

2.5 Different configurations of capacitors. (a) Electronic symbol of capacitor, surface mount capacitor (or chip capacitor) and other configurations. (b) Different types of capacitors. 16

2.6 Geometrical viewpoint of a capacitor. 19

2.7 Air core inductor (left) has less inductance and iron core inductor (right) has more inductance 20

2.8 Different configurations of inductors. (a) Electronic symbol of inductor, SMD inductors (or inductor chips) and other configurations. (b) Different types of inductors. . . 20

2.9 Geometry viewpoint of an inductor. 22

2.11 Memristance expression from a ϕ-q curve. Remark that, due to integration constants, this curve can be shifted horizontally and/or vertically. 25

2.12 Testing memristor device as a black box (left) and current-voltage response of the black box (right). 27

2.13 Demonstration of a memristor fingerprint for $R_{on} = 100\Omega$, $R_{off} = 16K\Omega$, $f_o = 1Hz$, $\omega_o = 2\pi f_o$ and $v(t) = 1.2sin(\omega t)$: $\omega = \omega_o$, $\omega = 2\omega_o$ and $\omega = 10\omega_o$. 29

2.14 (a) Self-crossing or transversal pinched hysteresis loop (PHL) and (b) Tangential or non-transversal pinched hysteresis loop (PHL). 31

2.15 Effect of increasing frequency on the PHL lobe area. (a) Hysteresis lobe area shrinkage due to the increase in the input frequency and (b) PHL lobe area versus frequency. 33

2.16 Calculating the area of PHL. 33

2.17 Memristor operating point from the constitutive relationship. 34

2.18 Third fingerprint illustration for tenfold increase in frequency: $\omega = 10\omega_o$, $\theta_2 \approx 0$. . . . 36

2.19 Memristor subjected to current and voltage excitation respectively 38

2.20 Results of Example 1: $I_o = 1A$, $f = 4Hz$, $\alpha = 1Wb.C^{-3}$, $\beta = 1mWb.C^{-1}$, (**a**)$q_0 = 0C$ and (**b**) $q_0 = 0.05C$. 39

2.21 Result obtained for example 2: $V_0 = 1V$,$f = 4Hz$, $\psi_1 = 1\ C.Wb^{-3}$, $\psi_2 = 1m\ C.Wb^{-1}$, (**a**) $\phi_0 = 0Wb$ and (**b**) $\phi_0 = 0.08Wb$. 41

2.22 Some memristor applications in analog and digital circuit [49]. 43

2.23 Simulation results comparison for the four basic passive circuit elements when $v(t) = V_0 sin(\omega t)$. r is a small resistor (say 100Ω) to allow easy measurements of the currents I_R, I_C, I_L and I_M. (**a1-a3**) Resistor $R = 920\Omega$: there is no phase difference in the $V(t)$ and I_R waveform and the I-V characteristic is a linear graph. (**b1-b3**) Capacitor $C = 12\mu F$: there is phase difference of $\frac{\pi}{2}$ in the V and I_C waveform, i.e I_C is leading the V by $\frac{\pi}{2}$ and the I-V characteristics is a clockwise circle. (**c1-c3**) Inductor $L = 10mH$: there is phase difference of $\frac{\pi}{2}$ in the I_L and V waveform, i.e V is leading I_L by $\frac{\pi}{2}$ and the I-V characteristic is a counter clockwise circle. (**d1-d3**) Memristor M: $R_{on} = 100\Omega$, $R_{off} = 16K\Omega$, there is no phase difference in the I_m and V waveform and the I-V characteristic is a pinched hysteresis loop. 45

2.24 Experimental results of the four fundamental passive circuit elements. (**a1-a3**) $R = 1K\Omega$, (**b1-b3**) $C = 10nF$, (**c1-c3**) $L = 10mH$ and (**d1-d3**) KNOWM memristor chip. The current through each component is measured and the corresponding I-V characteristics are given. There is no phase difference in $V(t)$ and $I(t)$ waveforms for R and M, while there is a phase difference of $\frac{\pi}{2}$ for C and L. In the capacitor C, $I(t)$ is leading the $V(t)$ by $\frac{\pi}{2}$ and in an inductor L, $V(t)$ is leading $I(t)$ by $\frac{\pi}{2}$. The I-V characteristic of R is a linear graph, for C and L it is a circle (respectively with clockwise and anticlockwise) and for M it is a pinched hysteresis loop. Scales: R: time t $[0.50ms/\text{div}]$, current I $[0.31mA/\text{div}]$ and voltage V $[0.50V/\text{div}]$, C: time t $[0.50ms/\text{div}]$, current I $[0.28mA/\text{div}]$ and voltage V $[0.50V/\text{div}]$, L: time t $[20\mu s/\text{div}]$, current I $[0.31mA/\text{div}]$ and voltage V $[0.50V/\text{div}]$ and M: time t $[0.50ms/\text{div}]$, current I $[4.45\mu A/\text{div}]$ and voltage V $[1.0V/\text{div}]$. . . . 46

3.1 Some memristor fabrications technologies. 48

3.2 Geometry of HP (TiO_2) memristor. (a) Crossbar arrays of wires with memristor in each junction [3, 105]. (b) Structural view of the TiO_2 memristor, i.e enlargement of the memristor in the junction. 49

3.3 Memristor internal behavioural response. $R'_{on} = R_{on}\dfrac{w(t)}{D}$, $R'_{off} = R_{off}\left(1 - \dfrac{w(t)}{D}\right)$, $V_1 = R'_{on}i(t)$ and $V_2 = R'_{off}i(t)$. 50

3.4 Window functions comparison. (a) Proposed window function and its comparison with the discussed functions. Joglekar ($p = 1$) and Prodromakis ($p = 10$), (b) Comparison of Joglekar and Prodromakis window functions, showing the effect of varying p. 55

3.5 Analytical results of CCM with Linear model, $R_{on} = 100\Omega$, $R_{off} = 16K\Omega$, $q_d = 100\mu C$ and three different input frequencies. (a) I-V characteristics, (b) state variable, (c) state variable and memristance for $f = 1Hz$, (d) memristance. 58

3.6 Analytical results of FCM with linear dopant drift model: $R_{on} = 100\Omega$, $R_{off} = 16K\Omega$, $q_d = 100\mu C$ and different input frequencies. (a) I-V characteristics, (b) state variable, (c) state variable and memristance for $f = 1Hz$, (d) memristance. 60

3.7 Analytical results of the CCM with nonlinear dopant drift model at different input frequencies. $I_0 = 2mA$, $x_0 = 0.05$, $q_d = 100\mu C$, $R_{off} = 16K\Omega$, $R_{on} = 100\Omega$ and $\delta R = 15.9K\Omega$. (a) I-V characteristics, (b) state variable and memristance for $f = 1Hz$, (c) state variable, (d) memristance. 62

3.8 Analytical results of FCM with nonlinear dopant drift modal at different input frequencies. $v(t) = V_0 sin(\omega t)$, $V_0 = 2V$, $x_0 = 0.1$, $q_d = 100\mu C$, $R_{off} = 16K\Omega$, $R_{on} = 100\Omega$ and $\delta R = 15.9K\Omega$. (a) I-V characteristics, (b) state variable and memristance for $f = 2Hz$, (c) state variable (d) memristance. 63

3.9 Memristance versus charge for linear and nonlinear drift models (Joglekar). It shows that as p increases, the nonlinear drift model tends to the linear model. Window function gives nonlinear model. Window function, in addition to nonlinearity, also increases the dynamics of the charge (or mobile carrier thereby affected by the value of q_d, because $q_d \propto \frac{1}{\mu_v} = \hat{h}(\mu_v)$). Therefore, for a fixed device dimension (i.e D) and doping, only μ_v is affected by the window function, hence q_d. This is due to the fact that window function ensures zero drift of the mobile carrier at the boundaries, thus significantly reduces their mobility and increases q_d. 64

3.10 Nonlinear models comparison of the full memristance transition between $R_{off} = 16K\Omega$ and $R_{on} = 100\Omega$ with respect to the quantity of charge $q(t)$. The results are obtained under the same initial conditions. This is to show the amount of charge q_R needed for each model to fully transit until R_{off} and then R_{on}. Note that $p = 1$ and $p = 20$ for Joglekar and Prodromakis respectively, and $g_{max}(x) = 1$ for both models allowing for accurate comparison. (**a**) $M(q)$ versus $q(t)$ for Strukov (Stru.), Joglekar (Jogl.) and Prodromakis (Prod.). (**b**) $M(q)$ and $q(t)$ transients. 64

3.11 Nonlinear models comparison of the full memristance transition between $R_{off} = 16K\Omega$ and $R_{on} = 100\Omega$ with respect to the quantity of the flowing charge $q(t)$. It shows the amount of charge q_R needed for each model to fully transit from R_{off} to R_{on}. Note that $p = 1$ and $p = 20$ for Joglekar and Prodromakis respectively, allowing to have $g_{max}(x) = 1$ for both models. (**a**) Prodromakis (Prodr.) $q_R = 0.145mC$ with $p = 20$, (**b**) Joglekar (Jogl.) $q_R = 0.365mC$ with $p = 1$ and (**c**) Strukov (Struk.) $q_R = 1.350mC$. 65

3.12 Comparison of the linear and nonlinear dopant drift models showing for each case, the nature of the flowing currents, the I-V characteristics, the memristance and the corresponding state variable transition respectively, for (**a1-a3**) $0.7V$, (**b1-b3**) $1V$ and (**c1-c3**) $1.2V$. Where: l and nl are linear and nonlinear models abbreviations, V(t) is the input voltage, i_l and i_{nl} are the flowing currents for linear and nonlinear drift model respectively, similarly, x_l, M_l, x_{nl} and M_{nl} are the state variables and memristances for the linear and nonlinear models. 67

3.13 Comparing the effect of a window function from the circuit point of view. Our proposed new(N) function is compared with the ones by Strukov(S), Jolekar(J) and Prodromakis(P), for **(a1-a4)** $1V$, **(b1-b4)** $1.2V$ and **(c1-c4)** $1.5V$. V(t) is the input voltage, i(t) is the current, x and M(x) are state variable and memristance. See the ordinate and abscissa of each figure. 68

3.14 SPICE implementation of TiO_2 memristor model for simulation purpose. (a) Block diagram representation of the memristance function: $V = R(x)i$ and $\frac{dx}{dt} = kf(x)i$, (b) Equivalent SPICE model: E is an E-type voltage source (i.e voltage controlled voltage source), G is a G-type current source (voltage dependent current source) and R_{sh} is the shunt resistance of the integrator. 69

3.15 Simulation results of the memristor netlist file given in Table A.1. $V = V_0 sin(\omega t)$, $V_0 = 1V$, $f = 1Hz$, $R_{on} = 100\Omega$, $R_{off} = 16K\Omega$, $\mu_v = 10fm^2/(V.s)$ and $D = 10nm$, which gives $q_d = 100\mu C$. (**a**) V and i transients, (**b**) I-V characteristic, (**c**) ϕ-q curve and (**d**) memristance and state variable transitions. 70

3.16 Analogue model of memristor [127]. 71

3.17 Results of the sinusoidal input voltage. Parameters set: $R = 1k\Omega$, $C = 1\mu F$, $G_0 = 0.5S$ and $K_G = 10SV^{-1}$ (a) $V_o = 0.6V$ and variation of input frequency, $\omega_o = 2\pi f_o$ with $f_o = 1Hz$. (b) memductance for ω_o and $V_o = 0.6V$, (c) at ω_o frequency and variation of voltage amplitude V_o, (d) the flux $\phi(t)$ for ω_o and $V_o = 0.6V$. 72

3.18 Triangular input voltage. 72

3.19 Results of triangular input voltage. $V_p = 0.4V$, $f = 1Hz$, $R = 1K\Omega$, $C = 1\mu F$, $G_0 = 10S$ and $KG = 0.2SV^{-1}$. 74

3.20 Results of square wave input voltage. $V = \pm 1V$, $f = 2Hz$, $R = 1K\Omega$, $C = 1\mu F$, $G_0 = 1S$ and $KG = 5SV^{-1}$. 76

3.21 Schematic of a passive memristor emulator [130]. 76

3.22 Response of the emulator in Fig. 3.21 (a) $R = 1.5M\Omega$, $R_G = 100M\Omega$, $C = 100pF$, $R_D = 1$, $V = 3V$ at $1KHz$. (b) $R = 1M\Omega$, $R_G = 100M\Omega$, $C = 100pF$, $R_D = 1$, $V = 3V$ at $1592KHz$ (i.e cutoff frequency). The response is affected by the value of of the input frequency, and the values of R and C which make the integrator causing different phase shifts. 77

3.23 Analogue model using current transformer (CT), $I_D = I$, while $I_R = \alpha I$, α being the CT coefficient. 78

3.24 Some examples of current mirror formations. (a) N-type MOSFET, (b) P-type MOSFET and (c) Cascode current mirror [Perfect current mirror ($V_{DS_{M1}} = V_{DS_{M2}}$)]. 79

3.25 Modified passive memristor emulator with hall effect sensor. 80

4.1 Memristance transition with respect to the flowing charges. 86

4.2 (a) The voltage and current waveforms in a memristor are always in phase. However, one can see that the current is not maximum even so the causative voltage is maximum (point 2), emphasizing the nonlinear nature of the device. Points 1, 3 and 5 are the evidence of pinched hysteresis loop at (0,0) i.e $I(t) = 0$ whenever $V(t) = 0$ and vice versa. (b) Effect of initial charge q_0 on the memristor I-V characteristic, thus reflecting the memory effect of the device. $R_{off} = 16K\Omega$, $R_{on} = 100\Omega$, $I_0 = 0.15mA$, $f = 1Hz$, $\mu_v = 10f\ m^2/V.s$, $D = 10nm$, then $q_d = 100\mu C$ and $q_0 = 0.1q_d,\ 0.3q_d$ and $0.4q_d$. 87

4.3 Memristance ϕ-q curve description of eq. (4.11). The flux ϕ is a continuous function of charge q and varies according to the operating point along the ϕ-q curve. Points b, c and d define some instances of memristance given by the lines T_1, T_2 and T_3 respectively. Point b is when $q(t) < 0$ and the memristance is R_{off} given by the slope of line T_1. However, points c and d describe the memristance transition as $q(t)$ increases until $q(t) = q_d$ where the ϕ-q loci leaves the parabolic path and becomes a straight line T_3 whose slope is R_{on}. For $q(t) > q_d$, the ϕ-q loci is no longer parabolic. Note that q_f is not far from q_d, see eq. (4.12). This curve is for $\phi_0 = 0$ and $q_0 = 0$. . 89

4.4 Characteristics of the memristor model given in eq. (4.11) by using a sine current input $i(t) = I_0\ sin(\omega t)$. The result is obtained for $R_{off} = 16K\Omega$, $R_{on} = 100\Omega$, $I_0 = 1.4mA$, $\mu_v = 10^{-14}m^2/V.s$, $D = 10^{-8}m$ which gives $q_d = 100\mu C$. (a) ϕ-q curve, (b) current and voltage transients and (c) I-V characteristics. 90

4.5 Results comparison of memristance as a function of charge for the HP model and our developed cubic model. Models 1 and 2 refer to the memristance expressions in (4.6) and (4.20) respectively. The charge $q(t)$ is taken in a larger interval, for example $q(t) = [-0.2,\ 1.2] \times 10^{-4}C$. Using the parameters value in [12]: $\mu_v = 10^{-14}m^2/V.s$, $D = 10nm$, $R_{off} = 16K\Omega$, $R_{on} = 100\Omega$, gives $q_d = 100\mu C$. Thus, $\frac{dM(q)}{dq}$ in eq. (4.6) has discontinuity at $q(t) = 0$ and $q(t) = q_d$ while $\frac{dM(q)}{dq}$ in eq. (4.20) is continuous at these q values. 95

4.6 Characteristics of the memristor model given in eq. (4.20) by using a sine current input $i(t) = I_0\ sin(\omega t)$. The result is obtained for $R_{off} = 16K\Omega$, $R_{on} = 100\Omega$, $I_0 = 1mA$, $f = 4Hz$ and $q_d = 100\mu C$. (a) ϕ-q curve, (b) current and voltage transients and (c) I-V characteristics. 96

4.7 SPICE simulation results of the new memristance function (Table A.2). Values of parameters used: $R_{on} = 100\Omega$, $R_{off} = 16K\Omega$, $f = 1Hz$ and $q_d = 100\mu C$. (**a1-a3**) for $V_{\text{amp}} = 0.75V$: ϕ-q curve, I-V graph, Memristance and state variable transition, respectively. (**b1-b3**) for $V_{\text{amp}} = 1.0V$: ϕ-q curve, I-V graph, Memristance and state variable transition, respectively. (**c1-c3**) for $V_{\text{amp}} = 1.2V$: ϕ-q curve, I-V graph, Memristance and state variable transition, respectively. 96

5.1 CNN – general formation. 100

5.2 2D CNNs prior to the inclusion of memristor [137]. 100

5.3 Three possibilities of memristor based 2D CNN. (a) Using memristor for coupling, thus replacing the linear resistor, (b) Using memristor in the cell unit by replacing the nonlinear resistor and (c) Using memristor in place of both R and R_{NL} in the system. 101

5.4 RC network. (a) 2D RC CNN (b) Case study: system of two cells. 102

5.5 Response of the RC network. (a) Charge $q(t)$ evolution given by equation (5.15). (b) The current $i(t)$ flowing through the coupling resistor R, that is from master to slave. $V_{m_0} = 1V$, $V_{s_0} = 0V$, $q_0 = 0$, $R_m = R_s = 100K\Omega$, $C_m = C_s = 1\mu F$ and $R = 10K\Omega$. The current $i(t)$ is zero when $V_m(t) = V_s(t)$ and the difference $V_m(t) - V_s(t)$ becomes zero eventually. 109

5.6 Response of the RC network. The time evolution of $V_m(t)$ and $V_s(t)$ according to the three approaches: (a) Analytical solution (b) Numerical solution (c) SPICE simulation (d) Comparison of the three methods showing a strong agreement. $V_{m_0} = 1V$, $V_{s_0} = 0V$, $R_m = R_s = 100k\Omega$, $C_m = C_s = 1\mu F$ and $R = 10k\Omega$. 109

5.7 Phase portraits of the RC network showing the evolution of the flowing charge through coupling linear resistor until $V_{m_0} = V_{s_0}$ i.e $V_{m_0} - V_{s_0} = 0$ which is given by the line $\mathscr{Y} = 0$. The longest trajectory is for $V_{m_0} = 1V$ and it is interesting that the magnitudes of the flowing charge and current are exactly the same with the ones observed in Figs. 5.5a and b respectively. 109

5.8 Two cells symbolic representation coupled together by a memristor. Although the system communicates bidirectionally, however the small red arrow shows transmission preference from master to slave in order to facilitate the description of the study. 110

5.9 2D cellular nonlinear network. (**a**) Target implementation of the memristor based 2D−CNN using memristors in the coupling mode. (**b**) Circuit schematic of two cells: master (m) and slave (s) cells. Each of them comprises one capacitor and one resistor coupled by a memristor M. 111

5.10 Plot of data from table 5.1. 119

5.11 Analytical results showing the evolution of $V_m(t)$, $V_s(t)$ and $q(t)$ for Memristor coupling mode according to the analytical description (5.50) of the circuit schematic in Fig. 5.9. $R_m = R_s = 100K\Omega$, $C_m = C_s = 1\mu F$, $V(C_m) = V_{m_0} = 1V$ and $V(C_s) = V_{s_0} = 0V$. Memristor parameters: $R_{off} = 16K\Omega$, $R_{on} = 100\Omega$, $D = 10^{-8}m$, $\mu_v = 10^{-14}m^2/V.s$ and $q_0 = 0.3\ q_d$. (**a**) $q(t)$ evolution, (**b**) $V_m(t)$ and $V_s(t)$ evolution. 121

5.12 Comparison - Memristor coupling mode with linear resistors in the cell unit: $V_m(t)$ and $V_s(t)$ versus time for the three approaches. $R_m = R_s = 100K\Omega$, $C_m = C_s = 1\mu F$, $V(C_m) = V_{m_0} = 1V$ and $V(C_s) = V_{s_0} = 0V$. Memristor parameters: $R_{off} = 16K\Omega$, $R_{on} = 100\Omega$, $D = 10^{-8}m$, $\mu_v = 10^{-14}m^2/V.s$, $R_{init} = 11K\Omega$ and $q_0 = 0.3\ q_d$. 121

5.13 Evolution of $V_m(t)$ and $V_s(t)$ showing the effect of initial memristance given by different q_0 instantiations i.e $q_0 = 0.1q_d$, $q_0 = 0.3q_d$ and $q_0 = 0.9q_d$ resectively. At $t = 0$, $V_m(t = 0) = V_{m_0} = 1V$, $V_s(t = 0) = V_{s_0} = 0V$, meanwhile $R_m = R_s = 100K\Omega$, $C_m = C_s = 1\mu F$, $R_{off} = 16K\Omega$, $R_{on} = 100\Omega$ and memristor technology parameters as suggested in [12]. 123

5.14 Time evolution of $V_m(t)$ and $V_s(t)$ and the corresponding charge $q(t)$ for $q_0 = [0.1q_d,\ 0.5q_d,\ 0.9q_d]$. 123

5.15 Variation of $V_{m_0} - V_{s_0}$ for a fixed (q_0). Expectantly, $q(t)$ slightly increases with increases in $(V_{m_0} - V_{s_0})$. The simulation time is determined by $q(t)$ and $(V_{m_0} - V_{s_0})$. Similarly, $V_m(t)$ and $V_s(t)$ fit the output data as shown in the plot window of each case.124

5.16 Illustration of some roots for $P_4(X)$ according to a value of h. (**a**) No real root, (**b**) double real root, the cubic functions are respectively for $X^3 - \frac{3}{2}X + \gamma_1$ and $X^3 - \frac{3}{2}X + \gamma_2$, (**c**) 2 distinct real roots and (**d**) 4 real roots. 141

5.17 Phase portraits for $Y_0 > 0$, describing the system dynamics from left to right, toward the equilibrium points with $Y = 0$. Each trajectory corresponds to a specific initial condition of the system. The trajectory in black is for $(X_0 \le X < 0)$, the ones in orange, green and pink are for $(X_0 < 0$ and $X(t \to \infty) < 1)$ and the one in blue is for $(X_0 < 0$ and $X(t \to \infty) > 1)$. 145

5.18 Phase portraits for $Y_0 < 0$ describing the system dynamics from right to left, toward equilibrium states with $Y = 0$. The trajectories in blue and pink are for $(1 < X \le X_0)$, the one in green is for $(X_0 > 1$ and $0 < X(t \to \infty) < 1)$, in orange is for $(0 < X \le X_0 < 1)$ and in black is for $(X_0 < 1$ and $X(t \to \infty) < 0)$. 146

5.19 Time evolution of $V_m(t)$ and $V_s(t)$ according to: (a) Analytical description, (b) SPICE circuit simulation, (c) Numerical solution with MatLab and (d) Comparison of the three methods. Here $V_{m_0} = 17V$, $V_{s_0} = -15V$, $q_0 = -50\mu C$, which corresponds to case A3 (blue line in Fig. 5.17) and $h = 6.682$. 148

5.20 Concentration of the dopants in relation to charge carrier mobility with respect to the polarity of input signal. **(a)** Virgin memristor, **(b)** symbolic representation, **(c)** application of positive bias causes the expansion of the doped region through the bulk of the device, **(d)** application of negative bias causes the contraction of the doped region [107]. Respectively, the overall process affects the device conducting channel widths w_p and w_n, and it gives the trend on how w approaches 0 or D, **(e)** the currents I_1 and I_2 through M_1 and M_2 respectively, and the corresponding I-V curves for $V(t) = V_o\ sin(\omega t)$, $V_o = 1V$, $R_{off} = 16K\Omega$ and $R_{on} = 100\Omega$. Reversing the polarity of the memristor also affects the absolute value of the following current. The I-V curve of the current $I_2(t)$ falls in the second and fourth quadrants due to the reversed polarity of the input voltage $V(t)$. 151

5.21 Memristor asymmetry from circuit point of view: two charged RC cells coupled together by a memristor. The circuit is invoked at time $t = 0$ by switchs S_1 and S_2. The cells are at different potentials so that the current $i(t)$ will flow through the memristor. The test is done for $V_1 > V_2$ and then $V_1 < V_2$. For example $V_1 = 1V,\ V_2 = 0V$ and then $V_1 = 0V,\ V_2 = 1V$. The voltage across the memristor is $V_m(t)$. (**a**) Cond-1 and $V_m(t) = V_1(t) - V_2(t)$. (**b**) Cond-2 and $V_m(t) = V_2(t) - V_1(t)$. 152

5.22 The interaction of the cells according to Cond-1 (solid curves) and Cond-2 (dash curves) for $q_0 = 38\mu C$, $R_{on} = 100\Omega$, $R_{off} = 16K\Omega$ with $V_{1_0} = 1V$, $V_{2_0} = 0V$ for Cond-1 and $V_{1_0} = 0V$, $V_{2_0} = 1V$ for Cond-2. **(a)** Memristance transition, **(b)** time evolution of $V_1(t)$ and $V_2(t)$. 153

5.23 System evolution using two different initial charges $q_{0_1} = 46\mu C$ and $q_{0_2} = 31\mu C$ with $V_{1_0} = 1V$, $V_{2_0} = 0V$ for Cond-1 (solid curves) and $V_{1_0} = 0V$, $V_{2_0} = 1V$ for Cond-2 (dash curves). **(a)** Memristance transition showing the variation effect of the initial charge, **(b)** the corresponding evolution of $V_1(t)$ and $V_2(t)$. 153

5.24 The effect of changing the initial voltage. $V_{0_a} = 1V$ and $V_{0_b} = 1.5V$ are the initial conditions of the cells and the initial charge $q_0 = 33.8\mu C$. For the black curve, $V_{1_0} = V_{0_a}$ and $V_{2_0} = 0V$ (solid) (and then $V_{1_0} = 0V$ and $V_{2_o} = V_{0_a}$ (dash)), meanwhile for the magenta one, $V_{1_0} = V_{0_b}$ and $V_{2_0} = 0V$ (solid) (and then $V_{1_0} = 0V$ and $V_{2_0} = V_{0_b}$ (dash)). **(a)** Memristance transition, **(b)** Voltage evolution. 154

5.25 The current flowing through the memristor, evolution of $V_1(t)$ and $V_2(t)$ for cells 1 and 2 respectively, and the voltage across the memristor $V_m(t)$. No current flows through the memristor when $V_1(t) = V_2(t)$ and the voltage across the memristor is also zero. $V_1(t)$ and $V_2(t)$ eventually decay to zero due to the resistive nature of the cells. (**a1** & **a2**) $V_{0_a} = 1V$ and (**b1** & **b2**) $V_{0_b} = 1.5V$. 154

5.26 Cond-1: the flowing charge and the corresponding memristance evolution. $V_{1_0} = 2V$, $V_{2_0} = 0V$, $R = 100K\Omega$, $C = 1\mu C$, $R_{off} = 16K\Omega$, $R_{on} = 100\Omega$ and $q_d = 100\mu C$. . . . 155

5.27 Phase portraits for cases A1 to B6, showing the charge evolution from left to right for $Y_0 > 0$ and from right to left for $Y_0 < 0$ under different initial conditions. For $X \le 0$ and $X \ge 1$ the memristance is constant, hence the curves happen to be parallel emphasizing a constant slope at the regions. The lack of symmetry is noticeable within the bulk of the device. 155

5.28 Four possible series connections of two memristors with respect to the input source. Memristive effect is retained for cases 1 and 2 whereas it is balanced for cases 3 and 4 [107]. Although cases 3 and 4 both formed a memristor fuse, case 3 is commonly considered as memristor fuse formation [160]. 156

5.29 Circuit response comparison of a memristor fuse with standalone memristors. **(a)** Circuit schematic with a sine input voltage source. M_p is the memristor with positive polarity preference, M_n with negative polarity preference and M_f is the memristor fuse, **(b)** current-voltage characteristics for M_p (red), M_n (orange) and M_f (black). . 157

5.30 Schematic of a memristor fuse formed by 2 TiO_2 memristors M_1 and M_2. The positive spot signifies the positive oxygen vacancies, which serve as the higher conducting part of each memristors. w_1 and w_2 represent the instantaneous width of the doped region, meanwhile the black and red arrows describe the trending expansion and contraction of the doped region, respectively. Hence, for any input voltage, say $V(t)$, an increase in the width w_1 corresponds to a decrease in w_2 and vice versa. 157

5.31 Analytical results of the memristor fuse showing the memristance transitions for $M_1(t)$, $M_2(t)$ and the memristor fuse $M_f(t)$. $\varrho = 2$, $q_{d_1} = 100\mu C$, $q_{d_2} = 200\mu C$, $R_{off} = 16K\Omega$ and $R_{on} = 100\Omega$. (**a**) memristance transitions for the memristors M_1 and M_2 (**b**) memristance of the memristor fuse M_f. 160

5.32 Analytical result of the memristor fuse using the new model. $\varrho = 2$, $q_{d_1} = 100\mu C$, $q_{d_2} = 200\mu C$, $R_{off} = 16K\Omega$ and $R_{on} = 100\Omega$. (**a**) memristance of M_1 and M_2, (**b**) memristance of the memristor fuse M_f. 162

5.33 Exploring the responses of the two memristors in the memristor fuse. 163

5.34 Memristance of M_1 and M_2 with respect to the flowing charge. It is clear that the increase in memristance of M_1 correspond to decrease in the one for M_2 and vice-versa. 165

5.35 Memristor fuse in the coupling mode. (a) Cond-1 (for $V_1 > V_2$) and (b) Cond-2 (for $V_1 < V_2$). 167

5.36 Comparing the system evolution using the circuit of **Figure 5.21** by considering memristor (M) and then memristor-fuse (M_f). Mc1 and Mc2 correspond respectively to a single memristor used according to Cond-1 and Cond-2, while Mf1 and Mf2 correspond respectively to a memristor fuse used according to Cond-1 and Cond-2. The results show the response for each case until the system stabilized: **(A)** the voltage evolution as $V_1(t)$ and $V_2(t)$, **(B)** the flowing currents through the memristor (I_{c1} and I_{c2} for Cond-1 and Cond-2 respectively) and memristor fuse (I_{f1} and I_{f2} for Cond-1 and Cond-2 respectively), **(C)** memristance transition. Given the same initial condition, the results show that memristor fuse conducts equally in both directions. For Mc1, Mc2, Mf1 and Mf2: c1, c2, f1 and f2 are subscripts denoting Cond-1 and Cond-2 accordingly. 168

5.37 Phase portraits of the analytical solution with memristor fuse in the coupling mode. The results showed a rather better symmetry than a standalone memristor. 171

6.1 Memristor-based 2D CNN – Display of 16 cells with memristors in the coupling mode, that is, adjacent neighbourhood connections. 174

6.2 Nonlinear resistance response. (a) I-V characteristic. (b) The corresponding potential energy showing the stable equilibrium state at $V_n = 0$ and $V_n = V_b$. $R_0 = 1023\Omega$ and the roots of the nonlinear resistance are $0V$, $V_a = 0.7V$ and $V_b = 1.2$. 175

6.3 Two cells coupled by a memristor. The interaction of the cells via memristor is studied by launching information from one cell (known as the master) to other (known as the slave), whose elements are labeled with subscript letters m and s respectively.175

6.4 Comparison of the evolution of $y(t)$ and its approximation, (**a**) $V_a = 0.12V$ and the steady state at V_b and (**b**) $V_a = 0.9V$ and the steady state at 0. 178

6.5 System evolution $V_m(t)$, $V_s(t)$, x and y. $R_o = 10K\Omega$, $C = 1\mu F$, $V_{m_0} = 1.5V$, $V_{s_0} = 0V$, $V_b = 1.2V$ and $V_a = 0.12V$. 179

6.6 System evolution showing the variation of V_a. $R_o = 10K\Omega$, $C = 1\mu F$, $V_{m_0} = 1.5V$, $V_{s_0} = 0V$, $V_b = 1.2V$, (**a**) $V_a = 0.2V$, (**b**) $V_a = 0.4V$, (**c**) $V_a = 0.6V$ and (**d**) $V_a = 0.8V$. . 180

6.7 Results for $R_0 = 10K\Omega$, $q_0 = 0.3q_d$, $V_s = 0V$ and $\Upsilon = [0.25, 0.45, 0.49, 0.5, 0.51, 0.55 \text{ and } 0.75]$ respectively indicated by the subscripts (**1-7**) down across the rows, showing the variations of V_a for three different values of V_m and V_b. The values of the other parameters are $R_{on} = 100\Omega$, $R_{off} = 16K\Omega$ and $C_m = C_s = 1\mu F$. (**a1**-**a7**) < First column > is for $V_m = V_b = 1V$ and V_a varies down across the column. (**b1**-**b7**) < Second column > is for $V_m < V_b$, here $V_m = 1V$, $V_b = 1.3V$. (**c1**-**c7**) < Third column > is for $V_m > V_b$ i.e $V_m = 1.3V$ and $V_b = 1V$. Down across the raw of each column, is the variation of V_a with respect to V_b according to Υ. With the exception of the fourth row (**a4**-**c4**) where $V_a = \frac{V_b}{2}$ and its vicinity, the results show that for $V_a < \frac{V_b}{2}$ the system stabilizes at V_b and for $V_a > \frac{V_b}{2}$ the system stabilizes at zero 0. However, for $V_a = \frac{V_b}{2}$ the values of parameters [i.e V_m, V_s, R_0, q_0, V_a, V_b and the memristive effect (R_{off} and R_{on})] decides the stability state and it is always 0 or V_b. The effect of changing parameters values on the system stability state can be clearly seen across the columns (**a4**-**c4**) where $V_a = \frac{V_b}{2}$. Note that figure (**a4**) can stabilize at 0 or V_b simply by changing the values of q_0, V_m or R_0. 183

6.8 Results for $R_0 = 2833\Omega$, $\Upsilon = [0.25, 0.45, 0.49, 0.5, 0.51, 0.55, 0.75]$ and $V_s = 0V$. (**a1**-**a7**) $V_{m_0} = V_b = 1V$. (**b1**-**b7**) $V_{m_0} < V_b$ i.e $V_{m_0} = 1V$ and $V_b = 1.3V$. (**c1**-**c7**) $V_{m_0} > V_b$ i.e $V_{m_0} = 1.3V$ and $V_b = 1V$. Down across the rows is the variation of V_a within $[0, V_b]$. Here, the values of parameters are similar to the ones in Fig. 6.7 with only the change in the value of R_0. It shows different evolution and stability for Figs. **b2** and **a4**. 184

6.9 Effect of initial memristance given by the initial charge q_0 on the system evolution and the steady state. Four different initial charges are considered as: $q_{0_1} = 20\mu C$, $q_{0_2} = 40\mu C$, $q_{0_3} = 60\mu C$ and $q_{0_4} = 80\mu C$, as indicated respectively by the subscripts numbers **1**-**4** in figures **a**, **b** and **c**. In each case, $V_a = 0.7V$, $V_b = 1.3V$, $V_{m_0} = 1.5V$ and $V_{s_0} = 0V$. (A) $R_0 = 1023\Omega$, (B) $R_0 = 2833\Omega$ and (C) $R_0 = 10K\Omega$. It shows that values of q_0 and R_0 have an effect on the evolution and steady state of the system. 185

6.10 Results obtained for parameters values comparable to SPICE showing the variations of $V_a \in [0, V_b]$. $R_0 = 2833\Omega$, $V_s = 0V$ and $\Upsilon = [0.25, 0.45, 0.49, 0.5, 0.51, 0.55, 0.75, 0.9]$ shown respectively by figures **a**, **b**, **c**, **d**, **e**, **f**, **g** and **h**. These results are based on reasonable values of parameters that can easily be compared with the one in SPICE simulations. For example, $V_b = 1.5$ is chosen to take into account threshold value of the diodes D_2 and D_3 (see Fig. 6.11), meanwhile $V_m = 2V$ is to ensure enough bias of the equivalent R_{NL}. 186

6.11 Nonlinear resistance circuit and its equivalent SPICE component. Nonlinear resistance circuit schematic representation (left) and the created two-terminals SPICE component of the onlinear resistance (right). 187

6.12 Complete circuit analysis of the SPICE R_{NL} component. (**a**) Circuit schematic: $V_{in} = 2V$, $R_1 = 6.8K\Omega$, $R_2 = 2K\Omega$, $R_3 = 7.2K\Omega$, $R_4 = 6.8K\Omega$, $R_5 = 1K\Omega$ and model of THAT4301 OpAmp. (**b**)Voltage V_{in} and V_{out} transient and it shows that $V_{out} > V_{in}$ confirming equation (6.20). This difference in potential forces the current flowing through R_2 to flow negatively. (**c**) Current flowing through the R_{NL}. First branch: I_x is small and positive. Second branch: I_y is negative. Third branch: I_z is high and positive. (**d**) DC sweep of V_{in} for Fig. c. See also Fig. 6.13. 189

6.13 Branch currents responses visualization of the R_{NL} circuit schematic. At point A, V_A is the potential when the first branch becomes active. Then, V_{in} increases and reaches the threshold value of diode D_1 at point B (i.e $V_B = 0.6V$), thus activates the second branch. When V_{in} becomes high enough, the combined threshold of diodes D_2 and D_3 is reached at point C (i.e $V_C = 1.2V$) and the third branch is activated. These systematic approaches always manifest itself in the nonlinear resistance response. 190

6.14 Verification of the created R_{NL} SPICE component based on the values of the resistors R_1-R_5. $V_{in} = 1.8V$. (**a**) Test-1: low resistances values, $V_a = 0.64V$ and $V_b = 1.28V$ (**b**) Test-2: medium resistances values, $V_a = 0.79V$ and $V_b = 1.49V$. (**c**) Test-3: high resistances values, $V_a = 0.62V$ and $V_b = 1.68V$. (**d**) Comparing figures **a**, **b** and **c** together. 191

6.15 Complete circuit analysis of the two-cells network. The result is obtained for: $R_1 = 10K\Omega$, $R_2 = 2.3K\Omega$, $R_3 = 11K\Omega$, $R_4 = 10K\Omega$, $R_5 = 1.3K\Omega$, thus it gives $V_a = 0.68V$ and $V_b = 1.77V$. $C_m = C_s = 1\mu C$, $R_{off} = 16K\Omega$, $R_{on} = 100\Omega$ and $q_d = 100\mu C$. The system stabilizes at V_b because $V_b - 2V_a > 0$. The initial conditions of the cells are: $V_{m_0} = 2V$ and $V_{s_0} = 0V$. At about $20ms$, $V_m(t) = V_s(t) =$ constant and then settled at V_b shortly (about $25ms$). At this point the current in each branch is zero, thus the network is completely stabilized. 193

6.16 Two cells SPICE Simulation for some chosen values of resistances, showing the steady state of the system based on the variations of resistors R_1-R_5. (a) low values of R_1-R_5, (b) medium values of R_1-R_5, (c) high values of R_1-R_5 and (d) arbitrary values of R_1-R_5. 194

6.17 Variations effect of R_3 and R_4 on the system steady state, using $R_1 = 10K\Omega$, $R_2 = 2K\Omega$ and $R_5 = 1K\Omega$. For a fixed value of R_2, it shows that the system stabilizes at V_b and 0 for $R_3 > R_4$ and $R_3 < R_4$ respectively. (a) $R_3 = 12K\Omega$, (b) $R_3 = 11K\Omega$, (c) $R_3 = 10K\Omega$, (d) $R_3 = 9K\Omega$, (e) $R_3 = 8K\Omega$ and (f) $R_3 = 6K\Omega$. Note that any change in the value of R_2 can affect the steady state of the system. 195

6.18 Result comparison for SPICE simulation and numerical solution. Similar behaviour is observed. 196

6.19 Effect of initial memristance on the evolution of $V_m(t)$ and $V_s(t)$. $q_{0_1} = 25\mu C$, $q_{0_2} = 50\mu C$, $q_{0_3} = 75\mu C$, $R_{on} = 100\Omega$, $R_{off} = 16K\Omega$, $C = 1\mu F$, $R_0 = 10K\Omega$, $V_{m_0} = 1.5V$ and $V_{s_0} = 0V$. In each case the initial memristance $M(q_0)$ affects the system evolution toward the equilibrium state V_b and 0 respectively. 196

6.20 Effect of initial memristance on the evolution of $V_m(t)$ and $V_s(t)$. $q_{0_1} = 25\mu C$, $q_{0_2} = 50\mu C$, $q_{0_3} = 75\mu C$, $R_{on} = 100\Omega$, $R_{off} = 16K\Omega$, $C = 1\mu F$, $R_0 = 10K\Omega$, $V_{m_0} = 1.5V$ and $V_{s_0} = 0.5V$. Using the same values of parameters except that V_{s_0} is nonzero. Similalrly, the effect of $M(q_0)$ is highly observable. 196

6.21 Schematic representation of the 1D-nonlinear diffusive electrical network for N number of identical cells. The coupling is made by the memristor, meanwhile each cell is composed of a linear capacitor C in parallel with a nonlinear resistor R_{NL}. . . . 198

List of Tables

2.1 Summary: Circuit elements visualization in tabular form. 11

3.1 Comparison of the three nonlinear dopant drift models 67

5.1 Variation of the initial voltage difference and the corresponding charge ratio. These measurements are taken with: $q_0 = 30\mu C$, $R_{off} = 16k\Omega$, $R_{on} = 100\Omega$, $C_m = C_s = 1\mu F$ and $R_m = R_s = 100k\Omega$. 119

5.2 Modified memristor SPICE netlist file 148

6.1 Table of values of Fig. 6.7 for the difference $V_b - 2V_a$ as a deterministic factor of system stability. $V_{s_0} = 0V$ and $V_a = \Upsilon V_b$. (**a1**-**a7**) $V_b = 1V$ and $V_{m_0} = 1V$, (**b1**-**b7**) $V_b = 1.3V$ and $V_{m_0} = 1V$ and (**c1**-**c7**) $V_b = 1V$ and $V_{m_0} = 1.3V$. 181

6.2 Table of $V_b - 2V_a$ for Fig. 6.10. $V_{s_0} = 0V$, $V_a = \Upsilon V_b$, $V_b = 1.5V$ and $V_{m_0} = 2V$. 182

6.3 Table of values for tests 1-3. 191

6.4 Table of values for R_1-R_5, for the two-cells simulations (Fig. 6.16). 194

6.5 Table of values for the variation of R_3 and R_4, for the two-cells simulations (Fig. 6.17). 195

A.1 Memristor SPICE netlist file 237

A.2 SPICE netlist file of the cubic memristor model. 238

B.1 The netlist file of figure 6.11 used for generating R_{NL} SPICE component. 240

V

APPENDICES

A

MEMRISTOR SPICE NETLIST FILE

Table A.1: Memristor SPICE netlist file

```
.SUBCKT memristor pl mn PARAMS: Ron=100 Roff=16K Ri=11K D=10N uv=10F p=1
* Differential state equation  *
Gx 0 x value={ I(Em)*uv*Ron*f(V(x),p)/D^2}
Cx x 0 1 IC= {(Roff-Ri)/(Roff-Ron)};
Rsh x 0 1T
* Resistive port equation *
Em pl aux value={-I(Em)*(Roff-Ron)*V(x)}
Roff aux mn {Roff}
* Note that I(Em)=I
* flux computation
Eflux flux 0 value={SDT(V(pl,mn))}
* charge computation
Echarge charge 0 value={SDT(I(Em))}
* Nonlinear drift modeling
.func f(x,p)={1-(2*x-1)^(2*p)}
.ENDS memristor
```

Table A.2: SPICE netlist file of the cubic memristor model.

```
.SUBCKT memcub pl mn PARAMS: Ron=100 Roff=16K D=10N uv=10F
.param qo={30uC}
.param a={-3/2}
.param b={0}
.param c={(Roff-Mo)/(2*(Roff-Ron))};
* qo is the last amount of charge flowed through the device
* Mo is the initial memristance given by qo
.param P={b-a^2/3}
.param Q={c+2*a^3/27-b*a/3}
.param Delt={Q^2/4+P^3/27}
.param v={(Q/2+sqrt(Delt))^(1/3)}
.param u={P/(3*v)}
.param Xo={u-v-a/3}; initial state of the memristance
* Xo=qo/qd normalized form of the charge and qd=D^2/(uv*Ron)
* Differential state equation  *
Gx 0 x value={ I(Emem)*uv*Ron/D^2}
Cx x 0 1 IC= {Xo};
Raux x 0 1T
* Resistive port equation *
Emem pl aux value={-I(Emem)*(Roff-Ron)*(3*V(x)^2-2*V(x)^3)}
Roff aux mn {Roff}
.ENDS memcub
```

B

R_{NL} SPICE NETLIST FILE

Table B.1: The netlist file of figure 6.11 used for generating R_{NL} SPICE component.

```
** Nonlinear resistance function RNL: Netlist **
.subckt RNL 111 112
Rnl0 111 112 6.8k
D1 115 111 Default
Rnl2 115 Vout 2K
Xrnl 111 116 p n 116 4301OA1_THAT
VP  p  0 15
Vn  n  0 -15
Rnl3 Vout 116 7.2k
Rnl4 116 112 6.8k
D2 111 113 Default
D3 113 114 Default
Rnl5 114 112 1K
.MODEL Default D
* .model Da1N4004 D (IS=18.8n RS=0      BV=400 IBV=5.00u CJO=30
* +M=0.333   N=2.0  TT=0)

* THAT4301 OA1 Macromodel
* connections: 1 = non-inverting input, 2 = inverting input,
* 3 = positive power supply 4 = negative power supply and 5 = output
.subckt 4301OA1_THAT  1 2 3 4 5
  c1   11 12 14.5E-12
  c2    6  7 25.00E-12
  dc    5 53 dx
  de   54  5 dx
  dlp  90 91 dx
  dln  92 90 dx
  dp    4  3 dx
  egnd 99  0 poly(2) (3,0) (4,0) 0 .5 .5
  fb    7 99 poly(5) vb vc ve vlp vln 0 3.255E6 -3E6 3E6 3E6 -3E6
  ga    6  0 11 12 785.4E-6
  gcm   0  6 10 99 7.854E-9
  iee   3 10 dc 50.30E-6
  hlim 90  0 vlim 1K
  q1   11  2 13 qx
  q2   12  1 14 qx
  r2    6  9 100.0E3
  rc1   4 11 1.273E3
  rc2   4 12 1.273E3
  re1  13 10 237.2
  re2  14 10 237.2
  ree  10 99 3.976E6
  ro1   8  5 220
  ro2   7 99 220
  rp    3  4 48.66E3
  vb    9  0 dc 0
  vc    3 53 dc 1.600
  ve   54  4 dc 1.200
  vlim  7  8 dc 0
  vlp  91  0 dc 3.40
  vln   0 92 dc 5.90
.model dx D(Is=800.0E-18)
.model qx PNP(Is=800.0E-18 Bf=166.7)
.ends 4301OA1_THAT
```

Document generated with LaTeX and:
the LaTeX style for PhD Thesis created by S. Galland — http://www.multiagent.fr/ThesisStyle
the tex-upmethodology package suite — http://www.arakhne.org/tex-upmethodology/

SPIM

école doctorale **sciences pour l'ingénieur et microtechniques**

Title: Memristors in Nonlinear Network: Application to Information (Signal and Image) Processing

Keywords: Memristor, Memristor fuse, Asymmetry, Symmetry, Bilaterality, Cellular nonlinear/neural networks (CNN), Charged RC cells, System dynamics, Diffusion, Signal processing, Binarization

Abstract:

Memristor is a two-terminal nonlinear dynamic electronic device. Typically, it is a passive nano-device whose conductivity is controlled by the flux, time-integral of the voltage across its terminals, or by the charge, time-integral of the current flowing through it, and it presents interesting features for versatile applications. This thesis considers memristor use as a neighborhood connection for 2D cellular nonlinear or neural network (CNN), essentially for information (image and signal) processing and electronic prosthesis. We develop a model of the memristor based 2D cellular nonlinear networks CNNs compatible to image applications by incorporating memristor in the adjacent neighborhood connection. This approach will offer many advantages with respect to previous known designs. Some of these advantages are higher pixel density due to the nano-nature of the memristor, lower power consumption, high-density connection flexibility and compatibility to CMOS technology, etc. Firstly, we present the State of the Art, that is, what is known about this new passive component - the memristor, along with an analog model of memristor for practical and demonstration purposes. Then, we present the quantitative and qualitative behaviour of a charge-controlled memristor by considering RC networks with memristor in the coupling mode, focusing specifically on the system of two initially charged RC cells. We extensively study the interaction of two Fitzhugh-Nagumo cells via a memristor by observing the transient and the steady state response of each cell, allowing us to have a good foresight of the memristor functionality in the memristor based 2D CNNs and the diffusion effect in a 1D cellular nonlinear electrical lattice. Furthermore, we present the generalized model of the memristor based 2D CNNs reliable for processing any number of cells.

Titre : Memristors en réseau non linéaire: Application au traitement de l'information (signal et image)

Mots-clés : Memristor, Memristor fuse, Asymétrie, Symétrie, Bilatéralité, Réseau cellulaire non linéaire (CNN), Cellules RC chargées, Dynamique du système, Diffusion, Traitement du signal, Binarisation

Résumé :

Le memristor est un dipôle électronique dynamique non linéaire. Typiquement, il s'agit d'un dispositif de nanotechnologie passif dont la conductivité est contrôlée par le flux, l'intégrale de la tension à ses bornes, ou par la charge, l'intégrale du courant qui le traverse, présentant des caractéristiques intéressantes pour des applications polyvalentes. Cette thèse est consacrée à l'utilisation de memristor comme élément de couplage d'un réseau cellulaire non linéaire, en vue du traitement de l'information (image et signal) ou comme prothèse électronique d'un système neuronal. Nous développons un modèle de réseaux cellulaires non linéaires 2D basés sur le memristor, en incorporant le memristor dans le couplage de cellules voisines. Cette approche offre de nombreux avantages par rapport à ce qui est utilisé actuellement. Parmi ces avantages, on peut citer une densité de pixels plus élevée en raison de la nano-nature du memristor, une consommation d'énergie plus faible, une flexibilité de connexion à haute densité, la compatibilité avec la technologie CMOS, etc... Tout d'abord, nous présentons l'état de l'art sur le memristor, ainsi qu'un modèle analogique de memristor à des fins pratiques et de démonstration. Ensuite, nous présentons le comportement quantitatif et qualitatif d'un memristor contrôlé par la charge en considérant les réseaux RC avec le memristor en mode couplage, en se concentrant spécifiquement sur le système de deux cellules RC initialement chargées. Nous étudions en détail l'interaction de deux cellules Fitzhugh-Nagumo via un memristor en observant la réponse transitoire de chaque cellule, ce qui nous permet d'avoir une bonne compréhension de la fonctionnalité memristor et de l'effet de diffusion dans un treillis électrique cellulaire non linéaire 1D. En outre, nous présentons le modèle généralisé des CNNs 2D basés sur le memristor pour le traitement de n'importe quel nombre de cellules.

UBFC UNIVERSITÉ BOURGOGNE FRANCHE-COMTÉ

Université Bourgogne Franche-Comté
32, avenue de l'Observatoire
25000 Besançon, France